Staggered fractional step numerical schemes for models for reactive flows

Dionysios Grapsas

Faculté des Sciences
Aix*Marseille Université

École Doctorale 184 – Mathématiques et Informatique

Thèse de doctorat

Discipline : Mathématiques appliquées

présentée par

Dionysios Grapsas

Staggered fractional step numerical schemes for models for reactive flows

---

dirigée par Raphaèle Herbin et Jean-Claude Latché

Soutenue le 11 décembre 2017 devant le jury composé de :

M. Christophe Chalons	Université de Versailles	Rapporteur
M. Stéphane Louis Clain	Université du Minho, Guimarães	Rapporteur
M^{me} Raphaèle Herbin	Université d'Aix-Marseille	Directeur
M. Frédéric Lagoutière	Université de Lyon 1	Examinateur
M. Jean-Claude Latché	IRSN	Codirecteur
M^{me} Marie-Hélène Vignal	Université de Toulouse 3	Examinateur

Institut de Mathématiques de Marseille
Technopôle Château-Gombert
39, rue Frédéric Joliot-Curie
13453 Marseille Cedex 13

Université Aix-Marseille
Ecole Doctorale de Mathématiques
et Informatique de Marseille
3 Place Victor Hugo
13331 Marseille Cedex 3
case 53, Bat7 - Bloc G1 - 1er étage - Bureau
02

À Phédias, éveilleur obstiné de ma curiosité,
à mes parents, qui m'ont donné les moyens de l'assouvir

Remerciements

Je voudrais évidement remercier mes directeurs de thèse, Raphaèle Herbin et Jean-Claude Latché, pour leur accompagnement pendant ces trois ans. Mais je voudrais les remercier davantage, ainsi que Thierry Gallouet, pour leur soutien et leur confiance pendant les années encore plus difficiles qui ont précédé et pour leurs efforts afin que je puisse commencer ce travail.

J'adresse mes remerciements à Christophe Chalons et Stéphane Louis Clain pour avoir accepté d'être rapporteurs de ce manuscrit. Je remercie aussi Frédéric Lagoutière et Marie-Hélène Vignal pour leur participation à mon jury de thèse.

Je tiens à remercier mes collègues de l'I2M pour un quotidien dans la bonne humeur : Chady, Benoît, Paolo, Rémi, Damien, Marie-Ève, Cécile, Ayouna, Samir et toute l'équipe d'Analyse Appliquée. Merci à Thomas, avec lequel je n'ai pas seulement partagé un appartement, mais aussi une grosse partie de ma vie ces quatre dernières années, à Vladimiro, pour les séances de tennis interminables (de préférence sous mistral très fort), à Nicolas, avec lequel j'ai eu le plaisir de partager, entre autres, l'expérience de la plupart de mes conférences.

Je tiens à remercier l'ensemble du LIE, qui m'accueille encore aujourd'hui comme si je ne suis jamais parti : Jean-Marc, Jean-Paul, Matthieu, Fabrice, François, Sylvain, Samuel, Marco, Philippe, Céline, Germain, Ahmed, Mohammed. Un grand merci à Fabien pour son soutien pendant le début de mon stage, à Laura, qui s'est toujours rendue disponible pour répondre à mes questions avec patience, à Khaled, qui m'a aidé préparer ma présentation.

Je voudrais remercier mes plus proches de m'avoir donné la possibilité de travailler dans les meilleurs conditions possibles : Miranda et Annie, vous le savez que je ne serais pas ici aujourd'hui sans votre soutien. Jean-Luc, Nicos, Hélène, Philippe, Néphélie, votre présence était toujours un cadeau précieux, une pause paisible dans un quotidien parfois bouleversant. Merci à Mari, Sofia et Giorgos de nous avoir aidé l'affronter. Et enfin un grand merci à Rim d'avoir assuré la tâche la plus difficile, d'être à mes côtés tous les jours.

Résumé

Dans cette thèse on développe et analyse des schémas numériques de projection pour les écoulements réactifs. La discrétisation en espace est effectuée sur des maillages décalés, et elle utilise soit le schéma Marker-And-Cell (MAC) pour des maillages rectangulaires soit une approximation non-conforme des éléments finis pour des maillages génériques quadrangulaires, hexaédrales ou simpliciaux.

La première partie de la thèse aborde la partie purement hydrodynamique du problème et propose un schéma numérique pour les équations de Navier-Stokes compressible. Pour le bilan de l'énergie, l'équation de conservation de l'énergie interne est discrétisée, ce qui garantit que celle-ci reste positive; cette relation contient un terme de correction numérique, qui permet au schéma de calculer la bonne vitesse des chocs dans la limite d'Euler. On montre que le schéma possède au moins une solution, et que dans tous les cas les propriétés de stabilité du problème continu sont préservées, indépendamment du pas d'espace et de temps. De plus, le schéma dégénère vers le schéma de projection usuel dans la limite des faibles nombres de Mach. Des test numériques confirment son bon comportement dans la limite non-visqueux incompressible ainsi que dans la limite d'Euler.

On s'intéresse ensuite au calcul des écoulements compressible réactifs pour des fluides partiellement prémélangés. La discrétisation est basée sur un modèle qui utilise une localisation explicite du front de flamme à travers une équation différentielle du type level-set, souvent appelée dans ce contexte équation G, couplée avec un système de lois de conservation (espèces chimiques, quantité de mouvement, énergie). On démontre que l'algorithme présenté possède au moins une solution et préserve les bornes physiques des inconnues; de plus on montre que toute suite de solutions approchées du système de lois de conservation converge (à une sous-suite près) vers une solution faible du problème continu. Dans le cas non-visqueux et pour des termes de réaction de plus en plus raides, le modèle doit dégénérer vers un modèle pour lequel la solution du problème de Riemann est établie. Les tests numériques effectués confirment que c'est bien le cas. Plusieurs discrétisation de l'opérateur convectif sont proposées afin de diminuer la diffusion numérique et améliorer la précision du schéma.

La dernière partie de cette thèse est consacrée à l'approximation de solutions d'un système de lois de conservation qui, modélise l'écoulement réactif généré par la combustion de poussières, à faible nombre de Mach et en une dimension d'espace. Ce modèle comporte des termes de diffusion massique assez génériques, dont les coefficients de diffusion dépendent de la composition locale du mélange, et qui sont différents pour chaque espèce chimique. L'algorithme préserve par construction les propriétés de stabilité du problème continu, notamment la positivité des fractions massiques des espèces chimiques, le fait que leur somme est égale à l'unité et la non-décroissance de la température étant donné une réaction chimique exothermique.

Abstract

In this thesis we develop and analyze fractional step numerical schemes for reactive flows. The space discretization is staggered, using either the Marker-And Cell (MAC) scheme for structured grids, or a nonconforming low-order finite element approximation for general quadrangular, hexahedral or simplicial meshes.

The first part of the thesis deals with the purely hydrodynamical part of the problem and proposes a numerical scheme for the compressible Navier-Stokes equations. For the energy balance equation, the scheme uses a discrete form of the conservation of the internal energy, which ensures that this latter variable remains positive; this relation includes a numerical corrective term, to allow the scheme to compute correct shock solutions in the Euler limit. The scheme is shown to have at least one solution, and to preserve the stability properties of the continuous problem irrespectively of the space and time steps. In addition, it naturally boils down to a usual projection scheme in the limit of vanishing Mach numbers. Numerical tests confirm its potentialities, both in the viscous incompressible and Euler limits.

Then we turn to the computation of partially premixed compressible reactive flows. The discretization is based on a model that uses an explicit localization of the flame brush location by a level-set-like partial differential equation often referred to as the G-equation, coupled with the system of balance laws (chemical species, momentum, energy). The algorithm presented here is shown to possess at least one solution that preserves the physical bounds of the unknowns; furthermore, any sequence of approximate solutions to the discretized system of balance laws is shown to tend (up to a subsequence) to a weak solution of the continuous problem. In the inviscid case, the model should boil down, as the stiffness of reaction term increases, to a model for which a closed form of the solution of Riemann problems is available. Numerical tests are performed to show that this is indeed the case. Various discretizations of the convection operators are proposed in order to diminish the numerical diffusion which, especially in this case, affects the convergence speed of the scheme.

The last part or the thesis is devoted to the approximation of solutions to a system of balance equations which models the low Mach number one- dimensional reactive flow generated by the combustion of a dust suspension. This model features rather general diffusion terms, with, in particular, mass diffusion coefficients that depend on the local composition and differ from one chemical species to another. The algorithm preserves by construction the stability properties of the continuous problem, namely the positivity of the chemical species mass fractions, the fact that they sum up to one, and the non-decrease of the temperature, provided that the chemical reaction is exothermic.

Contents

Chapter 0

Overview

The release of reactive gases, generally hydrogen, may occur during various accident scenarios in process industries as, more specifically, in nuclear facilities. For instance, high pressure hydrogen is used for cooling some devices of the tertiary circuit of Pressurized Water Reactors (PWRs), and consequences of a leak has to be assessed in safety studies. Severe accidents leading to the heating of the core of the reactor (possibly up to fusion) also generate large hydrogen releases (and, to some extent, of carbon monoxide) by oxydation of the structures of the primary circuit; as shown in the Fukushima accident, the risk of an explosion is present. Besides, several processes in the nuclear industry involve the manipulation or generation of fine dusts (about ten microns of characteristic diameter), the explosion of which may not be excluded: this is the case for graphite/gas reactors decommissioning activities, or during plasma reaction in the ITER torus (were explosion may occur in case of leakage of the torus wall, maintained to very low pressure in operating conditions, leading to a violent air ingress in the torus, dust resuspension and generation of a high temperature air/hydrogen/dust mixture). Consequently, it is crucial for the safety assessment of the facilities to be able to simulate the consequences of an explosion, essentially to check the capability of structures to prevent the release of radioactive materials in the surrounding environment. To this purpose, the Institut de Radioprotection et de Sûreté Nucléaire (IRSN) is developping an in-house computational tool for reactive gases/dusts dispersion, deflagration and blast wave propagation, named P^{2}REMICS. Works presented here are part of this project.

The P^{2}REMICS software (together with other applications such as the more mature ISIS code, devoted to fire simulations) relies on a C++ library of components for fluid flow simulation, named CALIF^{3}S, which may be seen as a generic CFD solver. Because of the wide range of applications, CALIF^{3}S incorporates numerical schemes for all flow regimes, from incompressible (or variable density low Mach number) to compressible flows, involving shock phenomena. These schemes are designed in a way to share as much as possible the same techniques, for obvious man-effort optimization purposes: the space discretization is the same, and relies on a staggered arrangement of the unknowns; for pollutant dispersion (low Mach number flow) and deflagration (compressible flow), the time discretization technique is based on a pressure correction strategy. Moreover, in some applications, the whole range of Mach numbers is encountered in the same simulation, so the scheme used for compressible flows is required to keep its accuracy in the low Mach number limit.

The work presented in this thesis is a contribution to the construction and assessment of CALIF^{3}S algorithms:

– We first develop a novel pressure correction scheme for the solution of the compressible Navier-Stokes equations, whose essential characteristics are the preservation of the stability properties of the continuous problem (conservation of the integral of the total energy over the computational

domain, positivity of the density and the internal energy), the accuracy in the Euler limit and the fact that the scheme boils down to a standard projection algorithm when the Mach number tends to zero.

– Then we propose a physical model for the simulation of deflagrations, which computes the limit of the burnt zone by solving a transport equation for the characteristic function of this area (similar to the balance relation called "G-equation" in the combustion litterature), and we extend the above-mentioned pressure correction scheme to this situation, inserting this building brick in a fractional step time-marching algorithm. Here also, the physical range of the unknowns is preserved by construction. The consistency of the scheme is not obvious, since we solve a discrete balance equation for the internal energy (or, equivalently, the so-called sensible enthalpy) and, due to the staggered space discretization, no conservative discrete total energy equation can be recovered. This issue was already tackled in previous works, but turns to be even more complicated here due to the considered time-splitting strategy, which leads to a decoupled specific time-discretization of the chemical species mass balances; the consistency is nevertheless proven. The accuracy of the scheme is then shown to dramatically depend on the space discretization of the chemical species mass balance, by numerically testing first and (formally) second order approximations of the convection operator.

– Finally, we turn to the modelling of dust explosions, focussing on two aspects: first, we develop a scheme for the standard form of the reactive flow governing equations (*i.e.* with standard reaction terms, without any *a priori* prediction of the location of the burnt zone), check on one-dimensional computations that the solution indeed takes the form of the progression of a flame brush and assess the consistency of the results obtained with the above-mentionned G-equation-like approach; second, for laminar flames, the diffusion of chemical species strongly differs from one species to another (the dust is supposed not to diffuse at all), thus a careful design of the diffusion operators and of the associated discretization is required.

This introductive chapter is intended to provide an overview of this work, which is developped further in Chapters 1, 2, 3, each of them corresponding to one item of the previous list. Each of these chapters is the object of a publication, either already published [30] or in preparation [23, 31]. The structure of the present chapter is as follows: in Section 0.1 we present, in a generic way, the space discretization used in the three following chapters. Each further Section (0.2, 0.3, 0.4) is devoted to one of the following chapters of the thesis, outlining the mathematical model, the developed numerical scheme and the main obtained results.

0.1 Meshes and unknowns

Let the computational domain Ω be an open polygonal subset of $\mathbb{R}^d$, $1 \leq d \leq 3$, with boundary $\partial\Omega$ and let $\mathcal{M}$ be a decomposition of Ω, supposed to be regular in the usual sense of the finite element literature (*e.g.* [10]). The cells may be:

– for a general domain Ω, either convex quadrilaterals ($d = 2$) or hexahedra ($d = 3$) or simplices, both type of cells being possibly combined in a same mesh,

– for a domain the boundaries of which are hyperplanes normal to a coordinate axis, rectangles ($d = 2$) or rectangular parallelepipeds ($d = 3$) (the faces of which, of course, are then also necessarily normal to a coordinate axis).

By $\mathcal{E}$ and $\mathcal{E}(K)$ we denote the set of all faces σ of the mesh and of the element $K \in \mathcal{M}$ respectively. The set of faces included in the boundary of Ω is denoted by $\mathcal{E}_{\rm ext}$ and the set of internal edges (*i.e.* $\mathcal{E} \setminus \mathcal{E}_{\rm ext}$) is denoted by $\mathcal{E}_{\rm int}$; a face $\sigma \in \mathcal{E}_{\rm int}$ separating the cells K and L is denoted by $\sigma = K|L$. The

outward normal vector to a face σ of K is denoted by $\boldsymbol{n}_{K,\sigma}$. For $K \in \mathcal{M}$ and $\sigma \in \mathcal{E}$, we denote by $|K|$ the measure of K and by $|\sigma|$ the $(d-1)$-measure of the face σ. For any $K \in \mathcal{M}$ and $\sigma \in \mathcal{E}(K)$, we denote by $d_{K,\sigma}$ the Euclidean distance between the center x_K of the mesh and the edge σ. For any $\sigma \in \mathcal{E}$, we define $d_\sigma = d_{K,\sigma} + d_{L,\sigma}$, if $\sigma \in \mathcal{E}_{\rm int}$ and $d_\sigma = d_{K,\sigma}$ if $\sigma \in \mathcal{E}_{\rm ext}$. The size of the mesh is denoted by h. For $1 \leq i \leq d$, we denote by $\mathcal{E}^{(i)} \subset \mathcal{E}$ and $\mathcal{E}_{\rm ext}^{(i)} \subset \mathcal{E}_{\rm ext}$ the subset of the faces of $\mathcal{E}$ and $\mathcal{E}_{\rm ext}$ respectively, which are perpendicular to the i^{th} unit vector of the canonical basis of $\mathbb{R}^d$.

The space discretization is staggered, using either the Marker-And Cell (MAC) scheme [39, 38], or nonconforming low-order finite element approximations, namely the Rannacher and Turek (RT) element [69] for quadrilateral or hexahedric meshes, or the lowest degree Crouzeix-Raviart (CR) element [14] for simplicial meshes.

For all these space discretizations, the degrees of freedom for the scalar variables (pressure, density etc.) are associated to the cells of the mesh $\mathcal{M}$ and, for a scalar variable x, are denoted by:

$$\big\{x_K,\ K \in \mathcal{M}\big\}.$$

Let us then turn to the degrees of freedom for the velocity (*i.e.* the discrete velocity unknowns).

– **Rannacher-Turek** or **Crouzeix-Raviart** discretizations: the degrees of freedom for the velocity components are located at the center of the faces of the mesh, and we choose the version of the element where they represent the average of the velocity through a face. The set of degrees of freedom reads:

$$\{\boldsymbol{u}_\sigma,\ \sigma \in \mathcal{E}\},\ \text{of components } \{u_{\sigma,i},\ \sigma \in \mathcal{E},\ 1 \leq i \leq d\}.$$

– **MAC** discretization: the degrees of freedom for the i^{th} component of the velocity are defined at the centre of the faces of $\mathcal{E}^{(i)}$, so the whole set of discrete velocity unknowns reads:

$$\big\{u_{\sigma,i},\ \sigma \in \mathcal{E}^{(i)},\ 1 \leq i \leq d\big\}.$$

For the definition of the schemes, we need a dual mesh which is defined as follows.

– **Rannacher-Turek** or **Crouzeix-Raviart** discretizations: for the RT or CR discretizations, the dual mesh is the same for all the velocity components. When $K \in \mathcal{M}$ is a simplex, a rectangle or a cuboid, for $\sigma \in \mathcal{E}(K)$, we define $D_{K,\sigma}$ as the cone with basis σ and with vertex the mass center of K (see Figure 1). We thus obtain a partition of K in m sub-volumes, where m is the number of faces of the mesh, each sub-volume having the same measure $|D_{K,\sigma}| = |K|/m$. We extend this definition to general quadrangles and hexahedra, by supposing that we have built a partition still of equal-volume sub-cells, and with the same connectivities; note that this is of course always possible, but that such a volume $D_{K,\sigma}$ may be no longer a cone; indeed, if K is far from a parallelogram, it may not be possible to build a cone having σ as basis, the opposite vertex lying in K and a volume equal to $|K|/m$. The volume $D_{K,\sigma}$ is referred to as the half-diamond cell associated to K and σ.
For $\sigma \in \mathcal{E}_{\rm int}$, $\sigma = K|L$, we now define the diamond cell D_σ associated to σ by $D_\sigma = D_{K,\sigma} \cup D_{L,\sigma}$; for an external face $\sigma \in \mathcal{E}_{\rm ext} \cap \mathcal{E}(K)$, D_σ is just the same volume as $D_{K,\sigma}$.

– **MAC** discretization: for the MAC scheme, the dual mesh depends on the component of the velocity. For each component, the MAC dual mesh only differs from the RT or CR dual mesh by the choice of the half-diamond cell, which, for $K \in \mathcal{M}$ and $\sigma \in \mathcal{E}(K)$, is now the rectangle or rectangular parallelepiped of basis σ and of measure $|D_{K,\sigma}| = |K|/2$.

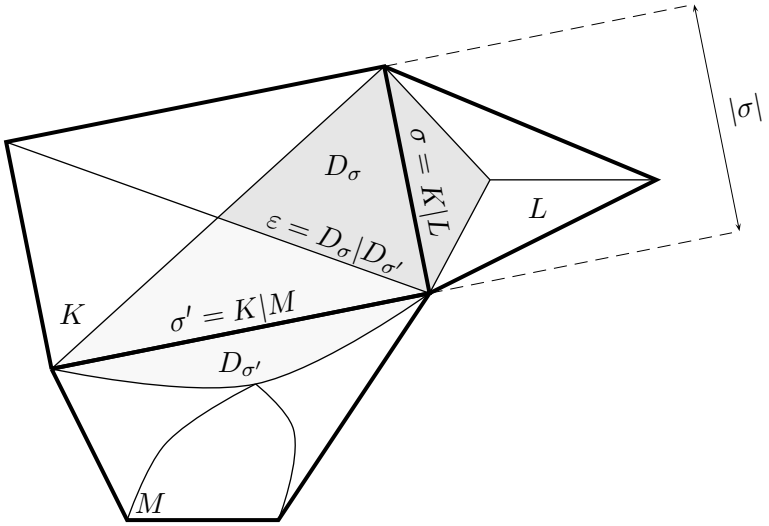

Figure 1: Primal and dual meshes for the Rannacher-Turek and Crouzeix-Raviart elements.

We denote by $|D_\sigma|$ the measure of the dual cell D_σ, and by $\varepsilon = D_\sigma|D_{\sigma'}$ the dual face separating two diamond cells D_σ and $D_{\sigma'}$.

In order to be able to write a unique expression of the discrete equations for both MAC and CR/RT schemes, we introduce the set of faces $\mathcal{E}_\mathcal{S}^{(i)}$ associated with the degrees of freedom of each component of the velocity ($\mathcal{S}$ stands for "scheme"). Note that the notations that follow are adopted to homogeneous Neumann boundary condition and small modifications need to be made for other boundary conditions.

$$\mathcal{E}_\mathcal{S}^{(i)} = \left| \begin{array}{l} \mathcal{E}^{(i)} \setminus \mathcal{E}_{\text{ext}}^{(i)} \text{ for the MAC scheme,} \\ \mathcal{E} \setminus \mathcal{E}_{\text{ext}}^{(i)} \text{ for the CR or RT schemes.} \end{array} \right.$$

Similarly, we unify the notation for the set of dual faces for both schemes by defining:

$$\bar{\mathcal{E}}_\mathcal{S}^{(i)} = \left| \begin{array}{l} \bar{\mathcal{E}}^{(i)} \setminus \bar{\mathcal{E}}_{\text{ext}}^{(i)} \text{ for the MAC scheme,} \\ \bar{\mathcal{E}} \setminus \bar{\mathcal{E}}_{\text{ext}}^{(i)} \text{ for the CR or RT schemes,} \end{array} \right.$$

where the symbol $\bar{}$ refers to the dual mesh; for instance, $\bar{\mathcal{E}}^{(i)}$ is thus the set of faces of the dual mesh associated with the i^{th} component of the velocity, and $\bar{\mathcal{E}}_{\text{ext}}^{(i)}$ stands for the subset of these dual faces included in the boundary. Note that, for the MAC scheme, the faces of $\bar{\mathcal{E}}^{(i)}$ are perpendicular to a unit vector of the canonical basis of $\mathbb{R}^d$, but not necessarily to the i^{th} one.

The time interval $[0, T]$ is uniformly split into $N \in \mathbb{N}^*$ sub-intervals, with length δt and so that $T = \delta t N$.

0.2 An unconditionally stable numerical scheme for the compressible Navier-Stokes equations

It seems natural, before tackling the more complex problem of reactive flows, that one should first have a robust numerical solver for non-reactive flows. Moreover, this solver may be used to calculate the concentrations of the different gases before the ignition. This is the subject of Chapter 1; in this section, a short description of this solver and of its properties.

As already mentioned, the proposed algorithm is based on staggered finite-volume space discretization; it is combined, to some extent, with finite-elements for some diffusion operators, whereas convection operators are clearly of finite-volume type. A fractional step strategy is implemented; it involves a prediction step for a tentative velocity followed by an elliptic pressure correction step. These steps are both implicit-in-time, to avoid any restriction of the time step other than the one imposed for accuracy reasons. This kind of approach has its roots in the late sixties, when the first attempts to build "all flow velocity" schemes [37, 38] were realized, based on the famous MAC scheme, introduced some years earlier [39]. These seminal papers have been the starting point for the development of numerous schemes with similar strategies to decouple the momentum balance equation (in a prediction step) from the mass and energy balance (correction step(s)); resulting algorithms may be iterative (prediction and correction are repeated up to obtain a fixed point, which corresponds to the/a solution of the backward Euler scheme for the coupled system – this is the spirit of the SIMPLE algorithm and its (numerous) variants) or, as here, non-iterative (the prediction step is followed by the correction step, and the time-step is over). The litterature on this topic is vast [7, 46, 47, 77, 48, 62, 4, 83, 13, 75, 80, 79, 76, 78, 53] (this list is restricted to staggered discretizations and certainly non-exhaustive). The risk when using a non-iterative pressure correction algorithm is to lose stability; we prove here an unconditional (*i.e.* independent of the time and space step) stability result and, to the best of our knowledge, this constitutes the first rigorous stability proof for such algorithms in the framework of the compressible Navier-Stokes equations.

One salient feature of the proposed scheme is that the energy balance balance rather than the total energy balance; the scheme is thus a discretization of a non-conservative form of the equations. This presents two advantages: first, for staggered discretizations, the total energy is a composite quantity, in the sense that it mixes cell and face variables, and its definition is not straighforward; second, the solved discrete internal energy balance ensures by construction the positivity of this variable, which is essential for the scheme stability. The counterpart is that the scheme is not *natively* consistent in the inviscid limit, *i.e.* for Euler equations: a correction term must be introduced in the discrete energy balance to ensure a correct capture of shock solutions. Roughly speaking, this term is the analogue of the dissipation term induced by viscosity in the Navier-Stokes case, but here associated to the numerical dissipation introduced in the momentum balance. Its derivation requires to establish a discrete kinetic energy balance equation from the discrete momentum balance; this is possible thanks to a careful (and specific) design of the velocity convection operator. This issue is already discussed in recent previous works [1, 20, 42], and we only develop here some qualitative aspects of this correction term.

Another feature of the scheme is that the numerical viscosity necessary for stabilization in highly convective cases is obtained by an upwinding of the convection operators with respect to the material velocity only, in opposition to what occurs with schemes based on Riemann solvers, in the spirit of AUSM or the so-called flux-splitting schemes [72, 58, 84, 57, 74]. Besides, Riemann solvers technology is not easy to implement neither in time-implicit schemes nor for staggered discretizations, and getting rid of the necessity to calculate exact or approximate Riemann problems solutions, facilitates the extension to more general hyperbolic systems, as performed in the following sections. This point is essential for the accuracy of the scheme for low Mach number flows, which is often lost because the numerical diffusion scales as the celerity of the fastest waves and not as the material velocity only. One way to tackle the low Mach number regime is to modify the solvers issued from the hyperbolic mainstream; this is a rather intricate task, and has been the subject of several works (see [36, 35, 34, 16, 8, 9]). Here, we take the opposite route, since we rather extend a solver natively designed for incompressible flows, or for the asymptotic model of low Mach number flows [61]; consequently, we observe that, formally, our algorithm boils down to the original incompressible scheme when the Mach number tends to zero (see [43] for a rigorous proof in the barotropic case). As a counterpart, the solver's accuracy and

stability in the Euler limit must be carefully investigated, and our numerical experiments are, in their majority, dedicated to this case; the numerical results, together with recently derived entropy estimates [21], confort the accuracy and the reliability of the proposed scheme.

0.2.1 Governing equations

The mathematical model reads:

$$\partial_t \rho + \mathrm{div}(\rho \boldsymbol{u}) = 0, \tag{1a}$$

$$\partial_t (\rho \boldsymbol{u}) + \mathrm{div}(\rho \boldsymbol{u} \otimes \boldsymbol{u}) + \boldsymbol{\nabla} p - \mathrm{div}(\boldsymbol{\tau}(\boldsymbol{u})) = 0, \tag{1b}$$

$$\partial_t (\rho e) + \mathrm{div}(\rho e \boldsymbol{u}) - \mathrm{div}(\boldsymbol{q}) + p\mathrm{div}(\boldsymbol{u}) = \boldsymbol{\tau}(\boldsymbol{u}) : \boldsymbol{\nabla} \boldsymbol{u}. \tag{1c}$$

$$E = \frac{1}{2} |\boldsymbol{u}|^2 + e, \tag{1d}$$

$$p = \wp(\rho, e), \tag{1e}$$

where t stands for the time, ρ, $\boldsymbol{u}$, p, E and e are the density, velocity, pressure, total energy and internal energy in the flow, $\boldsymbol{\tau}(\boldsymbol{u})$ stands for the shear stress tensor, $\boldsymbol{q}$ stands for the heat diffusion flux, and the function $\wp$ is the equation of state (EOS), which satisfies by hypothesis $\wp(\cdot, 0) = 0$ and $\wp(0, \cdot) = 0$ This allows to extend $\wp$ by continuity to $\mathbb{R}^2$ (without change of notation):

$$p = \wp(\rho, e), \text{ with } \wp(\rho, e) = 0 \text{ whenever } \rho \leq 0 \text{ or } e \leq 0. \tag{2}$$

The problem is supposed to be posed over $\Omega \times [0, T]$, where Ω is an open bounded connected subset of $\mathbb{R}^d$, $d \leq 3$ and $[0, T]$ is a finite time interval. This system must be supplemented by suitable boundary conditions, initial conditions and closure relations for the diffusion terms.

The closure relations for $\boldsymbol{\tau}(\boldsymbol{u})$ and $\boldsymbol{q}$ are given by:

$$\boldsymbol{\tau}(\boldsymbol{u}) = \mu(\boldsymbol{\nabla} \boldsymbol{u} + \boldsymbol{\nabla}^t \boldsymbol{u}) - \frac{2\mu}{3} \mathrm{div} \boldsymbol{u}\, \boldsymbol{I}, \qquad \boldsymbol{q} = -\lambda \boldsymbol{\nabla} e, \tag{3}$$

where λ and μ are two non-negative parameters. Consequently, the shear stress tensor satisfies:

$$\boldsymbol{\tau}(\boldsymbol{u}) : \boldsymbol{\nabla} \boldsymbol{u} \geq 0, \tag{4}$$

for any velocity field.

For the sake of simplicity, we assume that the velocity is prescribed to zero on the whole boundary $\partial\Omega$, and that the system is adiabatic:

$$\boldsymbol{u} = 0, \ \boldsymbol{q} \cdot \boldsymbol{n} = 0 \text{ on } \partial\Omega. \tag{5}$$

0.2.2 The algorithm

The fractional step algorithm considered here consists in the two following steps:

Pressure gradient scaling step:

$$\forall \sigma \in \mathcal{E}_{\mathrm{int}}, \quad (\overline{\boldsymbol{\nabla} p})_\sigma^{n+1} = \Big(\frac{\rho_{D_\sigma}^n}{\rho_{D_\sigma}^{n-1}} \Big)^{1/2} (\boldsymbol{\nabla} p^n)_\sigma. \tag{6a}$$

Prediction step – Solve for $\tilde{\boldsymbol{u}}^{n+1}$:

For $1 \leq i \leq d,\ \forall \sigma \in \mathcal{E}_{\mathcal{S}}^{(i)}$,

$$\frac{1}{\delta t}\left(\rho_{D_\sigma}^{n}\tilde{u}_{\sigma,i}^{n+1} - \rho_{D_\sigma}^{n-1}u_{\sigma,i}^{n}\right) + \mathrm{div}(\rho^{n}\tilde{u}_{i}^{n+1}\boldsymbol{u}^{n})_{\sigma} - \mathrm{div}\boldsymbol{\tau}(\tilde{\boldsymbol{u}}^{n+1})_{\sigma,i} + (\overline{\boldsymbol{\nabla} p})_{\sigma,i}^{n+1} = 0. \tag{6b}$$

Correction step – Solve for p^{n+1}, e^{n+1}, ρ^{n+1} and $\boldsymbol{u}^{n+1}$:

For $1 \leq i \leq d,\ \forall \sigma \in \mathcal{E}_{\mathcal{S}}^{(i)}$,

$$\frac{1}{\delta t}\,\rho_{D_\sigma}^{n}\,(u_{\sigma,i}^{n+1} - \tilde{u}_{\sigma,i}^{n+1}) + (\boldsymbol{\nabla} p^{n+1})_{\sigma,i} - (\overline{\boldsymbol{\nabla} p})_{\sigma,i}^{n+1} = 0, \tag{6c}$$

$$\forall K \in \mathcal{M}, \quad \frac{1}{\delta t}(\rho_K^{n+1} - \rho_K^{n}) + \mathrm{div}(\rho^{n+1}\boldsymbol{u}^{n+1})_K = 0 \tag{6d}$$

$\forall K \in \mathcal{M}$,

$$\begin{aligned}\frac{1}{\delta t}(\rho_K^{n+1}e_K^{n+1} - \rho_K^{n}e_K^{n}) + \mathrm{div}(\rho^{n+1}e^{n+1}\boldsymbol{u}^{n+1})_K + p_K^{n+1}(\mathrm{div}(\boldsymbol{u}^{n+1}))_K \\ -\lambda\,(\Delta e^{n+1})_K = \left(\boldsymbol{\tau}(\tilde{\boldsymbol{u}}^{n+1}) : \boldsymbol{\nabla}\tilde{\boldsymbol{u}}^{n+1}\right)_K + S_K^{n+1},\end{aligned} \tag{6e}$$

$$\forall K \in \mathcal{M}, \quad \rho_K^{n+1} = \varrho\big(e_K^{n+1}, p_K^{n+1}\big). \tag{6f}$$

Let us now give a little more details on the discrete terms appearing in the scheme (6). We begin with the discrete mass balance equation (6d) and the convection term, which reads:

$$\mathrm{div}(\rho\boldsymbol{u})_K = \frac{1}{|K|}\sum_{\sigma\in\mathcal{E}(K)} F_{K,\sigma}.$$

The quantity $F_{K,\sigma}$ stands for the mass flux across σ outward K. By the impermeability boundary condition, it vanishes on external faces and is given on internal faces by:

$$\forall \sigma \in \mathcal{E}_{\mathrm{int}},\ \sigma = K|L, \qquad F_{K,\sigma} = |\sigma|\ \rho_\sigma\ u_{K,\sigma}, \tag{7}$$

where $u_{K,\sigma}$ is an approximation of the normal velocity to the face σ outward K. This latter quantity is defined by:

$$u_{K,\sigma} = \left|\begin{array}{l} u_{\sigma,i}\ \boldsymbol{n}_{K,\sigma}\cdot\boldsymbol{e}^{(i)} \text{ for } \sigma \in \mathcal{E}^{(i)} \text{ in the MAC case,} \\ \boldsymbol{u}_\sigma \cdot \boldsymbol{n}_{K,\sigma} \text{ in the CR and RT cases,}\end{array}\right. \tag{8}$$

where $\boldsymbol{e}^{(i)}$ denotes the i-th vector of the orthonormal basis of $\mathbb{R}^d$. The density at the face $\sigma = K|L$ is approximated by the upwind technique, *i.e.* $\rho_\sigma = \rho_K$ if $u_{K,\sigma} \geq 0$ and $\rho_\sigma = \rho_L$ otherwise.

We now turn to the discrete momentum balance (6b), where the convection terms are approximated by a finite volume technique over the dual cells:

$$\mathrm{div}(\rho\tilde{u}_i\boldsymbol{u})_\sigma = \mathrm{div}\big(\tilde{u}_i(\rho\boldsymbol{u})\big)_\sigma = \frac{1}{|D_\sigma|}\sum_{\varepsilon\in\bar{\mathcal{E}}(D_\sigma)} F_{\sigma,\varepsilon}\tilde{u}_{\varepsilon,i},$$

where $F_{\sigma,\varepsilon}$ stands for a mass flux through the dual face ε, and $\tilde{u}_{\varepsilon,i}$ is a centered approximation of the i^{th} component of the velocity $\tilde{\boldsymbol{u}}$ on ε. The density ρ_{D_σ} ot the dual cell is obtained by a weighted average of the density in the neighbor cells:

$$\begin{array}{ll} \text{for } \sigma \in \mathcal{E}_{\mathrm{int}},\ \sigma = K|L, & |D_\sigma|\,\rho_{D_\sigma} = |D_{K,\sigma}|\,\rho_K + |D_{L,\sigma}|\,\rho_L, \\ \text{for an external face of a cell } K, & \rho_{D_\sigma} = \rho_K. \end{array} \tag{9}$$

The mass fluxes $(F_{\sigma,\varepsilon})_{\varepsilon\in\mathcal{E}(D_\sigma)}$ are evaluated as linear combinations, with constant coefficients, of the primal mass fluxes at the neighboring faces, in such a way that the following discrete mass balance over the dual cells is implied by the discrete mass balance (6d):

$$\forall \sigma \in \mathcal{E},\ \text{for } 0 \leq n < N, \qquad \frac{|D_\sigma|}{\delta t}\ (\rho_{D_\sigma}^{n+1} - \rho_{D_\sigma}^{n}) + \sum_{\varepsilon\in\mathcal{E}(D_\sigma)} F_{\sigma,\varepsilon}^{n+1} = 0. \tag{10}$$

In the rescaling step for the pressure gradient (6a) and in the correction equation (6c), the term $(\boldsymbol{\nabla} p)_{\sigma,i}$ stands for the i^{th} component of the discrete pressure gradient at the face σ, which is built as the transpose operator to the natural divergence:

$$\text{for } \sigma = K|L \in \mathcal{E}_{\rm int}, \qquad (\boldsymbol{\nabla} p)_{\sigma,i} = \frac{|\sigma|}{|D_\sigma|}\ (p_L - p_K)\ \boldsymbol{n}_{K,\sigma}\cdot \boldsymbol{e}^{(i)}. \tag{11}$$

This pressure gradient is only defined at the internal faces since, thanks to the impermeability boundary conditions, no momentum balance equation is written at the external faces. The quantity $(\overline{\boldsymbol{\nabla} p})_{\sigma,i}$ in (6a) is not, in the general case, discrete gradient.

In (6e), to guarantee the positivity of the internal energy, we define the convection operator by:

$$\mathrm{div}(\rho e \boldsymbol{u})_K = \mathrm{div}\big(e\,(\rho\boldsymbol{u})\big)_K = \frac{1}{|K|}\sum_{\sigma\in\mathcal{E}(K)} F_{K,\sigma} e_\sigma, \tag{12}$$

with, for $\sigma = K|L \in \mathcal{E}_{\rm int}$, $e_\sigma = e_K$ if $F_{K,\sigma} \geq 0$ and $e_\sigma = e_L$ otherwise. The divergence of the velocity, $(\mathrm{div}\boldsymbol{u})_K$, is discretized as follows:

$$\text{for } K \in \mathcal{M}, \qquad (\mathrm{div}\boldsymbol{u})_K = \frac{1}{|K|}\sum_{\sigma\in\mathcal{E}(K)} |\sigma|\ u_{K,\sigma}, \tag{13}$$

and, as announced, this definition implies that the discrete gradient and divergence operators are dual with respect to the L^2 inner product:

$$\sum_{K\in\mathcal{M}} |K|\ p_K\ (\mathrm{div}\boldsymbol{u})_K + \sum_{i=1}^{d}\sum_{\sigma\in\mathcal{E}_{\mathcal{S}}^{(i)}} |D_\sigma|\ u_{\sigma,i}\ (\boldsymbol{\nabla} p)_{\sigma,i} = 0. \tag{14}$$

The term S_K is necessary to obtain a consistent scheme in the Euler case [40] and is defined in the next section.

The viscous diffusion term $\mathrm{div}\boldsymbol{\tau}(\tilde{\boldsymbol{u}})_{\sigma,i}$ of the momentum balance equation (6b) and the viscous dissipation term $(\boldsymbol{\tau}(\tilde{\boldsymbol{u}}) : \boldsymbol{\nabla}\tilde{\boldsymbol{u}})_K$ of the internal energy balance equation (6e) are detailed in Chapter 1. They are defined so as to satisfy the following two constraints:

(i) non-negativity of the dissipation:

$$\forall K \in \mathcal{M}, \quad (\boldsymbol{\tau}(\tilde{\boldsymbol{u}}) : \boldsymbol{\nabla}\tilde{\boldsymbol{u}})_K \geq 0; \tag{15}$$

(ii) consistency of the diffusion and the dissipation, in the following sense:

$$-\sum_{i=1}^{d}\sum_{\sigma\in\mathcal{E}_{\mathcal{S}}^{(i)}} |D_\sigma|\ \mathrm{div}\boldsymbol{\tau}(\tilde{\boldsymbol{u}})_{\sigma,i}\ u_{\sigma,i} = \sum_{K\in\mathcal{M}} |K|\ \ (\boldsymbol{\tau}(\tilde{\boldsymbol{u}}) : \boldsymbol{\nabla}\tilde{\boldsymbol{u}})_K\,, \tag{16}$$

i.e. the discrete analogue of the identity $\displaystyle\int_\Omega \mathrm{div}\boldsymbol{\tau}(\boldsymbol{u})\cdot\boldsymbol{u} = -\int_\Omega \boldsymbol{\tau}(\boldsymbol{u}) : \boldsymbol{\nabla}\boldsymbol{u}$.

For meshes satisfying the usual orthogonality condition, the heat diffusion term is approximated thanks to the usual two-point approximation of the fluxes [19]:

$$\forall K \in \mathcal{M}, \qquad -\lambda\ (\Delta e)_K = \lambda \sum_{\sigma=K|L\in\mathcal{E}(K)} \frac{|\sigma|}{d_\sigma}\ (e_K - e_L). \tag{17}$$

With this definition, the discrete Laplace operator is monotone, in the following sense:

$$\forall\ (e_K)_{K\in\mathcal{M}} \subset \mathbb{R}, \qquad \sum_{K\in\mathcal{M}} -\lambda(\Delta e)_K\ (-e_K^-) \geq 0, \tag{18}$$

where $e_K^+ = \max(e_K, 0)$ and $e_K^- = -\min(e_K, 0)$. This property is necessary to ensure that the positivity of the internal energy is preserved by the sceme.

0.2.3 Properties of the scheme

We summarize here the main properties of the scheme. The first one concerns a discrete kinetic energy balance satisfied by any solution of the scheme, which is necessary so that the solutions of the scheme satisfy a discrete analogue of the overall balance (*i.e.* integrated over the computational domain) of the total energy balance equation.

Lemma 0.2.1 (Discrete kinetic energy balance, [40]).
A solution to the scheme (6) satisfies the following equality, for $1 \leq i \leq d$, $\sigma \in \mathcal{E}_{\mathcal{S}}^{(i)}$ and $0 \leq n \leq N-1$:

$$\begin{aligned}\frac{1}{2}\frac{|D_\sigma|}{\delta t}\Big[\rho_{D_\sigma}^n (u_{\sigma,i}^{n+1})^2 - \rho_{D_\sigma}^{n-1}(u_{\sigma,i}^n)^2\Big] + \frac{1}{2}\sum_{\varepsilon\in\bar{\mathcal{E}}(D_\sigma)} F_{\sigma,\varepsilon}^n\ \tilde{u}_{\sigma,i}^{n+1}\ \tilde{u}_{\sigma',i}^{n+1} \\ + |D_\sigma|\ (\boldsymbol{\nabla} p^{n+1})_{\sigma,i}\ u_{\sigma,i}^{n+1} - |D_\sigma|\,\mathrm{div}\boldsymbol{\tau}(\tilde{\boldsymbol{u}}^{n+1})_{\sigma,i}\ \tilde{u}_{\sigma,i}^{n+1} + P_{\sigma,i}^{n+1} - P_{\sigma,i}^n = -R_{\sigma,i}^{n+1},\end{aligned} \tag{19}$$

where

$$P_{\sigma,i}^{n+1} = \frac{\delta t\,|\sigma|^2}{2|D_\sigma|}\ \frac{1}{\rho_{D_\sigma}^n}\,(p_L^{n+1} - p_K^{n+1})^2, \quad R_{\sigma,i}^{n+1} = \frac{1}{2}\ \frac{|D_\sigma|}{\delta t}\ \rho_{D_\sigma}^{n-1}\ \left(\tilde{u}_{\sigma,i}^{n+1} - u_{\sigma,i}^n\right)^2. \tag{20}$$

The residual terms $R_{\sigma,i}^{n+1}$ may be seen as a numerical dissipation generated by the upwinding in time of the scheme (*i.e.* the use of a backward time discretization). For viscous flows, it may be anticipated that these terms tend to zero when the space and time steps tend to zero. On the opposite, it is not the case when dealing with Euler equations, where they may subsist as measures borne by the shocks. Since, in this context, the scheme needs to be consistent with the total energy balance, this dissipation has to be compensated in the internal energy balance; this is done by the corrective terms S_K in (6e), which we are now in position to define:

$$\forall K \in \mathcal{M},\ S_K^{n+1} = \sum_{i=1}^d S_{K,i}^{n+1},\ \text{with} \quad S_{K,i}^{n+1} = \frac{1}{2}\,\rho_K^{n-1} \sum_{\sigma\in\mathcal{E}(K)\cap\mathcal{E}_{\mathcal{S}}^{(i)}} \frac{|D_{K,\sigma}|}{\delta t}\ \left(\tilde{u}_{\sigma,i}^{n+1} - u_{\sigma,i}^n\right)^2. \tag{21}$$

Thanks to the definition (9) of the density on the duals cells, this relation results from a distribution of the residual terms associated to a face to its (one or two) adjacent cells. Therefore, we get:

$$\sum_{K\in\mathcal{M}} S_K^{n+1} = \sum_{i=1}^d \sum_{\sigma\in\mathcal{E}_{\mathcal{S}}^{(i)}} R_{\sigma,i}^{n+1}. \tag{22}$$

A theoretical justification of this process is provided in [40], where it is shown in the 1D case that, if the scheme is stable and converges to a limit, this limit indeed satisfies the weak form of the total energy balance. On the contrary, without corrective terms, the scheme is observed in numerical experiments to yield wrong shock solutions, which do not satisfy the Rankine-Hugoniot conditions.

As announced earlier, the discretization used, guarantees the positivity of the internal energy, a result which is stated below.

LEMMA 0.2.2 (Positivity of the internal energy).
Let us suppose that the discrete heat diffusion operator satisfies the monotonicity property (18), and that the equation of state satisfies (2). Let n be such that $0 \leq n \leq N-1$, and let us suppose that $e^n > 0$ (*i.e.* $e_K^n > 0, \forall K \in \mathcal{M}$). Then a solution to the scheme (6) satisfies $e^{n+1} > 0$.

The aformentioned discrete total energy equation is obtained by summation of the integrals over the mesh of the discrete internal energy (6e) and the discrete kinetic energy (19) equations and summing them up. Then, thanks to the relation (21) that holds between the remainder terms, the integral of the total energy over the mesh is shown to be conserved.

Theorem 0.2.1 (Unconditional stability of the scheme)
Let us suppose that the discrete heat diffusion operator satisfies the monotonicity property (18), that the equation of state satisfies (2), and that the initial conditions for ρ and e are positive. Then, for $0 \leq n \leq N-1$, a solution to the scheme (6) satisfies $\rho^{n+1} > 0$, $e^{n+1} > 0$ and the following estimate:

$$\sum_{K\in\mathcal{M}} |K|\ \rho_K^{n+1} e_K^{n+1} + \frac{1}{2}\sum_{i=1}^{d}\sum_{\sigma\in\mathcal{E}_{\mathcal{S}}^{(i)}} |D_\sigma|\ \rho_{D_\sigma}^{n}\ (u_{\sigma,i}^{n+1})^2 + \frac{\delta t^2}{2}\ \|p^{n+1}\|_{\rho^n,\mathcal{M}}^2$$
$$\leq \sum_{K\in\mathcal{M}} |K|\ \rho_K^{n} e_K^{n} + \frac{1}{2}\sum_{i=1}^{d}\sum_{\sigma\in\mathcal{E}_{\mathcal{S}}^{(i)}} |D_\sigma|\ \rho_{D_\sigma}^{n-1}\ (u_{\sigma,i}^{n})^2 + \frac{\delta t^2}{2}\ \|p^{n}\|_{\rho^{n-1},\mathcal{M}}^2 \quad (23)$$

where, for any discrete pressure q and density ρ,

$$\|q\|_{\rho,\mathcal{M}}^2 = \sum_{\sigma=K|L\in\mathcal{E}_{\rm int}} \frac{1}{\rho_{D_\sigma}}\ \frac{|\sigma|^2}{|D_\sigma|}\ (q_L - q_K)^2.$$

Given the above estimates, the scheme (6) admits at least one solution.

0.2.4 Numerical results

We present here two numerical tests that confirm the potentialities of the scheme:

- In the Euler limit, any sequence of solutions of the scheme converges to a weak solution of the problem (which satisfies the Rankine-Hugoniot conditions), thus the scheme calculates shocks that travel a the correct speed.
- At low Mach numbers, the scheme boils down to a stable scheme for the Navier-Stokes equations.

0.2.4.1 Behavior in the Euler limit

We address a two-dimensional Riemann problem introduced in [71]. The computational domain is $\Omega = (-0.5, 0.5)^2$ and the initial data consists in four constant states, in each of the four sub-squares of

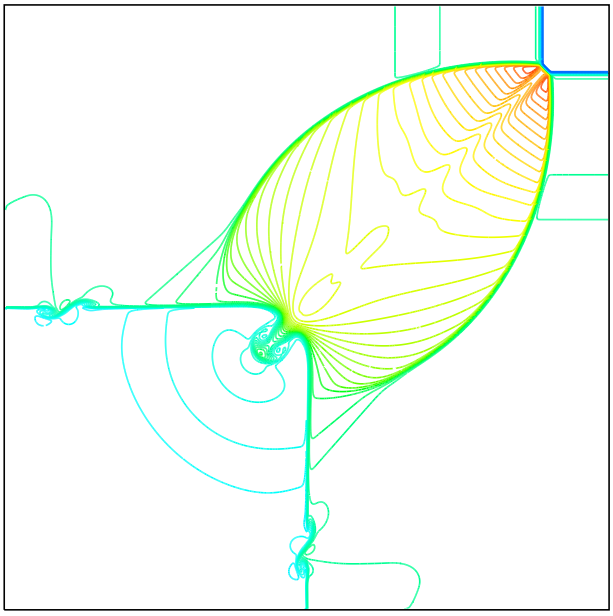

Figure 2: $2D$ Riemann problem – Isolines of the density in the domain.

Ω obtained by splitting it along the lines joining the mid-points of each segment of the boundary (*i.e.* in $\Omega_{1,1} = (-0.5, 0) \times (0, 0.5)$, $\Omega_{1,2} = (0, 0.5)^2$, $\Omega_{2,1} = (-0.5, 0)^2$ and $\Omega_{2,2} = (0, 0.5) \times (-0.5, 0)$). These constant states are chosen in such a way that each associated one-dimensional Riemann problem (*i.e.* each one-dimensional problem obtained by picking as left and right initial state the values of ρ, p in two adjacent sub-squares, together with the velocity component normal to the line separating these sub-squares) has for solution a single wave. The four constant states chosen here are:

$\Omega_{1,1}: \ \rho = 1, \ p = 1, \ \boldsymbol{u} = \begin{bmatrix} 0.7276 \\ 0 \end{bmatrix}$	$\Omega_{1,2}: \ \rho = 0.5313, \ p = 0.4, \ \boldsymbol{u} = \begin{bmatrix} 0 \\ 0 \end{bmatrix}$
$\Omega_{2,1}: \ \rho = 0.8, \ p = 1, \ \boldsymbol{u} = \begin{bmatrix} 0 \\ 0 \end{bmatrix}$	$\Omega_{2,2}: \ \rho = 1, \ p = 1, \ \boldsymbol{u} = \begin{bmatrix} 0 \\ 0.7276 \end{bmatrix}$

This configuration is referred to as the configuration 12 in [71]. Two shocks develop, the first one at the interface of $\Omega_{1,1}$ and $\Omega_{1,2}$ and the second one at the interface of $\Omega_{2,2}$ and $\Omega_{1,2}$; they move toward the right and the top of the domain, respectively. The other two interfaces (separating $\Omega_{2,1}$ from $\Omega_{1,2}$ and $\Omega_{2,2}$) do not move with time, and the tangential velocity is different on both sides of the interface; such an interface is called in [71] a slip line, and corresponds to a (steady) contact discontinuity of the system.

Results obtained with the MAC variant of the scheme, a 1000×1000 uniform grid, $\delta t = 2.5\,10^{-4}$ and an artificial viscosity fixed to $\mu = 5\,10^{-5}$ are shown in Figure 2. They are in good agreement with reference solutions (*e.g.* [71, 56, 51]). A more elaborate discussion of the results may be found in Chapter 1

0.2.4.2 Behavior in low Mach number flows

We now turn to the Navier-Stokes equations, and investigate the accuracy of the scheme in the quasi-incompressible limit. To this purpose, we consider a benchmark problem for (incompressible) Navier-Stokes solvers from [70]. The problem is two-dimensionnal, and consists in a flow between two

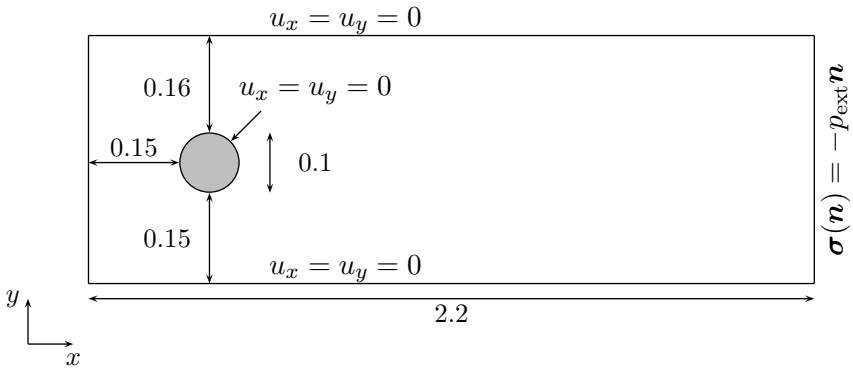

Figure 3: Low Mach flow past a cylinder – Geometry.

parallel plates past a cylindrical obstacle. The geometry of the problem is described in Figure 3. The fluid enters the domain on the left boundary, with an imposed velocity profile:

$$\boldsymbol{u} = \big(4u_m y \,\frac{H-y}{H},\, 0\big)^t,$$

where $H = 0.41$ is the height of the channel and $u_m = 1.5$; the velocity is prescribed to zero at the other boundaries except for the right-hand side, where we use a Neuman boundary condition:

$$(\boldsymbol{\tau}(\boldsymbol{u}) - p\,\boldsymbol{I})\;\boldsymbol{n} = -p_{\text{ext}}\,\boldsymbol{n},$$

where p_{ext} stands for a given external pressure. The initial pressure and p_{ext} are set both to 10^5, and the initial density is $\rho = 1$. With these values, the sound speed $c = (\gamma p/\rho)^{1/2}$ is $c \simeq 370$, so the characteristic Mach number is close to 0.003. The viscosity is $\mu = 0.001$, so the Reynolds number, defined as $Re = \rho\bar{u}D/\mu$, where $D = 0.1$ is the diameter of the cylinder and $\bar{u} = 2u_x(0,\, H/2)/3$, is equal to 100.

A "coarse version" of the meshes used for the presented computation is sketched in Figure 4; real meshes are considerably refined with respect to this one, by diminishing the discretization step along the characteristic lines (the boundaries and the concentric circles around the cylinder). In all the computations, we set the time step to $\delta t = 5 \cdot 10^{-4} s$.

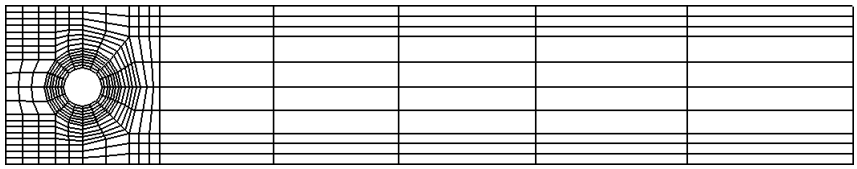

Figure 4: A "coarse version" of the mesh.

We observe in our computations the usual vortex-shedding phenomenon, well-known for incompressible flows (the so-called Von-Karmann alley), and the pressure and density show very small variations in space (the difference between the maximum and minimum value for the pressure and the density in the domain is in the range of 2 and 3.10^{-5} respectively). To assess in a quantitative way the accuracy of the results, several characteristic flow quantities have been computed (*cf.* Table 1 below), which indicate that the present algorithm seems as accurate as the incompressible pressure-correction solver based on the same space discretization studied in [5].

Mesh	Space unks	$c_{d,max}$	$c_{l,max}$	St
m2	64840	3.4937	0.9141	0.2850
m3	215545	3.2887	0.9891	**0.2955**
m4	381119	3.2614	**1.0062**	**0.2972**
m5	531301	**3.2365**	**1.0148**	**0.2976**
Reference range		3.22 - 3.24	0.99 - 1.01	0.295 - 0.305

Table 1: Characteristic flow quantities.

0.3 A model and a numerical scheme for partially premixed combustion

The second chapter deals with a model and a numerical scheme for partially premixed reactive flows. Existing models use a level-set-like partial differential equation, called in this context the G-equationto localize the flame brush location and separate the domain in a burnt and an unburnt subdomain; its unknown, the "color function", is the function G. This equation is coupled with the system of balance laws (chemical species, momentum, energy). The chemical mass fractions at any instant are calculated as a function of their initial values and the value of the function G, supposing an infinately fast chemical reaction; this model is called hereafter *the asymptotic model*. Unfortunately, it is impossible to take into account the mass diffusion in this class of models. Thus, we propose a more general model, *the relaxed model*, which includes balance equations for the chemical mass fractions. The information from the G function is integrated in the reactive source terms, which are present in the chemical mass fraction balance equations.

A numerical scheme is proposed for the solution of the model, whose solutions satisfy the stability properties of the continuous problem, irrespectively of the space and time steps if only implicit variants of the scalar convection operators are used or under a *CFL* condition the material velocity otherwise. We show that, under stability assumptions, any sequence of approximate solutions of the discretized system of balance laws converges (up to a subsequence) to a weak solution of the continuous problem. Furthermore, we show numerically that, ignoring the mass diffusion, the numerical solution of the proposed model converges to a solution of *the asymptotic model* [50] (developped in the next section), when the flame thickness and time and space steps tend to zero.

0.3.1 Governing equations

For the sake of simplicity, only four chemical species are supposed to be present in the flow, namely the fuel (denoted by F), the oxydant (O), the product (P) of the reaction, and a neutral gas (N). A one-step irreversible total chemical reaction is considered, which is written:

$$\nu_F F + \nu_O O + N \rightarrow \nu_P P + N,$$

where ν_F, ν_O and ν_P are the molar stoichiometric coefficients of the reaction. We denote by $\mathcal{I}$ the set $\mathcal{I} = \{F, O, N, P\}$ and the set of mass fractions of the chemical species in the flow reads $\{y_i,\ i \in \mathcal{I}\}$ (*i.e.* $\{y_F,\ y_O,\ y_N,\ y_P\}$).

The domain over which the problem is posed is a bounded domain Ω of $\mathbb{R}^d$, $d \in \{1, 2, 3\}$ and a finite time interval $[0, T]$. We suppose homogeneous Neumann boundary conditions for the velocity $\boldsymbol{u}$:

$$\boldsymbol{u} \cdot \boldsymbol{n} = 0 \quad \text{a.e. on } \partial\Omega, \tag{24}$$

where $\partial\Omega$ stands for boundary of Ω and $\boldsymbol{n}$ its outward normal vector.

The "asymptotic" model – We define the auxiliary unknowns $\{\tilde{y}_i,\ i \in \mathcal{I}\}$ as the result of the (inert) transport by the flow of the initial state, which means that the $\{\tilde{y}_i,\ i \in \mathcal{I}\}$ are the solutions to the following system of equations:

$$\partial_t(\rho\tilde{y}_i) + \mathrm{div}(\rho\tilde{y}_i\boldsymbol{u}) = 0, \quad \tilde{y}_i(\boldsymbol{x},0) = y_{i,0}(\boldsymbol{x}) \qquad \text{for } i \in \mathcal{I}, \tag{25}$$

where ρ stands for the fluid density and $y_{i,0}(\boldsymbol{x})$ is the initial mass fraction of the chemical species i in the flow. The initial conditions are supposed to verify $\sum_{i\in\mathcal{I}} y_{i,0} = 1$ everywhere in Ω, and this property is assumed to be valid for any $t \in [0,T]$, which is equivalent with the mixture mass balance, given below. The level-set function G is supposed to obey the following equation:

$$\partial_t(\rho G) + \mathrm{div}(\rho G\boldsymbol{u}) + \rho_u u_f|\boldsymbol{\nabla} G| = 0, \tag{26}$$

associated to the initial conditions $G = 0$ at the location where the flame starts and $G = 1$ elsewhere. The quantity ρ_u is a constant density, which, from a physical point of view, stands for a characteristic value for the unburnt gases density. The chemical mass fractions are now computed as:

$$\left|\begin{array}{l} \text{if } G > 0.5, \quad y_i = \tilde{y}_i \quad \text{for } i \in \mathcal{I}, \\ \text{if } G \le 0.5, \quad y_F = \nu_F W_F \tilde{z}^+,\ y_O = \nu_O W_O \tilde{z}^-,\ y_N = \tilde{y}_N, \text{ with } \tilde{z} = \dfrac{1}{\nu_F W_F}\tilde{y}_F - \dfrac{1}{\nu_O W_O}\tilde{y}_0. \end{array}\right. \tag{27}$$

In these relations, $\tilde{z}^+$ and $\tilde{z}^-$ stand for the positive and negative part of $\tilde{z}$, respectively, *i.e.* $\tilde{z}^+ = \max(\tilde{z},0)$ and $\tilde{z}^- = -\min(\tilde{z},0)$, and, for $i \in \mathcal{I}$, W_i is the molar mass of the chemical species i. The physical meaning of Relation (27) is that the chemical reaction is supposed to be infinitely fast, and thus that the flow composition is stuck to the chemical equilibrium composition in the so-called burnt zone, which explains why the model is called "asymptotic". The product mass fraction is given by $y_P = 1 - (y_F + y_O + y_N)$. The flow is governed by the Euler equations:

$$\partial_t\rho + \mathrm{div}(\rho\boldsymbol{u}) = 0, \tag{28a}$$

$$\partial_t(\rho u_i) + \mathrm{div}(\rho u_i\boldsymbol{u}) + \partial_i p = 0, \quad i = 1,d, \tag{28b}$$

$$\partial_t(\rho E) + \mathrm{div}(\rho E\boldsymbol{u}) + \mathrm{div}(p\boldsymbol{u}) = 0, \tag{28c}$$

$$p = (\gamma-1)\,\rho e_s, \qquad E = \frac{1}{2}|\boldsymbol{u}|^2 + e_s + \sum_{i\in\mathcal{I}} y_i \Delta h^0_{f,i}, \tag{28d}$$

where p stands for the pressure, E for the total energy, e_s for the so-called sensible energy and, for $i \in \mathcal{I}$, $\Delta h^0_{f,i}$ is the formation enthalpy of the chemical species i. The equation of state (28d) supposes that the fluid is a perfect mixture of ideal gases, with the same iso-pressure to iso-volume specific heat ratio $\gamma > 1$.

The "relaxed" model – This model retains the original form of the reactive flows governing equations, with a transport/reaction equation for all the chemical species mass fractions, and the value of G controls the reaction rates $\dot{\omega}$: $\dot{\omega}$ is set to zero when $G \ge 0.5$, and takes non-zero (and possibly large) values otherwise. The unknowns $\{y_i,\ i \in \mathcal{I}\}$ are thus now solution to the following balance equations:

$$\partial_t(\rho y_i) + \mathrm{div}(\rho y_i\boldsymbol{u}) = \dot{\omega}_i, \quad y_i(\boldsymbol{x},0) = y_{i,0}(\boldsymbol{x}) \qquad \text{for } i \in \mathcal{I}, \tag{29}$$

where the reactive term $\dot{\omega}_i$ is given by:

$$\dot{\omega}_i = \zeta_i\,\nu_i W_i\,\dot{\omega}, \quad \dot{\omega} = \frac{1}{\varepsilon}\,\eta(y_F,y_O)\ (G-0.5)^-, \quad \eta(y_F,y_O) = \min\Big(\frac{y_F}{\nu_F W_F}, \frac{y_O}{\nu_O W_O}\Big), \tag{30}$$

with $\zeta_F = \zeta_O = -1$, $\zeta_F = 1$ and $\zeta_N = 0$. The parameter ε defines the stiffness of the chemical reaction terms and is supposed to be proportional to the flame thickness. Note that, since $\nu_F W_F + \nu_O W_0 = \nu_P W_P$, we have $\sum_{i\in\mathcal{I}} \dot{\omega}_i = 0$, which, summing on $i \in \mathcal{I}$ the species mass balance, allows to recover the equivalence between the mass balance and the fact that $\sum_{i\in\mathcal{I}} y_i = 1$. The cut-off function $\eta(y_F, y_O)$ vanishes in the absence of fuel or oxydant and prevents the chemical species mass fractions to take negative values (and, equivalently, values greater than 1, since their sum is 1).

0.3.2 The algorithm

For the resolution of the model equations, we define the variable z as follows:

$$z = \frac{y_F + s(1 - y_O)}{1 + s}, \qquad s = \frac{\nu_F W_F}{\nu_O W_O}$$

Note that, combining the fuel and the oxydant mass balance equations, the variable z satisfies a homogeneous equation; for this reason, we replace the oxydant mass balance equation by the balance equation for z (since, given the values of z and y_F, we may deduce y_O). The fractional step algorithm for the relaxed model reads:

Reactive step:

$\forall K \in \mathcal{M}$:

Flame position indicator computation – Solve for G^{n+1}:

$$\frac{1}{\delta t}(\rho_K^n G_K^{n+1} - \rho_K^{n-1} G_K^n) + \mathrm{div}(\rho^n G^k \boldsymbol{u}^n)_K + (\rho_u^n u_f^n |\boldsymbol{\nabla} G|)_K = 0. \tag{31a}$$

Reduced variable computation – Solve for z^{n+1}:

$$\frac{1}{\delta t}(\rho_K^n z_K^{n+1} - \rho_K^{n-1} z_K^n) + \mathrm{div}(\rho^n z^k \boldsymbol{u}^n)_K = 0. \tag{31b}$$

Neutral gas mass fraction computation – Solve for y_N^{n+1}:

$$\frac{1}{\delta t}\big[\rho_K^n (y_N)_K^{n+1} - \rho_K^{n-1} (y_N)_K^n\big] + \mathrm{div}(\rho^n y_N^k \boldsymbol{u}^n)_K = 0. \tag{31c}$$

Fuel mass fraction computation – Solve for y_F^{n+1}:

$$\frac{1}{\delta t}\big[\rho_K^n (y_F)_K^{n+1} - \rho_K^{n-1} (y_F)_K^n\big] + \mathrm{div}(\rho^n y_F^{n+1} \boldsymbol{u}^n)_K = (\dot{\omega}_F)_K^{n+1}. \tag{31d}$$

Oxydant mass fraction computation – $(y_O)_K^{n+1} = 1 + \dfrac{1}{s}(y_F)_K^{n+1} - z_K^{n+1}(1 + \frac{1}{s})$. (31e)

Product mass fraction computation – $(y_P)_K^{n+1} = 1 - (y_F)_K^{n+1} - (y_O)_K^{n+1} - (y_N)_K^{n+1}$. (31f)

Euler step:

Pressure gradient scaling step – Solve for $(\widetilde{\boldsymbol{\nabla} p})^{n+1}$:

$$\forall \sigma \in \mathcal{E}, \qquad (\widetilde{\boldsymbol{\nabla} p})_\sigma^{n+1} = \Big(\frac{\rho_{D_\sigma}^n}{\rho_{D_\sigma}^{n-1}}\Big)^{1/2} (\boldsymbol{\nabla} p)_\sigma^n. \tag{32a}$$

Prediction step – Solve for $\tilde{\boldsymbol{u}}^{n+1}$:

For $1 \le i \le d,\ \forall \sigma \in \mathcal{E}_{\mathcal{S}}^{(i)}$,

$$\frac{1}{\delta t}(\rho_{D_\sigma}^n \tilde{u}_{\sigma,i}^{n+1} - \rho_{D_\sigma}^{n-1} u_{\sigma,i}^n) + \operatorname{div}(\rho^n \tilde{u}_i^{n+1} \boldsymbol{u}^n)_\sigma + (\widetilde{\boldsymbol{\nabla} p})_{\sigma,i}^{n+1} = 0. \tag{32b}$$

Correction step – Solve for ρ^{n+1}, p^{n+1} and $\boldsymbol{u}^{n+1}$:

For $1 \le i \le d,\ \forall \sigma \in \mathcal{E}_{\mathcal{S}}^{(i)}$,

$$\frac{1}{\delta t}\rho_{D_\sigma}^n (u_{\sigma,i}^{n+1} - \tilde{u}_{\sigma,i}^{n+1}) + (\boldsymbol{\nabla} p)_{\sigma,i}^{n+1} - (\widetilde{\boldsymbol{\nabla} p})_{\sigma,i}^{n+1} = 0, \tag{32c}$$

$$\forall K \in \mathcal{M}, \quad \frac{1}{\delta t}(\rho_K^{n+1} - \rho_K^n) + \operatorname{div}(\rho \boldsymbol{u})_K^{n+1} = 0, \tag{32d}$$

$$\begin{aligned} \forall K \in \mathcal{M}, \quad & \frac{1}{\delta t}\left[\rho_K^{n+1}(h_s)_K^{n+1} - \rho_K^n (h_s)_K^n\right] + \operatorname{div}(\rho h_s \boldsymbol{u})_K^{n+1} \\ & - \frac{1}{\delta t}(p_K^{n+1} - p_K^n) - \big(u \cdot \boldsymbol{\nabla} p\big)_K^{n+1} = (\dot{\omega}_\theta)_K^{n+1} + S_K^{n+1}, \end{aligned} \tag{32e}$$

$$\forall K \in \mathcal{M}, \qquad p_K^{n+1} = \frac{\gamma - 1}{\gamma}(h_s)_K^{n+1} \rho_K^{n+1}. \tag{32f}$$

Two equations from the continuous relaxed model have been replaced by the discretized form of three equivalent – at least formally at the continuous level – equations. The first one is the total energy equation (28c), that has been replaced by the sensible enthalpy, h_s, balance equation (*cf.* Chapter 2):

$$\partial_t(\rho h_s) + \operatorname{div}(\rho h_s \boldsymbol{u}) - \partial_t p - \boldsymbol{u} \cdot \boldsymbol{\nabla} p = \dot{\omega}_\theta,$$

where $\dot{\omega}_\theta = \sum_{i \in \mathcal{I}} \Delta h_{f,i}^0 \dot{\omega}$. The second one is the product mass balance equation, which is replaced by the algebraic relation $\sum_{i \in \mathcal{I}} y_i = 1$ that holds both in the continuous and at the discrete level.

Many of the discrete operators have already been defined in Section 0.2, we will focus here on the rest of the operators.

The discrete convection operator of any discrete field x defined on the primal cell is given by

$$\operatorname{div}(\rho x \boldsymbol{u})_K = \operatorname{div}\big(x(\rho \boldsymbol{u})\big)_K = \frac{1}{|K|} \sum_{\sigma \in \mathcal{E}(K)} F_{K,\sigma} x_\sigma,$$

where x_σ is an approximation of the unknown x on the edge σ. This approximation is either implicit ($k = n+1$ in relations (32a)–(31f)) with the classical upwind choice either an explicit ($k = n$) reconstruction of x_σ (*cf.* Chapter 2).

The sensible enthalpy equation is discretised in such a way that the present enthalpy formulation is strictly equivalent to the internal energy formulation of the energy balance equation used in 0.2. Consequently, the term $-\big(u \cdot \boldsymbol{\nabla} p\big)_K$ reads:

$$-\big(u \cdot \boldsymbol{\nabla} p\big)_K = \frac{1}{|K|} \sum_{\sigma \in \mathcal{E}(K)} |\sigma|\, u_{K,\sigma}\, (p_K - p_\sigma),$$

where p_σ is the upwind approximation of p at the face σ with respect to $u_{K,\sigma}$. The reaction heat, $(\dot\omega_\theta)_K$, is written in the following way:

$$(\dot\omega_\theta)_K = -\sum_{i=1}^{d} \Delta h^0_{f,i}\,(\dot\omega_i)_K = \big(\nu_F\,W_F\,\Delta h^0_{f,F} + \nu_O\,W_O\,\Delta h^0_{f,O} - \nu_P\,W_P\,\Delta h^0_{f,P}\big)\;\dot\omega_K.$$

The reaction term is approximated as follows:

$$\dot\omega_K^{n+1} = \eta\big((y_F)_K^{n+1}, (y_O)_K^{n+1}\big)(0.5 - G_K^{n+1})^-.$$

At the continuous level, the last term of equation (31a) may be written:

$$\rho_u\,u_f\,|\boldsymbol{\nabla} G| = \boldsymbol{a}\cdot\boldsymbol{\nabla} G = \mathrm{div}(G\,\boldsymbol{a}) - G\,\mathrm{div}(\boldsymbol{a}), \quad \text{with } \boldsymbol{a} = \rho_u\,u_f\,\frac{\boldsymbol{\nabla} G}{|\boldsymbol{\nabla} G|}.$$

Using an upwind finite volume discretization of both divergence terms in this relation, we get:

$$|K|\;(\rho_u^n\,u_f^n\;|\boldsymbol{\nabla} G|)_K = \sum_{\sigma\in\mathcal{E}(K)} |\sigma|\;(\tilde G_\sigma^{n+1} - G_K^{n+1})\,\boldsymbol{a}_\sigma^n\cdot\boldsymbol{n}_{K,\sigma},$$

where $\tilde G_\sigma^{n+1}$ stands for the upwind approximation of G^{n+1} on σ with respect to $\boldsymbol{a}^n\cdot\boldsymbol{n}_{K,\sigma}$. As for the chemical species mass balances, we also use an explicit variant, with a less diffusive discretization. The flame velocity on σ, $\boldsymbol{a}_\sigma^n$, is evaluated as

$$\boldsymbol{a}_\sigma^n = (\rho_u\,u_f)_\sigma^n\;\frac{(\boldsymbol{\nabla} G)_\sigma^n}{|(\boldsymbol{\nabla} G)_\sigma^n|},$$

where $(\rho_u\,u_f)_\sigma^n$ stands for an approximation of the product $\rho_u\,u_f$ on the face σ at t^n (this product is often constant in applications), and the gradient of G on $\sigma = K|L$ is computed as:

$$(\boldsymbol{\nabla} G)_\sigma = \frac{1}{|K\cup L|}\Big[\sum_{\sigma'\in\mathcal{E}(K)} |\sigma'|\;\hat G_{\sigma'}\;\boldsymbol{n}_{K,\sigma'} + \sum_{\sigma'\in\mathcal{E}(L)} |\sigma'|\;\hat G_{\sigma'}\;\boldsymbol{n}_{L,\sigma'}\Big],$$

with $\hat G_{\sigma'}$ a second order approximation of G at the barycenter of the face σ' (*cf.* Chapter 4, [73]).

0.3.3 Scheme properties

For any given family $(x_K^n)_{K\in\mathcal{M}} \in \mathbb{R}^{\mathcal{M}}$, where $\mathbb{R}^{\mathcal{M}}$ is a shorthand for $\mathbb{R}^{\mathrm{card}(\mathcal{M})}$ and $n\in\mathbb{N},\ n\le N$, we introduce the following notations:

$$\overline{x} = \max_{K\in\mathcal{M}} x_K^0, \qquad \underline{x} = \min_{K\in\mathcal{M}} x_K^0.$$

When no ambiguity arises, the notation x^n will be used to refer to the family $(x_K^n)_{K\in\mathcal{M}}$. For example $x^n > 1$, means $\forall K\in\mathcal{M},\ x_K^n > 1$.

The first two results concern the positivity of the density and the sensible energy (given that the chemical reaction is exothermic).

Lemma 0.3.1 (*cf.* [25]).
Let us suppose (32d) holds for any $n\in\mathbb{N},\ n\le N-1$, with $\rho^n > 0$. Then the linear system (32d) admits a unique solution that satisfies $\rho^{n+1} > 0$.

LEMMA 0.3.2 (Positivity of the sensible energy, *cf.* [30]).
Let us suppose $\underline{e_s} > 0$ and $\dot{\omega}_\theta^n \geq 0$ for $n \in \mathbb{N},\ n \leq N-1$. Then a solution to (31)-(32) satisfies for any $n \in \mathbb{N},\ n \leq N-1$ and $K \in \mathcal{M}$, $(e_s)_K^n > 0$.

Formally, for the continuous problem, taking the inner product of the momentum balance equation yields, after some partial derivatives combinations and using the mass balance, the so called kinetic energy balance:

$$\frac{1}{2}\partial_t(\rho|\boldsymbol{u}|^2) + \frac{1}{2}\mathrm{div}(\rho|\boldsymbol{u}|^2\boldsymbol{u}) = \boldsymbol{u}\cdot\big[\partial_t(\rho\boldsymbol{u}) + \mathrm{div}(\rho\boldsymbol{u}\otimes\boldsymbol{u})\big] = -\boldsymbol{u}\cdot\boldsymbol{\nabla}p.$$

Moreover, by replacing $h_s = e_s + p/\rho$ (where e_s is the sensible energy) in the sensible enthalpy equation, we obtain a sensible energy equation:

$$\partial_t(\rho e) + \mathrm{div}(\rho e\boldsymbol{u}) + p\mathrm{div}(\boldsymbol{u}) = 0.$$

Finally, multiplying each of the mass fraction balance equations by the formation enthalpy of the corresponding chemical species, gives rise to the reactive energy balance equation:

$$\partial_t\Big[\rho\big(\sum_{i\in\mathcal{I}}\Delta h_{f,i}^0 y_i\big)\Big] + \mathrm{div}\Big[\rho\big(\sum_{i\in\mathcal{I}}\Delta h_{f,i}^0 y_i\big)\boldsymbol{u}\Big] = \sum_{i\in\mathcal{I}}\Delta h_{f,i}^0\dot{\omega}_i = -\dot{\omega}_\theta.$$

We show that a discrete equivalent for this computation, and thus for these relations, may be derived for the proposed scheme. Moreover, summing these three energy balance equations and integrating in space (*i.e.* summing over $K \in \mathcal{M}$), we show that the integral of the discrete total energy balance of the system, is conserved over time.

LEMMA 0.3.3 (Total energy conservation, *cf.* [30]).
Let us suppose that e_s^0, ρ^0 and ρ^{-1} are positive. Then, a solution to (31)-(32) satisfies $\rho^{n+1} > 0$, $e^{n+1} > 0$ and the following stability result:

$$E^n = E^0,$$

where,

$$\forall n \in \mathbb{N},\ n \leq N-1, \qquad E^n = \sum_{K\in\mathcal{M}}|K|(\rho e)_K^n + \frac{1}{2}\sum_{i=1}^{d}\sum_{\sigma\in\mathcal{E}_\mathcal{S}^{(i)}}|D_\sigma|(u_{\sigma,i}^n)^2 + \delta t^2\sum_{\sigma\in\mathcal{E}_{\mathrm{int}}}\frac{|D_\sigma|}{\rho_{D_\sigma}^{n-1}}|(\boldsymbol{\nabla}p)_\sigma^n|^2,$$
$$(\rho e)_K^n = \rho_K^n(e_s)_K^n + \rho_K^n\sum_{i\in\mathcal{I}}\Delta h_{f,i}^0(y_i)_K^n.$$

The physical bounds of the unknowns, as imposed by the continuous model, are preserved; namely, the chemical mass fractions that are given by linear equations (no reactive term) stay between their initial maxima (and minima).

LEMMA 0.3.4.
Let us suppose that (32d) holds for any $n \in \mathbb{N},\ n \leq N-1$, with $\underline{\rho}^n > 0$. Then, for any $n \in \mathbb{N},\ n \leq N-1$ and $K \in \mathcal{M}$, the linear systems (31b) and (31c) admit unique solutions satisfying $z^{n+1} \in [\underline{z}, \overline{z}]$ and $(y_N)^{n+1} \in [\underline{y_N}, \overline{y_N}]$ respectively.

The chemical mass fractions that are given by non linear equations, are shown to stay positive, and thanks the definition of the reactive rates (such that the right hand sides of the chemical fraction balance equations vanish when summed up), guaranteeing that the some of the chemical species is equal to one, each one of them is bounded above by one (sharper bounds may be derived, but we let the reader refer to Chapter 2 for more details).

Lemma 0.3.5.
Let us suppose that (32d) holds for any $n \in \mathbb{N},\ n \leq N-1$, with $\underline{\rho} > 0$. Let $\left((y_i)_K^0\right)_{i\in\mathcal{I},\, K\in\mathcal{M}} \in \mathbb{R}^{4\mathcal{M}}$ be given and such that $\sum_{i\in\mathcal{I}}(y_i)_K^0 = 1$ for any $K \in \mathcal{M}$. Then, for any $n \in \mathbb{N},\ n \leq N-1$ and $K \in \mathcal{M}$, $\sum_{i\in\mathcal{I}}(y_i)_K^{n+1} = 1$ and the linear systems corresponding to the chemical mass fractions admit at least one solution satisfying $y_F^{n+1} \in [0, \overline{y_F}],\ y_O^{n+1} \in [0, \overline{y_O}]$ and $y_P^{n+1} \in [\underline{y_P}, 1]$.

The last two results show the capacity of the scheme to deal with discontinuities. The first result states its behaviour in contact discontinuities.

Lemma 0.3.6 (Contact discontinuities).
Let us suppose the initial velocity and the initial pressure constant, $u^0 = u$ and $p^0 = p$ and that the chemical reaction terms vanish. Then, there exists a solution to the scheme (31)-(32), satisfying, for any $n \in \mathbb{N},\ n \leq N$, $u^n = u$ and $p^n = p$.

The fact that, by construction of the scheme, we may derive the discrete equivalent of the total internal energy balance equation by simple algebraic manipulations, is crucial for the final result of this section, which states that under some stability hypothesis, any sequence of discrete solutions converges to a weak solution of the system of conservation laws, thus verifying the Rankine-Hugoniot conditions and calculating shocks that travel with the correct velocities. Before stating the result, let us introduce some notations.

Let $\mathrm{S}_{\mathcal{M}}(\Omega \times [0,T))$ be the space of piecewise constant functions in $K \times [t^n, t^{n+1})$, for any $n \in \mathbb{N},\ n \leq N$ and $K \in \mathcal{M}$. For any function $\psi \in \mathrm{C}_c^\infty(\Omega \times [0,T))$, its interpolate in $\mathrm{S}_{\mathcal{M}}(\Omega \times [0,T))$ is defined by

$$\psi_{\mathcal{M}}(\boldsymbol{x}, t) = \sum_{n\in\mathbb{N}} \sum_{K\in\mathcal{M}} \psi_K^n \, \chi_{K\times[t^n,t^{n+1})}(\boldsymbol{x}, t),$$

where $\psi_K^n = 1/|K| \int_K \psi(\boldsymbol{x}, t^n)$ and χ_P is the characteristic function of the set P. To any discrete family, $(f_K^n)_{K\in\mathcal{M}}^{n\in\mathbb{N},\ n\leq N}$, the following fuction of $\mathrm{S}_{\mathcal{M}}(\Omega \times [0,T))$ is naturally associated:

$$f_{\mathcal{M}}(\boldsymbol{x}, t) = \sum_{n\in\mathbb{N}} \sum_{K\in\mathcal{M}} f_K^n \, \chi_{K\times[t^n,t^{n+1})}(\boldsymbol{x}, t).$$

From here on, a function or a discrete family indexed by $\mathcal{M}$ will refer to the corresponding function of $\mathrm{S}_{\mathcal{M}}(\Omega \times [0,T))$. For any $g_{\mathcal{M}}$, the discrete $\mathrm{L}^1([0,T); \mathrm{BV}(\Omega))$ and $\mathrm{L}^1(\Omega; \mathrm{BV}([0,T)))$ norms read:

$$\|g_{\mathcal{M}}\|_{\mathrm{BV}x} = \sum_{n\in\mathbb{N}} \delta t \sum_{\sigma=K|L} |\sigma| |g_K^n - g_L^n|, \qquad \|g_{\mathcal{M}}\|_{\mathrm{BV}t} = \sum_{K\in\mathcal{M}} |K| \sum_{n\in\mathbb{N}} |g_K^{n+1} - g_K^n|.$$

The space of piecewise constant functions in $D_\sigma \times [t^n, t^{n+1})$, for any $n \in \mathbb{N},\ n \leq N$ and $\sigma \in \mathcal{E}$, is denoted by $\mathrm{S}_{\mathcal{D}}(\Omega \times [0,T))$. It is defined in the same way as $\mathrm{S}_{\mathcal{M}}(\Omega \times [0,T))$, but the interpolates here are defined by the mean value of the function over the primal edges, instead of the mean value over the primal the dual cell. Thus, for any regular function ψ, its interpolate in $\mathrm{S}_{\mathcal{D}}(\Omega \times [0,T))$ is defined by

$$\psi_{\mathcal{D}} = \sum_{n\in\mathbb{N}} \sum_{\sigma\in\mathcal{E}_{\mathrm{int}}} \psi_\sigma^n \, \chi_{D_\sigma\times[t^n,t^{n+1})}(\boldsymbol{x}, t),$$

where $\psi_\sigma^n = 1/|\sigma| \int_\sigma \psi(\boldsymbol{x}, t^n)$. To any discrete family $(f_\sigma^n)_{\sigma\in\mathcal{E}}^{n\in\mathbb{N},\ n\leq N}$, the following function of $\mathrm{S}_{\mathcal{D}}(\Omega \times [0,T))$ is naturally associated:

$$f_{\mathcal{D}} = \sum_{n\in\mathbb{N}} \sum_{\sigma\in\mathcal{E}} f_\sigma^n \, \chi_{D_\sigma\times[t^n,t^{n+1})}(\boldsymbol{x}, t).$$

From here on, a function or discrete family indexed by $\mathcal{D}$, will refer to the corresponding function of $\mathrm{S}_{\mathcal{D}}(\Omega \times [0,T))$. For any $g_{\mathcal{D}} \in \mathrm{S}_{\mathcal{D}}(\Omega \times [0,T))$, its discrete $\mathrm{L}^1([0,T);\mathrm{BV}_0(\Omega))$ and $\mathrm{L}^1(\Omega;\mathrm{BV}([0,T)))$ norms read, respectively:

$$\|g_{\mathcal{D}}\|_{\mathrm{BV}x} = \sum_{n\in\mathbb{N}} \delta t \sum_{\epsilon = D_\sigma | D_{\sigma'}} |\epsilon| |g^n_{\sigma'} - g^n_\sigma|, \qquad \|g_{\mathcal{D}}\|_{\mathrm{BV}t} = \sum_{\sigma\in\mathcal{E}} |D_\sigma| \sum_{n\in\mathbb{N}} |g^{n+1}_\sigma - g^n_{\sigma'}|.$$

Theorem 0.3.1 (Consistency)
Let $\Omega \subset \mathbb{R}^d$ be an open bounded domain and suppose initial conditions satisfying:

$$(\rho^0, p^0, h^0_s, \boldsymbol{u}^0) \in (\mathrm{L}^\infty(\Omega) \times \mathrm{BV}(\Omega) \times \mathrm{L}^\infty(\Omega) \times \mathrm{L}^\infty(\Omega)^d).$$

Let $(\mathcal{M}^{(m)}, \delta t^{(m)})_{m\in\mathbb{N},\ n\le N}$ be a sequence of discretizations in space and time, such that both the size of the mesh, $h^{(m)}$, and the time step, $\delta t^{(m)}$, tend to zero when $m \to \infty$. Let $(\rho_{\mathcal{M}}, p_{\mathcal{M}}, (h_s)_{\mathcal{M}}, \boldsymbol{u}_{\mathcal{D}}, \tilde{\boldsymbol{u}}_{\mathcal{D}})_{(m)}$ be the corresponding sequence of solutions. Suppose that this sequence verifies the following assertions:

(i) The sequence is uniformly bounded in $\mathrm{L}^\infty(\Omega \times [0,T))^5$, *i.e.* there exists $C \in \mathbb{R}$ such that, for $m \in \mathbb{N},\ n \le N$,

$$\max\left\{\rho^n_K, p^n_K, (h_s)^n_K\right\} \le C,\ \forall K \in \mathcal{M}^{(m)} \quad \text{and} \quad \max\left\{|\boldsymbol{u}^n_\sigma|, |\tilde{\boldsymbol{u}}^n_\sigma|\right\} \le C,\ \forall \sigma \in \mathcal{E}^{(m)}.$$

(ii) The sequence satisfies the following BV-stability assumption,

$$\lim_{m\to\infty} (h+\delta t)\left[\|\rho_{\mathcal{M}}\|_{\mathrm{BV}x} + \|p_{\mathcal{M}}\|_{\mathrm{BV}x} + \|(h_s)_{\mathcal{M}}\|_{\mathrm{BV}x} + \|\boldsymbol{u}_{\mathcal{D}}\|_{\mathrm{BV}x} + \|\boldsymbol{u}_{\mathcal{D}}\|_{\mathrm{BV}t} + \|\tilde{\boldsymbol{u}}_{\mathcal{D}}\|_{\mathrm{BV}x} + \|\tilde{\boldsymbol{u}}_{\mathcal{D}}\|_{\mathrm{BV}t}\right] = 0.$$

(iii) The sequence converges in $\mathrm{L}^p(\Omega\times[0,T))^{3+d}$, for $1 \le p < \infty$, to $(\bar\rho, \bar p, \bar h_s, \bar{\boldsymbol{u}}, \bar{\tilde{\boldsymbol{u}}}) \in \mathrm{L}^p(\Omega\times[0,T))^{3+2d}$.

Then, $\bar{\tilde u} = \bar u$ and $(\bar\rho, \bar p, \bar h_s, \bar{\boldsymbol{u}})$ satisfies the weak formulation of the system of balance laws (28).

0.3.4 Numerical results

As mentioned at the introduction of this section, at the continuous level, the boundedness of the chemical mass fractions formally implies that, when $\varepsilon \to 0$, the relaxed model converges to the asymptotic one.

A closed form of the solution of the Riemann problem for the asymptotic model is available [2]. In order to perform numerical tests, a Riemann problem with initial conditions such that the analytic solution has the profile presented in Figure 5 is chosen. The selected configuration imposes zero amplitude for the contact discontinuity and the left non linear wave, thus the solution consists of three different constant states: $\mathbf{W}^*_R, \mathbf{W}^{**}$ and $\mathbf{W}_R$.

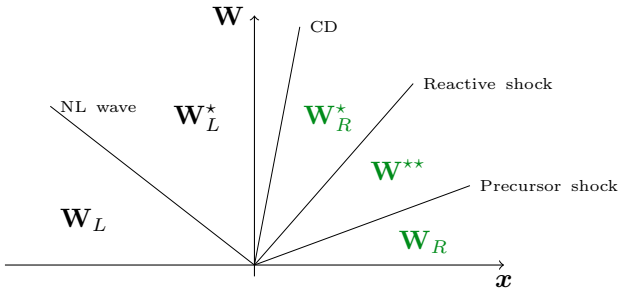

Figure 5: The analytic solution of the numerical test configuration.

The numerical tests performed aim at checking the convergence of the scheme to such a solution, which in fact results from two different properties: the convergence of the relaxed model to the asymptotic one when ε tends to zero, and the convergence of the scheme towards a numerical solution for vanishing time and space steps. To this purpose, we choose ε proportional to the space step and make it tend to zero, with a constant CFL number.

In a first tentative, an upwind approximation for the chemistry unknowns on the faces of the convection terms was used. The expected convergence is indeed observed, but the rate of convergence is poor. This seems to be due to the numerical diffusion of the upwind scheme; first, the scheme artificially introduces unburnt reactive masses (numerical diffusion in the chemical mass fraction equations) to the burnt zone and second, it fails to create the sharp interface which separates the burnt and the unburnt zone (numerical diffusion of the G-equation). As a result, the chemical reaction now artificially takes place also in what should be the burnt zone, supposed to be in chemical equilibrium (and governed by the corresponding equation of state). As expected in such a case, the results should be significantly improved with the use of a less diffusive scheme for the chemical species balance equations. This is why two different bound-preserving schemes (a MUSCL and an anti-diffusive (AD) scheme based on [17]), where used for the discretization of the convection operators of the chemistry part of the algorithm. The numerical results were significantly improved and our hypothesis seems to be verified: the less diffusive the scheme is, the faster the algorithm converges.

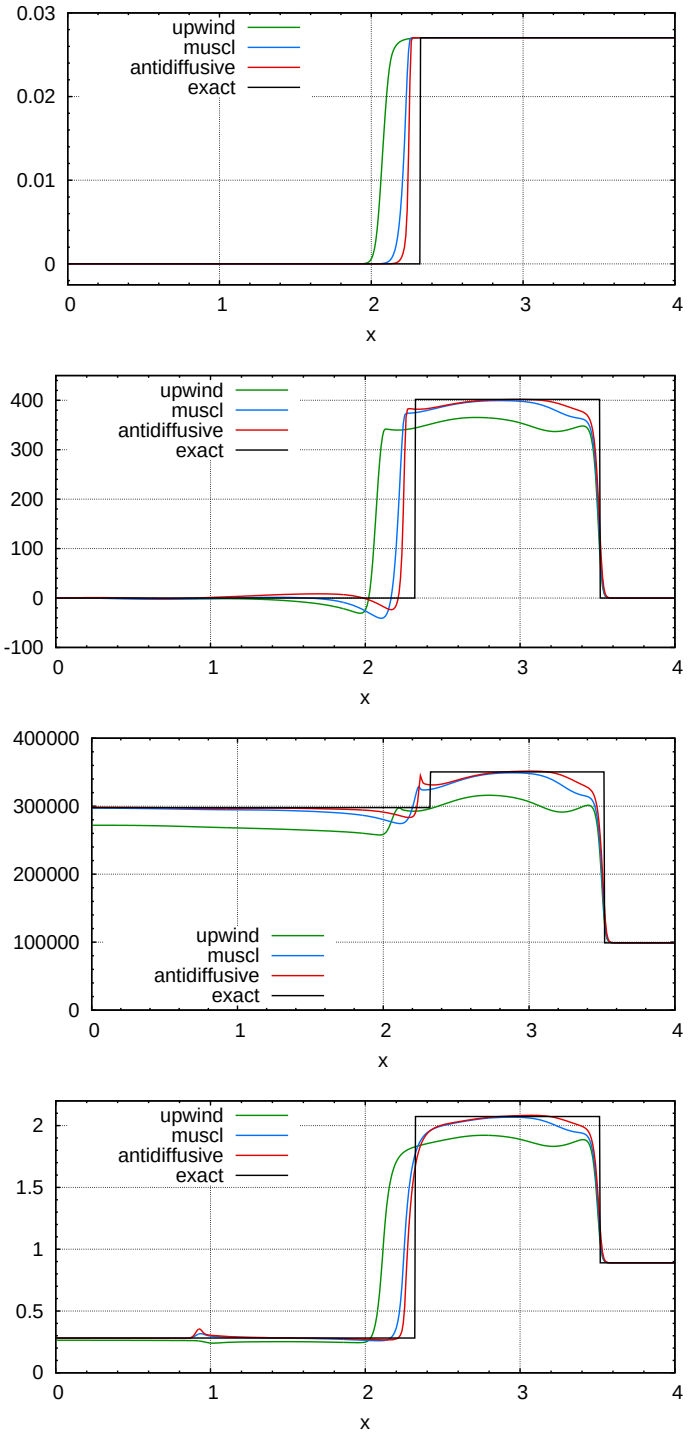

Figure 6: Comparison of the solutions obtained with the upwind, MUSCL and anti-diffusive scheme – From top to bottom, fuel mass fraction, velocity, pressure and density at $t =$, as a function of the space variable. Results obtained with a regular mesh composed of $n = 500$ cells.

0.4 A model and a numerical scheme to compute laminar flames in dust suspensions

In this last chapter we adress a model for the combustion of dust suspensions. The model is dedicated to the simulation of laminar flames, for which a one-dimensional representation, supposing a low Mach number flow, is sufficient. Particular care has to be paid to the formulation of the diffusion fluxes, since they determine the structure of the flame; in particular, the mass diffusion coefficients depend on the local composition of the mixture, and differ from one chemical species to another. Consequently, (standard) simplifications performed to derive the model will yield chemical species balance equations which preserve the positivity of the mass fractions and the fact that their sum is equal to 1, but do not satisfy a maximum principle (*i.e.* non-physical local accumulation of a species can not be excluded). On the opposite, the energy balance equation does satisfy a maximum principle so, provided that the chemical reaction is exothermic, the minimal temperature cannot decrease. We develop a fractional step finite volume scheme for the solution of a model that uses a rather general simplification for the mass diffusion coefficients, we show that it has at least one solution and such that any possible solution satisfies the above-mentionned physical bounds. Finally, make a comparison between the results obtained with the scheme from this chapter and the scheme proposed for *the relaxed model*, presented in Section 0.3.

0.4.1 Governing equations

As in the previous chapter, a one-step irreversible total chemical reaction is considered, which is written:

$$\nu_F F + \nu_O O + N \to \nu_P P + N,$$

where ν_F, ν_O and ν_P are the molar stoichiometric coefficients of the reaction. We denote by $\mathcal{I}$ the set $\mathcal{I} = \{F, O, N, P\}$ and the set of mass fractions of the chemical species in the flow reads $\{y_i,\ i \in \mathcal{I}\}$ (*i.e.* $\{y_F,\ y_O,\ y_N,\ y_P\}$). We also denote $\mathcal{I}_g$ (resp. $\mathcal{I}_s$) the set of the species that contsitute the gaseous (resp. solid) phase of the mixture, *i.e.* $\{O, N, P\}$ (resp. $\{F\}$).

The flow is supposed to be governed by the balance equations modelling a variable density flow in the asymptotic limit of low Mach number flows [61], namely the mass balance of the chemical species and of the mixture, the enthalpy balance, and the momentum balance equations. For a one-dimensional flow, the velocity may be seen as the solution of the mass balance equation, and the momentum balance yields the dynamic pressure. Since this latter unknown does not appear in the other equations, its computation is of poor interest, and the momentum balance equation may be disregarded.

Except of this aspect, the equations in this section are written in the usual multi-dimensional form. The computational domain is denoted by Ω, and its boundary $\partial\Omega$ is supposed to be split in an inflow part $\partial\Omega_I$ (where the flow enters the domain, *i.e.* $\boldsymbol{u} \cdot \boldsymbol{n}_{\partial\Omega} \leq 0$, with $\boldsymbol{u}$ the flow velocity and $\boldsymbol{n}_{\partial\Omega}$ the normal vector to $\partial\Omega$ outward Ω) and an outflow one $\partial\Omega_O$ (where the flow leaves the domain, *i.e.* $\boldsymbol{u} \cdot \boldsymbol{n}_{\partial\Omega} \geq 0$) of positive $(d-1)$-measure, with $\partial\Omega = \partial\Omega_I \cup \partial\Omega_O$ and $\partial\Omega_I \cap \partial\Omega_O = \varnothing$. The problem is supposed to be posed over the time interval $[0, T]$.

The model reads:

$$\partial_t \rho + \mathrm{div}(\rho \boldsymbol{u}) = 0, \tag{33a}$$

$$\partial_t (\rho y_i) + \mathrm{div}(\rho y_i \boldsymbol{u}) + \mathrm{div}(\boldsymbol{j}_i) = \dot{\omega}_i, \qquad \text{for } i \in \mathcal{I}, \tag{33b}$$

$$\sum_{i \in \mathcal{I}} c_{\mathrm{p},i} \left[\partial_t (\rho y_i \theta) + \mathrm{div}(\rho y_i \theta \boldsymbol{u}) + \mathrm{div}(\theta \boldsymbol{j}_i) \right] - \mathrm{div}(\lambda \boldsymbol{\nabla} \theta) = \dot{\omega}_\theta, \tag{33c}$$

$$\rho = \frac{1}{\dfrac{R\theta}{P_{th}} \displaystyle\sum_{i \in \mathcal{I}_g} \frac{y_i}{W_i} + \sum_{i \in \mathcal{I}_s} \frac{y_i}{\rho_i}}. \tag{33d}$$

Apart from the quantities already defined in the previous section, θ is the temperature, λ the heat diffusion coefficient, R the ideal gas constant, P_{th} the constant-in-time thermodynamic pressure, $\boldsymbol{j}_i$ the mass diffusion flux, $c_{\mathrm{p},i}$ the specific heat, W_i the molar weight and ρ_i the density of the i-th chemical species.

Equation (33c) is equivalent to the sensible enthalpy equation discretized in Section 0.3. Actually, the main difference between the two models – apart from the aforementioned mass diffusion – is that here, we do not perform an explicit flame front localization through the phase indicator function G, and the reactive source terms follow an Arrhenius equation. We opt for this latter approach, since we would like to switch to large scale models for the turbulence, where, practically, a G-function approach is impossible because of the complexity of the flame front structure.

Turning to the diffusion fluxes, since the size of the particles is large compared to the molecular Brownian motion ranges, we suppose that the diffusion of dust vanishes, so the diffusion phenomena only occur in the gas phase. We define the gas mass fraction as $y_g = \sum_{i \in \mathcal{I}_g} y_i$ and, for $i \in \mathcal{I}_g$, the mass fraction of the species i in the gas phase as $\tilde{y}_i = y_i / y_g$. A general expression of the diffusion fluxes read:

$$\text{for } i \in \mathcal{I}_s,\ \boldsymbol{j}_i = 0\ ; \qquad \text{for } i \in \mathcal{I}_g,\ \boldsymbol{j}_i = -\rho \sum_{j \in \mathcal{I}_g} D_{i,j} \boldsymbol{\nabla} \tilde{y}_j,$$

where the coefficients $(D_{i,j})_{i,j \in \mathcal{I}_g}$ depend on the local mixture concentration (*i.e.* on the mass fractions $(\tilde{y}_i)_{i \in \mathcal{I}_g}$ themselves). However, using a full tensor D and computing its coefficients is cost-consuming, and, moreover, the complete data necessary to their accurate computation is usually not available. This tensor is thus generally approximated. For instance, a "quasi-diagonal" approximation to this purpose for pure gaseous mixtures reads:

$$\text{for } i \in \mathcal{I}_g, \quad \boldsymbol{j}_i = \boldsymbol{j}_i^e + \tilde{y}_i \boldsymbol{J}, \quad \boldsymbol{j}_i^e = -\rho D_i \frac{W_i}{W} \boldsymbol{\nabla} \tilde{x}_i,$$

where $\tilde{x}_i$ stands for the molar mass fraction of the component i, so

$$\tilde{x}_i = \tilde{y}_i \frac{W}{W_i}, \quad \text{with } \frac{1}{W} = \sum_{i \in \mathcal{I}_g} \frac{\tilde{y}_i}{W_i}. \tag{34}$$

The quantity W is the so-called gaseous mixture molar mass. Complemented by the following expression for the mass diffusion coefficients, D_i:

$$\text{for } i \in \mathcal{I}_g, \quad D_i = \frac{1 - \tilde{y}_i}{\displaystyle\sum_{j \in \mathcal{I}_g,\ j \neq i} \frac{\tilde{x}_j}{D_{ji}}},$$

this formula is known as the Hirschfelder and Curtiss approximation (*cf.* [28, 45] and [68, pp. 14-15]). The term $\tilde{y}_i \boldsymbol{J}$ is a correction term added to ensure that $\sum_{j\in\mathcal{I}} \boldsymbol{j}_j = \sum_{j\in\mathcal{I}_g} \boldsymbol{j}_j = 0$, and so a suitable expression for $\boldsymbol{J}$ reads $\boldsymbol{J} = -\sum_{j\in\mathcal{I}_g} \boldsymbol{j}_j^e$ (note that, by definition, $\sum_{i\in\mathcal{I}_g} \tilde{y}_i = 1$).

The diffusion operator defined above is only positivity-preserving, since its divergence is not zero in the general case. This means that, because of the approximation made for the diffusion tensor, chemical fractions may locally exceed their initial and boundary values, which is of course unphysical (within the framework of the present model, where a possible drift of the particles with respect to the bulk flow velocity is not taken into account).

0.4.2 The algorithm

We implement a fractional-step algorithm, which consists in four steps, and reads, supposing that ρ^{n-1}, ρ^n, $(y_i)_{i\in\mathcal{I}}^n$, θ^n and u^n are known:

Reactive step:

$\forall K \in \mathcal{M}$:

Reduced variable computation – Solve for z^{n+1}:

$$\frac{1}{\delta t}(\rho_K^n z_K^{n+1} - \rho_K^{n-1} z_K^n) + \operatorname{div}(\rho^n z^k \boldsymbol{u}^n)_K = 0. \tag{35a}$$

Neutral gas mass fraction computation – Solve for y_N^{n+1}:

$$\frac{1}{\delta t}\big[\rho_K^n (y_N)_K^{n+1} - \rho_K^{n-1}(y_N)_K^n\big] + \operatorname{div}(\rho^n y_N^k \boldsymbol{u}^n)_K = 0. \tag{35b}$$

Fuel mass fraction computation – Solve for y_F^{n+1}:

$$\frac{1}{\delta t}\big[\rho_K^n (y_F)_K^{n+1} - \rho_K^{n-1}(y_F)_K^n\big] + \operatorname{div}(\rho^n y_F^{n+1} \boldsymbol{u}^n)_K = (\dot{\omega}_F)_K^{n+1}. \tag{35c}$$

Oxydant mass fraction computation – $(y_O)_K^{n+1} = 1 + \dfrac{1}{s}(y_F)_K^{n+1} - z_K^{n+1}(1 + \frac{1}{s})$. (35d)

Product mass fraction computation – $(y_P)_K^{n+1} = 1 - (y_F)_K^{n+1} - (y_O)_K^{n+1} - (y_N)_K^{n+1}$. (35e)

Hydrodynamics step:

Energy balance – Solve for θ^{n+1}:

$$\forall K \in \mathcal{M}, \qquad \sum_{i\in\mathcal{I}} c_{\mathrm{p},i}\Big[\frac{1}{\delta t}\big[\rho_K^n (y_i)_K^{n+1}\theta_K^{n+1} - \rho_K^{n-1}(y_i)_K^n\theta_K^n\big] + \operatorname{div}\big[\rho^n y_i^{n+1}\theta^{n+1}\boldsymbol{u}^n\big]_K + \operatorname{div}\big[\theta^{n+1}\boldsymbol{j}_i^n\big]_K\Big] - \operatorname{div}(\lambda\boldsymbol{\nabla}\theta^{n+1})_K = (\dot{\omega}_\theta)_K^{n+1}. \tag{36a}$$

Equation of state – $\rho_K^{n+1} = \varrho\big(\theta_K^{n+1}, ((y_i)_K^{n+1})_{i\in\mathcal{I}}\big), \quad$ for $K \in \mathcal{M}$. (36b)

Mass balance – Solve for $\boldsymbol{u}^{n+1}$:

$$\forall K \in \mathcal{M}, \qquad \frac{1}{\delta t}\big[\rho_K^{n+1} - \rho_K^n\big] + \operatorname{div}\big[\rho^{n+1}\boldsymbol{u}^{n+1}\big]_K = 0. \tag{36c}$$

The balance equation of the oxydant mass fraction has been replaced by a balance equation in the reduced variable z, which is a linear combination of the fuel and oxydant mass fraction balance equations, establish in order to solve for an equation without reactive source term. The mass balance

equation for the product has been replaced by the simple algebraic relation (35e), which is shown to hold in the discrete level.

For the convection fluxes, we use a nested structure that implies a discrete maximum principle. In the mass balance equation, let

$$\mathrm{div}[\rho \boldsymbol{u}]_K = \frac{1}{|K|} \sum_{\sigma \in \mathcal{E}(K)} F_{K,\sigma}.$$

We use this flux to define the convection fluxes in the species mass balance equations:

$$\mathrm{div}[\rho y_i \boldsymbol{u}]_K = \frac{1}{|K|} \sum_{\sigma \in \mathcal{E}(K)} F_{K,\sigma} (y_i)_\sigma^{\mathrm{up}},$$

where $(y_i)_\sigma^{\mathrm{up}}$ stands for the upwind approximation of y_i on the face σ with respect to $F_{K,\sigma}$. Similarly, let the convection and diffusion fluxes in this equation be written as:

$$\mathrm{div}[\rho y_i \boldsymbol{u}]_K + \mathrm{div}[\boldsymbol{j}_i]_K = \frac{1}{|K|} \sum_{\sigma \in \mathcal{E}(K)} G_{K,\sigma},$$

where, for short, we skip the index i for the flux $G_{K,\sigma}$. Then, in the energy mass balance,

$$\mathrm{div}[\rho y_i \theta \boldsymbol{u}]_K + \mathrm{div}[\theta \boldsymbol{j}_i]_K = \frac{1}{|K|} \sum_{\sigma \in \mathcal{E}(K)} G_{K,\sigma} \theta_\sigma^{\mathrm{up}},$$

where $\theta_\sigma^{\mathrm{up}}$ stands for the upwind approximation of θ on the face σ with respect to $G_{K,\sigma}$. The mass flux through the face σ reads:

$$F_{K,\sigma} = \rho_\sigma u_{K,\sigma}$$

where $u_{K,\sigma}$ stands for the value of the velocity oriented outward K and ρ_σ stands for any reasonable approximation of ρ on σ; here, we choose a centered approximation: $\rho_\sigma = \frac{1}{2}(\rho_K + \rho_L)$ for $\sigma = K|L$.

The discrete heat diffusion term in the enthalpy energy balance reads:

$$-\mathrm{div}[\lambda \boldsymbol{\nabla} \theta^{n+1}]_K = \sum_{\sigma = K|L} H_{K,\sigma}, \quad \text{with } H_{K,\sigma} = \lambda_\sigma (\theta_K - \theta_L),$$

where λ_σ stands for an approximation of the diffusion coefficient λ on σ.

The guiding line for the discretisation of the mass diffusion fluxes is that, as in the continuous case, the sum of the mass diffusion fluxes should vanish, so that the chemical fractions sum up to 1. The details of this discretization are given in Chapter 3.

0.4.3 Scheme properties

The following proposition summarizes the theoretical results for the solutions of the scheme: in accordance with the continuous model; the chemical mass fractions stay in the interval $[0, 1]$ and they sum up to 1, the temperature is non-decreasing (given an exothermic reaction and a sufficiently small time step) and the density stays positive.

Proposition 0.4.1 (Stability) Let the so-called *CFL*-number be defined by:

$$CFL^n = \max_{i \in \mathcal{I}} \max_{K \in \mathcal{M}} \frac{\delta t}{|K| \, \rho_K^{n-1} (y_i)_K} \sum_{\sigma = K|L} \frac{1}{d_\sigma} \frac{1}{2} (\rho_K D_i \frac{1}{(y_g)_K} + \rho_L D_i \frac{1}{(y_g)_L}) + (q_i)_{K,\sigma}^+ + \frac{1}{(y_g)_\sigma^{\mathrm{up}/q}} \, q_{K,\sigma}^+,$$

where, for short, the time-dependent quantities without time exponent are taken at t_n (*cf.* Chapter 3 for the exact definitions of the quantities q_i and q). Then, under the condition $CFL^n \leq 1$ for any $0 \leq n < N$, there exists a solution to (35)-(36) satisfying the following stability results:

(*i*) for $i \in \mathcal{I}$, $(y_i)^{n+1} \in [0,1]$ and $\sum_{i\in\mathcal{I}}(y_i)^{n+1} = 1$;

(*ii*) $\theta^{n+1} \geq \underline{\theta}$;

(*iii*) $0 < \rho^{n+1} \leq \max\Big\{\dfrac{P_{th}}{R\underline{\theta}}W_i,\ \text{for } i \in \mathcal{I}_g\ ;\ \rho_i,\ \text{for } i \in \mathcal{I}_s\Big\}$.

0.4.4 Numerical results

The following computations are performed with MATLAB. In Chapter 3, they are compared with computations performed by the open-source CALIF^{3}S software developped at IRSN [6] for the *relaxed model* of Section 0.3.

Data is chosen in order to check the scheme properties (*i.e.* to avoid unrealistic simplifications, as, for instance, a same specific heat diffusion coefficient for all the chemical species), and to be in the range of practical applications. The mixture is initially at rest, homogeneous and with an uniform temperature:

$$(y_F)_0 = (y_O)_0 = 0.4, \quad (y_N)_0 = 0.2, \quad (y_P)_0 = 0, \quad \theta_0 = 300^\circ K.$$

The reaction rate is given by the following Arrhenius law:

$$\dot{\omega}_K = 10^4\, y_F\, y_O\ e^{-900/\theta}. \tag{37}$$

The molar masses of the chemical species are considered to be equal to 20 g/mol for all the species, so the combustion reaction reads $F + O + N \longrightarrow 2P + N$, and the initial atmosphere composition is stoichiometric. The binary mass diffusion coefficients are

$$D_{NO} = 0.25 * 10^{-5}, \quad D_{NP} = 0.5 * 10^{-5}, \quad \text{and } D_{OP} = 10^{-5}.$$

The temperature diffusion coefficient is $\lambda = 0.005$, the specific heat coefficients (J/(Kg K)) are $c_{\mathrm{p},N} = 3.\,10^3$, $c_{\mathrm{p},F} = 1.\,10^3$, $c_{\mathrm{p},O} = 2.\,10^3$ and $c_{\mathrm{p},P} = 4.\,10^3$ and the formation enthalpies (J/Kg) are $\Delta h^0_{f,N} = 3.\,10^6$, $\Delta h^0_{f,F} = 1.\,10^6$, $\Delta h^0_{f,O} = -2.\,10^6$ and $\Delta h^0_{f,P} = -4.\,10^6$ (so the reaction is exothermic). The fuel density is equal to 100 Kg/m^3, and the density of the gaseous atmosphere is given by the ideal gases law.

Flame profiles obtained with the Hirschfelder and Curtiss diffusion coefficients – We present here results where the mass diffusion coefficients are calculated by the Hirschfelder and Curtis approximation. To initiate the transient, the reaction ignition is forced at the left part of the domain; then, the flame brush propagates to the right, while the solution progressively tends to a progressive wave (*i.e.* the translation at a constant speed of a constant profile). This establishment is quite long (for present computations, the final time is $t = 2$ s), and to capture this phenomena with a reasonable number of cells, we use a mobile frame attached to the flame front (or, equivalently, we impose a constant inlet flow rate of fresh gases at the right-hand section of the domain). However, the velocity of the flame front is influenced by the mesh, so the frame velocity (or the inlet flowrate) depends on the number of cells; to compare the established profiles, we thus have performed an abscissa translation up to obtain solutions as close as possible.

Obtained results with various meshes are plotted on Figures 7 and 8. First, we observe that numerical convergence (at least for an engineering point of view) is obtained for the coarsest mesh except for the velocity, which, unfortunately, is an important quantity, since the plane flame laminar velocity is a parameter often used to characterize the mixture, for instance to compute the turbulent flame velocity in the so-called TFC (for Turbulent Flame velocity Closure) deflagration mdels [85, 59]. For the velocity in the fresh gases, we obtain 3.343 cm/s, 3.017 cm/s 2.931 cm/s and 2.862 cm/s for

$n = 500$, $n = 1000$, $n = 2000$ and $n = 4000$ cells respectively, which suggests a first order convergence of this parameter, since the difference between two successive meshes roughly varies as the space step (of the coarsest or finest one, equivalently). Second, as expected, the expression of the mass diffusion operator produces, with the chosen binary diffusion coefficients, rather large (up to around 25% locally) unphysical variations of the inert gases mass fractions, which should remain constant in space and time. The temperature is larger in the burnt zone than in the fresh one (the reaction is exothermic); however, we observe a small temperature decrease on the upstream side (*i.e.* near the fresh zone) of the flame brush, which is not unconsistant with the theoretical study.

0.5 Perspectives

Starting from the Navier-Stokes equations and moving to reactive flows, during this work several models have been studied and suitable numerical schemes have been proposed, in order to deal with compressible reactive flows. Concerning the solvers for compressible Navier-Stokes equations already implemented, two points would definitely need further investigation:

(i) **The development of higher order schemes** – At the present point, only first-order upwinding (linear) schemes are implemented for convection operators in the mass and internal energy balance, in the pressure correction step, which generates excessive smoothing of contact discontinuities. In addition, using schemes of at least second order is a prerequisite for Large Eddy Simulation (LES, see below). The essential difficulty to implement second order (and thus necessarily non-linear for positivity preservation) schemes lies in the fact that the mass and energy balance equations are implicit in time. A possible way to avoid costly iterations, possibly leading to a lack of robustness of the solver, would be to try a defect-correction strategy [52], eventually associated to a Multi-dimensional Optimal Order Detection (MOOD) strategy [11].

(ii) **Non-conforming mesh refinement** – Non-conforming mesh refinement is already implemented in the CALIF^{3}S software, and convection operators have been derived to this purpose [67, 55]. However, the properties of the implemented diffusion term remains to be investigated, and the whole scheme would deserve a careful assessment, both in the viscous and inviscid cases.

In addition, extension to models dealing with turbulence for compressible flows is planned in a near future, both for Reynolds-Averaged (RANS) and Large Eddy Simulation (LES) formulations:

(i) **RANS models** – In RANS models, the turbulent kinetic energy appears in the balance equations of the momentum, the internal energy and in the equation of state as an additional pressure. This aspect is often neglected for the low Mach number flows (and may be neglected without loss of information for the incompressible flows). However, this is not possible when the compressibility effects are important (or, in other words, when the Mach number is close to the unity). This is a motivation for future works, that is to say, to extend the current schemes in order to be able to take into account the additional terms refered above. Two steps are in perspective:

- The first one, purely algorithmic, consists in extending the current pressure correction scheme to the two-pressure model while preserving its stability properties. The outcome of this step is a solver capable of calculating viscous flows.
- For the weak viscous case, the model may be seen as a perturbation of a hyperbolic system. This latter is a difficult problem, because the balance equation for the turbulent energy is non-conservative, which makes the definition of a weak formulation of the problem [3] and its numerical resolution very intricate (extension of the Rankine-Hugoniot conditions and a scheme that respects them, what permits to calculate correct shock positions).

(i) **LES models** – A LES model for compressible flows is given in Appendix A. To develop the associated solver, two routes may be followed: extending an already available explicit solver for Euler equations [27] or the present pressure correction scheme. Choosing an explicit scheme makes the implementation of non-linear convection operators easy, but the price to pay is that the explicit treatment of viscous terms may lead to stringent time-step restrictions (to this respect, note however that, in LES formulations, the viscosity scales as the space step). With the pressure correction scheme, as already mentioned, the implementation of higher-order convection schemes is difficult. For both solvers, the issue of second order time discretization must be addressed.

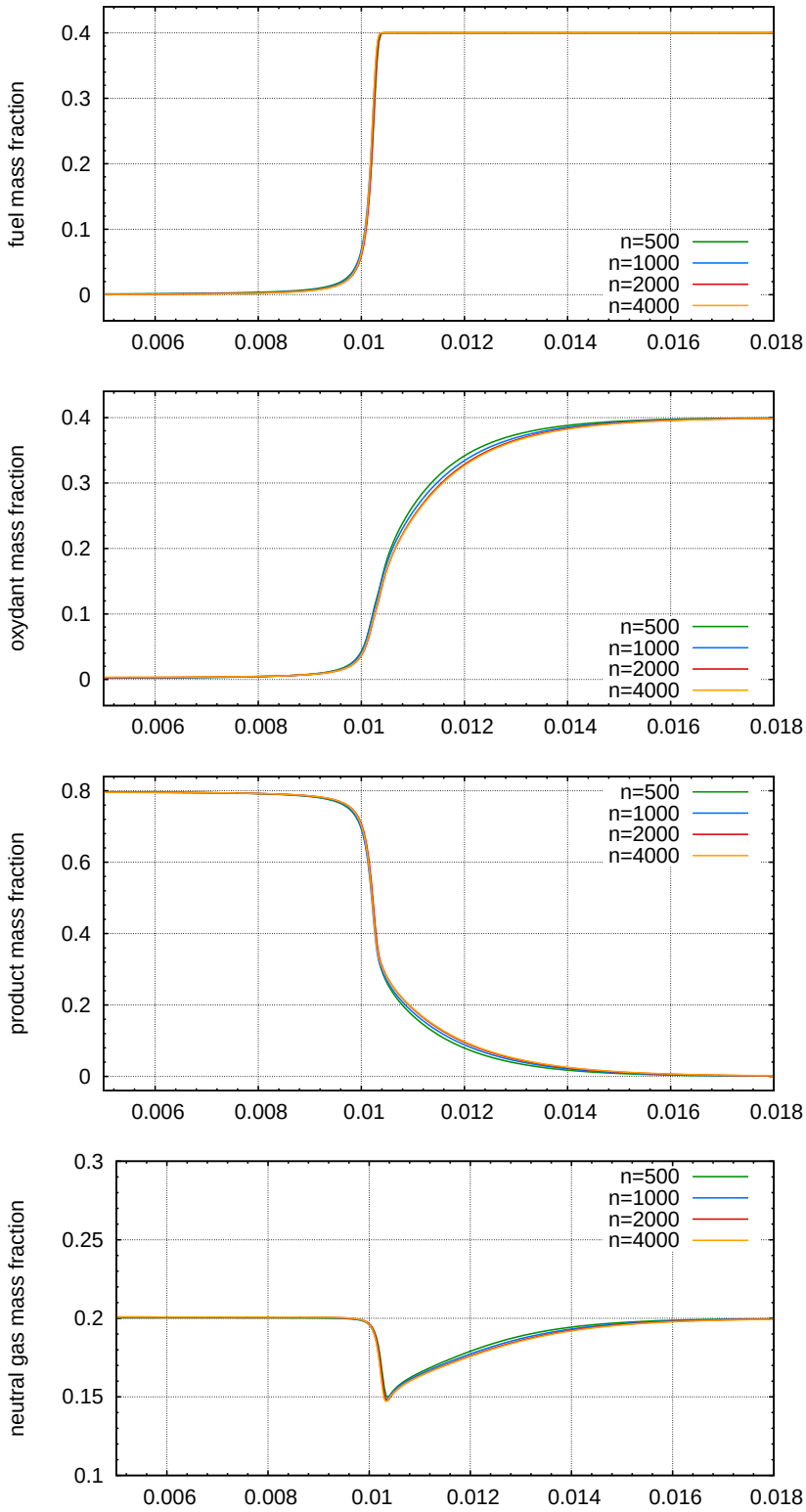

Figure 7: Results obtained with the Hirschfelder and Curtiss formula for the diffusion coefficients – From the top to the bottom, fuel, oxydant, product and neutral gas mass fractions obtained with 500 (green), 1000 (blue), 2000 (red) and 4000 (orange) cells.

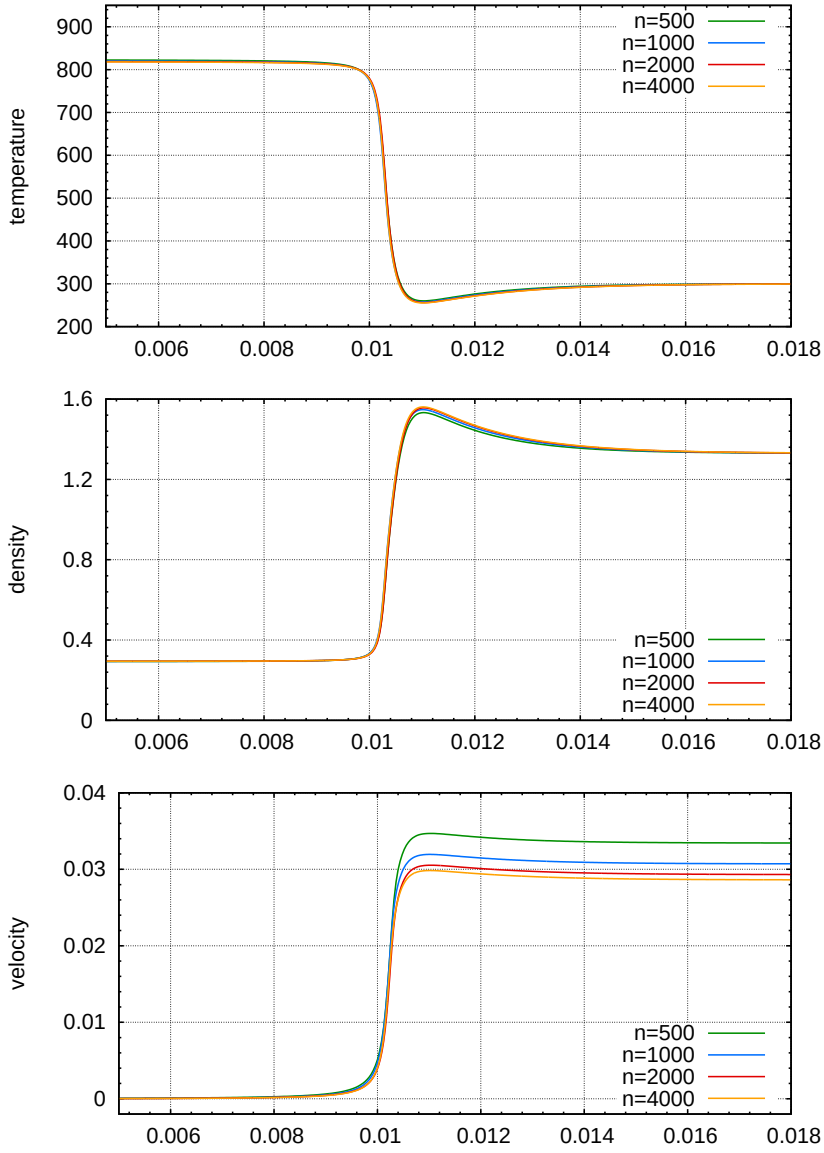

Figure 8: Results obtained with the Hirschfelder and Curtiss formula for the diffusion coefficients – From the top to the bottom, temperature, density and velocity obtained with 500 (green), 1000 (blue), 2000 (red) and 4000 (orange) cells.

Chapter 1

An unconditionally stable staggered pressure correction scheme for the compressible Navier-Stokes equations

Abstract

In this paper we present a pressure correction scheme for the compressible Navier-Stokes equations. The space discretization is staggered, using either the Marker-And-Cell (MAC) scheme for structured grids, or a nonconforming low-order finite element approximation for general quandrangular, hexahedral or simplicial meshes. For the energy balance equation, the scheme uses a discrete form of the conservation of the internal energy, which ensures that this latter variable remains positive; this relation includes a numerical corrective term, to allow the scheme to compute correct shock solutions in the Euler limit. The scheme is shown to have at least one solution, and to preserve the stability properties of the continuous problem, irrespectively of the space and time steps. In addition, it naturally boils down to a usual projection scheme in the limit of vanishing Mach numbers. Numerical tests confirm its potentialities, both in the viscous incompressible and Euler limits.

1.1 Introduction

We build in this paper a numerical scheme for the solution of the compressible Navier-Stokes equations:

$$\partial_t \rho + \mathrm{div}(\rho\, \boldsymbol{u}) = 0, \tag{1.1a}$$

$$\partial_t(\rho\, \boldsymbol{u}) + \mathrm{div}(\rho\, \boldsymbol{u} \otimes \boldsymbol{u}) + \boldsymbol{\nabla} p - \mathrm{div}(\boldsymbol{\tau}(\boldsymbol{u})) = 0, \tag{1.1b}$$

$$\partial_t(\rho\, E) + \mathrm{div}(\rho\, E\, \boldsymbol{u}) + \mathrm{div}(p\, \boldsymbol{u}) + \mathrm{div}(\boldsymbol{q}) = \mathrm{div}(\boldsymbol{\tau}(\boldsymbol{u})\ \cdot \boldsymbol{u}), \tag{1.1c}$$

$$E = \frac{1}{2}\ |\boldsymbol{u}|^2 + e, \tag{1.1d}$$

$$p = \wp(\rho, e). \tag{1.1e}$$

where t stands for the time, ρ, $\boldsymbol{u}$, p, E and e are the density, velocity, pressure, total energy and internal energy in the flow, $\boldsymbol{\tau}(\boldsymbol{u})$ stands for the shear stress tensor, $\boldsymbol{q}$ stands for the heat diffusion flux, and the function $\wp$ is the equation of state (EOS). The problem is supposed to be posed over $\Omega \times (0, T)$, where Ω is an open bounded connected subset of $\mathbb{R}^d$, $d \leq 3$ and $(0, T)$ is a finite time interval. This system must be supplemented by suitable boundary conditions, initial conditions and closure relations for the diffusion terms.

For the sake of simplicity, we assume in this paper that the velocity is prescribed to zero on the whole boundary $\partial\Omega$, and that the system is adiabatic:

$$\boldsymbol{u} = 0, \ \boldsymbol{q}\cdot\boldsymbol{n} = 0 \text{ on } \partial\Omega. \tag{1.2}$$

However, the modifications of the scheme and of the theoretical arguments to deal with more general boundary conditions are given in remarks, when useful. Suitable initial conditions must be provided for ρ, e and $\boldsymbol{u}$:

$$\rho(\boldsymbol{x},0) = \rho_0(\boldsymbol{x}), \quad e(\boldsymbol{x},0) = e_0(\boldsymbol{x}), \quad \boldsymbol{u}(\boldsymbol{x},0) = \boldsymbol{u}_0(\boldsymbol{x}), \text{ with } \rho_0 > 0, \ e_0 > 0. \tag{1.3}$$

Finally, the closure relations for $\boldsymbol{\tau}(\boldsymbol{u})$ and q are given by:

$$\boldsymbol{\tau}(\boldsymbol{u}) = \mu(\boldsymbol{\nabla}\boldsymbol{u} + \boldsymbol{\nabla}^t\boldsymbol{u}) - \frac{2\mu}{3}\operatorname{div}\boldsymbol{u}\,\boldsymbol{I}, \quad \boldsymbol{q} = -\lambda\boldsymbol{\nabla}e, \tag{1.4}$$

where $\boldsymbol{I}$ denotes the identity matrix and $\lambda, \mu \in L^\infty(\Omega)$ are such that there exists $\underline{\lambda} > 0$ and $\underline{\mu} > 0$ such that $\lambda \geq \underline{\lambda}$ a.e. and $\mu \geq \underline{\mu}$ a.e.. Consequently, the shear stress tensor satisfies:

$$\boldsymbol{\tau}(\boldsymbol{u}) : \boldsymbol{\nabla}\boldsymbol{u} \geq 0, \ \forall \boldsymbol{u} \in \mathbb{R}^d, \tag{1.5}$$

Replacing the total energy E by its expression (1.1d) in (1.1c) and developing some terms, we obtain:

$$\begin{aligned}\partial_t(\rho e) + \operatorname{div}(\rho e\boldsymbol{u}) + p\operatorname{div}\boldsymbol{u} + \operatorname{div}(\boldsymbol{q}) \\ + \frac{1}{2}\partial_t(\rho|\boldsymbol{u}|^2) + \frac{1}{2}\operatorname{div}(\rho|\boldsymbol{u}|^2\boldsymbol{u}) + \boldsymbol{u}\cdot\boldsymbol{\nabla}p - \operatorname{div}(\boldsymbol{\tau}(\boldsymbol{u}))\cdot\boldsymbol{u} = \boldsymbol{\tau}(\boldsymbol{u}) : \boldsymbol{\nabla}\boldsymbol{u}.\end{aligned} \tag{1.6}$$

Thanks to the mass balance equation (1.1a), we get formally, for any function z:

$$\partial_t(\rho z) + \operatorname{div}(\rho z\boldsymbol{u}) = \rho\,\partial_t z + \rho\boldsymbol{u}\cdot\boldsymbol{\nabla}z.$$

Using this identity twice and then the momentum balance equation (1.1b), we have for $1 \leq i \leq 3$:

$$\begin{aligned}\frac{1}{2}\partial_t(\rho u_i^2) + \frac{1}{2}\operatorname{div}(\rho u_i^2\boldsymbol{u}) = \rho u_i\partial_t u_i + \rho u_i\boldsymbol{u}\cdot\boldsymbol{\nabla}u_i = \\ u_i\left[\rho\partial_t u_i + \rho\boldsymbol{u}\cdot\boldsymbol{\nabla}u_i\right] = u_i\left[\partial_t(\rho u_i) + \operatorname{div}(\rho u_i\boldsymbol{u})\right] = -u_i\,\partial_i p + u_i\operatorname{div}(\boldsymbol{\tau}(\boldsymbol{u}))_i,\end{aligned}$$

so, summing for $i = 1$ to d:

$$\frac{1}{2}\partial_t(\rho|\boldsymbol{u}|^2) + \frac{1}{2}\operatorname{div}(\rho|\boldsymbol{u}|^2\boldsymbol{u}) = \boldsymbol{u}\cdot\left[\partial_t(\rho\boldsymbol{u}) + \operatorname{div}(\rho\boldsymbol{u}\otimes\boldsymbol{u})\right] = -\boldsymbol{u}\cdot\boldsymbol{\nabla}p + \operatorname{div}(\boldsymbol{\tau}(\boldsymbol{u}))\cdot\boldsymbol{u}.$$

Using this last relation in the total energy equation (1.6) yields the internal energy balance:

$$\partial_t(\rho e) + \operatorname{div}(\rho e\boldsymbol{u}) - \operatorname{div}(\boldsymbol{q}) + p\operatorname{div}(\boldsymbol{u}) = \boldsymbol{\tau}(\boldsymbol{u}) : \boldsymbol{\nabla}\boldsymbol{u}. \tag{1.7}$$

Since we assume that the initial condition for ρ is positive, the mass balance (1.1a) implies that the density ρ remains non-negative. Let us now suppose that the equation of state (1.1e) is such that $\wp(\cdot,0) = 0$ and $\wp(0,\cdot) = 0$, which allows to extend $\wp$ by continuity to $\mathbb{R}^2$ (without change of notation):

$$p = \wp(\rho, e), \text{ with } \wp(\rho, e) = 0 \text{ whenever } \rho \leq 0 \text{ or } e \leq 0. \tag{1.8}$$

Equation (1.7) then implies (thanks to (1.5)) that the internal energy e remains non-negative (at least formally).

Integrating now (1.1c) over Ω yields:

$$\frac{d}{dt}\int_\Omega \big(\frac{1}{2}\rho\,|\boldsymbol{u}|^2+\rho e\big)\,\mathrm{d}\boldsymbol{x}=0, \tag{1.9}$$

and, since $\rho \geq 0$ and $e \geq 0$, this inequality provides a stability estimate for the system.

In this paper, we propose and study a pressure correction scheme based on staggered-in-space discretizations (low order non-conforming finite elements or MAC scheme), solving the internal energy balance (1.7) instead of the total energy conservation equation (1.1d). As a consequence of these choices, this algorithm naturally boils down to a standard projection method in the vanishing Mach number (*i.e.* incompressible) asymptotic limit. We are able to prove, for this scheme, the same stability properties as in the continuous case: the approximate density and internal energy are non-negative (in fact, for discrete solutions, positive) and a discrete analogue to Relation (1.9) is derived. As a consequence of these properties, we are also able to prove the existence of a solution of the scheme.

This algorithm was already introduced in [40], for the Euler equations only, and its consistency (in the Lax-Wendroff sense) was proven in [40] in one space dimension. We complement this work here in several directions: we extend the scheme to the Navier-Stokes equations, prove the positivity of the internal energy and the existence of a solution to the scheme (while these properties are only claimed in [40]), provide some implementation details and some qualitative properties of the scheme (in particular, clarify its behaviour at contact discontinuities) and present two and three-dimensional numerical experiments, including a test to assess the behaviour in the low Mach number limit.

The fractional step strategy that we consider here involves an elliptic pressure correction step; this strategy has been used for compressible flows to obtain algorithms which are not limited by stringent stability conditions (such as CFL conditions based on the celerity of the fastest waves) since the late sixties, when first attempts were done to build "all flow velocity" schemes [37, 38]; these algorithms may be seen as an extension to the compressible case of the celebrated MAC scheme, introduced some years before [39]. These seminal papers have been the starting point for the development of numerous schemes falling in the class of pressure correction algorithms (possibly iterative, in the spirit of the SIMPLE method), some of them based on staggered finite volume space discretizations [7, 46, 47, 77, 48, 62, 4, 83, 13, 75, 80, 79, 76, 78, 53]; a bibliography extended to the schemes using other space discretizations may be found in [40]. To the best of our knowledge, the present paper provides the first rigorous stability proof for such algorithms in the framework of the Navier-Stokes equations. A key ingredient is the possibility to work with the internal energy balance to ensure the positivity of this quantity, without losing the consistency with the conservative equations (including the total energy balance) in the Euler case. Note also that, for the MAC scheme, a careful design of the viscous dissipation term is necessary to satisfy a discrete analogue of (1.5) (Section 1.3.2). Finally, the stability of the scheme also relies on the possibility to derive a local discrete kinetic energy balance, for which a rescaling step of the pressure gradient was introduced in [40]. Note also that the scheme proposed in this work implements a staggered finite-volume approach for first order terms (known for its efficiency) while being able to cope with unstructured meshes.

This paper is structured as follows. We first describe the space discretization (Section 1.2), then the scheme (Section 1.3). Section 1.4 is devoted to the proof of stability and existence of discrete solutions. Numerical tests are presented in Section 1.5. Since the scaling of the pressure gradient allowing to derive a discrete kinetic energy balance may be extended to other discretizations, we present the essential arguments for its design in a time-discrete (and space-continuous) setting in Appendix 1.A. The behaviour of the scheme on contact discontinuities of the Euler equations is adressed in Appendix 1.B. Finally, in Appendix 1.C, we provide some details about the numerical solution of the nonlinear algebraic system associated to the pressure correction step; we also discuss the issue of spurious

pressure boundary conditions which are known to be inherent to the pressure correction time-splitting technique.

1.2 Meshes and unknowns

Let $\mathcal{M}$ be a decomposition of the domain Ω, supposed to be regular in the usual sense of the finite element literature (*e.g.* [10]). The cells may be:

- for a general domain Ω, either convex quadrilaterals ($d = 2$) or hexahedra ($d = 3$) or simplices, both types of cells being possibly combined in a same mesh in two space dimensions,
- for a domain whose boundaries are hyperplanes normal to a coordinate axis, rectangles ($d = 2$) or rectangular parallelepipeds ($d = 3$) (the faces of which, of course, are then also necessarily normal to a coordinate axis).

By $\mathcal{E}$ and $\mathcal{E}(K)$ we denote the set of all $(d-1)$-faces σ of the mesh and of the element $K \in \mathcal{M}$ respectively. The set of faces included in the boundary of Ω is denoted by $\mathcal{E}_{\rm ext}$ and the set of internal faces (*i.e.* $\mathcal{E} \setminus \mathcal{E}_{\rm ext}$) is denoted by $\mathcal{E}_{\rm int}$. A face $\sigma \in \mathcal{E}_{\rm int}$ separating the cells K and L is denoted by $\sigma = K|L$. The outward normal vector to a face σ of K is denoted by $\boldsymbol{n}_{K,\sigma}$. For $1 \leq i \leq d$, we denote by $\mathcal{E}^{(i)}$, $\mathcal{E}^{(i)}_{\rm int}$ and $\mathcal{E}^{(i)}_{\rm ext}$ the subset of the faces of $\mathcal{E}$, $\mathcal{E}_{\rm int}$ and $\mathcal{E}_{\rm ext}$ respectively which are perpendicular to the i^{th} unit vector of the canonical basis of $\mathbb{R}^d$. For $K \in \mathcal{M}$ and $\sigma \in \mathcal{E}$, we denote by $|K|$ the measure of K and by $|\sigma|$ the $(d-1)$-measure of the face σ.

The space discretization is staggered, using either the Marker-And Cell (MAC) scheme [39, 38], or nonconforming low-order finite element approximations, namely the Rannacher and Turek (RT) element [69] for quadrilateral or hexahedral meshes, or the lowest degree Crouzeix-Raviart (CR) element [14] for simplicial meshes.

For all these space discretizations, the degrees of freedom for the pressure, the density and the internal energy (*i.e.* the discrete pressure, density and internal energy unknowns) are associated to the cells of the mesh $\mathcal{M}$, and are denoted by:

$$\big\{p_K,\ \rho_K,\ e_K,\ K \in \mathcal{M}\big\}.$$

Let us then turn to the degrees of freedom for the velocity.

- **Rannacher-Turek** or **Crouzeix-Raviart** discretizations – The discrete velocity unknowns are located at the center of the faces of the mesh, and we choose the version of the element where they represent the average of the velocity through a face. The Dirichlet boundary conditions are taken into account by setting the velocity unknowns associated to an external face to zero, so the set of discrete velocity unknowns reads:

$$\{u_{\sigma,i},\ \sigma \in \mathcal{E}_{\rm int},\ 1 \leq i \leq d\}.$$

- **MAC** discretization – The degrees of freedom for the i^{th} component of the velocity are located at the centre of the faces $\sigma \in \mathcal{E}^{(i)}$, so the whole set of discrete velocity unknowns reads:

$$\big\{u_{\sigma,i},\ \sigma \in \mathcal{E}^{(i)}_{\rm int},\ 1 \leq i \leq d\big\}.$$

Hence there are d unknowns per face of the primal mesh in the case of the CR-RT scheme, namely the d components of the velocity, while there is only one unknown per face of the primal mesh in the case of the MAC scheme, namely the normal component of the velocity.

We now introduce a dual mesh, for the finite volume approximation of the time derivative and convection terms in the momentum balance equation.

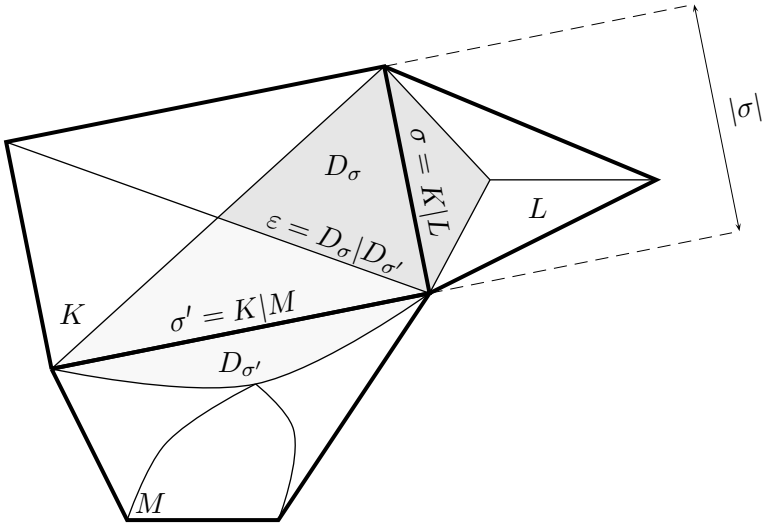

Figure 1.1: Primal and dual meshes for the Rannacher-Turek and Crouzeix-Raviart elements.

- **Rannacher-Turek** or **Crouzeix-Raviart** discretizations – For the RT or CR discretizations, the dual mesh is the same for all the velocity components. When $K \in \mathcal{M}$ is a simplex, a rectangle or a cuboid, for $\sigma \in \mathcal{E}(K)$, we define $D_{K,\sigma}$ as the cone with basis σ and with vertex the mass center of K (see Figure 1.1). We thus obtain a partition of K in m sub-volumes, where m is the number of faces of the cell, each sub-volume having the same measure $|D_{K,\sigma}| = |K|/m$. We extend this definition to general quadrangles and hexahedra, by supposing that we have built a partition still of equal-volume sub-cells, and with the same connectivities. The volume $D_{K,\sigma}$ is referred to as the half-diamond cell associated to K and σ. For $\sigma \in \mathcal{E}_{\rm int}$, $\sigma = K|L$, we now define the diamond cell D_σ associated to σ by $D_\sigma = D_{K,\sigma} \cup D_{L,\sigma}$.
- **MAC** discretization – For the MAC scheme, the dual mesh depends on the component of the velocity. For each component, the MAC dual mesh only differs from the RT or CR dual mesh by the choice of the half-diamond cell, which, for $K \in \mathcal{M}$ and $\sigma \in \mathcal{E}(K)$, is now the rectangle or rectangular parallelepiped of basis σ and of measure $|D_{K,\sigma}| = |K|/2$ (see Figures 1.2 and 1.3).

We denote by $|D_\sigma|$ the measure (area of volume) of the dual cell D_σ, and by $\varepsilon = D_\sigma|D_{\sigma'}$ the face separating two diamond cells D_σ and $D_{\sigma'}$. The set of the (dual) faces of D_σ is denoted by $\bar{\mathcal{E}}(D_\sigma)$.

Finally, in order to be able to write a unique expression of the discrete equations for both MAC and CR/RT schemes, we introduce the set of faces $\mathcal{E}_{\mathcal{S}}^{(i)}$ associated to the degrees of freedom of the i^{th} component of the velocity ($\mathcal{S}$ stands for "scheme"):

$$\mathcal{E}_{\mathcal{S}}^{(i)} = \left| \begin{array}{l} \mathcal{E}_{\rm int}^{(i)} \text{ for the MAC scheme,} \\ \mathcal{E}_{\rm int} \text{ for the CR or RT schemes.} \end{array} \right.$$

In addition, for the definition of the discrete diffusion terms in the momentum balance equation (1.1b) and in the internal energy equation (1.7), we need to distinguish two classes of meshes: the so-called super-admissible meshes, and the others, referred to as general meshes. In the present particular

framework, super-admissible meshes are obtained under the following condition:

$$\left|\begin{array}{l}\text{Each cell } K \text{ of the mesh is either:}\\ \quad\text{- a rectangle } (d=2) \text{ or a rectangular parallelepiped } (d=3);\text{ in this case, we denote by } \boldsymbol{x}_K \text{ the mass center of } K;\\ \quad\text{- a simplex, the circumcenter } \boldsymbol{x}_K \text{ of which is located inside } K.\end{array}\right. \tag{1.10}$$

This condition implies that, for each neighboring control volumes K and L, the segment $[x_K, x_L]$ is orthogonal to the face $K|L$ separating K from L, even when, in two space dimensions, one cell is a rectangle and the other one a triangle (we recall that, in three space dimensions, the two types of cells cannot be mixed). For each internal face $\sigma = K|L$, we denote by d_σ the distance $d(x_K, x_L)$.

Definition (Impermeability and Neumann boundary conditions). If the velocity is not prescribed to zero at the boundary, the space discretization is adapted as follows:

- if $\boldsymbol{u}\cdot\boldsymbol{n} = 0$ is the only condition imposed on the boundary, the degrees of freedom do not change for the MAC scheme, but the velocity unknowns corresponding to the tangential component(s) of the velocity must be added for the RT and CR discretizations. We thus first need a definition of the dual cell at a boundary face $\sigma \in \mathcal{E}_{\rm ext}$; denoting by K the adjacent cell, we take for D_σ the same volume as $D_{K,\sigma}$. Next, we must extend $\mathcal{E}_{\mathcal{S}}^{(i)}$. This can be done in a straightforward way if the boundary is always normal to a vector of the canonical basis of $\mathbb{R}^d$; then we get $\mathcal{E}_{\mathcal{S}}^{(i)} = \mathcal{E} \setminus \mathcal{E}_{\rm ext}^{(i)}$. This is the situation that we will consider here. The extension to the general case is just technical: a change of unknown must be done to make the velocity in the direction normal to each external face appear as a degree of freedom.
- when the velocity is free at a boundary face σ, this face must be treated in the definition of $\mathcal{E}_{\mathcal{S}}^{(i)}$ as an internal face, and the associated dual cell is defined as previously.

1.3 The pressure correction scheme

1.3.1 The algorithm

Let us consider a partition $0 = t_0 < t_1 < \ldots < t_N = T$ of the time interval $(0, T)$, which we suppose uniform. Let $\delta t = t_{n+1} - t_n$ for $n = 0, 1, \ldots, N-1$ be the constant time step. The pressure correction scheme considered here consists in the two following steps:

Pressure gradient scaling step:

$$\forall \sigma \in \mathcal{E}_{\rm int}, \quad \overline{\boldsymbol{\nabla}}_\sigma(p^{n+1}) = \Big(\frac{\rho^n_{D_\sigma}}{\rho^{n-1}_{D_\sigma}}\Big)^{1/2}\, \boldsymbol{\nabla}_\sigma(p^n). \tag{1.11a}$$

Prediction step – Solve for $\tilde{\boldsymbol{u}}^{n+1}$:

For $1 \le i \le d$, $\forall \sigma \in \mathcal{E}_{\mathcal{S}}^{(i)}$,

$$\frac{1}{\delta t}\left(\rho^n_{D_\sigma}\tilde{u}^{n+1}_{\sigma,i} - \rho^{n-1}_{D_\sigma} u^n_{\sigma,i}\right) + \mathrm{div}_\sigma(\rho^n \tilde{u}^{n+1}_i \boldsymbol{u}^n) - \mathrm{div}_{\sigma,i}\,\boldsymbol{\tau}(\tilde{\boldsymbol{u}}^{n+1}) + \overline{\boldsymbol{\nabla}}_{\sigma,i}(p^{n+1}) = 0. \tag{1.11b}$$

Correction step – Solve for p^{n+1}, e^{n+1}, ρ^{n+1} and $\boldsymbol{u}^{n+1}$:

For $1 \le i \le d$, $\forall \sigma \in \mathcal{E}_{\mathcal{S}}^{(i)}$,

$$\frac{1}{\delta t}\, \rho_{D_\sigma}^n\, (u_{\sigma,i}^{n+1} - \tilde{u}_{\sigma,i}^{n+1}) + \boldsymbol{\nabla}_{\sigma,i}(p^{n+1}) - \overline{\boldsymbol{\nabla}}_{\sigma,i}(p^{n+1}) = 0, \tag{1.11c}$$

$$\forall K \in \mathcal{M}, \quad \frac{1}{\delta t}(\rho_K^{n+1} - \rho_K^n) + \mathrm{div}_K(\rho^{n+1}\boldsymbol{u}^{n+1}) = 0, \tag{1.11d}$$

$\forall K \in \mathcal{M}$,

$$\begin{aligned}\frac{1}{\delta t}(\rho_K^{n+1} e_K^{n+1} - \rho_K^n e_K^n) + \mathrm{div}_K(\rho^{n+1} e^{n+1}\boldsymbol{u}^{n+1}) + p_K^{n+1}\,\mathrm{div}_K(\boldsymbol{u}^{n+1}) \\ -\lambda\,(\Delta e^{n+1})_K = \big(\boldsymbol{\tau}(\tilde{\boldsymbol{u}}^{n+1}) : \boldsymbol{\nabla}\tilde{\boldsymbol{u}}^{n+1}\big)_K + S_K^{n+1},\end{aligned} \tag{1.11e}$$

$$\forall K \in \mathcal{M}, \quad \rho_K^{n+1} = \varrho\big(e_K^{n+1}, p_K^{n+1}\big). \tag{1.11f}$$

The first step is a pressure gradient scaling step which is introduced in order to recover a discrete kinetic energy inequality (see Appendix 1.A). The second step is a classical semi-implicit solution of the momentum balance equation to obtain a tentative velocity field. The third step is a nonlinear pressure correction step, which couples the mass balance equation with the internal energy balance equation. However expensive, this coupling seems to be the price to pay to obtain an unconditional stability property (see Section 1.4.1, and [64, 65] for a discussion on this issue). In addition, in the Euler case, it also allows the scheme to keep the velocity and pressure constant across (1D) contact discontinuities (see Appendix 1.B). The last equation of this step is the equation of state, which is recast here as $\rho = \varrho(e, p)$ (instead of $p = \wp(\rho, e)$) because, at the algebraic level, the density is first eliminated from the system, this latter is solved for e^{n+1} and p^{n+1}, and ρ^{n+1} is finally given by (1.11f) (see Appendix 1.C for the solution process).

We now give the expression of each term of this algorithm, except for the diffusion and dissipation terms, which are defined in sections 1.3.2 and 1.3.3 below. The space discretization follows a specific order, which is explained on Flow chart 1.1. We begin with the discrete mass balance equation (1.11d). The convection term in this relation reads:

$$\mathrm{div}(\rho\boldsymbol{u})_K = \frac{1}{|K|}\sum_{\sigma\in\mathcal{E}(K)} F_{K,\sigma},$$

where $F_{K,\sigma}$ stands for the mass flux across σ outward K. By the impermeability boundary conditions, it vanishes on external faces and is given on internal faces by:

$$\forall \sigma \in \mathcal{E}_{\mathrm{int}},\ \sigma = K|L, \qquad F_{K,\sigma} = |\sigma|\ \rho_\sigma\ u_{K,\sigma}, \tag{1.12}$$

where $u_{K,\sigma}$ is an approximation of the normal velocity to the face σ outward K. This latter quantity is defined by:

$$u_{K,\sigma} = \begin{cases} u_{\sigma,i}\ \boldsymbol{n}_{K,\sigma}\cdot\boldsymbol{e}^{(i)} \text{ for } \sigma \in \mathcal{E}^{(i)} \text{ in the MAC case,} \\ \boldsymbol{u}_\sigma \cdot \boldsymbol{n}_{K,\sigma} \text{ in the CR and RT cases,} \end{cases} \tag{1.13}$$

where $\boldsymbol{e}^{(i)}$ denotes the i-th vector of the orthonormal basis of $\mathbb{R}^d$. The density at the face $\sigma = K|L$ is approximated by the upwind technique, *i.e.* $\rho_\sigma = \rho_K$ if $u_{K,\sigma} \ge 0$ and $\rho_\sigma = \rho_L$ otherwise.

We now turn to the discrete momentum balance (1.11b). For both the MAC and the RT-CR discretizations, the time derivative and convection terms are approximated in (1.11b) by a finite

(i) (For the mass balance) Define the mass flux at each primal face:

$$\mathrm{div}_K(\rho\boldsymbol{u}) = \frac{1}{|K|}\sum_{\sigma\in\mathcal{E}(K)} F_{K,\sigma}, \quad F_{K,\sigma} = |\sigma|\ \rho_\sigma\ u_{K,\sigma},$$

$u_{K,\sigma}$ =normal velocity, ρ_σ =upwind density (*ensures the positivity of the density*).

(ii) From this primal mass flux,

(a) (For the momentum balance) Define the density at the faces ρ_{D_σ} and the mass fluxes through the dual faces $F_{\sigma,\varepsilon}$ in such a way that a mass balance holds on dual cells, and define the flux of the i^{th} velocity component through a dual face by $F_{\sigma,\varepsilon}u_{\varepsilon,i}$, with $u_{\varepsilon,i}$ centered (*yields a discrete kinetic energy balance*);

(b) (For the internal energy balance) Define the energy flux through each primal face by $F_{K,\sigma}\,e_\sigma$, with e_σ =upwind energy (*yields a maximum-principle-preserving convection operator*);

(c) (For the internal energy balance) Define the velocity divergence (just set ρ equal to 1 in the expression of $\mathrm{div}_K(\rho\boldsymbol{u})$), and the pressure gradient by transposition (*yields a total energy estimate*).

Flow chart 1.1: Process for the construction of the space discretization of the hyperbolic part of the system of partial differential equations (*i.e.* Euler equations, written in non-conservative form using the internal energy balance). This process must be combined with a time stepping strategy which, in practice, may be of pressure correction type (present paper, to ensure unconditional stability) or explicit (*cf.* [40]).

volume technique over the dual cells, so that the convection term reads:

$$\mathrm{div}_\sigma(\rho\tilde{u}_i\boldsymbol{u}) = \mathrm{div}_\sigma\big(\tilde{u}_i(\rho\boldsymbol{u})\big) = \frac{1}{|D_\sigma|}\sum_{\varepsilon\in\bar{\mathcal{E}}(D_\sigma)} F_{\sigma,\varepsilon}\tilde{u}_{\varepsilon,i},$$

where $F_{\sigma,\varepsilon}$ stands for a mass flux through the dual face ε outward D_σ, and $\tilde{u}_{\varepsilon,i}$ is a centered approximation of the i^{th} component of the velocity $\tilde{\boldsymbol{u}}$ on ε. The density at the dual cell ρ_{D_σ} is obtained by a weighted average of the density in the neighbouring cells:

$$\begin{array}{ll} \text{for } \sigma\in\mathcal{E}_{\rm int},\ \sigma = K|L, & |D_\sigma|\,\rho_{D_\sigma} = |D_{K,\sigma}|\,\rho_K + |D_{L,\sigma}|\,\rho_L, \\ \text{for an external face of a cell } K, & \rho_{D_\sigma} = \rho_K. \end{array} \tag{1.14}$$

The mass fluxes $(F_{\sigma,\varepsilon})_{\varepsilon\in\mathcal{E}(D_\sigma)}$ are evaluated as linear combinations, with constant coefficients, of the primal mass fluxes at the neighboring faces, in such a way that the following discrete mass balance over the dual cells is implied by the discrete mass balance (1.11d):

$$\forall\sigma\in\mathcal{E},\ \text{for } 0\le n<N, \qquad \frac{|D_\sigma|}{\delta t}\,(\rho_{D_\sigma}^{n+1}-\rho_{D_\sigma}^{n}) + \sum_{\varepsilon\in\mathcal{E}(D_\sigma)} F_{\sigma,\varepsilon}^{n+1} = 0. \tag{1.15}$$

This relation is critical to derive a discrete kinetic energy balance (see Section 1.4.1 below). The computation of the dual mass fluxes $F_{\sigma,\varepsilon}$ is such that the flux through a dual face lying on the boundary, which is then also a primal face, is the same as the primal flux, that is zero. This computation yields the expression (1.14) for the densities, and some linear combination of the primal fluxes for the dual fluxes [24, 40, 41]. Since the mass balance is not yet solved at the velocity prediction stage, the

densities and dual fluxes have to be built from the mass balance at the previous time step: hence the backward time shift for the densities in the time-derivative term.

In the rescaling step for the pressure gradient (1.11a) and in the correction equation (1.11c), the term $\boldsymbol{\nabla}_{\sigma,i}(p)$ stands for the i^{th} component of the discrete pressure gradient at the face σ, which is built as the transposed operator to the natural divergence (see Equations (1.18) and (1.19) below):

$$\text{for } \sigma = K|L \in \mathcal{E}_{\rm int}, \qquad \boldsymbol{\nabla}_{\sigma,i}(p) = \frac{|\sigma|}{|D_\sigma|}\ (p_L - p_K)\ \boldsymbol{n}_{K,\sigma} \cdot \boldsymbol{e}^{(i)}. \tag{1.16}$$

This pressure gradient is only defined at internal faces since, thanks to the impermeability boundary conditions, no momentum balance equation is written at the external faces. The quantity $\overline{\boldsymbol{\nabla}}_{\sigma,i}(p)$ in (1.11a) is obtained by a simple rescaling of the pressure gradient, which is needed to obtain a discrete kinetic energy balance (see Section 1.4.1 and Appendix 1.A). Note that $\overline{\boldsymbol{\nabla}}(p)$ is not a discrete gradient, in the sense that there does not exist in the general case a discrete pressure $\overline{p}$ such that $\overline{\boldsymbol{\nabla}}(p) = \boldsymbol{\nabla}(\overline{p})$.

Equation (1.11e) is a finite-volume approximation of the internal energy balance over the primal cell K. To ensure the positivity of the convection operator, the convection flux is defined as the product of the mass flux with an upwind approximation of the internal energy [54]:

$$\mathrm{div}_K(\rho e \boldsymbol{u}) = \mathrm{div}_K\big(e\,(\rho \boldsymbol{u})\big) = \frac{1}{|K|} \sum_{\sigma \in \mathcal{E}(K)} F_{K,\sigma} e_\sigma, \tag{1.17}$$

with, for $\sigma = K|L \in \mathcal{E}_{\rm int}$, $e_\sigma = e_K$ if $F_{K,\sigma} \geq 0$ and $e_\sigma = e_L$ otherwise. The divergence of the velocity, $\mathrm{div}_K(\boldsymbol{u})$, is discretized as follows:

$$\text{for } K \in \mathcal{M}, \qquad \mathrm{div}_K(\boldsymbol{u}) = \frac{1}{|K|} \sum_{\sigma \in \mathcal{E}(K)} |\sigma|\ u_{K,\sigma}, \tag{1.18}$$

and, as announced, this definition implies that the discrete gradient and divergence operators are dual with respect to the L^2 inner product:

$$\sum_{K \in \mathcal{M}} |K|\ p_K\ \mathrm{div}_K(\boldsymbol{u}) + \sum_{i=1}^{d} \sum_{\sigma \in \mathcal{E}_{\mathcal{S}}^{(i)}} |D_\sigma|\ u_{\sigma,i}\ \boldsymbol{\nabla}_{\sigma,i}(p) = 0. \tag{1.19}$$

The term S_K at the right-hand side of (1.11e) is necessary to obtain a consistent scheme in the Euler case [40]; its purpose is to compensate some numerical dissipation terms appearing in the discrete kinetic energy balance equation, which may not tend to 0 as the mesh and time step tend to 0. Its expression is derived in Section 1.4.1.

Definition (Outflow or Neuman boundary conditions). When the normal velocity is not prescribed to zero at the boundary face $\sigma \in \mathcal{E}(K)$, we suppose that the flow leaves the domain (*i.e.* $u_{K,\sigma} \geq 0$), so the definition (1.12) of $F_{K,\sigma}$ remains unchanged (and $\rho_\sigma = \rho_K$). The face σ is also an external dual face of the diamond cell D_σ, and the above mentioned construction procedure of the dual mass fluxes yields $F_{\sigma,\varepsilon} = F_{K,\sigma}$; at this face, we set $\tilde{u}_{\varepsilon,i} = \tilde{u}_{\sigma,i}$. The expression (1.18) of the discrete divergence of the velocity still holds, but now takes into account a (possibly) non-zero normal velocity $u_{K,\sigma}$ at the external face σ. Therefore, the gradient-divergence duality property becomes:

$$\sum_{K \in \mathcal{M}} |K|\ p_K\ \mathrm{div}_K(\boldsymbol{u}) + \sum_{i=1}^{d} \sum_{\sigma \in \mathcal{E}_{\mathcal{S}}^{(i)}} |D_\sigma|\ u_{\sigma,i}\ \boldsymbol{\nabla}_{\sigma,i}(p) = \sum_{\sigma \in \mathcal{E}_{\rm ext}} -|\sigma|\ p_{\rm ext}$$

where p_{ext} stands for the external pressure involved in the Neumann boundary condition, and we have supposed that the Neumann boundary condition is applied on the whole boundary (otherwise, the sum at the right-hand side should be restricted to the faces included in the part of $\partial\Omega$ where Neumann boundary conditions are prescribed). We thus obtain the following definition of the gradient on the external face σ adjacent to the cell K:

$$\boldsymbol{\nabla}_{\sigma,i}(p^{n+1}) = \frac{|\sigma|}{|D_\sigma|}\ (p_{\text{ext}} - p_K^{n+1})\ \boldsymbol{n}_{K,\sigma}\cdot\boldsymbol{e}^{(i)}.$$

Finally, the definition of the internal energy flux (1.17) remains unchanged (and $e_\sigma = e_K$).

In order to obtain a stability estimate, the dual mass balance (1.15) has to be satisfied when performing the first velocity prediction step, and this complicates the initialization of the scheme. The initial approximations for ρ, e and $\boldsymbol{u}$ are given by the average of the initial conditions ρ_0, e_0 and $\boldsymbol{u}_0$ on the primal and dual cells respectively:

$$\begin{aligned}
&\forall K\in\mathcal{M},\quad \rho_K^{(-1)} = \frac{1}{|K|}\int_K \rho_0(\boldsymbol{x})\,\mathrm{d}\boldsymbol{x}, \qquad e_K^0 = \frac{1}{|K|}\int_K e_0(\boldsymbol{x})\,\mathrm{d}\boldsymbol{x},\\
&\text{for } 1\le i\le d,\ \forall\sigma\in\mathcal{E}_{\mathcal{S}}^{(i)},\quad u_{\sigma,i}^0 = \frac{1}{|D_\sigma|}\int_{D_\sigma}(\boldsymbol{u}_0(\boldsymbol{x}))_i\,\mathrm{d}\boldsymbol{x}.
\end{aligned} \tag{1.20}$$

Then the discrete mass balance (1.11d), written for $n=-1$, is solved for ρ^0, and the initial pressure is given by the equation of state (1.1e).

1.3.2 The viscous diffusion and dissipation term

The aim of this section is to define the viscous diffusion term $\mathrm{div}_{\sigma,i}\,\boldsymbol{\tau}(\tilde{\boldsymbol{u}})$ of the momentum balance equation (1.11b) and the viscous dissipation term $(\boldsymbol{\tau}(\tilde{\boldsymbol{u}}):\boldsymbol{\nabla}\tilde{\boldsymbol{u}})_K$ of the internal energy balance equation. Besides usual numerical consistency considerations, we would like these quantities to satisfy the two following constraints:

(i) non-negativity of the dissipation:

$$\forall K\in\mathcal{M},\quad (\boldsymbol{\tau}(\tilde{\boldsymbol{u}}):\boldsymbol{\nabla}\tilde{\boldsymbol{u}})_K \ge 0; \tag{1.21}$$

(ii) consistency of the diffusion and the dissipation, in the following sense:

$$-\sum_{i=1}^{d}\sum_{\sigma\in\mathcal{E}_{\mathcal{S}}^{(i)}} |D_\sigma|\ \mathrm{div}_{\sigma,i}\,\boldsymbol{\tau}(\tilde{\boldsymbol{u}})\ u_{\sigma,i} = \sum_{K\in\mathcal{M}} |K|\ \ (\boldsymbol{\tau}(\tilde{\boldsymbol{u}}):\boldsymbol{\nabla}\tilde{\boldsymbol{u}})_K\,, \tag{1.22}$$

i.e. the discrete analogue of the identity $\displaystyle\int_\Omega \mathrm{div}\boldsymbol{\tau}(\boldsymbol{u})\cdot\boldsymbol{u} = -\int_\Omega \boldsymbol{\tau}(\boldsymbol{u}):\boldsymbol{\nabla}\boldsymbol{u}$.

Since the discretization of the diffusion term is different for the RT or CR discretization, on one side, and for the MAC scheme, on the other side, we deal with these two cases separately.

1.3.2.1 Unstructured meshes, CR-RT discretization.

For the RT or CR discretization, we use the usual finite element discretization of the viscous term:

$$-\mathrm{div}_{\sigma,i}\,\boldsymbol{\tau}(\tilde{\boldsymbol{u}}) = -\frac{1}{|D_\sigma|}\sum_{K\in\mathcal{M}}\int_K \boldsymbol{\tau}(\tilde{\boldsymbol{u}}):\boldsymbol{\nabla}\boldsymbol{\varphi}_\sigma^{(i)}\,\mathrm{d}\boldsymbol{x}, \tag{1.23}$$

where $\boldsymbol{\varphi}_\sigma^{(i)}$ stands for the vector-valued finite element shape function associated to the i^{th} component of the velocity and to the face σ; by definition of the RT or CR finite elements, this shape function reads $\varphi_\sigma \boldsymbol{e}^{(i)}$, where φ_σ is the real-valued function of the approximation space whose mean value is 1 over σ and 0 over the other faces of the mesh.

The dissipation term is given by:

$$(\boldsymbol{\tau}(\tilde{\boldsymbol{u}}) : \boldsymbol{\nabla}\tilde{\boldsymbol{u}})_K = \frac{1}{|K|}\int_K \boldsymbol{\tau}(\tilde{\boldsymbol{u}}) : \boldsymbol{\nabla}\tilde{\boldsymbol{u}}\,\mathrm{d}\boldsymbol{x}. \tag{1.24}$$

The non-negativity of this term is a classical result, which is a consequence of the following elementary computation. By symmetry,

$$\boldsymbol{\tau}(\tilde{\boldsymbol{u}}) : \boldsymbol{\nabla}\tilde{\boldsymbol{u}} = \mu\,(\boldsymbol{\nabla}\tilde{\boldsymbol{u}}+\boldsymbol{\nabla}^t\tilde{\boldsymbol{u}}) : \boldsymbol{\nabla}\tilde{\boldsymbol{u}} - \frac{2\mu}{3}\,\mathrm{div}(\tilde{\boldsymbol{u}})\,\boldsymbol{I} : \boldsymbol{\nabla}\tilde{\boldsymbol{u}} = \mu\,\big((\boldsymbol{\nabla}\tilde{\boldsymbol{u}}+\boldsymbol{\nabla}^t\tilde{\boldsymbol{u}}) : (\boldsymbol{\nabla}\tilde{\boldsymbol{u}}+\boldsymbol{\nabla}^t\tilde{\boldsymbol{u}}) - \frac{2}{3}\,(\mathrm{div}\tilde{\boldsymbol{u}})^2\big).$$

This expression is thus the sum of the squares of the off-diagonal entries of $\boldsymbol{\nabla}\tilde{\boldsymbol{u}} + \boldsymbol{\nabla}^t\tilde{\boldsymbol{u}}$ and of the following quantity

$$\frac{2\mu}{3}\Big(3\sum_{i=1}^{3}(\partial_i u_i)^2 - \big(\sum_{i=1}^{3}\partial_i u_i\big)^2\Big),$$

which is non-negative.

Finally, by a simple reordering of the sums,

$$\begin{aligned}
&-\sum_{i=1}^{d}\sum_{\sigma\in\mathcal{E}_{\mathcal{S}}^{(i)}} |D_\sigma|\ \mathrm{div}_{\sigma,i}\,\boldsymbol{\tau}(\tilde{\boldsymbol{u}})\ u_{\sigma,i} \\
&\qquad = \sum_{i=1}^{d}\sum_{\sigma\in\mathcal{E}_{\mathcal{S}}^{(i)}} u_{\sigma,i}\sum_{K\in\mathcal{M}}\int_K \boldsymbol{\tau}(\tilde{\boldsymbol{u}}) : \boldsymbol{\nabla}\boldsymbol{\varphi}_\sigma^{(i)}\,\mathrm{d}\boldsymbol{x} = \sum_{K\in\mathcal{M}}\int_K \boldsymbol{\tau}(\tilde{\boldsymbol{u}}) : \boldsymbol{\nabla}\Big(\sum_{i=1}^{d}\sum_{\sigma\in\mathcal{E}_{\mathcal{S}}^{(i)}} u_{\sigma,i}\boldsymbol{\varphi}_\sigma^{(i)}\Big)\,\mathrm{d}\boldsymbol{x} \\
&\qquad\qquad = \sum_{K\in\mathcal{M}}\int_K \boldsymbol{\tau}(\tilde{\boldsymbol{u}}) : \boldsymbol{\nabla}\tilde{\boldsymbol{u}}\,\mathrm{d}\boldsymbol{x} = \sum_{K\in\mathcal{M}} |K|\ \ (\boldsymbol{\tau}(\tilde{\boldsymbol{u}}) : \boldsymbol{\nabla}\tilde{\boldsymbol{u}})_K\,,
\end{aligned}$$

that is (1.22).

1.3.2.2 MAC scheme

For the MAC scheme, the strategy used to build the viscous diffusion and dissipation terms is to mimic the computation performed in the previous section. Hence, we first need to define the (discrete) partial derivatives of the discrete velocities *a.e* in Ω, and then a finite volume analogue of the shape functions. With these ingredients, expressions (1.23) and (1.24) still make sense, and their consequences (namely Relations (1.21) and (1.22)) hold.

The arguments presented in this section were already used in [24], but with a rather different approach and notations; they are detailed here in the present framework.

The two-dimensional case - Since we have to deal with differential quotient formula on structured grids, we use the standard notations in this context given on Figures 1.2 and 1.3. For the sake of clarity, we first concentrate on the inner cells; the cells neighbouring the boundary and the boundary conditions are dealt with later.

The discrete partial derivatives of the velocity are defined as follows (see Figures 1.4 and 1.5):

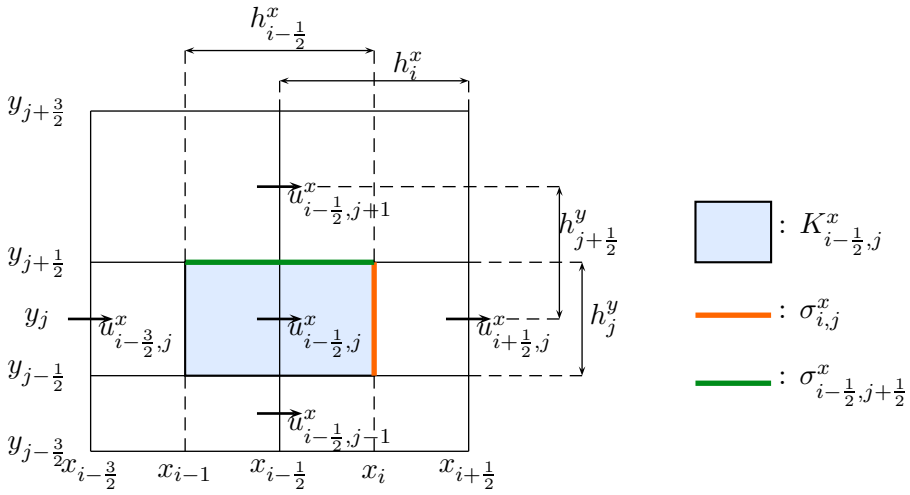

Figure 1.2: Unknown and dual cell for the x-component of the velocity, notations for staggered discretizations.

– Let the primal cells be denoted by $K_{i,j} = (x_{i-1/2}, x_{i+1/2}) \times (y_{j-1/2}, y_{j+1/2})$. The derivatives involved in the divergence, $\partial_x^{\mathcal{M}} u^x$ and $\partial_y^{\mathcal{M}} u^y$, are defined over the primal cell by, $\forall \boldsymbol{x} \in K_{i,j}$:

$$\partial_x^{\mathcal{M}} u^x(\boldsymbol{x}) = \frac{u^x_{i+\frac{1}{2},j} - u^x_{i-\frac{1}{2},j}}{h^x_i}, \quad \partial_y^{\mathcal{M}} u^y(\boldsymbol{x}) = \frac{u^y_{i,j+\frac{1}{2}} - u^y_{i,j-\frac{1}{2}}}{h^y_j}. \tag{1.25}$$

– For the other derivatives, we introduce a fourth mesh which is vertex-centred, and we denote by K^{xy} the generic cell of this new mesh, with $K^{xy}_{i-\frac{1}{2},j-\frac{1}{2}} = (x_{i-1}, x_i) \times (y_{j-1}, y_j)$. Then, $\forall \boldsymbol{x} \in$

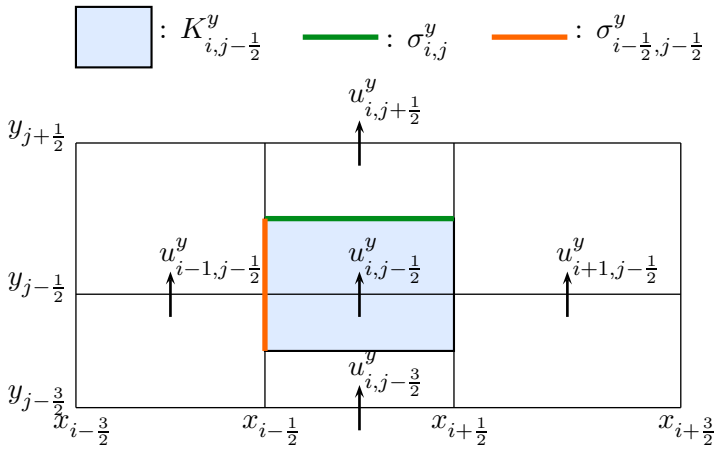

Figure 1.3: Unknowns and dual cell for the y-component of the velocity, notations for staggered discretizations (continued).

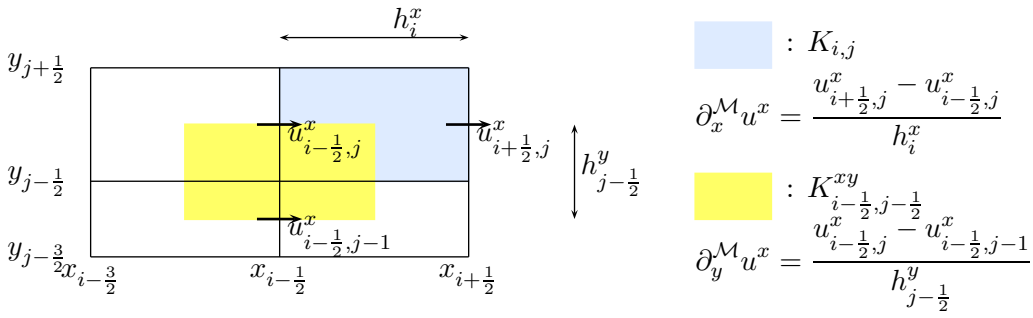

Figure 1.4: Discrete partial derivatives of the x-component of the velocity

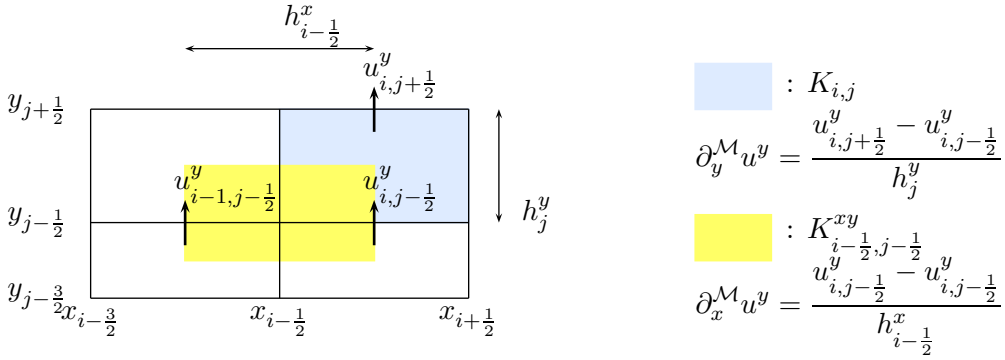

Figure 1.5: Discrete partial derivatives of the y-component of the velocity

$K^{xy}_{i-\frac{1}{2},j-\frac{1}{2}}$:

$$\partial_y^{\mathcal{M}} u^x(\boldsymbol{x}) = \frac{u^x_{i-\frac{1}{2},j} - u^x_{i-\frac{1}{2},j-1}}{h^y_{j-\frac{1}{2}}}, \quad \partial_x^{\mathcal{M}} u^y(\boldsymbol{x}) = \frac{u^y_{i,j-\frac{1}{2}} - u^y_{i-1,j-\frac{1}{2}}}{h^x_{i-\frac{1}{2}}}. \tag{1.26}$$

We are now in position to define the discrete stress tensor of $\tilde{\boldsymbol{u}}$ by:

$$(\mu\boldsymbol{\nabla})^{\mathcal{M}}\tilde{\boldsymbol{u}} = \begin{bmatrix} \mu_{xx}\,\partial_x^{\mathcal{M}}\tilde{u}^x & \mu_{xy}\,\partial_y^{\mathcal{M}}\tilde{u}^x \\ \mu_{yx}\,\partial_x^{\mathcal{M}}\tilde{u}^y & \mu_{yy}\,\partial_y^{\mathcal{M}}\tilde{u}^y \end{bmatrix}, \quad (\mu\,\mathrm{div})^{\mathcal{M}}(\tilde{\boldsymbol{u}}) = \mu_{xx}\,\partial_x^{\mathcal{M}}\tilde{u}^x + \mu_{yy}\,\partial_y^{\mathcal{M}}\tilde{u}^y,$$

$$\boldsymbol{\tau}^{\mathcal{M}}(\tilde{\boldsymbol{u}}) = (\mu\boldsymbol{\nabla})^{\mathcal{M}}\tilde{\boldsymbol{u}} + \big((\mu\boldsymbol{\nabla}^{\mathcal{M}})\tilde{\boldsymbol{u}}\big)^t - \frac{2}{3}\,(\mu\,\mathrm{div})^{\mathcal{M}}\tilde{\boldsymbol{u}}\,\boldsymbol{I},$$

where μ_{xx}, μ_{xy}, μ_{yx} and μ_{yy} are approximations of the viscosity field on the various meshes; here, we choose to use the same piecewise constant fields for μ_{xx} and μ_{yy} (respectively μ_{xy} and μ_{yx}), with the same mesh as their associated partial derivatives, namely the primal cells (respectively the vertex-centred cells). The value of μ_{xx} and μ_{yy} over $K_{i,j}$ (respectively μ_{xy} and μ_{yx} over $K^{xy}_{i-\frac{1}{2},j-\frac{1}{2}}$) is denoted by $\mu_{i,j}$ (respectively $\mu_{i-\frac{1}{2},j-\frac{1}{2}}$).

We now introduce the "finite-volume shape functions" for the components of the velocity. Let us denote by $\mathcal{I}^x \subset \mathbb{N}^2$ (resp. $\mathcal{I}^y \subset \mathbb{N}^2$) the set of pairs (i,j) which are admissible in the sense that $\boldsymbol{x}_{i-\frac{1}{2},j}$ (resp. $\boldsymbol{x}_{i,j-\frac{1}{2}}$) is the mass center of a vertical (resp. horizontal) face of the mesh. For $(i,j) \in \mathcal{I}^x$, we denote by $\boldsymbol{\varphi}^{x,(i-\frac{1}{2},j)}$ the shape function associated to the degree of freedom of the x-component of the velocity located at $\boldsymbol{x}_{i-\frac{1}{2},j}$; this discrete function is defined by:

$$(\boldsymbol{\varphi}^{x,(i-\frac{1}{2},j)})^x_{k-\frac{1}{2},\ell} = \delta^i_k\ \delta^j_\ell,\ \forall (k,\ell) \in \mathcal{I}^x \text{ and } (\boldsymbol{\varphi}^{x,(i-\frac{1}{2},j)})^y_{k,\ell-\frac{1}{2}} = 0,\ \forall (k,\ell) \in \mathcal{I}^y.$$

Similarly, for $(i,j) \in \mathcal{I}^y$, we denote by $\boldsymbol{\varphi}^{y,(i,j-\frac{1}{2})}$ the shape function associated to the degree of freedom for the y-component of the velocity located at $\boldsymbol{x}_{i,j-\frac{1}{2}}$, which is defined by

$$(\boldsymbol{\varphi}^{y,(i,j-\frac{1}{2})})^x_{k-\frac{1}{2},\ell} = 0,\ \forall (k,\ell) \in \mathcal{I}^x \text{ and } (\boldsymbol{\varphi}^{y,(i,j-\frac{1}{2})})^y_{k,\ell-\frac{1}{2}} = \delta^i_k\ \delta^j_\ell,\ \forall (k,\ell) \in \mathcal{I}^y.$$

Then, the viscous diffusion and dissipation terms are defined by the following analogues of (1.23) and (1.24):

$$\begin{aligned} &\forall (i,j) \in \mathcal{I}^x, \qquad -(\mathrm{div}\boldsymbol{\tau}(\tilde{\boldsymbol{u}}))^x_{i-\frac{1}{2},j} = \frac{1}{|K^x_{i-\frac{1}{2},j}|}\int_\Omega \boldsymbol{\tau}^{\mathcal{M}}(\tilde{\boldsymbol{u}}) : \boldsymbol{\nabla}^{\mathcal{M}}\boldsymbol{\varphi}^{x,(i-\frac{1}{2},j)}\,\mathrm{d}\boldsymbol{x}, \\ &\forall (i,j) \in \mathcal{I}^y, \qquad -(\mathrm{div}\boldsymbol{\tau}(\tilde{\boldsymbol{u}}))^y_{i,j-\frac{1}{2}} = \frac{1}{|K^y_{i,j-\frac{1}{2}}|}\int_\Omega \boldsymbol{\tau}^{\mathcal{M}}(\tilde{\boldsymbol{u}}) : \boldsymbol{\nabla}^{\mathcal{M}}\boldsymbol{\varphi}^{y,(i,j-\frac{1}{2})}\,\mathrm{d}\boldsymbol{x}, \end{aligned} \tag{1.27}$$

and:

$$(\boldsymbol{\tau}(\tilde{\boldsymbol{u}}) : \boldsymbol{\nabla}\tilde{\boldsymbol{u}})_K = \frac{1}{|K|}\int_K \boldsymbol{\tau}^{\mathcal{M}}(\tilde{\boldsymbol{u}}) : \boldsymbol{\nabla}^{\mathcal{M}}\tilde{\boldsymbol{u}}\,\mathrm{d}\boldsymbol{x}. \tag{1.28}$$

As a consequence of these definitions, as announced, the constraints (1.21) and (1.22) are satisfied. Let us now check that the definition (1.27) coincides with the usual definition of the viscous diffusion term for the MAC scheme. To this purpose, we consider the equation corresponding to the $(i-\frac{1}{2},j)$ unknown for the x-component of the velocity. The shape function associated to this equation is $\boldsymbol{\varphi}^{x,(i-\frac{1}{2},j)}$ and its non-zero partial derivatives are $\partial^{\mathcal{M}}_x\boldsymbol{\varphi}^{x,(i-\frac{1}{2},j)}$ and $\partial^{\mathcal{M}}_y\boldsymbol{\varphi}^{x,(i-\frac{1}{2},j)}$:

$$\partial^{\mathcal{M}}_x\boldsymbol{\varphi}^{x,(i-\frac{1}{2},j)} = \left|\begin{array}{l} \dfrac{1}{h^x_{i-1}} \text{ over } K_{i-1,j}, \\ \dfrac{-1}{h^x_i} \text{ over } K_{i,j}, \\ 0 \text{ elsewhere,} \end{array}\right. \qquad \partial^{\mathcal{M}}_y\boldsymbol{\varphi}^{x,(i-\frac{1}{2},j)} = \left|\begin{array}{l} \dfrac{1}{h^y_{j-\frac{1}{2}}} \text{ over } K^{xy}_{i-\frac{1}{2},j-\frac{1}{2}}, \\ \dfrac{-1}{h^y_{j+\frac{1}{2}}} \text{ over } K^{xy}_{i-\frac{1}{2},j+\frac{1}{2}}, \\ 0 \text{ elsewhere.} \end{array}\right.$$

The corresponding entries of the discrete stress tensor of $\tilde{\boldsymbol{u}}$ (recall that, at the continuous level, this tensor is defined by $\boldsymbol{\tau}^{xx}(\tilde{u}) = \frac{4}{3}\,\mu\partial_x\tilde{u}^x - \frac{2}{3}\,\mu\partial_y\tilde{u}^y$ and $\boldsymbol{\tau}^{xy} = \mu(\partial_y\tilde{u}^x + \partial_x\tilde{u}^x)$) read over $K_{i-1+\varepsilon,j}$, with $\varepsilon = 0$ and $\varepsilon = 1$:

$$\boldsymbol{\tau}^{\mathcal{M}}(\tilde{\boldsymbol{u}})^{xx}_{i-1+\varepsilon,j} = \frac{4}{3}\,\mu_{i-1+\varepsilon,j}\frac{\tilde{u}^x_{i-\frac{1}{2}+\varepsilon,j} - \tilde{u}^x_{i-\frac{3}{2}+\varepsilon,j}}{h^x_{i-1+\varepsilon}} - \frac{2}{3}\,\mu_{i-1+\varepsilon,j}\frac{\tilde{u}^y_{i+\varepsilon,j+\frac{1}{2}} - \tilde{u}^y_{i+\varepsilon,j-\frac{1}{2}}}{h^y_j},$$

and, over $K^{xy}_{i-\frac{1}{2},j-\frac{1}{2}+\varepsilon}$, still with $\varepsilon = 0$ and $\varepsilon = 1$:

$$\boldsymbol{\tau}^{\mathcal{M}}(\tilde{\boldsymbol{u}})^{xy}_{i-\frac{1}{2},j-\frac{1}{2}+\varepsilon} = \mu_{i-\frac{1}{2},j-\frac{1}{2}+\varepsilon}\Big[\frac{\tilde{u}^x_{i-\frac{1}{2},j+\varepsilon} - \tilde{u}^x_{i-\frac{1}{2},j-1+\varepsilon}}{h^y_{j-\frac{1}{2}+\varepsilon}} + \frac{\tilde{u}^y_{i-1,j-\frac{1}{2}+\varepsilon} - \tilde{u}^y_{i,j-\frac{1}{2}+\varepsilon}}{h^x_{i-\frac{1}{2}}}\Big].$$

We thus get:

$$\int_\Omega \boldsymbol{\tau}^{\mathcal{M}}(\tilde{\boldsymbol{u}})^{xx}\ \partial^{\mathcal{M}}_x\boldsymbol{\varphi}^{x,(i-\frac{1}{2},j)}\,\mathrm{d}\boldsymbol{x} = F_{i,j} - F_{i-1,j},$$

where, for $\varepsilon = 0$ and $\varepsilon = 1$, $F_{i-1+\varepsilon,j} = h^y_j\ \boldsymbol{\tau}^{\mathcal{M}}(\tilde{\boldsymbol{u}})^{xx}_{i-1+\varepsilon,j}$, which is the usual viscous diffusion flux across the face $\sigma^x_{i-1+\varepsilon,j}$ (see Figure 1.2). Similarly,

$$\int_\Omega \boldsymbol{\tau}^{\mathcal{M}}(\tilde{\boldsymbol{u}})^{xy}\ \partial^{\mathcal{M}}_y\boldsymbol{\varphi}^{x,(i-\frac{1}{2},j)}\,\mathrm{d}\boldsymbol{x} = F_{i-\frac{1}{2},j+\frac{1}{2}} - F_{i-\frac{1}{2},j-\frac{1}{2}},$$

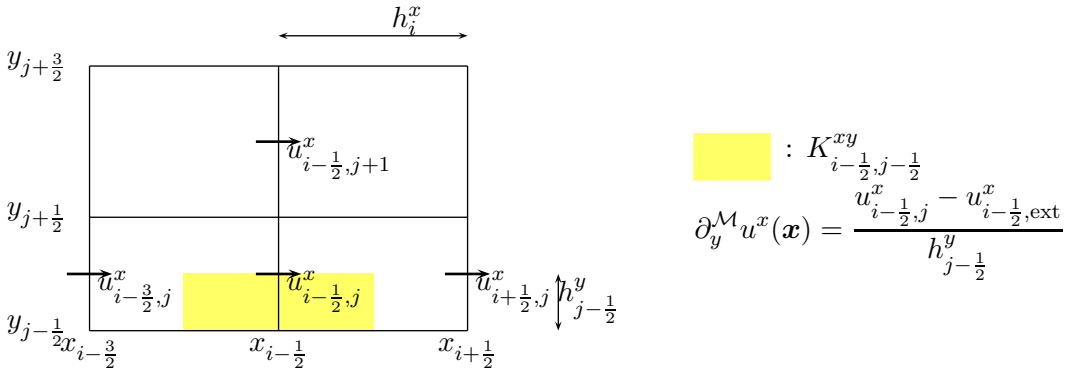

Figure 1.6: Boundary conditions, x-component of the velocity

where, for $\varepsilon = 0$ and $\varepsilon = 1$, $F_{i-\frac{1}{2},j-\frac{1}{2}+\varepsilon} = h^x_{i-1/2}\ \boldsymbol{\tau}^{\mathcal{M}}(\tilde{\boldsymbol{u}})^{xy}_{i-\frac{1}{2},j-\frac{1}{2}+\varepsilon}$, which is the usual expression of the MAC viscous flux across the face $\sigma^x_{i-\frac{1}{2},j-\frac{1}{2}+\varepsilon}$ (once again defined on Figure 1.2). The same arguments apply for the y-component of the momentum balance equation.

Let us now show how to extend these definitions up to the boundary and how to deal with Dirichlet boundary conditions. Modification of the above material is necessary only for the definition of a "twice-staggered cell" K^{xy} associated to a vertex lying on the boundary, and for one of the discrete partial derivatives on this cell: $\partial_y^{\mathcal{M}} u^x$ near an horizontal boundary and $\partial_x^{\mathcal{M}} u^y$ near a vertical boundary. Let us deal for instance with the first case, using the notations of Figure 1.6. Roughly speaking, everything is done as if we were supposing that there is an additional horizontal stripe of mesh at the boundary, with zero height and where the x-velocity is set at the prescribed value, let us say $u^x_{i-\frac{1}{2},\text{ext}}$ (which is zero in case of homogeneous Dirichlet boundary conditions). Therefore, $K^{xy}_{i-\frac{1}{2},j-\frac{1}{2}} = (x_{i-1}, x_i) \times (y_{j-\frac{1}{2}}, y_j)$, $h^y_{j-\frac{1}{2}} = h^y_j/2$ and

$$\partial_y^{\mathcal{M}} u^x(\boldsymbol{x}) = \frac{u^x_{i-\frac{1}{2},j} - u^x_{i-\frac{1}{2},\text{ext}}}{h^y_{j-\frac{1}{2}}}, \quad \forall \boldsymbol{x} \in K^{xy}_{i-\frac{1}{2},j-\frac{1}{2}}.$$

The other partial derivative $\partial_x^{\mathcal{M}} u^y$ defined on $K^{xy}_{i-\frac{1}{2},j-\frac{1}{2}}$ is computed with its usual expression, but using the prescribed value for $u^y_{i-1,j-\frac{1}{2}}$ and $u^y_{i,j-\frac{1}{2}}$; this derivative vanishes in case of homogeneous boundary conditions (in fact, as soon as the prescribed value for u^y does not depend on x). For the computation of the partial derivative of the shape functions, the external value is always zero (which is consistent with the fact that a test function for an elliptic boundary value problem is supposed to vanish on the boundary).

Definition (Neumann or perfect slip boundary conditions). In the case of Neumann or perfect slip boundary condition, the quantity at the boundary is supposed to be the same as in the domain (*i.e.*, for the example chosen above, $u^x_{i-\frac{1}{2},\text{ext}} = u^x_{i-\frac{1}{2},j}$). If the considered Neumann boundary condition involves a non-zero shear surface force, this latter must be added at the righ-hand side of the balance equation.

The three-dimensional case – Extending the computations of the preceding section to three space

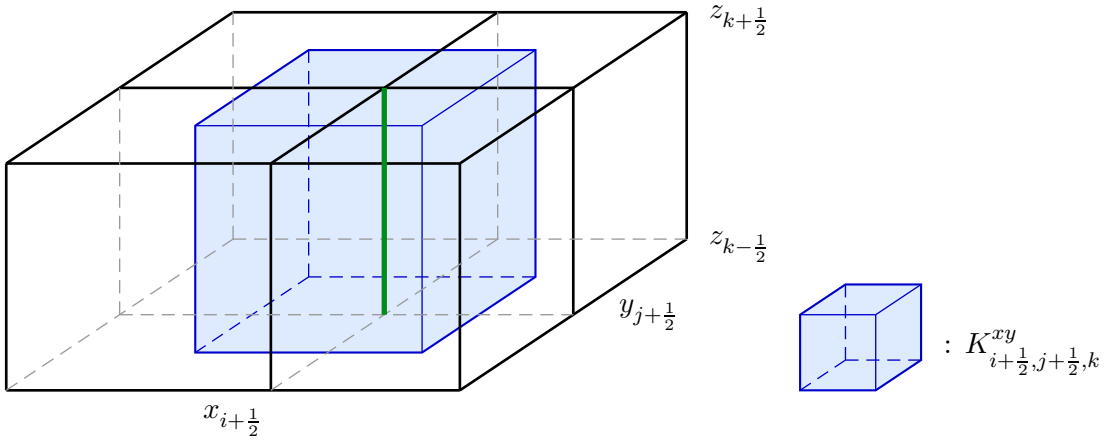

Figure 1.7: The xy-staggered cell $K^{xy}_{i+\frac{1}{2},j+\frac{1}{2},k}$, used in the definition of $\partial_y^{\mathcal{M}} u^x$, $\partial_x^{\mathcal{M}} u^y$, and $\boldsymbol{\tau}^{\mathcal{M}}(\boldsymbol{u})_{x,y} = \boldsymbol{\tau}^{\mathcal{M}}(\boldsymbol{u})_{y,x}$.

dimensions yields the following construction.

- First, define three new meshes, which are "edge-centred": $K^{xy}_{i+\frac{1}{2},j+\frac{1}{2},k}$ is staggered from the primal mesh $K_{i,j,k}$ in the x and y direction (so $K^{xy}_{i+\frac{1}{2},j+\frac{1}{2},k} = (x_i, x_{i+1}) \times (y_i, y_{j+1}) \times (z_{k-\frac{1}{2}}, z_{k+\frac{1}{2}})$, see Figure 1.7), $K^{xz}_{i+\frac{1}{2},j,k+\frac{1}{2}}$ in the x and z direction, and $K^{yz}_{i,j+\frac{1}{2},k+\frac{1}{2}}$ in the y and z direction.
- The partial derivatives of the velocity components are then defined as piecewise constant functions, the value of which is obtained by natural finite differences:
  - for $\partial_x^{\mathcal{M}} u^x$, $\partial_y^{\mathcal{M}} u^y$ and $\partial_z^{\mathcal{M}} u^z$, on the primal mesh,
  - for $\partial_y^{\mathcal{M}} u^x$ and $\partial_x^{\mathcal{M}} u^y$ on the cells $(K^{xy}_{i+\frac{1}{2},j+\frac{1}{2},k})$,
  - for $\partial_z^{\mathcal{M}} u^x$ and $\partial_x^{\mathcal{M}} u^z$ on the cells $(K^{xz}_{i+\frac{1}{2},j,k+\frac{1}{2}})$,
  - for $\partial_y^{\mathcal{M}} u^z$ and $\partial_z^{\mathcal{M}} u^y$ on the cells $(K^{yz}_{i,j+\frac{1}{2},k+\frac{1}{2}})$.
- Then, define four families of values for the viscosity field, μ, μ^{xy}, μ^{xz} and μ^{yz}, associated to the primal and the three edge-centred meshes respectively.
- The shear stress tensor is obtained by the extension of (1.27) to $d = 3$, and the dissipation term is given by (1.28).

1.3.3 The heat diffusion term

The discretization of the diffusion term depends on whether the mesh is super-admissible (in the sense of Section 1.2, Condition (1.10)) or not. In the first case, we use the usual finite volume scheme based on a two-point approximation of the fluxes [19]:

$$\forall K \in \mathcal{M}, \qquad -\lambda\,(\Delta e)_K = \lambda \sum_{\sigma = K|L \in \mathcal{E}(K)} \frac{|\sigma|}{d_\sigma}\,(e_K - e_L). \tag{1.29}$$

Note that, in this relation, no flux is computed on the external faces, which is consistent with homogeneous Neumann boundary conditions. In the second case, we use the so-called SUSHI scheme, in the variant described in [67, Section 3.1] for general meshes.

For $a \in \mathbb{R}$, let us denote by a^+ and a^- the positive and negative part of a respectively, *i.e.* $a^+ = \max(a, 0)$ and $a^- = -\min(a, 0)$, so $a^+ \geq 0$, $a^- \geq 0$ and $a = a^+ - a^-$. For the scheme to ensure the positivity of the internal energy, we need the Laplace operator to be monotone, in the following sense:

$$\forall\ (e_K)_{K\in\mathcal{M}} \subset \mathbb{R}, \qquad \sum_{K\in\mathcal{M}} -\lambda\ (\Delta e)_K\ (-e_K^-) \geq 0. \tag{1.30}$$

Lemma 1.3.1.
The finite volume scheme based on the two-point approximation of the fluxes (1.29) satisfies the property (1.30).

Proof. Let $(e_K)_{K\in\mathcal{M}} \subset \mathbb{R}$ be given. Then, by definition and then reordering the sums:

$$\begin{aligned}\sum_{K\in\mathcal{M}} -\lambda\ (\Delta e)_K\ (-e_K^-) &= \sum_{K\in\mathcal{M}} (-e_K^-) \sum_{\sigma=K|L\in\mathcal{E}(K)} \frac{|\sigma|}{d_\sigma}\ (e_K - e_L) \\ &= \sum_{\sigma=K|L\in\mathcal{E}_{\rm int}} \frac{|\sigma|}{d_\sigma}\ (e_K - e_L)\ (e_L^- - e_K^-),\end{aligned}$$

and the conclusion follows by remarking that the function $s \mapsto s^-$ is non-increasing. □

Definition (Two-points flux discrete Laplace operator with Dirichlet boundary conditions). In case of Dirichlet boundary conditions, the definition (1.29) of the discrete Laplace operator must be changed to:

$$-(\Delta e)_K = \sum_{\sigma=K|L\in\mathcal{E}(K)} \frac{|\sigma|}{d_\sigma}\ (e_K - e_L) + \sum_{\sigma\in\mathcal{E}(K)\cap\mathcal{E}_{\rm ext}} \frac{|\sigma|}{d_\sigma}\ (e_K - e_{\sigma,D}),$$

where $e_{\sigma,D}$ stands for the prescribed value for e on the face σ, and, for an external face, d_σ stands for the distance between σ and $\boldsymbol{x}_K$. Let us suppose that $e_{\sigma,D} \geq 0$. The additional terms (compared to the Neumann case) in the expression of $\sum_{K\in\mathcal{M}} -\lambda\ (\Delta e)_K\ (-e_K^-)$ read:

$$\lambda \sum_{\sigma\in\mathcal{E}_{\rm ext},\ \sigma\in\mathcal{E}(K)} \frac{|\sigma|}{d_\sigma}\ (e_K - e_{\sigma,D})(-e_K^-),$$

and this sum is non-negative, since, by definition of the negative part of a real number, both products $e_K\ (-e_K^-)$ and $-e_{\sigma,D}\ (-e_K^-)$ are non-negative. The two-point fluxes discrete Laplace operator thus still satisfies the assumption (1.30) in case of Dirichlet boundary conditions.

Unfortunately, the fact that the discrete Laplace operator obtained by the SUSCHI scheme satisfies (1.30) is wrong on general meshes; this restricts the applicability of the following analysis to super-admissible meshes or to the Euler equations. As a matter of fact, however, this seems unavoidable that the stability of the scheme be conditioned to the fact that internal energy remains non-negative, and thus that the diffusion operator is monotone; circumventing this problem will require to build a discrete Laplace operator satisfying a maximum principle, which is still an active subject of research (and, of course, out of the scope of the present paper).

1.4 Properties of the scheme

1.4.1 A priori estimates

The following lemma is an easy extension of [40, Lemma 3.11], to cope with diffusion terms (while [40] only deals with Euler equations). Its proof follows, at the discrete level, the computation performed in Appendix 1.A, which clarifies the effects of the pressure gradient scaling step.

LEMMA 1.4.1 (Discrete kinetic energy balance).
A solution to the scheme (1.11) satisfies the following equality, for $1 \leq i \leq d$, $\sigma \in \mathcal{E}_{\mathcal{S}}^{(i)}$ and $0 \leq n \leq N-1$:

$$\frac{1}{2}\frac{|D_\sigma|}{\delta t}\Big[\rho_{D_\sigma}^n (u_{\sigma,i}^{n+1})^2 - \rho_{D_\sigma}^{n-1}(u_{\sigma,i}^n)^2\Big] + \frac{1}{2}\sum_{\varepsilon\in\bar{\mathcal{E}}(D_\sigma)} F_{\sigma,\varepsilon}^n\ \tilde{u}_{\sigma,i}^{n+1}\ \tilde{u}_{\sigma',i}^{n+1}$$
$$+ |D_\sigma|\ \boldsymbol{\nabla}_{\sigma,i}(p^{n+1})\ u_{\sigma,i}^{n+1} - |D_\sigma|\,\mathrm{div}_{\sigma,i}\,\boldsymbol{\tau}(\tilde{\boldsymbol{u}}^{n+1})\ \tilde{u}_{\sigma,i}^{n+1} + P_{\sigma,i}^{n+1} - P_{\sigma,i}^n = -R_{\sigma,i}^{n+1}, \quad (1.31)$$

where

$$P_{\sigma,i}^{n+1} = \frac{\delta t\,|\sigma|^2}{2|D_\sigma|}\ \frac{1}{\rho_{D_\sigma}^n}\,(p_L^{n+1} - p_K^{n+1})^2, \quad R_{\sigma,i}^{n+1} = \frac{1}{2}\ \frac{|D_\sigma|}{\delta t}\ \rho_{D_\sigma}^{n-1}\ \big(\tilde{u}_{\sigma,i}^{n+1} - u_{\sigma,i}^n\big)^2. \quad (1.32)$$

The residual terms $R_{\sigma,i}^{n+1}$ may be seen as a numerical dissipation generated by the upwinding in time of the scheme (*i.e.* the use of a backward time discretization). For viscous flows, it may be anticipated that these terms tend to zero when the space and time steps tend to zero. On the opposite, it is not the case when dealing with Euler equations, where they may subsist as measures borne by the shocks (see Remark 1.4.1 below). Since, in this context, the scheme needs to be consistent with the total energy balance, this dissipation (as the usual physical viscous dissipation) has to be compensated in the internal energy balance; this is done by the corrective terms S_K in (1.11e), which we are now in position to define:

$$\forall K \in \mathcal{M},\ S_K^{n+1} = \sum_{i=1}^d S_{K,i}^{n+1},\ \text{with}\quad S_{K,i}^{n+1} = \frac{1}{2}\,\rho_K^{n-1} \sum_{\sigma\in\mathcal{E}(K)\cap\mathcal{E}_{\mathcal{S}}^{(i)}} \frac{|D_{K,\sigma}|}{\delta t}\ \big(\tilde{u}_{\sigma,i}^{n+1} - u_{\sigma,i}^n\big)^2. \quad (1.33)$$

Thanks to the definition (1.14) of the density on the duals cells, this relation results from a distribution of the residual terms associated to a face to its (one or two) adjacent cells. Therefore, we get:

$$\sum_{K\in\mathcal{M}} S_K^{n+1} = \sum_{i=1}^d \sum_{\sigma\in\mathcal{E}_{\mathcal{S}}^{(i)}} R_{\sigma,i}^{n+1}. \quad (1.34)$$

A theoretical justification of this process is provided in [40], where it is shown in the 1D case that, if the scheme is stable and converges to a limit, this limit indeed satisfies the weak form of the total energy balance (1.1c). Note however that the scheme does not provide a conservative discretization of the (conservative) total energy balance. Indeed, the discrete kinetic energy balance(s) and the internal energy balance are not posed on the same mesh: precisely speaking, the kinetic energy is the sum of the terms $\frac{1}{2}\rho u_i^2$, for $1 \leq i \leq d$, and the discrete balance equation (1.31) for each of these terms is posed on the mesh associated to the i^{th} velocity component (that is d different meshes for the MAC scheme, and a single mesh for the RT-CR discretization), while the internal energy balance is posed on the primal mesh. To the best of our knowledge, these $d+1$ relations cannot be combined to obtain a consistent discrete analogue of the total energy balance. This latter equation is only obtained in

the weak sense at the limit of vanishing time and space steps. A similar algorithm was developed for co-located discretization in [44], in which case the discrete kinetic energy inequality and internal energy equation are written on the same mesh, so that local conservation of the total energy can be ensured. Note that for both types of discretizations (staggered or colocated), without corrective terms, the scheme is observed in numerical experiments to yield wrong shock solutions, which do not satisfy the Rankine-Hugoniot conditions.

Definition (Behaviour of the remainder R (or the corrective term S)). Let us consider a one-dimensional problem posed over $\Omega = (0,1)$ and $t \in (0,1)$, and let u be a discrete function increasing with x and such that, for $x \in (0,1)$, $u(x,t) = 0$ for $t \in (0, T_0(x))$, $u(x,t) = 1$ for $t \in (T_1(x), 1)$ and $u(x,.)$ affine in the interval $(T_0(x), T_1(x))$. We suppose in addition that the number of time steps in the interval $(T_0(x), T_1(x))$ does not depend on x, and is equal to N. This situation is obtained, for instance, when u is a travelling-in-time piecewise-affine profile (with $T_0(x) = x_0 + c\,t$ and $T_1(x) = x_1 + c\,t$, c being the travelling velocity). In these conditions, for $\sigma \in \mathcal{E}$, the difference $u_\sigma^{n+1} - u_\sigma^n$ is, up to side effects, equal to $1/N$ for N time steps and to zero for the other ones, so we get, for the space-time L^1-norm of R or S:

$$\sum_{n=0}^{N-1} \sum_{\sigma \in \mathcal{E}} \delta t \; R_\sigma^{n+1} = \sum_{n=0}^{N-1} \sum_{K \in \mathcal{M}} \delta t \; S_K^{n+1} \sim |\Omega| \; N \; \frac{1}{N^2} = \frac{|\Omega|}{N}.$$

Let us now make this computation for a sequence of more and more refined meshes. We then have two situations: either N is bounded, and the L^1-norm of R or S does not vanish, or N tends to $+\infty$ when h tends to zero. These two situations seem to be encountered in the computations [40]:

- Shocks appear to be captured in a finite number of cells, for any space step, and so, when h tends to zero, R and S tend to measures borne by the shocks (the L^1-norm remains constant while the measure of the support tends to zero); consequently, for solutions combining only shocks, one may expect a near-to-one order of convergence in L^1-norm. This behaviour may be explained by the fact that the flow is compressive, and the convection counterbalances the numerical diffusion.
- On the contrary, the scheme is much more diffusive at contact discontinuities; if we suppose a diffusion induced by the upwinding, with a velocity which remains constant at the contact discontinuity (so the diffusion is also constant, and of range h), we may anticipate a smearing of the solution jump over a distance scaling like $h^{1/2}$. In this case, R and S tend to zero. Moreover, the first order convergence is lost: the order is reduced to approximately $1/2$ (still in L^1-norm) in numerical experiments.

We now turn to the positivity of the scalar variables. The positivity of the density is a consequence of the upwind discretization of the mass balance equation [26, Lemma 2.1]. To prove that the internal energy remains positive, we need a preliminary lemma, which we now state. Let ψ a regular real function. Then, at the continuous level, the following computation holds (formally), using twice the mass balance equation:

$$\begin{aligned}\psi'(e)\big(\partial_t(\rho e) + \mathrm{div}(\rho e \boldsymbol{u})\big) &= \rho\psi'(e)\big(\partial_t e + \boldsymbol{u}\cdot\boldsymbol{\nabla} e\big) \\ &= \rho\Big(\partial_t\big(\psi(e)\big) + \boldsymbol{u}\cdot\boldsymbol{\nabla}\big(\psi(e)\big)\Big) = \partial_t\big(\rho\psi(e)\big) + \mathrm{div}\big(\rho\psi(e)\boldsymbol{u}\big).\end{aligned}$$

Thus, integrating over the domain Ω and using the boundary conditions:

$$\int_\Omega \psi'(e)\big(\partial_t(\rho e) + \mathrm{div}(\rho e\boldsymbol{u})\big)\,\mathrm{d}\boldsymbol{x} = \frac{d}{dt}\int_\Omega \rho\psi(e)\,\mathrm{d}\boldsymbol{x}.$$

The following lemma states a discrete analogue of this identity, which holds only for convex functions ψ, because of the diffusion generated by the upwinding of the convection term. Its proofs is a straightforward consequence of [40, Lemma A.2],

Lemma 1.4.2.
Let ψ, $\mathbb{R} \longrightarrow \mathbb{R}$, be a continuously differentiable convex function. A solution to the scheme (1.11) satisfies the following inequality:

$$\sum_{K\in\mathcal{M}} |K|\ \psi'(e_K^{n+1})\Big[\frac{1}{\delta t}\left(\rho_K^{n+1}e_K^{n+1}-\rho_K^n e_K^n\right)+\mathrm{div}_K(\rho^{n+1}e^{n+1}\boldsymbol{u}^{n+1})\Big] \geq \frac{1}{2}\sum_{K\in\mathcal{M}}\frac{|K|}{\delta t}\ \Big[\rho_K^{n+1}\,\psi(e_K^{n+1})-\rho_K^n\,\psi(e_K^n)\Big]. \quad (1.35)$$

We are now in position to state and prove the following result.

Lemma 1.4.3 (Positivity of the internal energy).
Let us suppose that the discrete heat diffusion operator satisfies the monotonicity property (1.30), and that the equation of state satisfies (1.8). Let n be such that $0 \leq n \leq N-1$, and let us suppose that $e^n > 0$ (*i.e.* $e_K^n > 0,\ \forall K \in \mathcal{M}$). Then a solution to the scheme (1.11) satisfies $e^{n+1} > 0$.

Proof. Let us multiply the discrete internal energy equation (1.11e) by $-|K|\ (e_K^{n+1})^-$ and sum over $K \in \mathcal{M}$. We obtain $T_1 + T_2 + T_3 = T_4$ with:

$$T_1 = \sum_{K\in\mathcal{M}} -|K|\ (e_K^{n+1})^-\Big[\frac{1}{\delta t}\left(\rho_K^{n+1}e_K^{n+1}-\rho_K^n e_K^n\right)+\mathrm{div}_K(\rho^{n+1}e^{n+1}\boldsymbol{u}^{n+1})\Big],$$

$$T_2 = \sum_{K\in\mathcal{M}} -|K|\ (e_K^{n+1})^-\,p_K^{n+1}\,\mathrm{div}_K(\boldsymbol{u}^{n+1}),$$

$$T_3 = \sum_{K\in\mathcal{M}} \lambda\,|K|\ (e_K^{n+1})^-\,(\Delta e^{n+1})_K,$$

$$T_4 = \sum_{K\in\mathcal{M}} -|K|\ (e_K^{n+1})^-\ \Big[\big(\boldsymbol{\tau}(\tilde{\boldsymbol{u}}^{n+1}):\boldsymbol{\nabla}\tilde{\boldsymbol{u}}^{n+1}\big)_K + S_K^{n+1}\Big].$$

Thanks to Lemma 1.4.2 applied with the continuously differentiable convex function $\psi(s) = (s^-)^2/2$, we have for the term T_1, since $e^n \geq 0$:

$$T_1 \geq \frac{1}{2}\sum_{K\in\mathcal{M}}\frac{|K|}{\delta t}\ \Big[\rho_K^{n+1}\left((e_K^{n+1})^-\right)^2-\rho_K^n\left((e_K^n)^-\right)^2\Big] = \frac{1}{2}\sum_{K\in\mathcal{M}}\frac{|K|}{\delta t}\rho_K^{n+1}\left((e_K^{n+1})^-\right)^2.$$

Thanks to Assumption (1.8), we have $T_2 = 0$, since, when $(e_K^{n+1})^- \neq 0$, $e_K^{n+1} \leq 0$ and so the pressure satisfies $p_K^{n+1} = \wp(\rho_K^{n+1}, e_K^{n+1}) = 0$. The relation (1.30) yields $T_3 \geq 0$. Finally, by construction, the viscous dissipation term and S_K^{n+1} are non-negative, so $T_4 \leq 0$. Gathering all the terms, we obtain:

$$\sum_{K\in\mathcal{M}}\frac{|K|}{\delta t}\rho_K^{n+1}\left((e_K^{n+1})^-\right)^2 \leq 0,$$

which shows that $(e_K^{n+1})^- = 0$, for all $K \in \mathcal{M}$, and thus $e^{n+1} \geq 0$. Let us now consider a cell K such that $e_K^{n+1} = 0$. The internal energy balance on K reads:

$$-\frac{1}{\delta t}\rho_K^n e_K^n - \sum_{\sigma=K|L} (F_{K,\sigma})^- e_L^{n+1} - \lambda \sum_{\sigma=K|L} \frac{|\sigma|}{d_\sigma} e_L^{n+1} = \left(\boldsymbol{\tau}(\tilde{\boldsymbol{u}}^{n+1}) : \boldsymbol{\nabla}\tilde{\boldsymbol{u}}^{n+1}\right)_K + S_K^{n+1}.$$

The first term at the left-hand side is by assumption negative, the other terms are non-positive and the right-hand side is non-negative, which raises a contradiction. This concludes the proof. □

Finally, we obtain the following estimate, which is a discrete analogue of the conservation of the total energy.

Theorem 1.4.1 (Unconditional stability of the scheme)
Let us suppose that the discrete heat diffusion operator satisfies the monotonicity property (1.30), that the equation of state satisfies (1.8), and that the initial conditions for ρ and e are positive. Then, for $0 \leq n \leq N-1$, a solution to the scheme (1.11) satisfies $\rho^{n+1} > 0$, $e^{n+1} > 0$ and the following estimate:

$$\sum_{K\in\mathcal{M}} |K|\ \rho_K^{n+1} e_K^{n+1} + \frac{1}{2}\sum_{i=1}^{d}\sum_{\sigma\in\mathcal{E}_{\mathcal{S}}^{(i)}} |D_\sigma|\ \rho_{D_\sigma}^n\ (u_{\sigma,i}^{n+1})^2 + \frac{\delta t^2}{2}\ |p^{n+1}|^2_{\rho^n,\mathcal{M}}$$
$$\leq \sum_{K\in\mathcal{M}} |K|\ \rho_K^n e_K^n + \frac{1}{2}\sum_{i=1}^{d}\sum_{\sigma\in\mathcal{E}_{\mathcal{S}}^{(i)}} |D_\sigma|\ \rho_{D_\sigma}^{n-1}\ (u_{\sigma,i}^{n})^2 + \frac{\delta t^2}{2}\ |p^{n}|^2_{\rho^{n-1},\mathcal{M}} \quad (1.36)$$

where, for any discrete pressure q and density ρ,

$$|q|^2_{\rho,\mathcal{M}} = \sum_{\sigma=K|L\in\mathcal{E}_{\rm int}} \frac{1}{\rho_{D_\sigma}}\ \frac{|\sigma|^2}{|D_\sigma|}\ (q_L - q_K)^2.$$

Proof. Since the initial condition for ρ and e are assumed to be positive, by induction, the positivity of the density is ensured by the upwind discretization of the scheme, and the positivity of the internal energy follows from Lemma 1.4.3. Summing the discrete internal energy equation (1.11e) over the cells $K \in \mathcal{M}$, we obtain, by conservativity of the diffusion fluxes:

$$\sum_{K\in\mathcal{M}} \frac{|K|}{\delta t}\ \left[\rho_K^{n+1}\, e_K^{n+1} - \rho_K^n\, e_K^n\right] + \sum_{K\in\mathcal{M}} |K|\ p_K^{n+1}\ \mathrm{div}_K(\boldsymbol{u}^{n+1})$$
$$= \sum_{K\in\mathcal{M}} |K|\ (\boldsymbol{\tau}(\tilde{u}^{n+1}) : \boldsymbol{\nabla}\tilde{\boldsymbol{u}}^{n+1})_K + S_K^{n+1}.$$

On the other hand, summing over the edges and the components i the equation of discrete kinetic energy balance (1.31) yields, by conservativity of the convection flux of the kinetic energy:

$$\frac{1}{2}\sum_{i=1}^{d}\sum_{\sigma\in\mathcal{E}_{\mathcal{S}}^{(i)}} \Big[\frac{|D_\sigma|}{\delta t}\Big(\rho_{D_\sigma}^n (u_{\sigma,i}^{n+1})^2 - \rho_{D_\sigma}^{n-1}(u_{\sigma,i}^n)^2\Big) + |D_\sigma|\ \boldsymbol{\nabla}_{\sigma,i}(p^{n+1})\ u_{\sigma,i}^{n+1} + P_{\sigma,i}^{n+1} - P_{\sigma,i}^n\Big]$$
$$= \sum_{i=1}^{d}\sum_{\sigma\in\mathcal{E}_{\mathcal{S}}^{(i)}} \Big[|D_\sigma|\,\mathrm{div}_{\sigma,i}\,\boldsymbol{\tau}(\tilde{\boldsymbol{u}}^{n+1})\ \tilde{u}_{\sigma,i}^{n+1} - R_{\sigma,i}^{n+1}\Big].$$

Summing these two relations and using the $\boldsymbol{\nabla} - \mathrm{div}$ duality property (1.19), the consistency property (1.22) of the viscous diffusion and dissipation terms, the fact that the residual term in the kinetic energy balance and the corrective term in the internal energy equation are designed to compensate themselves (Equation (1.34)) and the definition (1.32) of $P_{\sigma,i}^{n+1}$ concludes the proof. □

1.4.2 Existence of a discrete solution

We recall the following theorem, which is a consequence of the topological degree theory (see *e.g.* [18]), and which is a very powerful tool for the proof of existence of a solution to non-linear systems arising from the discretization of non-linear partial differential equations.

Theorem 1.4.2 (Application of the topological degree, finite dimensional case)
Let V be a finite dimensional vector space on $\mathbb{R}$, $\|.\|$ a norm on V, let f be a continuous function from V to V and let $R > 0$. Let us assume that there exists a continuous function $\mathcal{F} : V \times [0,1] \to V$ satisfying:

(i) $\mathcal{F}(.,1) = f$,

(ii) $\forall \alpha \in [0,1]$, if $v \in V$ is such that $\mathcal{F}(v,\alpha) = 0$ then $v \in B_R = \{v \in V\ ; \|v\| < R\}$,

(iii) the topological degree of $\mathcal{F}(.,0)$ with respect to 0 and to B_R is equal to $d_0 \neq 0$.

Then the topological degree of $\mathcal{F}(.,1)$ with respect to 0 and to B_R is also equal to $d_0 \neq 0$; consequently, there exists at least a solution $v \in B_R$ such that $f(v) = 0$.

Theorem 1.4.3
Under the assumptions of Theorem 1.4.1, there exists a solution to the scheme (1.11).

Proof. Let us begin with the velocity prediction step. The step is a linear system of unknown $\tilde{\boldsymbol{u}}$ and, applying Lemma 1.4.2 with $\psi(s) = s^2$ to each component of the velocity yields:

$$\frac{1}{2}\sum_{i=1}^{d}\sum_{\sigma\in\mathcal{E}_{\mathcal{S}}^{(i)}}\Big[\frac{|D_\sigma|}{\delta t}\,\rho_{D_\sigma}^{n}(\tilde{u}_{\sigma,i}^{n+1})^2 - |D_\sigma|\ \mathrm{div}_{\sigma,i}\,\boldsymbol{\tau}(\tilde{\boldsymbol{u}}^{n+1})\ \tilde{u}_{\sigma,i}^{n+1}\Big]$$

$$\leq \sum_{i=1}^{d}\sum_{\sigma\in\mathcal{E}_{\mathcal{S}}^{(i)}}\Big[|D_\sigma|\ \rho_{D_\sigma}^{n-1}(u_{\sigma,i}^{n})^2 - |D_\sigma|\ \overline{\boldsymbol{\nabla}}_{\sigma,i}(p^{n+1})\ \tilde{u}_{\sigma,i}^{n+1}.\Big]$$

Since $\rho^n > 0$ and the sum associated to the viscous diffusion (which is equal, by construction, to the integral of the viscous dissipation over the domain) is non-negative, this relation yields an estimate for $\tilde{\boldsymbol{u}}^{n+1}$ by the Young's inequality. The system thus has one and only one solution.

Let us now define $M \in \mathbb{N}$ and $X \in \mathbb{R}^M$ by:

$$M = \sum_{i=1}^{d}\mathrm{card}(\mathcal{E}_{\mathcal{S}}^{(i)}) + 2\mathrm{card}(\mathcal{M}),\ X = \big((u_{\sigma,i}^{n+1})_{\sigma\in\mathcal{E}_{\mathcal{S}}^{(i)},\,1\leq i\leq d},\ (\rho_K^{n+1})_{K\in\mathcal{M}},\ (\rho_K^{n+1}e_K^{n+1})_{K\in\mathcal{M}}\big).$$

Let $\mathcal{F} : \mathbb{R}^M \times [0,1] \longrightarrow \mathbb{R}^M$ be the continuous function defined by

$$\mathcal{F}(X,\alpha) = \big((\mathcal{F}_{\sigma,i}^{u})_{\sigma\in\mathcal{E}_{\mathcal{S}}^{(i)},\,1\leq i\leq d},\ (\mathcal{F}_K^{\rho})_{K\in\mathcal{M}},\ (\mathcal{F}_K^{e})_{K\in\mathcal{M}}\big)$$

with:

$$\forall \sigma \in \mathcal{E}_{\mathcal{S}}^{(i)},\ 1 \le i \le d, \qquad \mathcal{F}_{\sigma,i}^{u} = \frac{1}{\delta t}\rho_{D_\sigma}^{n}(u_{\sigma,i}^{n+1} - \tilde{u}_{\sigma,i}^{n+1}) + \alpha\ \boldsymbol{\nabla}_{\sigma,i}(p^{n+1}) - \overline{\boldsymbol{\nabla}}_{\sigma,i}(p^{n+1}),$$

$$\forall K \in \mathcal{M}, \qquad \mathcal{F}_{K}^{\rho} = \frac{1}{\delta t}(\rho_K^{n+1} - \rho_K^{n}) + \alpha \mathrm{div}_K(\rho^{n+1}\boldsymbol{u}^{n+1}),$$

$$\forall K \in \mathcal{M}, \qquad \mathcal{F}_{K}^{e} = \frac{1}{\delta t}(\rho_K^{n+1}e_K^{n+1} - \rho_K^{n}e_K^{n}) - \big(\boldsymbol{\tau}(\tilde{\boldsymbol{u}}^{n+1}) : \boldsymbol{\nabla}\tilde{\boldsymbol{u}}^{n+1}\big)_K - S_K^{n+1}$$
$$+ \alpha\ \Big[\mathrm{div}_K(\rho^{n+1}e^{n+1}\boldsymbol{u}^{n+1}) + p_K^{n+1}\ \mathrm{div}_K(\boldsymbol{u}^{n+1}) - \lambda\ (\Delta e^{n+1})_K\Big],$$

where, $\forall K \in \mathcal{M}$, $p_K^{n+1} = \wp\big(\rho_K^{n+1}, e_K^{n+1}\big)$. The system of equations $\mathcal{F}(X,1) = 0$ corresponds to the correction step. The function $X \mapsto \mathcal{F}(X,0)$ is linear (note that ρ^n, $\tilde{\boldsymbol{u}}^{n+1}$, $\overline{\boldsymbol{\nabla}}(p^{n+1})$ and S^{n+1} are known quantities) and one to one. In addition, the positivity of ρ^{n+1} and e^{n+1} solution to $\mathcal{F}(X,\alpha) = 0$ is preserved for $\alpha \in [0,1]$, by the same arguments as for the scheme itself (*cf.* Theorem 1.4.1). By conservativity of the convection fluxes, the equation:

$$\begin{aligned} &\sum_{K\in\mathcal{M}} |K|\mathcal{F}_K^{\rho} = 0 \\ \Leftrightarrow\quad &\sum_{K\in\mathcal{M}} \frac{|K|}{\delta t}(\rho_K^{n+1} - \rho_K^{n}) = 0, \end{aligned}$$

yields a uniform (with respect to α) bound for ρ^{n+1} (for any norm, since we are in finite dimension). Let us now consider the equation:

$$\begin{aligned} &\sum_{i=1}^{d}\sum_{\sigma\in\mathcal{E}_{\mathcal{S}}^{(i)}} D_\sigma u_{\sigma,i}^{n+1}\mathcal{F}_{\sigma,i}^{u} + \sum_{K\in\mathcal{M}} |K|\mathcal{F}_K^{e} = 0 \\ \Leftrightarrow\quad &\sum_{i=1}^{d}\sum_{\sigma\in\mathcal{E}_{\mathcal{S}}^{(i)}} D_\sigma u_{\sigma,i}^{n+1}\Big[\frac{1}{\delta t}\rho_{D_\sigma}^{n}(u_{\sigma,i}^{n+1} - \tilde{u}_{\sigma,i}^{n+1}) + \alpha\big(\boldsymbol{\nabla}_{\sigma,i}(p^{n+1}) - \overline{\boldsymbol{\nabla}}_{\sigma,i}(p^{n+1})\big)\Big] \\ &\qquad + \sum_{K\in\mathcal{M}} |K|\Big[\frac{1}{\delta t}(\rho_K^{n+1}e_K^{n+1} - \rho_K^{n}e_K^{n}) - \big(\boldsymbol{\tau}(\tilde{\boldsymbol{u}}^{n+1}) : \boldsymbol{\nabla}(\tilde{\boldsymbol{u}}^{n+1})\big)_K - S_K^{n+1} \\ &\qquad\qquad +\alpha\big(\mathrm{div}_K(\rho^{n+1}e^{n+1}\boldsymbol{u}^{n+1}) + p_K^{n+1}\mathrm{div}_K(\boldsymbol{u}^{n+1}) - \lambda(\Delta e^{n+1})_K\big)\Big] = 0. \end{aligned}$$

Thanks to the conservativity of the diffusion and convection fluxes,

$$\sum_{K\in\mathcal{M}} |K|\mathrm{div}_K(\rho^{n+1}e^{n+1}\boldsymbol{u}^{n+1}) = \sum_{K\in\mathcal{M}} |K|\lambda(\Delta e^{n+1})_K = 0,$$

the $\boldsymbol{\nabla}$-div duality argument (1.19) reads:

$$\sum_{K\in\mathcal{M}} |K|\ p_K^{n+1}\mathrm{div}_K(\boldsymbol{u}^{n+1}) + \sum_{i=1}^{d}\sum_{\sigma\in\mathcal{E}_{\mathcal{S}}^{(i)}} |D_\sigma| u_{\sigma,i}^{n+1}\boldsymbol{\nabla}_{\sigma,i}(p^{n+1}) = 0,$$

and since, as mentioned above, ρ^n, $\tilde{\boldsymbol{u}}^{n+1}$, $\overline{\boldsymbol{\nabla}}(p^{n+1})$ and S^{n+1} are known quantities, we rewrite the last relation:

$$\frac{D_\sigma}{\delta t}\sum_{i=1}^{d}\sum_{\sigma\in\mathcal{E}_{\mathcal{S}}^{(i)}} u_{\sigma,i}^{n+1}\Big[\rho_{D_\sigma}^{n}(u_{\sigma,i}^{n+1} - \tilde{u}_{\sigma,i}^{n+1})\Big] + \frac{|K|}{\delta t}\sum_{K\in\mathcal{M}} \rho_K^{n+1}e_K^{n+1} \le C,$$

where the bound C only depends on known quantities (and is independent of α). Invoking the identity $2a(a-b) = a^2 + (a-b)^2 - b^2$, we obtain:

$$\frac{D_\sigma}{2\delta t} \sum_{i=1}^{d} \sum_{\sigma \in \mathcal{E}_S^{(i)}} \rho_{D_\sigma}^n (u_{\sigma,i}^{n+1})^2 + \frac{|K|}{\delta t} \sum_{K \in \mathcal{M}} \rho_K^{n+1} \, e_K^{n+1} \leq C',$$

where C' is still a constant that only depends on known quantities and independent of α. Since ρ^{n+1} and e^{n+1} are positive and ρ^{n+1} bounded, we thus get a uniform bound on $\boldsymbol{u}^{n+1}$ and thus on X. Hence Theorem 1.4.2 applies (with $V = \mathbb{R}^M$ and $\|.\|$ the uniform norm), and the correction step admits at least one solution. This concludes the proof. □

1.5 Numerical tests

We present in this section numerical tests, to assess the behaviour of the scheme. We begin with a convergence study, on a two-dimensional analytical solution (Section 1.5.1). Then we address the limiting cases which the scheme should be able to cope with, namely the computation of high speed inviscid flows and of low Mach number viscous flows. Consequently, sections 1.5.2, 1.5.3 and 1.5.4 are dedicated to classical benchmarks for Euler solvers, while we compute in the first part of Section 1.5.5 an (almost) incompressible flow around a cylinder. Since the three first Euler tests are performed with the MAC space discretization, we continue this study in the remaining of Section 1.5.5 by computing a high speed viscous flow on a general geometry (with the Rannacher-Turek space discretization), obtained by keeping the same domain as in the previous incompressible case and decreasing the pressure range (and thus the range of the speed of sound) up to get a supersonic flow. Finally, we address a three dimensional inviscid case in Section 1.5.6.

For all the following test-cases, the fluid is supposed to obey the equation of state:

$$p = (\gamma - 1)\, \rho\, e, \qquad \text{with } \gamma = 1.4.$$

Computations are performed with the software component library CALIF^{3}S, developed at IRSN [6].

1.5.1 A convergence study

In this section, we compare the numerical results obtained by implementing the above algorithm in CALIF^{3}S with an analytical solution. This latter is built as follows: we first derive an exact analytical solution to stationary Euler equations, by extending to compressible flows the classical test for incompressible flows often referred to as the "standing-vortex" problem; then the diffusion in the momentum balance equation and in the energy balance, and the viscous dissipation in this latter equation are dealt with by a compensation at the right-hand side; finally, the problem is made unstationary by a time translation (*i.e.*, given a constant vector field $\boldsymbol{a}$, the density ρ, the internal energy e and the velocity $\boldsymbol{v}$ are deduced from the steady state solution $\hat{\rho}$, $\hat{e}$ and $\hat{\boldsymbol{v}}$ by $\rho(\boldsymbol{x}, t) = \hat{\rho}(\boldsymbol{x} - \boldsymbol{a}t)$, $e(\boldsymbol{x}, t) = \hat{e}(\boldsymbol{x} - \boldsymbol{a}t)$ and $\boldsymbol{v}(\boldsymbol{x}, t) = \hat{\boldsymbol{v}}(\boldsymbol{x} - \boldsymbol{a}t) + \boldsymbol{a}$; the change of variable $\boldsymbol{x} = \hat{\boldsymbol{x}} - \boldsymbol{a}t$ is also performed on the right hand sides).

By construction, the velocity field is divergence-free, without consequence on the convergence study (this specificity is not seen by the scheme whose solution is not discretely divergence-free); in addition, letting the sound speed tend to infinity (*i.e.* the Mach number tend to zero), we obtain a problem which tends to an incompressible flow problem. This allows us to check the behaviour of the scheme in the zero Mach number limit. We therefore address four problems: Euler or Navier-Stokes equations, for a Mach number in the range of unity and in the range of 10^{-3}.

Steady solution to the Euler equations – As in the standing-vortex problem, we search for a velocity perpendicular to the position vector $\boldsymbol{x} = (x, y)$, with a magnitude only depending on the radius:

$$\boldsymbol{u}(\boldsymbol{x}) = \begin{bmatrix} u_1 \\ u_2 \end{bmatrix} = f(\xi) \begin{bmatrix} -y \\ x \end{bmatrix},$$

where $\xi = |\boldsymbol{x}|^2 = (x^2 + y^2)^2$. Since this velocity field is divergence-free, we have, for $i = 1,\ 2$,

$$\mathrm{div}(\rho u_i \boldsymbol{u}) = \boldsymbol{u} \cdot \boldsymbol{\nabla}(\rho u_i) = \rho \boldsymbol{u} \cdot \boldsymbol{\nabla} u_i + u_i \boldsymbol{u} \cdot \boldsymbol{\nabla}\rho.$$

Choosing $\rho = \varrho(\xi)$, we observe that

$$\mathrm{div}(\rho \boldsymbol{u}) = \boldsymbol{u} \cdot \boldsymbol{\nabla}\rho = 0,$$

and the mass balance equation is thus satisfied. In addition, $\mathrm{div}(\rho u_i \boldsymbol{u}) = \rho \boldsymbol{u} \cdot \boldsymbol{\nabla} u_i$, and an easy computation yields:

$$\rho \begin{bmatrix} \boldsymbol{u} \cdot \boldsymbol{\nabla} u_1 \\ \boldsymbol{u} \cdot \boldsymbol{\nabla} u_2 \end{bmatrix} = -\varrho(\xi)\ f(\xi)^2 \begin{bmatrix} x \\ y \end{bmatrix}$$

Let us now suppose that the pressure reads $p = g(\xi)$. We thus have:

$$\boldsymbol{\nabla} p = 2g'(\xi) \begin{bmatrix} x \\ y \end{bmatrix}.$$

The momentum balance equation is therefore satisfied provided that

$$g' = \frac{1}{2}\rho f^2,\ \text{so}\ g(\xi) = p_0 + \frac{1}{2}\int_0^\xi \varrho(s)\, f(s)^2\, \mathrm{d}s,$$

with p_0 a given pressure. Finally, the equation of state yields $e = p/((\gamma - 1)\rho)$, thus e is a function of ξ only, and we have:

$$\mathrm{div}(\rho e \boldsymbol{u}) + p\, \mathrm{div}\boldsymbol{u} = \boldsymbol{u} \cdot \boldsymbol{\nabla}(\rho e) + p\, \mathrm{div}\boldsymbol{u},$$

and both terms vanish since $\boldsymbol{\nabla}(\rho e)$ is normal to $\boldsymbol{u}$ and $\mathrm{div}\boldsymbol{u} = 0$, which shows that the energy balance is satisfied.

Numerical tests – We choose for f and ϱ the following functions:

$$f(\xi) = \left| \begin{array}{l} 40\ \xi^2\,(1-\xi)^2 \text{ if } \xi \le 1 \\ 0 \text{ otherwise} \end{array} \right. , \qquad \varrho = 1 + f,$$

so the vortex is local (*i.e.* of finite spatial extension) and both functions are in $\mathrm{H}^2(\Omega)$. The center of the vortex is initially located at $\boldsymbol{x}_0 = (0, 0)^t$, the translation velocity $\boldsymbol{a}$ is set to $\boldsymbol{a} = (1, 1)^t$ and $\Omega = (-1.5,\ 2.5)^2$. The range of variation of each unknown is $\rho \in [1,\ 3.5]$, $v_i \in [-0.8,\ 2.8]$ for $i = 1, 2$ and $p \in [p_0,\ p_0 + 3.93]$. The final time is $t = 1$, and the solution is constant over the boundary all over the computational interval, and thus may be fixed to this value if the diffusion is taken into account (for the Euler equations, the normal velocity is set to zero, and so are all the convection fluxes; since the pressure gradient operator is built as the transposed of the divergence, it vanishes on the boundaries). The considered meshes are $n \times n$ grids, with $n \in \{80,\ 160,\ 320,\ 640,\ 1280\}$, and the time step is $\delta t = 0.01 \times 80/n$, so the CFL number is constant, and close to 2 (with a CFL number related to the material velocity only, defined by CFL$=(\rho|\boldsymbol{u}|\,\delta t)/h$). The space discretization is performed with the MAC scheme.

Two tests are performed or the full Navier-Stokes equations with diffusion coefficients equal to $\mu = 0.1$ and $\lambda = 0.1\,\gamma$: in the first one, $p_0 = 10$, so the celerity of sound waves is close to 4 and

the maximum Mach number is close to 0.75; in the second one, $p_0 = 10^5$, so the Mach number is everywhere lower than 0.01.

Then we turn to the Euler equations, still with $p_0 = 10$ and $p_0 = 10^5$. For these two tests, a numerical viscosity μ_h is added to compensate the fact that we use a centered discretization in the convection term of the momentum balance equation. The quantity μ_h scales as the space step and is taken equal to $\mu = 0.01 * 80/n$, so close to $(\rho|\boldsymbol{u}|)_{\max} h/50$ where $(\rho|\boldsymbol{u}|)_{\max}$ stands for the maximum value of the quantity $\rho|\boldsymbol{u}|$; this value has to be compared with the range of the numerical viscosity which would be induced by an upwind discretization, which reads $\rho|\boldsymbol{u}|h/2$. Since this diffusion is a numerical artefact, no compensating term is added at the right hand side of the momentum and energy balance (contrary to what is done in the Navier-Stokes case). The transport of the internal energy is performed with an upwind discretization, so no stabilization has to be added (*i.e.* $\lambda = 0$).

On Figure 1.8, we plot the difference between the computed and the analytical solution at $t = 1$, as a function of the time and space step. This difference is evaluated in discrete L^2-norm, defined for both a regular and a discrete function ξ by:

$$||\xi|| = \Big(\sum_{K \in \mathcal{M}} |K| \; \xi(\boldsymbol{x}_K)^2 \Big)^{1/2},$$

where, for $K \in \mathcal{M}$, $\boldsymbol{x}_K$ stands for the mass center of K. There errors are normalized with respect to the error found for $n = 80$. We observe a very similar convergence for the two considered values of the Mach number, both in the Navier-Stokes and Euler case. For diffusive cases, the order of convergence is close to one; it is slightly lower (close to 0.8) without diffusion.

1.5.2 The Mach 3 facing step

We begin with a classical benchmark popularized in [81]. The computational domain is $\Omega = \overline{\Omega} \setminus \mathcal{S}$, where $\overline{\Omega} = (0,\, 3) \times (0,\, 1)$ and $\mathcal{S} = (0.6,\, 3) \times (0,\, 0.2)$, and the computation time interval is $(0,\, 0.25)$. The flow enters the domain through the left boundary $\{0\} \times (0, 1)$ with a velocity corresponding to Mach= 3:

$$\begin{bmatrix} \rho \\ \boldsymbol{u} \\ p \end{bmatrix} \big((0, x_2)^t, t \big) = \begin{bmatrix} 1.4 \\ (3, 0)^t \\ 1 \end{bmatrix}, \qquad \forall x_2 \in (0, 1), \; \forall t \in (0, 0.25).$$

The initial data is the same as the inflow conditions:

$$\begin{bmatrix} \rho \\ \boldsymbol{u} \\ p \end{bmatrix} (\boldsymbol{x}, 0) = \begin{bmatrix} 1.4 \\ (3, 0)^t \\ 1 \end{bmatrix}, \qquad \forall \boldsymbol{x} \in \Omega.$$

At the right boundary $\{3\} \times (0, 1)$, the flow should be free, since it leaves the domain at a velocity greater than the sound speed. However, at the discrete level, an external pressure p_{ext} is needed to evaluate the pressure gradient on the boundary faces; it is taken here at the same value as the pressure at the entrance of the domain, so $p_{\text{ext}} = 1$; we discuss later on the effects of this numerical artefact. An impermeability and perfect slip condition (*i.e.* $\boldsymbol{u} \cdot \boldsymbol{n} = 0$, with $\boldsymbol{n}$ the unit outward normal on $\partial\Omega$, and $\boldsymbol{\tau}(\boldsymbol{n}) \cdot \boldsymbol{t} = 0$ for any vector $\boldsymbol{t}$ such that $\boldsymbol{t} \cdot \boldsymbol{n} = 0$) is prescribed on the rest of the boundary. At $t = 0$, a shock is generated by this boundary condition at the flow-facing step, and then moves upflow, and reaches and reflects on the upper and lower horizontal boundaries of the domain.

We display on Figure 1.9 the results obtained with the MAC space discretization, with a mesh built from a 1200×400 uniform grid, by removing the cells included in $\mathcal{S}$. The time step is $\delta t = h/4 = 0.001$, which corresponds to a CFL number in the range of unity with respect to the celerity of the fastest

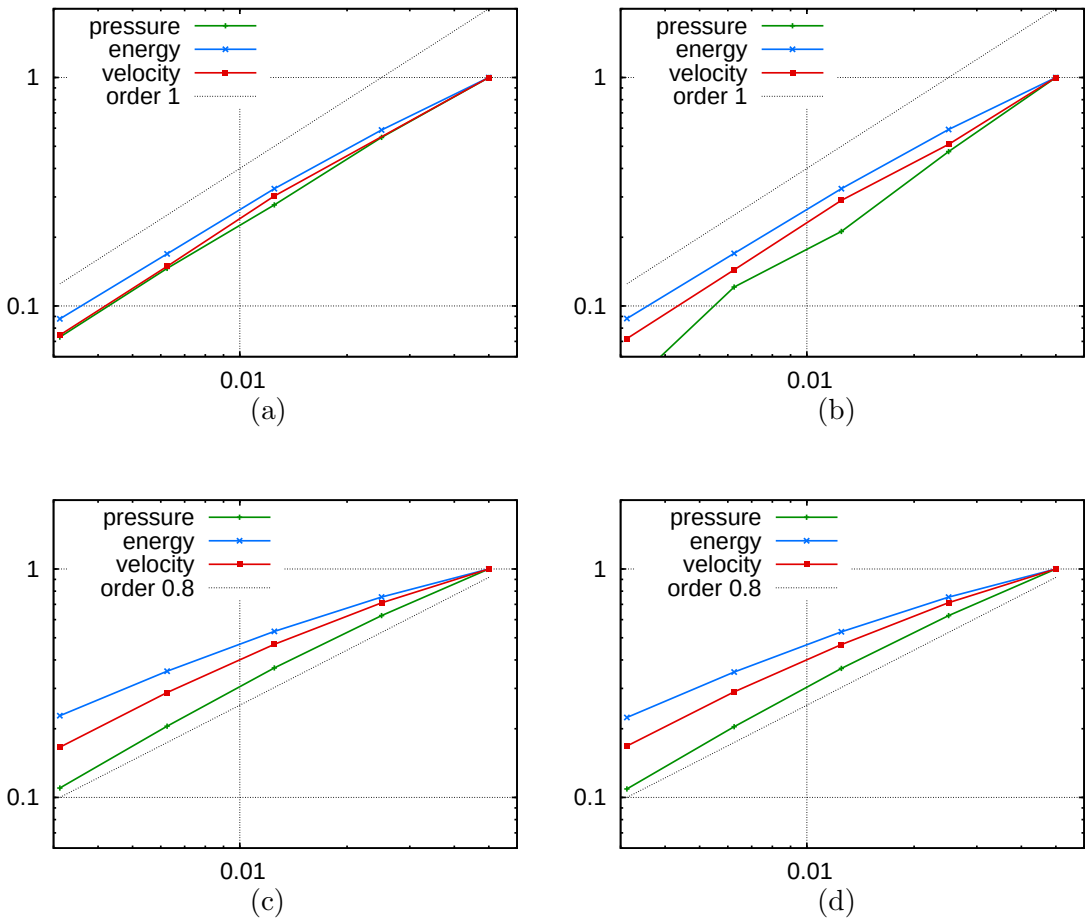

Figure 1.8: Numerical errors in the Navier-Stokes (plots (a) and (b)) and Euler cases (plots (c) and (d)), for a Mach number in the range of unity (plots (a) and (c)) or lower than 0.01 (plots (b) and (d)).

wave ($u_1 + c = 4$ at the inlet boundary, where c stands for the speed of sound). The artificial viscosity is set to $\mu = 0.001$, which roughly corresponds to a fifth of the numerical viscosity introduced by the classical upwinding $\mu_{\text{upw}} \simeq \rho\,|\boldsymbol{u}|\,h/2$ of the convection term.

At first glance, the results are comparable to those presented in the recent literature [12, 33, 82, 11]. As could be expected, the stability of the scheme seems to be paid by a greater diffusion: some authors observe a Kelvin-Helmholtz instability at the contact discontinuity line issued from the Mach triple point (whose occurrence, even in the absence of any shear-stress, is plausible, since the slip line is unstable) which does not appear here, and we also obtain a spurious Mach reflection at the bottom boundary, probably caused by perturbations issued from the step corner. One way to circumvent this problem would be to use (nonconforming) local mesh refinement; the development of such a scheme is underway.

Pressure correction schemes are known to generate spurious boundary conditions for the pressure, which, for the discretization used here, are implicit in the pressure elliptic operator in the correction step (see [15, Section 2.3] for a discussion on this topic, with the same space discretization as here but for the toy problem of the time-dependent incompressible Stokes equations, and Appendix 1.C of the present paper). For a free outlet boundary (as for a Neuman condition), the artificial boundary condition is a non-homogeneous Dirichlet boundary condition for the pressure, with the prescribed

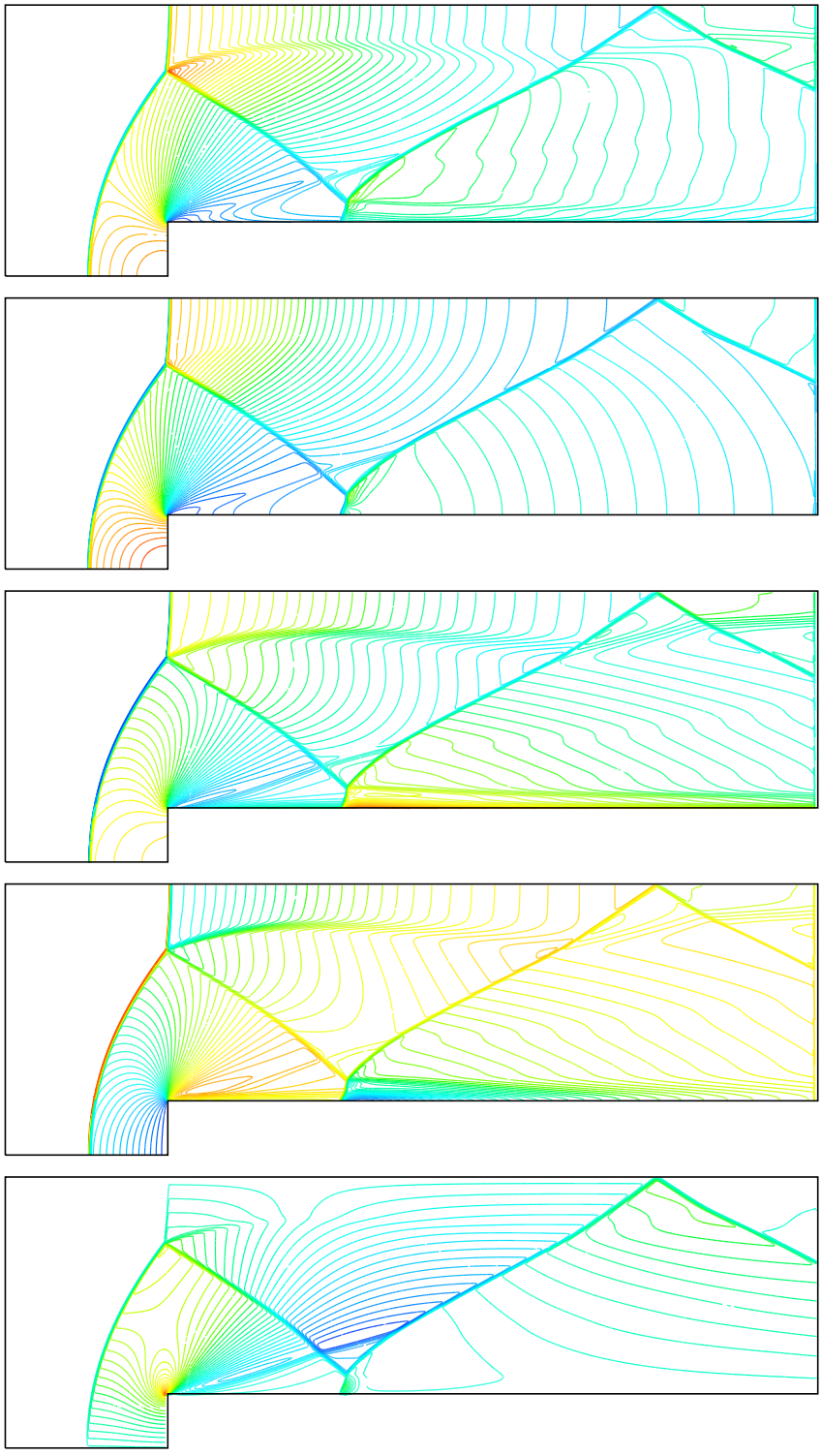

Figure 1.9: Mach 3 step – From top to bottom: density, pressure, enthalpy ($\mathcal{H} = e + p/\rho$), first and second component of the velocity at $t = 4$, obtained with $h = 2.5 \times 10^{-3}$, $\delta t = 10^{-3}$ and $\mu = 10^{-3}$. The variation intervals of the unknowns are $\rho \in [0.235,\ 6.4]$, $p \in [0.216,\ 12.04]$, $\mathcal{H} \in [2.46, 8.11]$, $u_1 \in [0.,\ 3.046]$, and $u_2 \in [-0.92,\ 1.82]$.

value p_{ext} corresponding to the external pressure used in the gradient approximation at the boundary faces. This boundary condition may be observed on Figure 1.9 to generate a very narrow boundary layer near the outlet section, but without any effect in the remainder of the domain. A similar behaviour was already observed for a similar scheme in the case of barotropic flows [49, Section 4].

1.5.3 The double Mach reflection

We now consider the classical test case (*e.g.* [33]) of a Mach=10 shock in air ($\gamma = 1.4$) impinging a wall with a 60° angle. The right state (pre-shock) initial conditions correspond to a fluid at rest and the left state is given by the Rankine-Hugoniot conditions, supposing that the velocity of the shock is $\omega = 10$ (while the speed of sound in the pre-shock state is $c = 1$, hence the denomination "Mach=10 shock"):

$$\begin{bmatrix} \rho_L \\ \boldsymbol{u}_L \\ p_L \end{bmatrix} = \begin{bmatrix} 8 \\ 8.25\ (\sqrt{3}/2, 1/2)^t \\ 116.5 \end{bmatrix}, \qquad \begin{bmatrix} \rho_R \\ \boldsymbol{u}_R \\ p_R \end{bmatrix} = \begin{bmatrix} 1.4 \\ (0,0)^t \\ 1 \end{bmatrix}.$$

The computational domain is $\Omega = (0,4) \times (0,1)$. The reflecting wall lies at the bottom of the domain and starts at $x_1 = 1/6$, i.e. impermeability and free slip boundary conditions are enforced on $\partial\Omega_r = (1/6, 4) \times \{0\}$ and outflow boundary conditions are prescribed at $\partial\Omega_o = (0, 1/6) \times \{0\}$. At $t = 0$, the shock impinges the reflecting wall (at $x_1 = 1/6$), so the fluid is in the left state for $x_1 \leq 1/6 + x_2/\sqrt{3}$ and in the right state in the rest of the domain. Then, in the zones of Ω which are not perturbed by the reflections, the shock moves with a velocity equal to $\omega\ (\sqrt{3}/2, -1/2)^t$. The external pressure at the outflow boundary $\partial\Omega_o$ is thus prescribed throughout the transient state to $p_L = 116.5$. On the top of the domain $(0,4) \times \{1\}$, the boundary condition is consistent to the undisturbed shock wave, thus the unknowns ρ, $\boldsymbol{u}$ and p are prescribed to the left state values for $x_1 \leq 1/6 + 1/\sqrt{3} + (2 * \omega/\sqrt{3})\ t$ and to the right state values on the other part of the boundary. Finally, on $\{4\} \times (0,1)$, the velocity is prescribed to $\boldsymbol{u}_R = (0,0)^t$.

We plot on Figure 1.11 the results obtained with the MAC scheme, for $t = 0.2$ with a 1600×400 grid (consisting of square cells) and a time step $\delta t = h/100$. The artificial viscosity is $\mu = 0.01$ (to be compared, for instance, with $\rho_L\, |\boldsymbol{u}_L|\, h/2 = 0.0825$). Once again, the results are comparable to those presented in the recent literature (*e.g.* [33]).

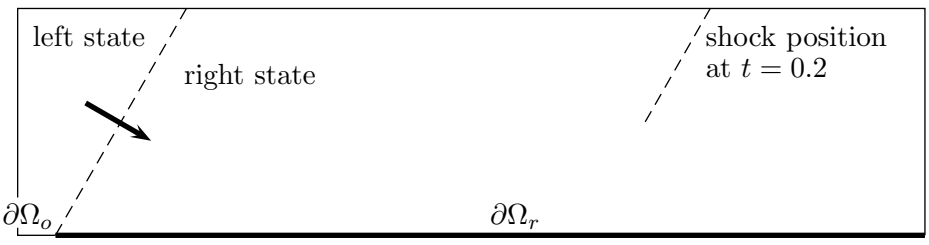

Figure 1.10: Double Mach reflection – Geometry and initial conditions.

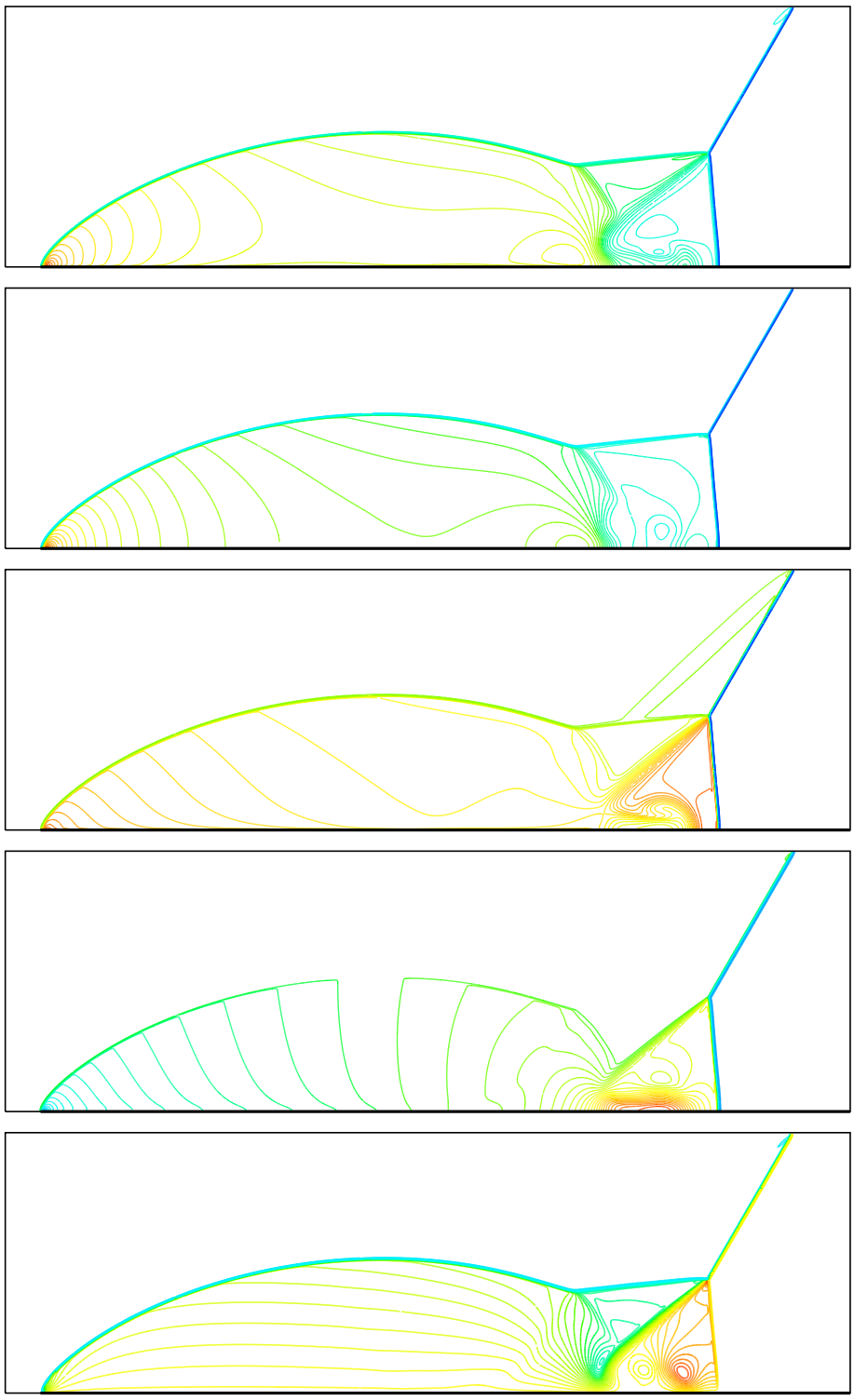

Figure 1.11: Double Mach reflection – From top left to bottom right: density, pressure, enthalpy ($\mathcal{H}$) and first and second component of the velocity at $t = 0.2$, obtained with $h = 2.5\ 10^{-3}$, $\delta t = 2.5\ 10^{-5}$ and $\mu = 0.01$. The variation ranges of the unknowns are $\rho \in [1.4,\ 22.4]$, $p \in [1,\ 559]$, $\mathcal{H} \in [2.5,\ 87.8]$, $u_1 \in [-1.74,\ 15.9]$, and $u_2 \in [-5.53,\ 1.74]$. A right part of the domain, where the solution is constant, is not drawn.

1.5.4 A two-dimensional Riemann problem

We address in this section a two-dimensional Riemann problem introduced in [71]. The computational domain is $\Omega = (-0.5, 0.5)^2$ and the initial data consists in four constant states, in each of the four sub-squares of Ω obtained by splitting it along the lines joining the mid-points of each segment of the boundary (*i.e.* in $\Omega_{1,1} = (-0.5, 0) \times (0, 0.5)$, $\Omega_{1,2} = (0, 0.5)^2$, $\Omega_{2,1} = (-0.5, 0)^2$ and $\Omega_{2,2} = (0, 0.5) \times (-0.5, 0)$). These constant states are chosen in such a way that each associated one-dimensional Riemann problem (*i.e.* each one-dimensional problem obtained by picking as left and right initial state the values of ρ, p in two adjacent sub-squares, together with the velocity component normal to the line separating these sub-squares) has for solution a single wave. The four constant states chosen here are:

$\Omega_{1,1}: \ \rho = 1, \ p = 1, \ \boldsymbol{u} = \begin{bmatrix} 0.7276 \\ 0 \end{bmatrix}$	$\Omega_{1,2}: \ \rho = 0.5313, \ p = 0.4, \ \boldsymbol{u} = \begin{bmatrix} 0 \\ 0 \end{bmatrix}$
$\Omega_{2,1}: \ \rho = 0.8, \ p = 1, \ \boldsymbol{u} = \begin{bmatrix} 0 \\ 0 \end{bmatrix}$	$\Omega_{2,2}: \ \rho = 1, \ p = 1, \ \boldsymbol{u} = \begin{bmatrix} 0 \\ 0.7276 \end{bmatrix}$

This configuration is referred to as the configuration 12 in [71]. Two shocks develop, the first one at the interface of $\Omega_{1,1}$ and $\Omega_{1,2}$ and the second one at the interface of $\Omega_{2,2}$ and $\Omega_{1,2}$; they move toward the right and the top of the domain, respectively. The other two interfaces (separating $\Omega_{2,1}$ from $\Omega_{1,2}$ and $\Omega_{2,2}$) do not move with time, and the tangential velocity is different on both sides of the interface; such an interface is called in [71] a slip line, and corresponds to a (steady) contact discontinuity of the system.

Results obtained with the MAC variant of the scheme, a 1000×1000 uniform grid, $\delta t = 2.5\,10^{-4}$ and an artificial viscosity fixed to $\mu = 5\,10^{-5}$ are shown on Figures 1.12 and 1.13. They are in good agreement with reference solutions (*e.g.* [71, 56, 51]). However, the used stabilization technique, namely adding a physical-like artificial diffusion term, generates shear-stress instabilities along the slip lines, as zoomed in Figure 1.13. This seems to be unavoidable, and more elaborate techniques are necessary to avoid this phenomenon. Note however that the solution is not destabilized (in particular, we do not observe the generation of spurious pressure waves polluting the solution in the whole domain). In addition, the problem of computing accurately a standing slip line may look rather academic, since actual difficulties appear when the slip line moves, *i.e.* when the (constant across the line) normal component of the velocity is not zero; up to our knowledge, avoiding significant perturbation of the solution in this latter case indeed remains a challenging issue for numerical Euler solvers (see Appendix 1.B).

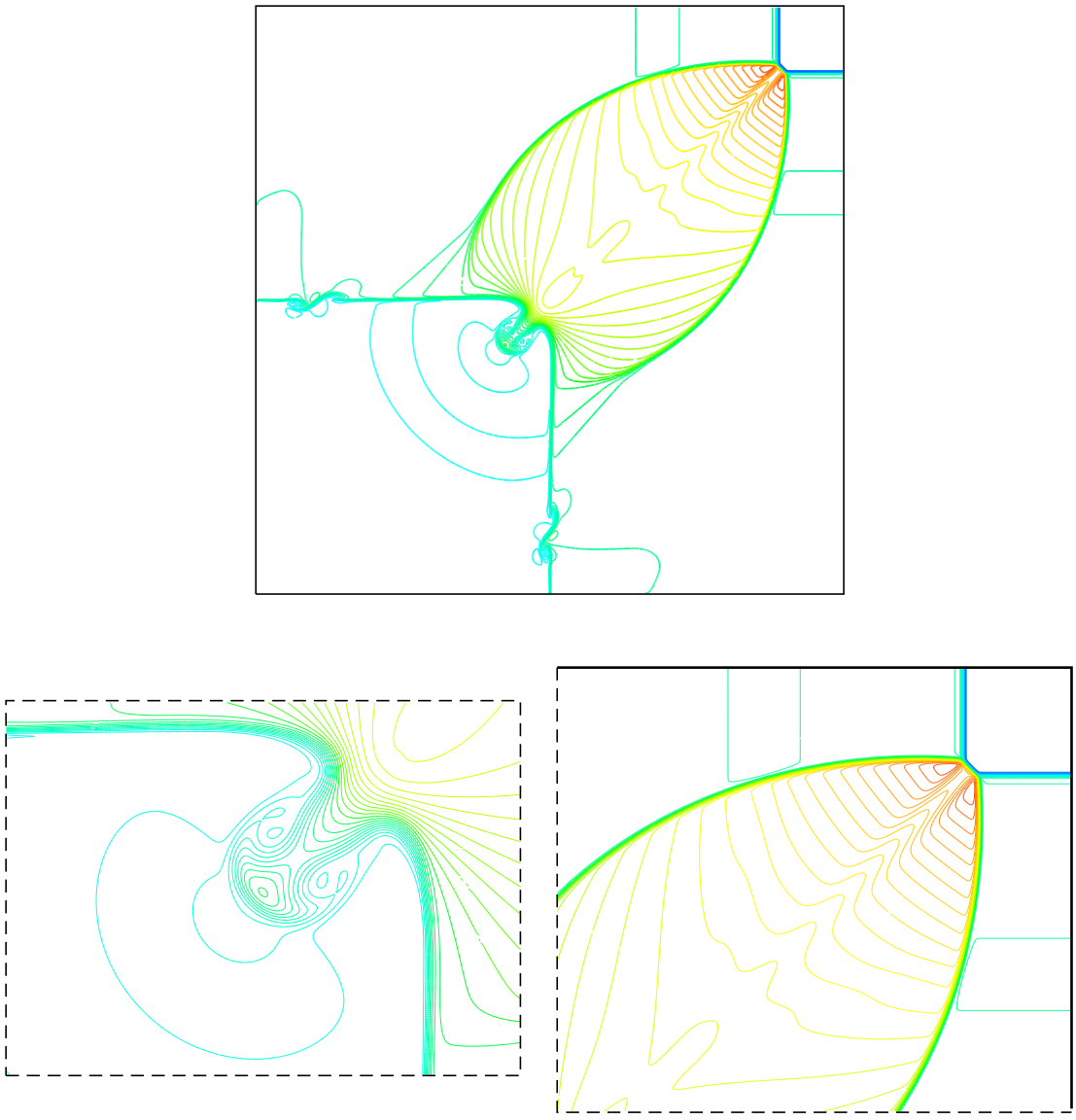

Figure 1.12: 2D Riemann problem – Isolines of the density in the domain, and zoom at the center and the upper right corner of the domain.

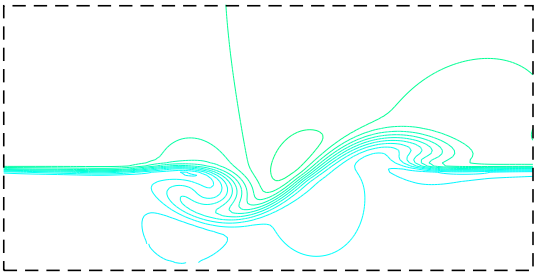

Figure 1.13: 2D Riemann problem – Isolines of the density along the horizontal slip line.

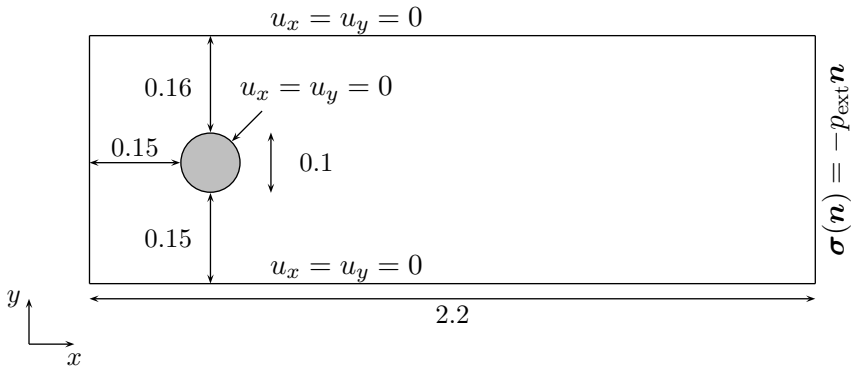

Figure 1.14: Low Mach flow past a cylinder – Geometry.

1.5.5 Navier-Stokes flows past a cylinder

We turn now to the Navier-Stokes equations, and first investigate the accuracy of the scheme in the quasi-incompressible limit. To this purpose, we consider a problem addressed as a benchmark for (incompressible) Navier-Stokes solvers in [70]. The problem is two-dimensionnal, and consists in a flow between two parallel plates past a cylindrical obstacle. The geometry of the problem is described in Figure 1.14. The fluid enters the domain on the left boundary, with an imposed velocity profile:

$$\boldsymbol{u} = \big(4u_m y \frac{H-y}{H}, 0\big)^t,$$

where $H = 0.41$ is the height of the channel and $u_m = 1.5$; the velocity is prescribed to zero at the other boundaries except for the right-hand side, where we use a Neuman boundary condition:

$$(\boldsymbol{\tau}(\boldsymbol{u}) - p\,\boldsymbol{I})\,\boldsymbol{n} = -p_{\text{ext}}\,\boldsymbol{n},$$

where p_{ext} stands for a given external pressure. The initial pressure and p_{ext} are set both to 10^5, and the initial density is $\rho = 1$. With these values, the sound speed $c = (\gamma p/\rho)^{1/2}$ is $c \simeq 370$, so the characteristic Mach number is close to 0.003. The viscosity is $\mu = 0.001$, so the Reynolds number, defined as $Re = \rho\bar{u}D/\mu$, where $D = 0.1$ is the diameter of the cylinder and $\bar{u} = 2u_x(0, H/2)/3$, is equal to 100.

A "coarse version" of the meshes used for the presented computation is sketched in Figure 1.15; real meshes are considerably refined with respect to this one, by diminishing the discretization step along the characteristic lines (the boundaries and the concentric circles around the cylinder). In all the computations, we set the time step to $\delta t = 5 \cdot 10^{-4} s$.

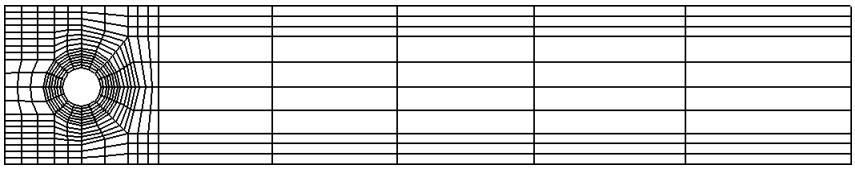

Figure 1.15: A "coarse version" of the mesh.

We observe in our computations the usual vortex-shedding phenomenon, well-known for incompressible flows (the so-called Von-Karmann alley), and the pressure and density show very small variations in space (the difference between the maximum and minimum value for the pressure and the density in the domain is in the range of 2 and 3.10^{-5} respectively). To assess in a quantitative way the accuracy of the results, we compute some characteristic flow quantities. The drag and lift coefficients, denoted by c_d and c_l respectively, are given by

$$c_d = \frac{2F_d}{\rho \bar{u}^2 D}\,, \qquad c_l = \frac{2F_l}{\rho \bar{u}^2 D},$$

where F_d and F_l are the drag and lift forces respectively:

$$F_d = \int_{\mathcal{D}} (\mu \frac{\partial u_t}{\partial n} n_y - p n_x)\, \mathrm{d}\gamma,, \qquad F_l = \int_{\mathcal{D}} (-\mu \frac{\partial u_t}{\partial n} n_x - p n_y)\, \mathrm{d}\gamma.$$

with $\mathcal{D}$ the disk surface, $\boldsymbol{n} = (n_x, n_y)^t$ its outward normal vector and u_t the velocity in the direction tangent to the disk, *i.e.* collinear to $\boldsymbol{t} = (n_y, -n_x)^t$. In Table 1.2 below, we denote by $c_{d,max}$ and $c_{l,max}$ the maximum absolute values of these coefficients. The Strouhal number is defined as $St = Df/\bar{u}$, where f is the frequency of separation, calculated directly from the period of F_l. We gather in Table 1.2 the obtained values for these parameters for different meshes, together with their plausible range derived from the set of the contributions to the benchmark [70]. Values entering this reference interval are typeset in bold. The present algorithm seems as accurate as the incompressible pressure-correction solver based on the same space discretization studied in [5].

Mesh	Space unks	$c_{d,max}$	$c_{l,max}$	St
m2	64840	3.4937	0.9141	0.2850
m3	215545	3.2887	0.9891	**0.2955**
m4	381119	3.2614	**1.0062**	**0.2972**
m5	531301	**3.2365**	**1.0148**	**0.2976**
Reference range		`3.22-3.24`	`0.99-1.01`	`0.295-0.305`

Table 1.2: Characteristic flow quantities.

We now turn to a compressible version of this test, with a high characteristic Mach number, close to Ma$=\sqrt{10}$. To this purpose, we set the initial pressure and the external pressure p_{ext} at the value $\gamma/10\,\rho$, so that the sound speed is now given by $c^2 = 0.1$. In this case, since the heating on the surface of the cylinder is important, we prescribe the internal energy at its inlet value at the surface of the disk, and fix the thermal conductivity of the fluid to $\lambda = 10^{-3}$. To avoid to complicate the flow structure near the domain boundaries, we impose an impermeability and perfect slip condition at

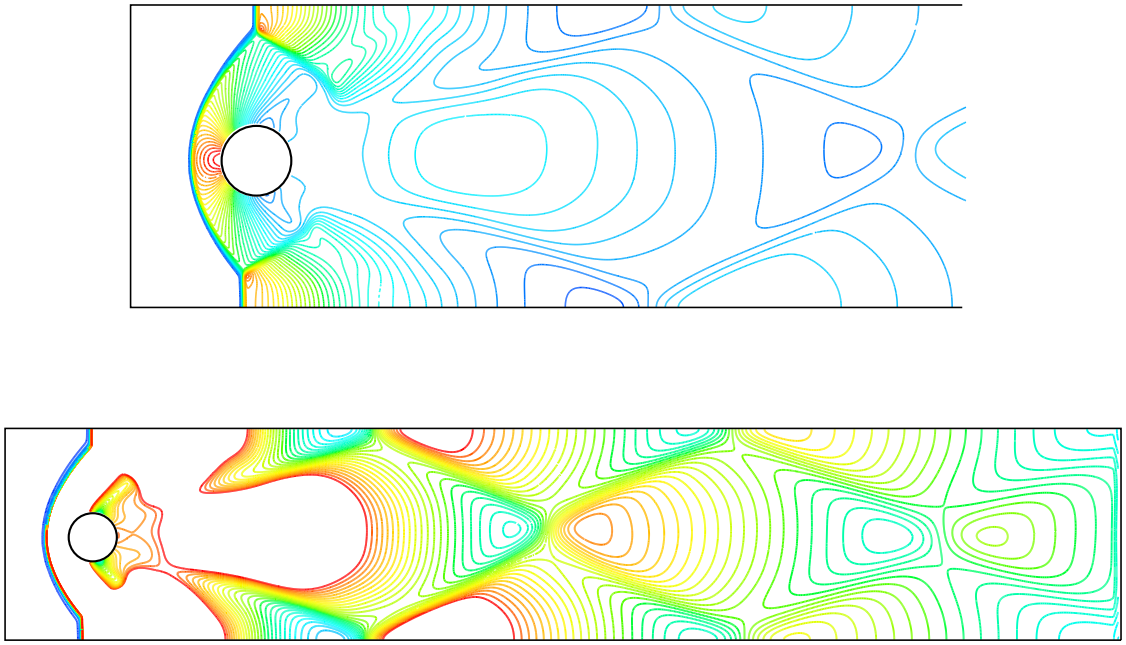

Figure 1.16: Mach=10 flow past a cylinder – Top: iso-lines of pressure near the disk ($p \in (0.0713,\ 0.957)$) at $t = 5$; bottom: still pressure iso-lines but on the whole computational domain, and restricted to the interval $(0.0713,\ 0.2)$) (so the areas left in white on the figure correspond to zones where $p > 0.2$).

the upper and lower boundaries and the inlet velocity is prescribed to a constant in space (and time) value $\boldsymbol{u} = (1, 0)^t$. The time step is $\delta t = 10^{-4}$. The rest of the configuration is unchanged, and the initial values are still the same as the inlet values.

Results obtained at $t = 5$ with a mesh of about 10^6 cells are shown on Figures 1.16 and 1.17. We observe a strong shock upstream the disk, with a Mach reflection at the upper and lower boundaries. Subsequent (downstream) reflections yield "*X-structures*" for the pressure field; they are progressively damped, both by the physical viscosity and (probably) by the scheme diffusion. As in the Euler case, the artificial boundary conditions imposed by the pressure correction technique to the pressure at the outlet section spoil the flow only on a narrow (numerical) boundary layer.

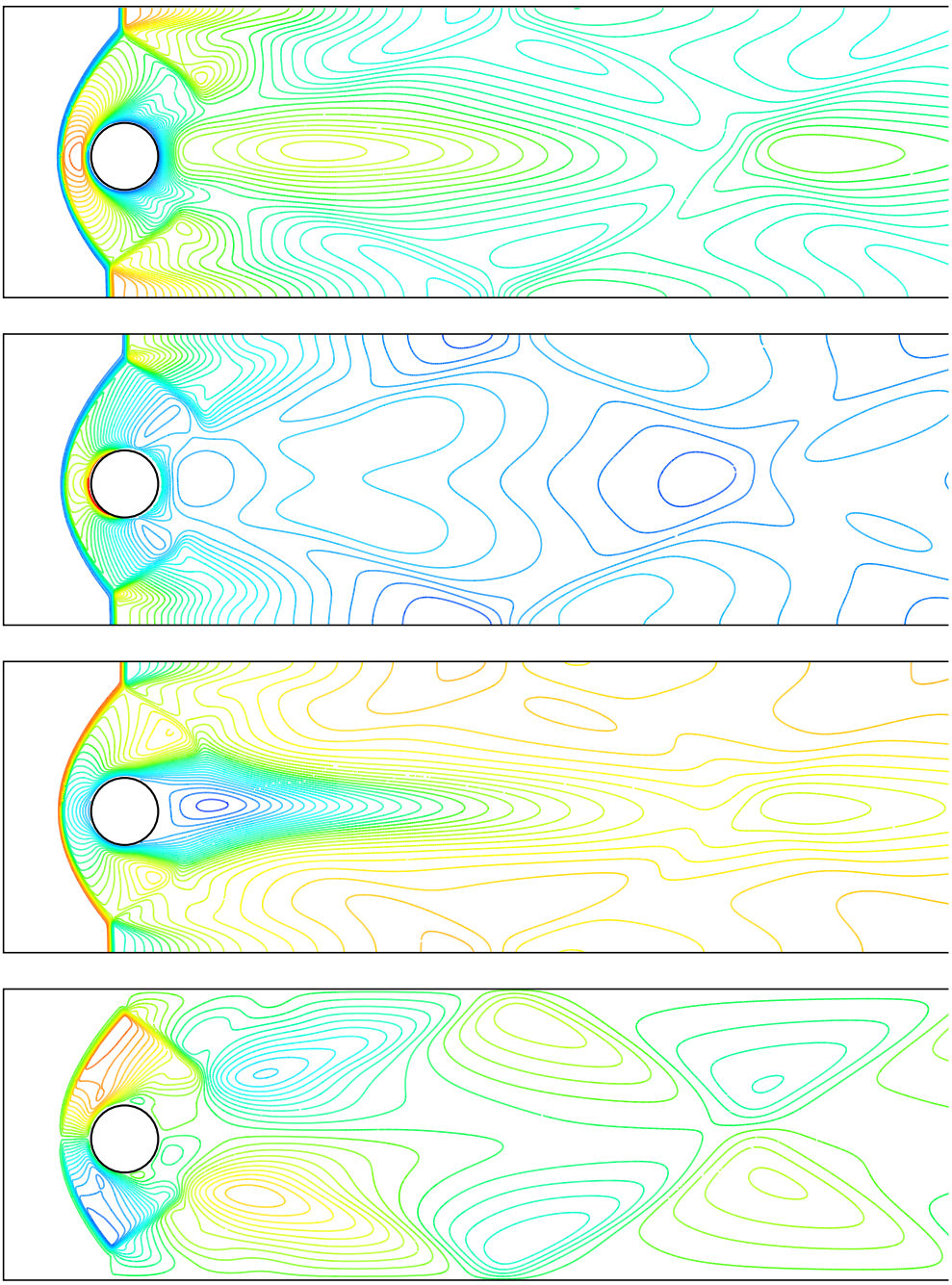

Figure 1.17: Mach=10 flow past a cylinder – From top to bottom: internal energy, density, x-component of velocity, y-component of velocity at $t = 5$. The variation ranges of the unknowns are $e \in [0.178,\ 0.536]$, $\rho \in [0.804,\ 12.23]$, $u_1 \in [-0.11,\ 1]$, and the value $u_1 = 0$ corresponds to the fourth iso-line starting from the center of the vortex attached to the cylinder, $u_2 \in [-0.326,\ 0.327]$.

1.5.6 Interaction of a shock and a cube

To conclude this section, we turn to a three-dimensional problem, which consists in the interaction of a shock wave and a cube. We consider the same pure shock wave as for the double Mach reflection problem, which now travels in the x_1-direction:

$$\begin{bmatrix} \rho_L \\ \boldsymbol{u}_L \\ p_L \end{bmatrix} = \begin{bmatrix} 8 \\ 8.25\ (1,0,0)^t \\ 116.5 \end{bmatrix}, \qquad \begin{bmatrix} \rho_R \\ \boldsymbol{u}_R \\ p_R \end{bmatrix} = \begin{bmatrix} 1.4 \\ (0,0,0)^t \\ 1 \end{bmatrix},$$

and $(\rho, \boldsymbol{u}, p) = (\rho_L, \boldsymbol{u}_L, p_L)$ (resp. $(\rho, \boldsymbol{u}, p) = (\rho_R, \boldsymbol{u}_R, p_R)$) for $x_1 \leq -1.3$ (resp. $x_1 \geq -1.3$). The obstacle is the cube $(-1, 1)^3$. Since the problem presents two symmetry planes, defined by $x_2 = 0$ and $x_3 = 0$ respectively, the chosen computational domain is $\Omega = (-3, 5) \times (0, 4) \times (0, 4)$. The cells are cubes of edges 0.02 long, which leads to a $400 \times 200 \times 200$ uniform grid from which the cells corresponding to the interior of the obstacle have been removed; the mesh finally includes 15 750 000 control volumes. The final time is $T = 0.6$ (remember that, in absence of obstacle, the shock speed is equal to 10, so the front location at the final time should be the plane $x_1 = 4.7$), and the chosen time step is $\delta t = 0.0005$, which corresponds to a CFL number close to 1/3 with respect to the maximum wave celerity in the left state ($c \simeq 4.5$). The MAC scheme is used for the space discretization, and the convection operator in the momentum balance equation is centered and stabilized with an artificial viscosity $\mu = 0.5$ (lower than the diffusion entailed by the classical upwinding $\rho\,|\boldsymbol{u}|\,h/2$ of this term, which is greater than 1 locally in space and time during the computation).

The obtained pressure field is shown on Figures 1.18 and 1.19. A strong reflection is observed on the obstacle: the maximum pressure rises to $p \simeq 900$ at the first reflections, and then progressively decreases to $p \simeq 500$. Then the pressure wave overpasses the obstacle, and a "shock-against-shock" recomposition is observed at a time close to $t = 0.45$ (first illustration on Figure 1.18) at the intersection of the symmetry planes, which leads to a maximum pressure close to the pressure observed on the left face of the obstacle, *i.e.* $p \simeq 500$; the pressure field at $t = 0.456$ on the plane $x_1 = 2$ (so at a distance of 1 after the obstacle) is shown on Figure 1.19. This recomposition leads to an irregular Mach reflection, which clearly appears later (second illustration on Figure 1.18, $t = 0.6$).

Since this test is representative of industrial applications, we give now some information about the numerical resolution. The computation is performed in parallel (the CALIF^{3}S software uses PETSc primitives) on an infiniband linux cluster and involves 60 Intel Xeon X5660 2.8GHz processors, for about 14 hours of restitution time. The solution of the linear system for the prediction step is performed with a GMRES algorithm, preconditioned on each subdomain by ILU0; the solution of the system takes about 1.5 hours (cumulated over the 1200 time steps), for about $47\,10^6$ unknowns (the degrees of freedom of the 3 components of the velocity, which are coupled in the same system, to allow the discretization of the viscous tensor under its general form, used here only for stabilization purposes). The correction step is solved by a Newton algorithm (see Appendix 1.C), which converges in 4 to 5 iterations. Each internal system is solved by the same GMRES solver as in the prediction step, with now about $30\,10^6$ unknowns (pressure and internal energy degrees of freedom), for a cumulated time close to 3.3 hours. The rest of the CPU time (about 8 hours) is used for the assembling of these systems.

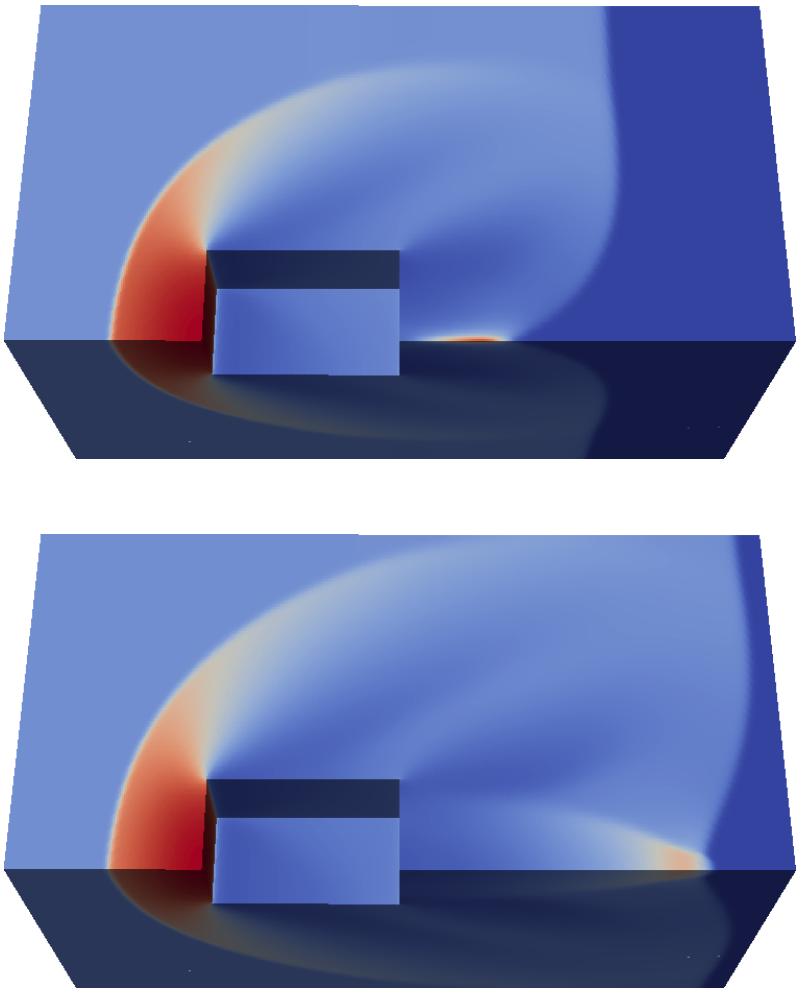

Figure 1.18: Interaction between a shock and a cube – Pressure on the symmetry planes $x_{=}20$ and $x_3 = 0$ at times $t = 0.456$ (top) and $t = 0.6$ (bottom).

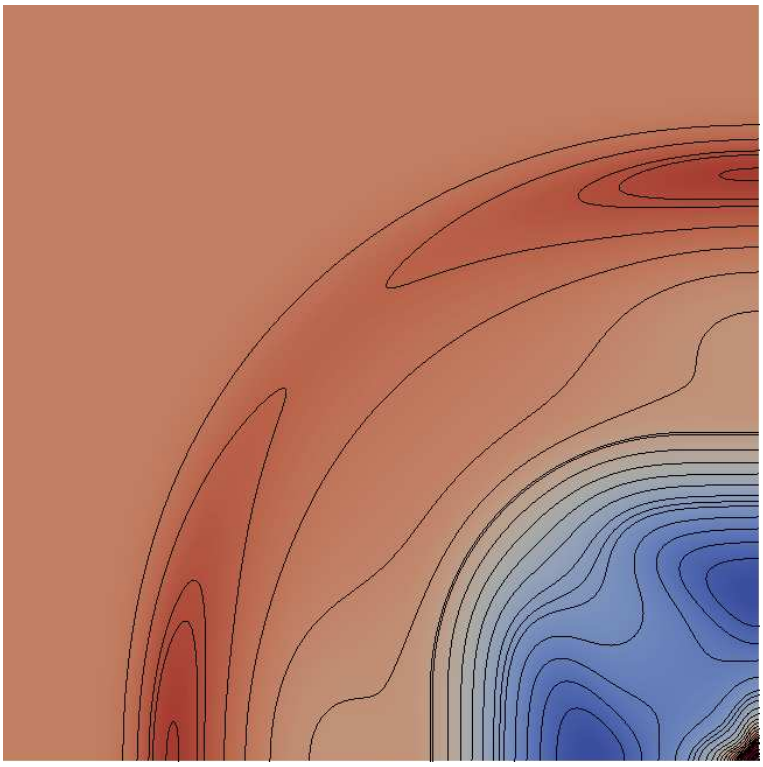

Figure 1.19: Interaction between a shock and a cube – Pressure at $t = 0.456$ on the plane $x_1 = 2$.

Appendix

1.A Pressure correction methods and kinetic energy balance

When applying a pressure correction method to the computation of a variable density flow, a specific treatment of the pressure is necessary to obtain a kinetic energy identity. To this purpose, an *ad hoc* technique was introduced in [32] and, to our knowledge, it is still today the only work on this topic. We propose here a different method, and briefly compare it with the algorithm described in [32].

To present the difficulty which we face, let us work in the time semi-discrete formalism, and let us denote by $\overline{\boldsymbol{\nabla}} p^{n+1}$ the pressure gradient used in the velocity prediction step, postponing its definition for a while. Let us also denote by $\mathcal{C}(\tilde{\boldsymbol{u}}^{n+1})$ the convection operator for the velocity, and let us suppose that this operator satisfies an identity of the form:

$$\mathcal{C}(\tilde{\boldsymbol{u}}^{n+1})\cdot\tilde{\boldsymbol{u}}^{n+1}=\frac{1}{2\,\delta t}\Big[\rho^{m+1}|\tilde{\boldsymbol{u}}^{n+1}|^2-\rho^{m}|\boldsymbol{u}^{n}|^2\Big]+\frac{1}{2}\mathrm{div}(|\tilde{\boldsymbol{u}}^{n+1}|^2\,\boldsymbol{q}^{\ell})+\mathcal{R}^{n+1}, \tag{1.37}$$

where ℓ and m stand for time indices depending on n and $\boldsymbol{q}^{\ell}$ stands for an approximation of the mass flux, and with $\mathcal{R}^{n+1}\geq 0$. In the present paper, we have:

$$\mathcal{C}(\tilde{\boldsymbol{u}}^{n+1})=\frac{1}{\delta t}(\rho^{n}\tilde{\boldsymbol{u}}^{n+1}-\rho^{n-1}\boldsymbol{u}^{n})+\mathrm{div}(\rho^{n}\tilde{\boldsymbol{u}}^{n+1}\otimes\boldsymbol{u}^{n}),$$

and Relation (1.37) is satisfied with $m=n-1$ and $\boldsymbol{q}=\rho\,\boldsymbol{u}$, $\ell=n$. Other choices for the convection operator are possible [32, 60, 63]. With the above notations, the velocity prediction step reads:

$$\mathcal{C}(\tilde{\boldsymbol{u}}^{n+1})-\mathrm{div}\big(\boldsymbol{\tau}(\tilde{\boldsymbol{u}}^{n+1})\big)+\overline{\boldsymbol{\nabla}} p^{n+1}=0. \tag{1.38}$$

Our aim here is to obtain a discrete equivalent of the kinetic energy balance, which we recall:

$$\frac{1}{2}\partial_t(\rho\,|\boldsymbol{u}|^2)+\frac{1}{2}\mathrm{div}(\rho\,|\boldsymbol{u}|^2\,\boldsymbol{u})-\mathrm{div}(\boldsymbol{\tau}(\boldsymbol{u}))\cdot\boldsymbol{u}+\boldsymbol{\nabla} p\cdot\boldsymbol{u}=0. \tag{1.39}$$

This relation is obtained by taking the inner product of the momentum balance equation by the velocity. Thus, let us take the inner product of (1.38) by $\tilde{\boldsymbol{u}}^{n+1}$. Using (1.37), we get:

$$\begin{aligned}\frac{1}{2\,\delta t}\Big[\rho^{m+1}|\tilde{\boldsymbol{u}}^{n+1}|^2-\rho^{m}|\boldsymbol{u}^{n}|^2\Big]+\frac{1}{2}\mathrm{div}(|\tilde{\boldsymbol{u}}^{n+1}|^2\,\boldsymbol{q}^{\ell})&\\ -\mathrm{div}\big(\boldsymbol{\tau}(\tilde{\boldsymbol{u}}^{n+1})\big)\cdot\tilde{\boldsymbol{u}}^{n+1}+\overline{\boldsymbol{\nabla}} p^{n+1}\cdot\tilde{\boldsymbol{u}}^{n+1}&=-\mathcal{R}^{n+1}.\end{aligned} \tag{1.40}$$

This relation is not a discrete analogue of (1.39), since the first two terms cannot be interpreted as a discrete time derivative, due to the presence in the first term of $|\tilde{\boldsymbol{u}}^{n+1}|^2$ instead of $|\boldsymbol{u}^{n+1}|^2$. Hence, we now turn to the correction step, and write the velocity correction equation as:

$$\frac{1}{\delta t}\,\rho^{m+1}\boldsymbol{u}^{n+1}+\boldsymbol{\nabla} p^{n+1}=\frac{1}{\delta t}\,\rho^{m+1}\tilde{\boldsymbol{u}}^{n+1}+\overline{\boldsymbol{\nabla}} p^{n+1}.$$

Let us multiply this relation by $[\delta t/(2\rho^{m+1})]^{1/2}$ and square the resulting equation, to obtain:

$$\frac{1}{2\delta t}\,\rho^{m+1}|\boldsymbol{u}^{n+1}|^2+\boldsymbol{\nabla} p^{n+1}\cdot\boldsymbol{u}^{n+1}+\frac{\delta t}{2\rho^{m+1}}\,|\boldsymbol{\nabla} p^{n+1}|^2 \\ =\frac{1}{2\delta t}\,\rho^{m+1}|\tilde{\boldsymbol{u}}^{n+1}|^2+\overline{\boldsymbol{\nabla}} p^{n+1}\cdot\tilde{\boldsymbol{u}}^{n+1}+\frac{\delta t}{2\rho^{m+1}}\,|\overline{\boldsymbol{\nabla}} p^{n+1}|^2.$$

Adding this relation with (1.40), we get:

$$\frac{1}{2\,\delta t}\Big[\rho^{m+1}|\boldsymbol{u}^{n+1}|^2-\rho^m|\boldsymbol{u}^n|^2\Big]+\frac{1}{2}\mathrm{div}(|\tilde{\boldsymbol{u}}^{n+1}|^2\,\boldsymbol{q}^\ell) \\ -\mathrm{div}\big(\boldsymbol{\tau}(\tilde{\boldsymbol{u}}^{n+1})\big)\cdot\tilde{\boldsymbol{u}}^{n+1}+\boldsymbol{\nabla} p^{n+1}\cdot\boldsymbol{u}^{n+1}=-\mathcal{R}^{n+1}-\mathcal{R}_{\boldsymbol{\nabla}}^{n+1}. \quad (1.41)$$

with:

$$\mathcal{R}_{\boldsymbol{\nabla}}^{n+1}=\frac{\delta t}{2\rho^{m+1}}\,|\boldsymbol{\nabla} p^{n+1}|^2-\frac{\delta t}{2\rho^{m+1}}\,|\overline{\boldsymbol{\nabla}} p^{n+1}|^2.$$

Equation (1.41) is now a discrete analogue to (1.39). However, it is interesting to recast $\mathcal{R}_{\boldsymbol{\nabla}}^{n+1}$ as a difference of the same quantity at two different time levels, for at least two reasons:

- first, summing (1.41) in time, we obtain in this case a stability estimate.
- Second, if Relation (1.41) is multiplied by a regular test function, lest us say φ^{n+1}, and, once again, summed in time, a discrete integration by parts in time makes δt times the (discrete) time derivative of φ appear. The factor δt is decisive to prove that the corresponding sum, *i.e.* the sum over n of $\mathcal{R}_{\boldsymbol{\nabla}}^{n+1}\,\varphi^{n+1}$, tends to zero, even for an irregular (shock) solution. No counterpart of the remainder term $\mathcal{R}_{\boldsymbol{\nabla}}^{n+1}$ thus needs to be introduced in the internal energy balance in the case of the Euler equations.

To reach this goal, we thus need to have:

$$\frac{\delta t}{2\rho^{m+1}}\,|\overline{\boldsymbol{\nabla}} p^{n+1}|^2=\frac{\delta t}{2\rho^m}\,|\boldsymbol{\nabla} p^n|^2$$

which yields the following definition for $\overline{\boldsymbol{\nabla}} p^{n+1}$:

$$\overline{\boldsymbol{\nabla}} p^{n+1}=\Big[\frac{\rho^{m+1}}{\rho^m}\Big]^{1/2}\,\boldsymbol{\nabla} p^n. \quad (1.42)$$

Note that this quantity is not necessarily the (discrete) gradient of a discrete pressure field (hence, the notation $\overline{\boldsymbol{\nabla}} p$ instead of $\boldsymbol{\nabla}\overline{p}$).

Finally, we thus only need to multiply the beginning-of-step pressure gradient by a factor (hopefully known, which is the case here with $m=n-1$), which almost leaves unchanged the count of algebraic operations associated to a time step.

On the contrary, the method proposed in [32] consists in solving for $\overline{p}^{n+1}$ the following elliptic problem:

$$\mathrm{div}\Big[\frac{1}{\rho^{m+1}}\boldsymbol{\nabla}\overline{p}^{n+1}\Big]=\mathrm{div}\Big[\frac{1}{(\rho^{m+1}\,\rho^m)^{1/2}}\boldsymbol{\nabla} p^n\Big]. \quad (1.43)$$

By more intricate arguments than for (1.42) (especially for the issue of the introduction of corrective terms in the internal balance energy), it may be shown that (1.43) provides the same benefits as (1.42). In addition, in one space dimension, both relations yields the same corrected gradient (*i.e.* $\overline{\boldsymbol{\nabla}} p^{n+1}=\boldsymbol{\nabla}\overline{p}^{n+1}$).

1.B Behaviour of the scheme on contact discontinuities

In this section, we check the ability of the proposed scheme to deal with contact discontinuities without generating numerical perturbations. We forget boundary conditions, or, in other words, suppose that $\Omega = \mathbb{R}^d$, $1 \leq d \leq 3$.

In 1D, this just amounts to check that the scheme is able to propagate a discontinuity for ρ and e while keeping the velocity and the pressure constant. Let us thus suppose that, at the time level n, u^n and p^n are constant, let us say $u^n \equiv \bar{u}$ and $p^n \equiv \bar{p}$, and let us examine the consequences of this assumption in the scheme (1.11):

- Since the pressure gradient $\boldsymbol{\nabla} p^n$ vanishes, so does $\overline{\boldsymbol{\nabla}} p^{n+1}$;
- Thanks to the fact that the convection operator in the momentum balance equation (1.11b) vanishes for constant advected fields $\tilde{u}^{n+1}$ (or, in other words, thanks to the fact that the mass balance over dual cells (1.15) holds), we obtain that $\tilde{u}^{n+1} \equiv \bar{u}$. In addition, the expression (1.32) of the remainder terms (R_σ^{n+1}) shows that they vanish, and so do the corrective terms (S_K^{n+1}) (see Equation (1.33)).
- Let us now suppose that the equation of state is such that the product ρe is a function of the pressure only:
$$\rho e = f(p). \tag{1.44}$$
Typical exampled of such a situation are perfect gases ($p = (\gamma - 1)\rho e$) or stiffen gases ($p = (\gamma - 1)\rho e + \gamma p_\infty$, with p_∞ a fixed positive constant). Then it is easy to see the $p^{n+1} \equiv \bar{p}$ and $u^{n+1} \equiv \bar{u}$ satisfy Equations (1.11c) and (1.11e). Equation (1.11d) can then be seen as a transport equation (since u^{n+1} is constant) and yields ρ^{n+1} while the equation of state yields e^{n+1}.

This shows that the pressure and velocity remain constant through contact discontinuities, provided that the assumption (1.44) holds.

Let us now turn to the two-dimensional case. The preceding reasoning still holds for the specific solutions where $\boldsymbol{u}$ and p are constant and ρ and e are transported. We now consider the contact discontinuity wave (specific to the two-dimensional case) which consists of the transport of one component of the velocity, let us say $\boldsymbol{u} \cdot \boldsymbol{t}$, by a velocity field constant in the direction $\boldsymbol{n}$, with $\boldsymbol{n} \cdot \boldsymbol{t} = 0$. For instance, such a situation is obtained for the initial data:

$$\rho_0 = 1,\ p_0 = 1,\ \boldsymbol{u} = \begin{bmatrix} 1 \\ 5 \end{bmatrix} \text{ on } (-\infty, 0) \times \mathbb{R} \text{ and } \boldsymbol{u} = \begin{bmatrix} 1 \\ -5 \end{bmatrix} \text{ on } (0, +\infty) \times \mathbb{R}.$$

By similar arguments as previously, we would obtain that $u_1 \equiv 1$, $\rho \equiv 1$ and $p \equiv 1$ while u_2 is a solution of a transport equation given by the second component of the momentum balance, provided that the corrective terms (S_K^n) identically vanish. Unfortunately, the discrete kinetic energy balance is not exactly satisfied (see the expression (1.32) of the remainder terms), the terms (S_K^n) are not equal to zero, and we cannot expect the constant solution for ρ, p (and e) and u_1 to be preserved. This may be observed on Figure 1.B.1, where we plot the solution obtained with $\Omega = (-0.5, 0.5) \times (-0.5, 0.5)$, a mesh consisting of 3 horizontal stripes of $n = 500$, $n = 1000$ and $n = 2000$ cells, at $t = 0.12$. The equation of state is:

$$p = (\gamma - 1)\rho e, \quad \gamma = 1.4,$$

so that the constant sound speed satisfies $c^2 = 1.4$. The time step is set to $\delta t = 1/(4n)$ (the CFL number is therefore close to $1/2$), and the artificial viscosity is set to $\mu = 1/(40n)$ (so 20 times lower than the viscosity which would be generated by an upwind discretization of the velocity convection term). As shown by the profile for u_2, this diffusion is sufficient to damp most of the oscillations

which should be generated by the transport of a discontinuity by a centered convection operator. Numerically, we observe a strong heating at the contact discontinuity, which leads to a strong decrease of the density, and subsequent perturbations on the pressure and the horizontal velocity (recall that these quantities are constant in the continuous solution). The difference between the numerical and the exact solutions seems to be only bounded in the L^∞-norm (in fact, for ρ and e only) and to tend to zero in L^1 (and therefore in L^p, for any finite p).

To the best of our knowledge, the observed behaviour is common to all Euler solvers. Moreover, the previous analysis shows that, to avoid perturbations, the scheme should satisfy an exact discrete kinetic balance (*i.e.* without remainder term). As soon as ρ is constant, this can be achieved by switching from a backward Euler to a Crank-Nicolson time discretization of the momentum balance and setting to zero the artificial viscosity [5]; however, it is of little interest, since the second component of the velocity then suffers from numerical oscillations and, essentially, since ρ varies across a contact discontinuity in the general case. For our scheme, a solution could be also to arbitrarily set the corrective terms (S_K^n) to zero, since they are probably not necessary *at contact discontinuities* to the consistency of the scheme (indeed, contrary to what happens at shocks, they are expected to tend to zero in L^1 as the mesh and time steps tend to 0, see Remark 1.4.1); however, this would require to be able to distinguish dynamically (*i.e.* in view of the results, during the computation) a contact discontinuity from a shock, which does not seems to be an easy task.

1.C Numerical solution of the correction step

First case: Euler equations, $\rho e = f(p)$ – When the equation of state is such that the product ρe is a function of the pressure only, and in the absence of heat diffusion (*i.e.* $\lambda = 0$), the correction step may be solved in two decoupled substeps:

- **First step** - From Equation (1.11c), the end-of-step velocity may be written as a function of the end-of-step pressure (and of known quantities). Inserting this expression in the internal energy balance (1.11e) yields a discrete nonlinear parabolic problem for the pressure only, which thus allows to compute p^{n+1}. Then, (1.11c) gives $\boldsymbol{u}^{n+1}$.
- **Second step** - The mass balance (1.11d) is now a linear problem for ρ^{n+1} (or $1/e^{n+1}$), and the equation of state finally yields e^{n+1} (or ρ^{n+1}).

Let us now write the discrete parabolic problem for the pressure as:

$$\forall K \in \mathcal{M}, \quad \frac{|K|}{\delta t}\left[f(p_K^{n+1}) - f(p_K^n)\right] + \sum_{\sigma \in \mathcal{E}(K)} G_{K,\sigma}^{n+1} = S_K^{n+1}. \tag{1.45}$$

We are now going to give the expression of each of the terms of this equation. From (1.11c), we get:

$$\text{For } 1 \le i \le d,\ \forall \sigma \in \mathcal{E}_{\mathcal{S}}^{(i)}, \qquad u_{\sigma,i}^{n+1} = \tilde{u}_{\sigma,i}^{n+1} - \frac{\delta t}{\rho_{D_\sigma}^n}\,\boldsymbol{\nabla}_{\sigma,i}(p^{n+1}) + \frac{\delta t}{\rho_{D_\sigma}^n}\,\overline{\boldsymbol{\nabla}}_{\sigma,i}(p^{n+1}).$$

Considering only the normal component of the velocity at the face and using the definition (1.16) of the discrete gradient, we get:

$$\forall \sigma = K|L \in \mathcal{E}_{\mathrm{int}}, \quad u_{K,\sigma}^{n+1} = \tilde{u}_{K,\sigma}^{n+1} + \frac{\delta t\ |\sigma|}{\rho_{D_\sigma}^n\ |D_\sigma|}(p_K^{n+1} - p_L^{n+1}) - \frac{\delta t\ |\sigma|}{(\rho_{D_\sigma}^n)^{1/2}(\rho_{D_\sigma}^{n-1})^{1/2}\ |D_\sigma|}(p_K^n - p_L^n),$$

where, to define $\tilde{u}_{K,\sigma}^{n+1}$, we adopt the same convention for $\tilde{\boldsymbol{u}}$ as for $\boldsymbol{u}$, *i.e.* Relation (1.13). When the normal velocity is prescribed to zero at the external faces, so is the pressure gradient, and thus

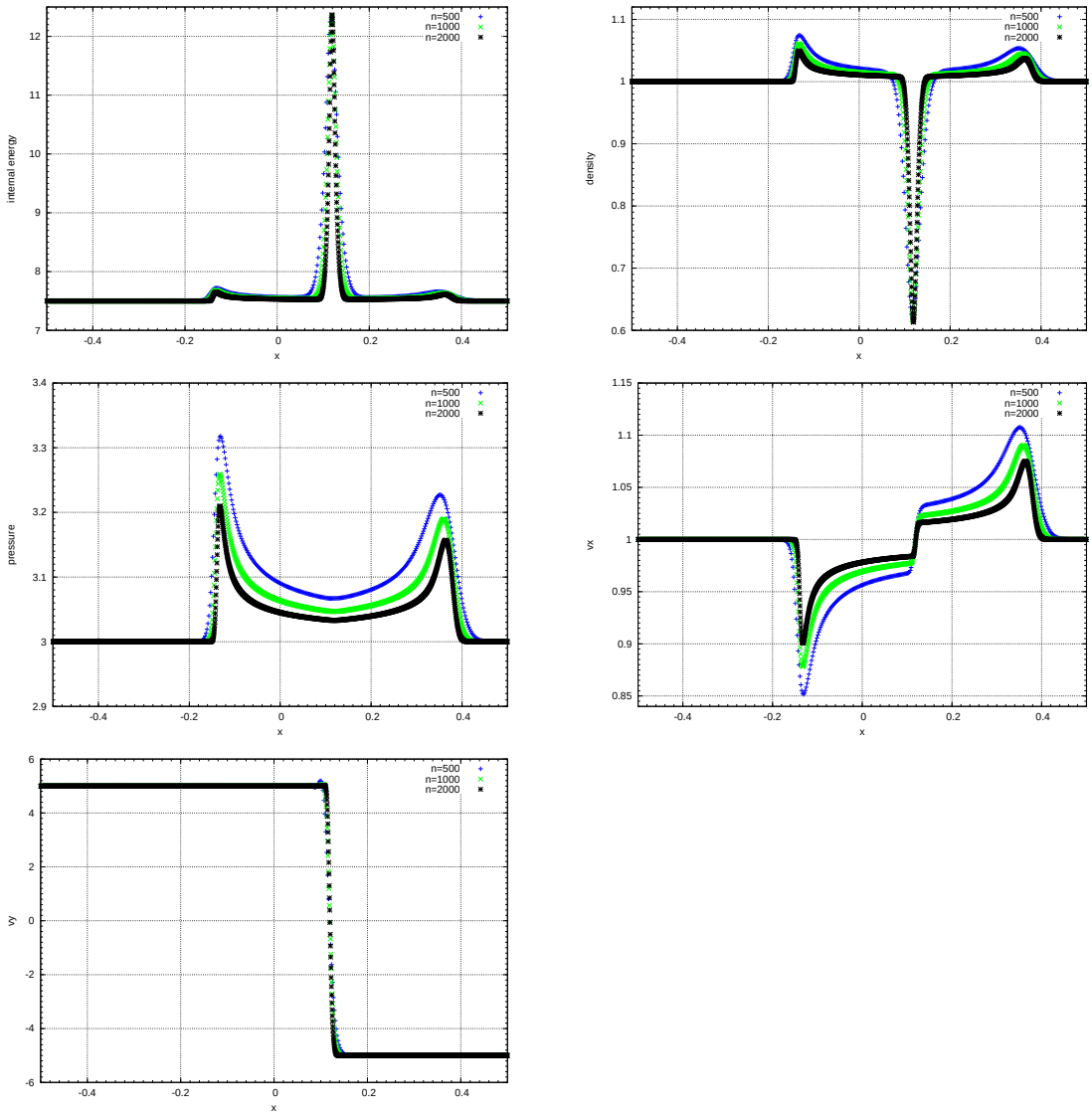

Figure 1.B.1: Slip contact discontinuity – Results for $h = 1/500$, $h = 1/1000$ and $h = 1/2000$, along a line parallel to the x-axis. Internal energy (top-left), density (top-right), pressure (middle-left), x-velocity (middle-right) and y-velocity (bottom).

$u_{K,\sigma}^{n+1} = 0$. Let us denote by $\tilde{v}_{K,\sigma}^{n+1}$ the known part of the right-hand side in the previous relation, *i.e.*:

$$\forall \sigma = K|L \in \mathcal{E}_{\rm int}, \quad \tilde{v}_{K,\sigma}^{n+1} = \tilde{u}_{K,\sigma}^{n+1} - \frac{\delta t \ |\sigma|}{(\rho_{D_\sigma}^n)^{1/2}(\rho_{D_\sigma}^{n-1})^{1/2} \ |D_\sigma|}(p_K^n - p_L^n).$$

Using this relation in (1.11e), we get:

$$\forall \sigma = K|L \in \mathcal{E}_{\rm int}, \quad G_{K,\sigma}^{n+1} = (G_{K,\sigma}^{n+1})_{\rm conv} + (G_{K,\sigma}^{n+1})_{\rm diff}, \text{ with}$$

$$(G_{K,\sigma}^{n+1})_{\rm conv} = |\sigma| \ f(p_\sigma^{n+1}) \ \tilde{v}_{K,\sigma}^{n+1}, \quad (G_{K,\sigma}^{n+1})_{\rm diff} = \frac{\delta t \ |\sigma|^2}{\rho_{D_\sigma}^n \ |D_\sigma|} \left[f(p_\sigma^{n+1}) + p_K^{n+1}\right] (p_K^{n+1} - p_L^{n+1}),$$

where p_σ^{n+1} stands for the upwind value of p^{n+1} with respect to $u_{K,\sigma}^{n+1}$. On the external faces, still with impermeability conditions, $G_{K,\sigma}^{n+1} = 0$. This nonlinear problem is solved by a quasi-Newton iteration, and the upwinding of p^{n+1} is performed with respect to the normal velocity at the previous Newton iteration, which does not seem to pose any problem of convergence. The system (1.45) may be seen as a discrete parabolic problem, with a discrete convection-diffusion operator the diffusion part of which obeys a Neumann boundary condition (since the flux $(G_{K,\sigma}^{n+1})_{\text{diff}}$ is zero at the external faces). Note that this problem is not conservative (the "diffusion coefficient" is proportional to $f(p_\sigma^{n+1}) + p_K^{n+1}$ on one side of the face and to $f(p_\sigma^{n+1}) + p_L^{n+1}$ on the other side), which is a consequence of the fact that the internal energy balance itself is non-conservative.

When the normal velocity is free at some external face σ, the predicted velocity and the pressure gradient at σ no longer vanishes, and we get, denoting by K the cell adjacent to σ:

$$G_{K,\sigma}^{n+1} = \frac{\delta t \ |\sigma|^2}{\rho_{D_\sigma}^n \ |D_\sigma|} \left[f(p_K^{n+1}) + p_K^{n+1} \right] \ (p_K^{n+1} - p_{\text{ext}}) + f(p_K^{n+1}) \tilde{v}_{K,\sigma}^{n+1},$$

where we have supposed that the flow leaves the domain, so the upwind value for p^{n+1} at σ is p_K^{n+1}, and p_{ext} stands for the external pressure used to approximate the gradient at the face. The discrete diffusion operator for p thus now incorporates an implicit Dirichlet boundary condition on σ.

General case – In the general case, the above-mentioned decoupling of equations in the correction step is not possible, and we use a procedure which is more standard in pressure correction algorithms: as previously, from Equation (1.11c), the end-of-step velocity is written as a function of the end-of-step pressure (and of known quantities), but this expression is now inserted in the mass balance (1.11d), to produce an equation which once again looks like a discrete nonlinear parabolic problem for the pressure, but unfortunately still involves the internal energy, through the computation of the density thanks to the equation of state; then this equation is solved simultaneously with the internal energy balance (1.11e), by a coupled Newton iteration.

This algorithm seems rather robust, and has been used for all the tests of this paper; it typically converged in five or less iterations. However, switching to the decoupled version sometimes proved useful (in the sense that it allowed significantly greater time steps) in industrial cases, combining stiff shocks with a space grid resolution limited by the computing time; for instance, this was done to compute a jet generated by a leak through a wall separating a low pressure (some Pa) large containment from the outside atmosphere ("loss-of-vacuum" accident scenario in the ITER facility). Note that, as soon as the equation of state gives ρe as a function of p only, using the decoupled solution may be done, at the price to postpone the treatment of the diffusion in the internal energy balance to an additional step of the algorithm.

Chapter 2

A staggered pressure correction numerical scheme to compute a travelling reactive interface between two compressible media

Abstract

We address in this paper a model often used for the simulation of turbulent deflagrations in industrial applications. The flow is governed by the Euler equations for a variable composition mixture and the combustion modelling is based on a phenomenological approach: the flame propagation is represented by the transport of the characteristic function of the burnt zone, where the chemical reaction is complete; outside of this zone, the atmosphere remains in its fresh state. Numerically, we approximate this problem by a penalization-like approach, *i.e.* using a finite conversion rate with a characteristic time tending to zero with the space and time seps. The numerical scheme works on staggered, possibly unstructured, meshes. The time-marching algorithm is of segregated type, and consists in solving in a first step the chemical species mass balances and then, in a second step, mass, momentum and energy balances. For this latter stage of the algorithm, we use a pressure correction technique. The scheme is shown to satisfy the same stability properties as the continuous problem: the chemical species mass fractions are kept in the $[0, 1]$ interval, the density and the sensible internal energy stay positive and the integral over the computational domain of a discrete total energy is conserved. In addition, supposing for a while that the chemical rate is finite, the scheme is proved to be weakly consistant, in the Lax-Wendroff sense. Finally, we observe numerically that the penalization procedure converges, *i.e.* that making the chemical time scale tend to zero allow to converge to the solution of the target (infinitely fast chemistry) continuous problem. Tests also evidence that the scheme accuracy dramatically depends on the discretization of the convection operator in the chemical species mass balances.

2.1 Problem position

We study in this paper a numerical scheme for the computation of large scale turbulent deflagrations occurring in a partially premixed atmosphere. In usual situations, such a physical phenomena is driven by the progress in the atmosphere of shell-shaped thin zone, where the chemical reaction occurs and which thus separates the burnt area from fresh gases; this zone is called the flame brush. The onset

of the chemical reaction is due to the temperature elevation, so the displacement of the flame brush is driven by the heat transfers inside and in the neighbouring of this zone. Modelling of deflagrations still remains a challenge, since the flame brush has a very complex structure (sometimes presented as fractal in the literature), due to by thermo-convective instabilities or turbulence [68, 66]. Whatever the modelling strategy may be, the problem thus needs a multiscale approach, since the local flame brush structure is out of reach of the computations aimed at simulating the flow dynamics at the observation scale, *i.e.* the whole reactive atmosphere scale. A possible way to completely circumvent this problem is to perform an explicit computation of the flame brush location, solving a transport-like equation for a characteristic function of the burnt zone; such an approach transfers the modelling difficulty to the evaluation of the flame brush velocity, by an adequate closure relation, and the resulting model is generally referred to as a Turbulent Flame velocity Closure (TFC) model [85]. The transport equation for burnt zone is called in this context the G-equation, its unknown (the characteristic function) being denoted by G [66]. Such a modelling is implemented in the in-house software P^2REMICS (for Partially PREMIxed Combustion Solver) developped, on the basis of the software components library CALIF^{3}S (for Components Adaptative Library For Fluid Flow Simulations, see [6]) at the French Institut de Radioprotection et Sûreté Nucléaire (IRSN) for safety evaluation purposes; this is the context of the work presented in the present paper.

Usually, TFC models applies to perfectly premixed flows (*i.e.* flows with constant initial composition), and the chemical state of the flow is governed by the value of G only: $G \in [0, 1]$, for $G \geq 0.5$, the mixture is supposed to be in its fresh (initial) state and $G < 0.5$ is supposed to correspond to the burnt state; in both cases, the composition of the fuel is known (to the initial value in the fresh zones, and to the state resulting from a complete chemical reaction in the burnt one).

However, for partially premixed turbulent flows (*i.e.* flows with non-constant initial composition), the situation is more complex, since the composition of the mixture can no more be deduced from the value of G.An extension for this situation, in the inviscid case, is proposed in [2]. The line followed to formulate this model is to write transport equations for the chemical species initially present in the flow, as if no chemical reaction occured, and then to compute the actual composition in the burnt zone (*i.e.* the part of the physical space where $G < 0.5$) as the chemical equilibrium composition, thus supposing an infinitely fast reaction. This model is referred to in the following as the *"asymptotic model"*, and is recalled in the first part of Section 2.2.

We propose here an alternate extension, which consists in keeping the classical reactive formulation of the chemical species mass balance, but evaluating the reaction term as a function of G: it is set to zero in the fresh zone ($G \geq 0.5$), and to a finite (but possibly large) value in the burnt zone ($G < 0.5$). This model is referred to as the *"relaxed model"*; it is in fact more general, as it may be readily extended to cope with diffusion terms, while the "asymptotic model" does not (for this purpose, a balance for the actual mass fractions is necessary). We then build a numerical scheme, based on a staggered discretization of the unknowns, for the solution of the relaxed model; this algorithm is of fractional step type, and employs a pressure correction technique for hydrodynamics. It enjoys the same stability properties as the continuous model: positivity of the density and the internal energy, conservation of the total energy, chemical species mass fractions lying in the interval $[0, 1]$. In addition, its is shown to be weakly consistent with the continuous problem (in the Lax-Wendroff sense). This algorithm is an extension to the reactive case of the numerical scheme for compressibe Navier-Stokes equations described and tested in [30].

Making the reaction term stiffer and stiffer, the relaxed model should boil down to the asymptotic one, for which a closed form of the solution of Riemann problems is available. We perform numerical tests to check this property, which confort this assumption. In addition, we observe that the accuracy of the scheme (for this kind of application) dramatically depends on the numerical diffusion introduced

by the scheme in the mass balance equation for the chemical species, comparing the results for three approximation of the convection operator in these equations: the standard upwind scheme, a MUSCL-like scheme introduced in [67] and a first ordre scheme designed to reduce diffusion proposed in [17].

The presentation is structured as follows. We first introduce the asymptotic and the relaxed models in Section 2.2. Then we give an overview of the content of this paper in Section 2.3, writing the scheme in the time semi-discrete setting and stating its stability and consistency property. The fully discrete setting is given in two steps, first describing the space discretization (Section 2.4) and then the scheme itself (Section 2.5). Section 2.6 is devoted to the stability and consistency analysis. Finally, numerical experiments are presented in Section 2.7.

2.2 The physical models

We begin with the description of the asymptotic model introduced in [2] and then turn to the relaxed model proposed in the present work.

The asymptotic model - For the sake of simplicity, only four chemical species are supposed to be present in the flow, namely the fuel (denoted by F), the oxydant (O), the product (P) of the reaction, and a neutral gas (N). A one-step irreversible total chemical reaction is considered, which is written:

$$\nu_F F + \nu_O O + N \to \nu_P P + N,$$

where ν_F, ν_O and ν_P are the molar stoichiometric coefficients of the reaction. We denote by $\mathcal{I}$ the set of the subscripts used to refer to the chemical species in the flow, so $\mathcal{I} = \{F, O, N, P\}$ and the set of mass fractions of the chemical species in the flow reads $\{y_i,\ i \in \mathcal{I}\}$ (*i.e.* $\{y_F,\ y_O,\ y_N,\ y_P\}$). We now define the auxiliary unknowns $\{\tilde{y}_i,\ i \in \mathcal{I}\}$ as the result of the (inert) transport by the flow of the initial state, which means that the $\{\tilde{y}_i,\ i \in \mathcal{I}\}$ are the solutions to the following system of equation:

$$\partial_t(\rho\tilde{y}_i) + \mathrm{div}(\rho\tilde{y}_i\boldsymbol{u}) = 0, \quad \tilde{y}_i(\boldsymbol{x}, 0) = y_{i,0}(\boldsymbol{x}) \qquad \text{for } i \in \mathcal{I}, \tag{2.1}$$

where ρ stands for the fluid density, $\boldsymbol{u}$ for the velocity, and $y_{i,0}(\boldsymbol{x})$ is the initial mass fraction of the chemical species i in the flow. These equations are supposed to be posed over a bounded domain Ω of $\mathbb{R}^d$, $d \in \{1, 2, 3\}$ and a finite time interval $(0, T)$. The initial conditions are supposed to verify $\sum_{i\in\mathcal{I}} y_{i,0} = 1$ everywhere in Ω, and this property is assumed to be valid for any $t \in (0, T)$, which is equivalent with the mixture mass balance, given below. The characteristic function G is supposed to obey the following equation:

$$\partial_t(\rho G) + \mathrm{div}(\rho G\boldsymbol{u}) + \rho_u u_f |\boldsymbol{\nabla} G| = 0, \tag{2.2}$$

associated to the initial conditions $G = 0$ at the location where the flame starts and $G = 1$ elsewhere. The quantity ρ_u is a constant density, which, from a physical point of view, stands for a characteristic value for the unburnt gases density. The chemical mass fractions are now computed as:

$$\left|\begin{array}{l} \text{if } G > 0.5, \quad y_i = \tilde{y}_i \quad \text{for } i \in \mathcal{I}, \\ \text{if } G \leq 0.5, \quad y_F = \nu_F W_F \tilde{z}^+,\ y_O = \nu_O W_O \tilde{z}^-,\ y_N = \tilde{y}_N, \text{ with } \tilde{z} = \dfrac{1}{\nu_F W_F}\tilde{y}_F - \dfrac{1}{\nu_O W_O}\tilde{y}_0. \end{array}\right. \tag{2.3}$$

In these relation, $\tilde{z}^+$ and $\tilde{z}^-$ stand for the positive and negative part of $\tilde{z}$, respectively, *i.e.* $\tilde{z}^+ = \max(\tilde{z}, 0)$ and $\tilde{z}^- = -\min(\tilde{z}, 0)$, and, for $i \in \mathcal{I}$, W_i is the molar mass of the chemical species i. The physical meaning of Relation (2.3) is that the chemical reaction is supposed to be infinitely fast, and thus that the flow composition is stuck to the chemical equilibrium composition in the so-called burnt

zone, which explains why the model is qualified of "asymptotic". The product mass fraction is given by $y_P = 1 - (y_F + y_O + y_N)$. The flow is governed by the Euler equations:

$$\partial_t \rho + \mathrm{div}(\rho \boldsymbol{u}) = 0, \tag{2.4a}$$

$$\partial_t(\rho u_i) + \mathrm{div}(\rho u_i \boldsymbol{u}) + \partial_i p = 0, \quad i = 1, d, \tag{2.4b}$$

$$\partial_t(\rho E) + \mathrm{div}(\rho E \boldsymbol{u}) + \mathrm{div}(p\boldsymbol{u}) = 0, \tag{2.4c}$$

$$p = (\gamma - 1)\,\rho e_s, \qquad E = \frac{1}{2}|\boldsymbol{u}|^2 + e_s + \sum_{i\in\mathcal{I}} y_i \Delta h^0_{f,i} \tag{2.4d}$$

where p stands for the pressure, E for the total energy, e_s for the so-called sensible energy and, for $i \in \mathcal{I}$, $\Delta h^0_{f,i}$ is the formation enthalpy of the chemical species i. The equation of state (2.4d) supposes that the fluid is a perfect mixture of ideal gases, with the same iso-pressure to iso-volume specific heat ratio $\gamma > 1$. This set of equations is complemented by homogeneous Neumann boundary conditions for the velocity:

$$\boldsymbol{u} \cdot \boldsymbol{n} = 0 \quad \text{a.e. on } \partial\Omega, \tag{2.5}$$

where $\partial\Omega$ stands for boundary of Ω and $\boldsymbol{n}$ its outward normal vector.

The "relaxed" model – This model retains the original form of the reactive flows governing equations, with a transport/reaction equation for all the chemical species mass fractions, and the value of G controls the reaction rates $\dot\omega$: $\dot\omega$ is set to zero when $G \geq 0.5$, and takes non-zero (and possibly large) values otherwise. The unknowns $\{y_i,\ i \in \mathcal{I}\}$ are thus now solution to the following balance equations:

$$\partial_t(\rho y_i) + \mathrm{div}(\rho y_i \boldsymbol{u}) = \dot\omega_i, \quad \tilde y_i(\boldsymbol{x}, 0) = y_{i,0}(\boldsymbol{x}) \qquad \text{for } i \in \mathcal{I}, \tag{2.6}$$

where the reactive term $\dot\omega_i$ is given by:

$$\dot\omega_i = \frac{1}{\varepsilon}\,\zeta_i\,\nu_i W_i\,\dot\omega, \quad \dot\omega = \eta(y_F, y_O)\ (G - 0.5)^-, \quad \eta(y_F, y_O) = \min\Big(\frac{y_F}{\nu_F W_F}, \frac{y_O}{\nu_O W_O}\Big), \tag{2.7}$$

with $\zeta_F = \zeta_O = -1$, $\zeta_F = 1$ and $\zeta_N = 0$. Note that, since $\nu_F W_F + \nu_O W_0 = \nu_P W_P$, we have $\sum_{i\in\mathcal{I}} \dot\omega_i = 0$, which, summing on $i \in \mathcal{I}$ the species mass balance, allows to recover the equivalence between the mass balance the fact that $\sum_{i\in\mathcal{I}} y_i = 1$. The factor $\eta(y_F, y_O)$ is a cutt-off function, which prevents the chemical species mas fractions to take negative values (and, equivalently, values greater than 1, since their sum is 1).

The rest of the model is left unchanged.

2.3 General description of the scheme and main results

Instead of the total energy balance equation, the scheme solves a balance equation for the sensible enthalpy, defined by $h_s = e_s + p/\rho$. Let us now derive this equation. The first step is to establish the kinetic energy balance and subtract from (2.4c) to obtain a balance equation for the internal energy. Thanks to the mass balance equation, for any function ψ

$$\partial_t(\rho\psi) + \mathrm{div}(\rho\psi\boldsymbol{u}) = \rho\partial_t\psi + \rho\boldsymbol{u}\cdot\boldsymbol{\nabla}\psi.$$

Using twice this identity and then the momentum balance equation, we have for $1 \leq i \leq d$:

$$\frac{1}{2}\partial_t(\rho u_i^2) + \frac{1}{2}\mathrm{div}(\rho u_i^2\,\boldsymbol{u}) = \rho\,u_i\partial_t u_i + \rho u_i \boldsymbol{u}\cdot\boldsymbol{\nabla}u_i = u_i\big[\partial_t(\rho u_i) + \mathrm{div}(\rho u_i\boldsymbol{u})\big] = -u_i\partial_i p,$$

so, summing for $i = 1$ to d, we establish the kinetic energy balance:

$$\frac{1}{2}\partial_t(\rho|\boldsymbol{u}|^2) + \frac{1}{2}\mathrm{div}(\rho|\boldsymbol{u}|^2\boldsymbol{u}) = \boldsymbol{u}\cdot\big[\partial_t(\rho\boldsymbol{u}) + \mathrm{div}(\rho\boldsymbol{u}\otimes\boldsymbol{u})\big] = -\boldsymbol{u}\cdot\boldsymbol{\nabla}p.$$

Substituting the expression of the total energy in (2.4c), yields

$$\partial_t(\rho e) + \mathrm{div}(\rho e\boldsymbol{u}) + \frac{1}{2}\partial_t(\rho|\boldsymbol{u}|^2) + \frac{1}{2}\mathrm{div}(\rho|\boldsymbol{u}|^2) + \boldsymbol{u}\cdot\boldsymbol{\nabla}p + p\mathrm{div}(\boldsymbol{u}) = 0,$$

which, using the kinetic energy balance, gives the internal energy balance:

$$\partial_t(\rho e) + \mathrm{div}(\rho e\boldsymbol{u}) + p\mathrm{div}(\boldsymbol{u}) = 0. \tag{2.8}$$

Using the linearity of the mass balance of the chemical species i, for any $i \in \mathcal{I}$, we establish the reactive energy balance:

$$\partial_t\Big[\rho\big(\sum_{i\in\mathcal{I}}\Delta h^0_{f,i}y_i\big)\Big] + \mathrm{div}\Big[\rho\big(\sum_{i\in\mathcal{I}}\Delta h^0_{f,i}y_i\big)\boldsymbol{u}\Big] = \sum_{i\in\mathcal{I}}\Delta h^0_{f,i}\dot{\omega}_i = -\dot{\omega}_\theta. \tag{2.9}$$

Then, the equality on the difference between internal and sensible enthalpy, $h - h_s = \sum_{i\in\mathcal{I}}\Delta h^0_{f,i}y_i$,

$$\partial_t(\rho h) + \mathrm{div}(\rho h\boldsymbol{u}) = \partial_t(\rho h_s) + \mathrm{div}(\rho h_s\boldsymbol{u}) - \dot{\omega}_\theta,$$

substituting the expression for the total enthalpy, $h = e + p/\rho$,

$$\partial_t(\rho e) + \partial_t p + \mathrm{div}(\rho e\boldsymbol{u}) + p\mathrm{div}(\boldsymbol{u}) + \boldsymbol{u}\cdot\boldsymbol{\nabla}p = \partial_t(h_s) + \mathrm{div}(\rho h_s\boldsymbol{u}) - \dot{\omega}_\theta,$$

and finally using the internal energy balance, we obtain the sensible enthalpy balance:

$$\partial_t(\rho h_s) + \mathrm{div}(\rho h_s\boldsymbol{u}) - \partial_t p - \boldsymbol{u}\cdot\boldsymbol{\nabla}p = \dot{\omega}_\theta. \tag{2.10}$$

The numerical resolution of the mathematical model is realized by a fractional step algorithm, which employs a pressure correction technique for hydrodynamics in order to separate the resolution of the momentum balance from the other equations of the Euler system. The semi-discretized version of the algorithm is given by:

Reactive step:

$$\frac{1}{\delta t}(\rho^n G^{n+1} - \rho^{n-1}G^n) + \mathrm{div}(\rho^n G^k\boldsymbol{u}^n) + \rho_u u_f\,|\boldsymbol{\nabla}G^{n+1}| = 0. \tag{2.11a}$$

$$\frac{1}{\delta t}\big[\rho^n y_N^{n+1} - \rho^{n-1}y_N^n\big] + \mathrm{div}(\rho^n y_N^k\boldsymbol{u}^n) = 0. \tag{2.11b}$$

$$\frac{1}{\delta t}(\rho^n z^{n+1} - \rho^{n-1}z^n) + \mathrm{div}(\rho^n z^k\boldsymbol{u}^n) = 0. \tag{2.11c}$$

$$\frac{1}{\delta t}\big[\rho^n y_F^{n+1} - \rho^{n-1}y_F^n\big] + \mathrm{div}(\rho^n y_F^k\boldsymbol{u}^n) = \nu_F W_F\,\dot{\omega}(y_F^{n+1}, z^{n+1}). \tag{2.11d}$$

$$y_O^{n+1} = 1 + \frac{1}{s}y_F^{n+1} - \big(1 + \frac{1}{s}\big)z^{n+1}. \tag{2.11e}$$

$$y_F^{n+1} + y_O^{n+1} + y_N^{n+1} + y_P^{n+1} = 1. \tag{2.11f}$$

Euler step:

$$\frac{1}{\delta t}(\rho^n \tilde{u}_i^{n+1} - \rho^{n-1} u_i^n) + \mathrm{div}(\rho^n \tilde{u}_i^{n+1} \boldsymbol{u}^n) + \Big(\frac{\rho^n}{\rho^{n-1}}\Big)^{1/2} \partial_i p^n = 0, \quad i = 1, \ldots, d. \tag{2.12a}$$

$$\left|\begin{array}{l} \dfrac{1}{\delta t}\ \rho^n(u_i^{n+1} - \tilde{u}_i^{n+1}) + \partial_i p^{n+1} - \Big(\dfrac{\rho^n}{\rho^{n-1}}\Big)^{1/2} \partial_i p^n = 0, \quad i = 1, \ldots, d, \\ \dfrac{1}{\delta t}(\rho^{n+1} - \rho^n) + \mathrm{div}(\rho^{n+1} \boldsymbol{u}^{n+1}) = 0, \\ \dfrac{1}{\delta t}\ \big[(\rho h_s)^{n+1} - (\rho h_s)^n\big] + \mathrm{div}(\rho h_s \boldsymbol{u})^{n+1} - \dfrac{1}{\delta t}\,(p^{n+1} - p^n) - (u \cdot \boldsymbol{\nabla} p)^{n+1} = \dot{\omega}_\theta^{n+1} + S^{n+1}, \\ p^{n+1} = \dfrac{\gamma - 1}{\gamma}\ \rho^{n+1}\, h_s^{n+1}. \end{array}\right. \tag{2.12b}$$

Thus the value of y_O^{n+1} is deduced from y_F^{n+1} and z^{n+1}, which allows to express $\dot{\omega}$ as a function of y_F^{n+1} and z^{n+1}, instead of y_F^{n+1} and y_O^{n+1} as suggested by Relation (2.7). The product mass fraction y_F^{n+1} is deduced from the relation $y_F^{n+1} + y_O^{n+1} + y_N^{n+1} + y_P^{n+1} = 1$. The updates of y_O and y_N are both performed after (2.11d), so the term $\dot{\omega}_\theta^{n+1}$ in the third relation of (2.12b) is fully defined.

The space dicretization is performed by a finite volume technique, using a staggered arrangement of the unknowns (the scalar variables are approximated at the cell centers and the velocity components at the face centers), using either a MAC scheme (for structured discretizations) or the degrees of freedom of low-order non-conforming finite elements: Crouzeix-Raviart for simplicial cells and Rannacher-Turek for quadrangles ($d = 2$) or hexahedra ($d = 3$). For Euler equations (*i.e.* Steps (2.12a)- (2.12b)), upwinding is performed by building positivity-preserving convection operators, in the spirit of the so-called Flux-Splitting methods, and only first-order upwinding is implemented. The pressure gradient is built as the transpose (with respect to the L^2 inner product) of the natural velocity divergence operator. For the balance equations for the othe scalar unknowns, the time discretization is implicit when first-order upwinding is used in the convection operator (in other words, $k = n + 1$ in (2.11a)-(2.11d)) or explicit ($k = n$ in (2.11a)-(2.11d)) when a higher order (of MUSCL type, *cf.* Appendix 2.A) flux or an anti-diffusive flux (*cf.* Appendix 2.B) is used.

Scheme properties – First, the positivity of the density is ensured by construction of the discrete mass balance equation.

At the continuous level, the physical bounds of the mass fractions are preserved – with appropriate boundary conditions – thanks to the mass balance equation, which permits to transform the chemical species mass balance equations to transport equations, *i.e.*

$$\partial_t(\rho y_i) + \mathrm{div}(\rho y_i \boldsymbol{u}) = \rho(\partial_t y_i + \boldsymbol{u} \cdot \boldsymbol{\nabla} y_i) + y_i\big[\partial_t \rho + \mathrm{div}(\rho \boldsymbol{u})\big] = \rho(\partial_t y_i + \boldsymbol{u} \cdot \boldsymbol{\nabla} y_i).$$

The same holds at the discrete level: building a discrete convection operator for the mass fractions from the discrete mass balance equation yields the same physical bounds [54], under a CFL condition if an explicit time approximation is used. Since the mass balance is solved only in the last step of the algorithm, this leads to shift in time the densities in (2.11a)-(2.11d).

The positivity of the sensible energy stems from two essential arguments: first, a discrete analog of the internal energy equation (2.8) may be obtained from the discrete sensible enthalpy balance, by mimicking the continuous computation; second, this discrete relation may be shown to have only positive solutions, once again thanks to the consistency of the discrete convection operator and the mass balance. This holds provided that the equation is exothermic ($\dot{\omega}_\theta \geq 0$) and thanks to the non-negativity of S^{n+1} (see below).

In order to calculate correct shocks, it is crucial for the scheme to be consistent with the following weak formulation of the problem:

$$
\begin{aligned}
&\forall \phi \in \mathrm{C}_c^\infty(\Omega \times [0,T)\big),\\
&\int_0^T \int_\Omega \big[\rho \partial_t \phi + \rho \boldsymbol{u} \cdot \boldsymbol{\nabla} \phi\big] \mathrm{d}\boldsymbol{x}\, \mathrm{d}t + \int_\Omega \rho_0(\boldsymbol{x}) \phi(\boldsymbol{x},0) \mathrm{d}\boldsymbol{x} = 0,\\
&\int_0^T \int_\Omega \big[\rho u_i \partial_t \phi + (\rho \boldsymbol{u} u_i) \cdot \boldsymbol{\nabla} \phi + p \partial_i \phi\big] \mathrm{d}\boldsymbol{x}\, \mathrm{d}t\\
&\qquad\qquad + \int_\Omega \rho_0(\boldsymbol{x}) (u_i)_0(\boldsymbol{x}) \phi(\boldsymbol{x},0) \mathrm{d}\boldsymbol{x} = 0, \quad 1 \le i \le d,\\
&\int_0^T \int_\Omega \big[\rho E \partial_t \phi + (\rho E + p) \boldsymbol{u} \cdot \boldsymbol{\nabla} \phi\big] \mathrm{d}\boldsymbol{x}\, \mathrm{d}t + \int_\Omega \rho_0(\boldsymbol{x}) E_0(\boldsymbol{x}) \phi(\boldsymbol{x},0) \mathrm{d}\boldsymbol{x} = 0,\\
&\int_0^T \int_\Omega \big[\rho y_i \partial_t \phi + \rho y_i \boldsymbol{u} \cdot \boldsymbol{\nabla} \phi\big] \mathrm{d}\boldsymbol{x}\, \mathrm{d}t + \int_0^T \int_\Omega \rho_0(\boldsymbol{x}) y_{i,0}(\boldsymbol{x}) \phi(\boldsymbol{x},0) \mathrm{d}\boldsymbol{x}\\
&\qquad\qquad = -\int_0^T \int_\Omega \dot{\omega}_i \phi \, \mathrm{d}\boldsymbol{x}\, \mathrm{d}t, \quad 1 \le i \le d,\\
&p = (\gamma - 1) \rho e_s.
\end{aligned}
\tag{2.13}
$$

Remark that this system contains the total energy balance equation and not the dicretized sensible enthalpy balance equation. This is why a discrete equivalent of the internal energy balance (2.8) is derived, with a particular time discretization of this latter quantity, which is unusual but suitable to pass to the limit in the scheme (so as to get consistency in the Lax-Wendroff sense). We also observe that the kinetic energy balance, obtained by taking the inner product of the discretized momentum balance equation with $\tilde{\boldsymbol{u}}^{n+1}$, features numerical (non-negative) dissipation terms which, in the presence of shocks, do not tend to zero with the time and space steps; these remainders are compensated by the corrective term S^{n+1}.

Finally, the integral of the total energy over the domain is conserved, which yields a stability result for the scheme (irrespectively of the time and space step, for this relation; recall however that the overall stability of the scheme needs a CFL condition if an explicit version of the convection operator for chemical species is used). The main steps of the scheme analysis are listed in Table 2.1.

2.4 Meshes and unknowns

Let us simply clarify here that the degrees of freedom for the new (comparing to the previous chapter) unknowns, *i.e.* the enthalpy, the mixture, fuel and neutral gas mass fractions and the flame indicator are associated to the cells of the mesh $\mathcal{M}$ and are denoted by:

$$\big\{p_K,\ \rho_K,\ h_K,\ y_{F,K},\ y_{N,K},\ z_K,\ G_K,\ K \in \mathcal{M}\big\},$$

since the rest of the space discretization is the same as the one presented in Chapter 1, Section 1.2.

$\partial_t(\rho h_s) + \cdots = \dot{\omega}_\theta$	
$\downarrow$	*(algebraic manipulations)*
$\partial_t(\rho e_s) + \cdots = \dot{\omega}_\theta$	Implies the positivity of e_s (thanks to the sign of S and $\dot{\omega}_\theta^{n+1}$)
$\downarrow$	*(using the mass balance for the chemical species)*
$\partial_t(\rho e) + \cdots = 0$	
$\downarrow$	
$\int_0^T \int_\Omega \pi_{\mathcal{M}}\phi \left[\partial_t(\rho e) + \ldots\right]$ $+\pi_{\mathcal{E}}\phi \left[\partial_t(\rho E_k) + \ldots\right] = 0$	Allows to conclude to the consistency of the scheme, by passing to the limit in this equation, using the fact that the scheme satisfies a discrete kinetic energy balance, and thanks to the *ad hoc* corrective term S in the enthalpy balance.

Table 2.1: Main steps of the scheme analysis.

2.5 The scheme

2.5.1 Euler step

Pressure gradient scaling step – Solve for $(\widetilde{\boldsymbol{\nabla} p})^{n+1}$:

$$\forall \sigma \in \mathcal{E}, \qquad (\widetilde{\boldsymbol{\nabla} p})_\sigma^{n+1} = \Big(\frac{\rho_{D_\sigma}^n}{\rho_{D_\sigma}^{n-1}}\Big)^{1/2} (\boldsymbol{\nabla} p)_\sigma^n. \tag{2.14a}$$

Prediction step – Solve for $\tilde{\boldsymbol{u}}^{n+1}$:

For $1 \le i \le d$, $\forall \sigma \in \mathcal{E}_{\mathcal{S}}^{(i)}$,

$$\frac{1}{\delta t}(\rho_{D_\sigma}^n \tilde{u}_{\sigma,i}^{n+1} - \rho_{D_\sigma}^{n-1} u_{\sigma,i}^n) + \operatorname{div}(\rho^n \tilde{u}_i^{n+1} \boldsymbol{u}^n)_\sigma + (\widetilde{\boldsymbol{\nabla} p})_{\sigma,i}^{n+1} = 0. \tag{2.14b}$$

Correction step – Solve for ρ^{n+1}, p^{n+1} and $\boldsymbol{u}^{n+1}$:

For $1 \le i \le d$, $\forall \sigma \in \mathcal{E}_{\mathcal{S}}^{(i)}$,

$$\frac{1}{\delta t}\rho_{D_\sigma}^n (u_{\sigma,i}^{n+1} - \tilde{u}_{\sigma,i}^{n+1}) + (\boldsymbol{\nabla} p)_{\sigma,i}^{n+1} - (\widetilde{\boldsymbol{\nabla} p})_{\sigma,i}^{n+1} = 0, \tag{2.14c}$$

$$\forall K \in \mathcal{M}, \quad \frac{1}{\delta t}(\rho_K^{n+1} - \rho_K^n) + \operatorname{div}(\rho \boldsymbol{u})_K^{n+1} = 0, \tag{2.14d}$$

$$\begin{aligned} \forall K \in \mathcal{M}, \quad \frac{1}{\delta t}\left[\rho_K^{n+1}(h_s)_K^{n+1} - \rho_K^n (h_s)_K^n\right] + \operatorname{div}(\rho h_s \boldsymbol{u})_K^{n+1} \\ - \frac{1}{\delta t}\left(p_K^{n+1} - p_K^n\right) - \left(u \cdot \boldsymbol{\nabla} p\right)_K^{n+1} = (\dot{\omega}_\theta)_K^{n+1} + S_K^{n+1}, \end{aligned} \tag{2.14e}$$

$$\forall K \in \mathcal{M}, \qquad p_K^{n+1} = \frac{\gamma - 1}{\gamma}(h_s)_K^{n+1} \rho_K^{n+1}. \tag{2.14f}$$

Then, ρ^0 is computed by the mass balance equation (2.14d) and p^0 is computed by the equation of state (2.14f).

The discretization of the mass and momentum balance equations is the same as the one presented in Chapter 1, Section 1.3 (apart the diffusion operators which are absent here), so we pass directly to the discretization of the sensible enthalpy balance equation.

2.5.1.1 Sensible enthalpy equation

The equation is discretised in such a way that the present enthalpy formulation is strictly equivalent to the internal energy formulation of the energy balance equation used in [30]. Consequently, the term $-\big(u \cdot \boldsymbol{\nabla} p\big)_K$ reads:

$$-\big(u \cdot \boldsymbol{\nabla} p\big)_K = \frac{1}{|K|} \sum_{\sigma \in \mathcal{E}(K)} |\sigma|\, u_{K,\sigma}\, (p_K - p_\sigma),$$

where p_σ is the upwind approximation of p at the face σ with respect to $u_{K,\sigma}$. The reaction heat, $(\dot{\omega}_\theta)_K$, is written in the following way:

$$(\dot{\omega}_\theta)_K = -\sum_{i=1}^{N_s} \Delta h^0_{f,i}\, (\dot{\omega}_i)_K = \left(\nu_F\, W_F\, \Delta h^0_{f,F} + \nu_O\, W_O\, \Delta h^0_{f,O} - \nu_P\, W_P\, \Delta h^0_{f,P}\right)\, \dot{\omega}_K.$$

The definition of $\dot{\omega}_K$ is given in Section 2.5.2.

The term S_K is chosen to compensate the numerical dissipation terms appearing in the kinetic energy balance, in the sense that a limit of a converging sequence of discrete solutions satisfies the weak form of the conservative total energy balance (which is the only valid formulation of the energy balance for Euler equations). It reads,

$$\forall K \in \mathcal{M} \text{ and } n \in \mathbb{N},\ n \leq N,\ S_K^{n+1} = \sum_{i=1}^{d} S_{K,i}^{n+1}, \quad \text{with } S_{K,i}^{n+1} = \frac{1}{2} \rho_K^{n-1} \sum_{\sigma \in \mathcal{E}(K) \cap \mathcal{E}_{\mathcal{S}}^{(i)}} \frac{|D_{K,\sigma}|}{\delta t} (\tilde{u}_{\sigma,i}^{n+1} - u_{\sigma,i}^n)^2.$$

Thus,

$$\sum_{K \in \mathcal{M}} S_K^{n+1} = \sum_{i=1}^{d} \sum_{\sigma \in \mathcal{E}_{\mathcal{S}}^{(i)}} R_{\sigma,i}^{n+1}.$$

2.5.2 Reactive step

$\forall K \in \mathcal{M}$:

Flame position indicator computation – Solve for G^{n+1}:

$$\frac{1}{\delta t}(\rho_K^n G_K^{n+1} - \rho_K^{n-1} G_K^n) + \mathrm{div}(\rho^n G^k \boldsymbol{u}^n)_K + (\rho_u^n u_f^n |\boldsymbol{\nabla} G|)_K = 0. \tag{2.15a}$$

Reduced variable computation – Solve for z^{n+1}:

$$\frac{1}{\delta t}(\rho_K^n z_K^{n+1} - \rho_K^{n-1} z_K^n) + \mathrm{div}(\rho^n z^k \boldsymbol{u}^n)_K = 0. \tag{2.15b}$$

Neutral gas mass fraction computation – Solve for y_N^{n+1}:

$$\frac{1}{\delta t}\left[\rho_K^n (y_N)_K^{n+1} - \rho_K^{n-1} (y_N)_K^n\right] + \mathrm{div}(\rho^n y_N^k \boldsymbol{u}^n)_K = 0. \tag{2.15c}$$

Fuel mass fraction computation – Solve for y_F^{n+1}:

$$\frac{1}{\delta t}\left[\rho_K^n (y_F)_K^{n+1} - \rho_K^{n-1} (y_F)_K^n\right] + \mathrm{div}(\rho^n y_F^{n+1} \boldsymbol{u}^n)_K = (\dot{\omega}_F)_K^{n+1}. \tag{2.15d}$$

Oxydant mass fraction computation – $(y_O)_K^{n+1} = 1 + \frac{1}{s}(y_F)_K^{n+1} - \left(1 + \frac{1}{s}\right) z_K^{n+1}$. (2.15e)

Product mass fraction computation – $(y_P)_K^{n+1} = 1 - (y_F)_K^{n+1} - (y_O)_K^{n+1} - (y_N)_K^{n+1}$. (2.15f)

The initialization of the chemical variables is given by the mean values of the initial conditions over the primal cells:

$$\forall K \in \mathcal{M},\ G_K^0 = \frac{1}{|K|}\int_K G_0(\boldsymbol{x})\,\mathrm{d}\boldsymbol{x}, \quad z_K^0 = \frac{1}{|K|}\int_K z_0(\boldsymbol{x})\,\mathrm{d}\boldsymbol{x}, \quad (y_i)_K^0 = \frac{1}{|K|}\int_K (y_i)_0(\boldsymbol{x})\,\mathrm{d}\boldsymbol{x},\ i = N, F,$$

where the reduced variable z is a linear combination of y_F and y_O, such that the balance equation of z is homogeneous. Equations (2.15a)-(2.15d) may be solved sequentially, after the first iteration of the hydrodynamics part of the algorithm, *i.e.* once $(\rho_K^0)_{K\in\mathcal{M}}$ is calculated. In the fuel mass fraction computation step, the reaction term is approximated as follows:

$$\dot{\omega}_K^{n+1} = \eta\big((y_F)_K^{n+1}, (y_O)_K^{n+1}\big)(0.5 - G_K^{n+1})^-.$$

The oxydant mass fraction, $(y_O)_K^{n+1}$, may be expressed as a function of $(y_F)_K^{n+1}$ and z_K^{n+1}; since z^{n+1} is known at this step, equation (2.15d) may be solved for y_F^{n+1}. Finally, y_P^{n+1} is calculated directly from the expression (2.15f) since, as it will be shown later (*cf.* Lemma 2.6.7), the sum of the mass fractions is equal to 1 for $n \in \mathbb{N}, n \leq N$.

At the continuous level, the last term of equation (2.15a) may be written:

$$\rho_u\, u_f\, |\boldsymbol{\nabla} G| = \boldsymbol{a}\cdot\boldsymbol{\nabla} G = \mathrm{div}(G\,\boldsymbol{a}) - G\,\mathrm{div}(\boldsymbol{a}), \quad \text{with } \boldsymbol{a} = \rho_u\, u_f\, \frac{\boldsymbol{\nabla} G}{|\boldsymbol{\nabla} G|}.$$

Using an upwind finite volume discretization of both divergence terms in this relation, we get:

$$|K|\ (\rho_u^n\, u_f^n\ |\boldsymbol{\nabla} G|)_K = \sum_{\sigma\in\mathcal{E}(K)} |\sigma|\ (\tilde{G}_\sigma^{n+1} - G_K^{n+1})\,\boldsymbol{a}_\sigma^n\cdot\boldsymbol{n}_{K,\sigma},$$

where $\tilde{G}_\sigma^{n+1}$ stands for the upwind approximation of G^{n+1} on σ with respect to $\boldsymbol{a}^n\cdot\boldsymbol{n}_{K,\sigma}$. The flame velocity on σ, $\boldsymbol{a}_\sigma^n$, is evaluated as

$$\boldsymbol{a}_\sigma^n = (\rho_u\, u_f)_\sigma^n\ \frac{(\boldsymbol{\nabla} G)_\sigma^n}{|(\boldsymbol{\nabla} G)_\sigma^n|},$$

where $(\rho_u\, u_f)_\sigma^n$ stands for an approximation of the product $\rho_u\, u_f$ on the face σ at t^n (this product being often constant in applications), and the gradient of G on $\sigma = K|L$ is computed as:

$$(\boldsymbol{\nabla} G)_\sigma = \frac{1}{|K\cup L|}\Big[\sum_{\sigma'\in\mathcal{E}(K)} |\sigma'|\ \hat{G}_{\sigma'}\ \boldsymbol{n}_{K,\sigma'} + \sum_{\sigma'\in\mathcal{E}(L)} |\sigma'|\ \hat{G}_{\sigma'}\ \boldsymbol{n}_{L,\sigma'}\Big],$$

with $\hat{G}_{\sigma'}$ a second order approximation of G at the barycenter of the face σ'.

2.6 Scheme properties

For any given family $(x_K^n)_{K\in\mathcal{M}} \in \mathbb{R}^{\mathcal{M}}$, where $\mathbb{R}^{\mathcal{M}}$ is a shorthand for $\mathbb{R}^{\mathrm{card}(\mathcal{M})}$, we introduce the following notations:

$$\overline{x} = \max_{K\in\mathcal{M}} x_K^0, \qquad \underline{x} = \min_{K\in\mathcal{M}} x_K^0.$$

When no ambiguity arises, the notation x^n will be used to refer to the family $(x_K^n)_{K\in\mathcal{M}}$. For example $x^n > 1$, means $\forall K\in\mathcal{M},\ x_K^n > 1$.

Lemma 2.6.1 (*cf.*[25]).
Let us suppose (2.14d) holds for any $n \in \mathbb{N}, n \leq N$, with $\underline{\rho} > 0$. Then the linear system (2.14d) admits a unique solution that satisfies $\rho^{n+1} > 0$.

Replacing the discrete analogue of the expresion for the sensible enthalpy, $h_s = e_s + p/\rho$, in (2.14e), leads to:

$$\frac{1}{\delta t}\big[\rho_K^{n+1}(e_s)_K^{n+1} - \rho_K^n(e_s)_K^n\big] + \mathrm{div}(\rho e_s \boldsymbol{u})_K^{n+1} + \mathrm{div}(p\boldsymbol{u})_K^{n+1} - \big(\boldsymbol{u}\cdot\boldsymbol{\nabla} p\big)_K^{n+1} = (\dot{\omega}_\theta)_K^{n+1} + S_K^{n+1}. \quad (2.16)$$

The obvious choice for $\mathrm{div}(p\boldsymbol{u})_K$ is

$$\mathrm{div}(p\boldsymbol{u})_K = \frac{1}{|K|}\sum_{\sigma\in\mathcal{E}(K)} |\sigma| u_{K,\sigma} p_\sigma,$$

where p_σ denotes the upwind approximation of p on the face σ, with respect to the velocity on the face, $u_{K,\sigma}$. Thus, by construction of the discrete operator $\big(\boldsymbol{u}\cdot\boldsymbol{\nabla} p\big)$, we obtain the discrete sensible energy balance equation:

$$\frac{1}{\delta t}\big[\rho_K^{n+1}(e_s)_K^{n+1} - \rho_K^n(e_s)_K^n\big] + \mathrm{div}(\rho e_s \boldsymbol{u})_K^{n+1} + p_K^{n+1}\mathrm{div}(\boldsymbol{u})_K^{n+1} = (\dot{\omega}_\theta)_K^{n+1} + S_K^{n+1}, \quad (2.17)$$

where the convection operator on the primal cell is approached using the upwind choice with respect to the flux for the discrete field e_s.

Lemma 2.6.2 (Positivity of the sensible energy, *cf.* [30]).
Let us suppose $\underline{e_s} > 0$ and $\dot{\omega}_\theta^n \geq 0$, for $n \in \mathbb{N}, n \leq N$. Then a solution to (2.14)-(2.15) satisfies for any $n \in \mathbb{N}, n \leq N$ and $K \in \mathcal{M}$, $(e_s)_K^n > 0$.

From the discrete sensible energy balance, a discrete internal energy balance may be established.

Lemma 2.6.3 (Discrete internal energy balance).
A solution to (2.14)-(2.15) satisfies the following equality, for any $K \in \mathcal{M}$ and $n \in \mathbb{N}, n \leq N$:

$$\frac{1}{\delta t}\big((\rho e)_K^{n+1} - (\rho e)_K^n\big) + \widetilde{\mathrm{div}}(\rho e\boldsymbol{u})_K^{n+1} + p_K^{n+1}\mathrm{div}(u)_K^{n+1} = S_K^{n+1}, \quad (2.18)$$

where

$$(\rho e)_K^{n+1} = \rho_K^{n+1}(e_s)_K^{n+1} + \rho_K^n \sum_{i\in\mathcal{I}} \Delta h_{f,i}^0 (y_i)_K^{n+1},$$
$$\widetilde{\mathrm{div}}(\rho e\boldsymbol{u})_K^{n+1} = \mathrm{div}\big[(\rho e_s)^{n+1}\boldsymbol{u}^{n+1} + \rho^n \sum_{i\in\mathcal{I}} \Delta h_{f,i}^0 y_i^{n+1}\boldsymbol{u}^n\big]_K.$$

Proof. Multiplying the mass fraction balance equations by the corresponding formation enthalpy $(\Delta h_{f,i}^0)_{i\in\mathcal{I}}$, then summing over $i \in \mathcal{I}$, yields:

$$\frac{1}{\delta t}\sum_{i\in\mathcal{I}} \Delta h_{f,i}^0\big(\rho_K^n(y_i)_K^{n+1} - \rho_K^{n+1}(y_i)_K^n\big) + \mathrm{div}\big[\rho^n \sum_{i\in\mathcal{I}} \Delta h_{f,i}^0 y_i^{n+1}\boldsymbol{u}^n\big]_K = \sum_{i\in\mathcal{I}} \Delta h_{f,i}^0 (\dot{\omega}_i)_K^{n+1} = (\dot{\omega}_\theta)_K^{n+1}. \quad (2.19)$$

Adding the obtained discrete analogue of the reactive energy equation (2.9) to the discrete sensible energy, and using the above definitions for $(\rho e)_K^{n+1}$ and $\widetilde{\mathrm{div}}(\rho e\boldsymbol{u})_K^{n+1}$, leads to the discrete internal energy balance (2.18). □

A discrete kinetic energy balance and a total energy balance conservation result, essentially related to the hydrodynamics part of the problem, have already been established.

Lemma 2.6.4 (Discrete kinetic energy balance, *cf.* [30]).
A solution to (2.14)-(2.15) satisfies the following equality, for any $K \in \mathcal{M}$ and $n \in \mathbb{N}, n \leq N$:

$$\frac{|D_\sigma|}{2\delta t}\left[\rho^n_{D_\sigma}(u^{n+1}_{\sigma,i})^2 - \rho^{n-1}_{D_\sigma}(u^n_{\sigma,i})^2\right] + \frac{1}{2}\sum_{\epsilon\in\bar{\mathcal{E}}(D_\sigma)} F^n_{\sigma,\varepsilon}\tilde{u}^{n+1}_{\sigma,i}\tilde{u}^{n+1}_{\sigma',i} + |D_\sigma|(\boldsymbol{\nabla} p)^{n+1}_{\sigma,i}u^{n+1}_{\sigma,i} = -R^{n+1}_{\sigma,i} - P^{n+1}_{\sigma,i}, \quad (2.20)$$

where

$$R^{n+1}_{\sigma,i} = \frac{|D_\sigma|\rho^{n-1}_{D_\sigma}}{2\delta t}(\tilde{u}^{n+1}_{\sigma,i} - u^{n+1}_{\sigma,i})^2 \quad \text{and} \quad P^{n+1}_{\sigma,i} = \frac{|D_\sigma|}{2\delta t\rho^n_{D_\sigma}}\left[\left((\boldsymbol{\nabla} p)^{n+1}_{\sigma,i}\right)^2 - \left((\widetilde{\boldsymbol{\nabla} p})^{n+1}_{\sigma,i}\right)\right)^2\right].$$

Lemma 2.6.5 (Total energy conservation, *cf.* [30]).
Let us suppose that e^0_s, ρ^0 and ρ^{-1} are positive. Then, a solution to (2.14)-(2.15) satisfies $\rho^{n+1} > 0$, $e^{n+1} > 0$ and the following stability result:

$$E^n = E^0,$$

where,

$$\forall n \in \mathbb{N}, n \leq N, \qquad E^n = \sum_{K\in\mathcal{M}} |K|(\rho e)^n_K + \frac{1}{2}\sum_{i=1}^{d}\sum_{\sigma\in\mathcal{E}^{(i)}_{\mathcal{S}}} |D_\sigma|(u^n_{\sigma,i})^2 + \delta t^2 \sum_{\sigma\in\mathcal{E}_{\rm int}} \frac{|D_\sigma|}{\rho^{n-1}_{D_\sigma}}|(\boldsymbol{\nabla} p)^n_\sigma|^2.$$

Let us now turn to the existence (and uniqueness) of solutions for the chemical variables, such as in their stability properties. The following two results are proven – in a more general context, *i.e.* for a problem where the mass diffusion is present – in Chapter 3, Section 3.4.

Lemma 2.6.6.
Let us suppose (2.14d) holds for any $n \in \mathbb{N}, n \leq N$, with $\underline{\rho} > 0$. Then, for any $n \in \mathbb{N}, n \leq N$ and $K \in \mathcal{M}$, the linear systems (2.15b) and (2.15c) admit unique solutions satisfying for any $K \in \mathcal{M}$, $z^{n+1}_K \in [\underline{z}, \overline{z}]$ and $(y_N)^{n+1}_K \in [\underline{y_N}, \overline{y_N}]$ respectively.

Proof. *cf.* Chapter 3, Section 3.4. □

Lemma 2.6.7.
Let us suppose (2.14d) holds for any $n \in \mathbb{N}, n \leq N$, with $\underline{\rho} > 0$. Let $\left((y_i)^0_K\right)_{i\in\mathcal{I},\, K\in\mathcal{M}} \in \mathbb{R}^{4\mathcal{M}}$ be given and such that $\sum_{i\in\mathcal{I}}(y_i)^0_K = 1$ for any $K \in \mathcal{M}$. Then, for any $n \in \mathbb{N}, n \leq N$ and $K \in \mathcal{M}$, $\sum_{i\in\mathcal{I}}(y_i)^{n+1}_K = 1$ and the linear systems corresponding to the chemical mass fractions admit at least one solution satisfying $y^{n+1}_F \in [0, \overline{y_F}]$, $y^{n+1}_O \in [0, \overline{y_O}]$ and $y^{n+1}_P \in [\underline{y_P}, 1]$.

Proof. *cf.* Chapter 3, Section 3.4. □

Lemma 2.6.8 (Contact discontinuities).
Let us suppose the initial velocity and the initial pressure constant, $u^0 = u$ and $p^0 = p$. Then, there exists a solution to the scheme (2.14)-(2.15), given by, for any $n \in \mathbb{N}, n \leq N$, $u^n = u$ and $p^n = p$.

Proof. Let us suppose for $n \in \mathbb{N}, n \leq N$, p^n and u^n constant. The pressure gradient scaling step (2.14a) gives immediately $(\widetilde{\boldsymbol{\nabla} p})_\sigma^{n+1} = 0$. Thus, $\tilde{u}_\sigma^{n+1} = u_\sigma^n$ verifies the prediction step (2.14b), and for $p^{n+1} = p^n$ equation (2.14c) gives $u_\sigma^{n+1} = \tilde{u}_\sigma^{n+1}$. The mass balance equation (2.14d) becomes an homogeneous transport equation for the density ρ with constant velocity $\boldsymbol{u}$, thus, by the equation of state (2.14f), the sensible enthalpy is also transported with constant velocity u. On the left hand side of the sensinble enthalpy balance equation (2.14e), the only terms that survive are the ones associated to the transport operator. Since S^{n+1} vanishes, this implies that $\dot{\omega}_\theta = 0$. □

To state and prove the consistency result, the discrete unknowns and the test functions need to be associated to piecewise constant functions. Let $\mathrm{S}_\mathcal{M}(\Omega \times [0,T))$ be the space of piecewisely constant functions in $K \times [t^n, t^{n+1})$, for any $n \in \mathbb{N}, n \leq N$ and $K \in \mathcal{M}$. For any function $\psi \in \mathrm{L}^1(\Omega \times [0,T))$, its interpolate in $\mathrm{S}_\mathcal{M}(\Omega \times [0,T))$ is defined by

$$\psi_\mathcal{M}(\boldsymbol{x}, t) = \sum_{n \in \mathbb{N}} \sum_{K \in \mathcal{M}} \psi_K^n \, \chi_{K \times [t^n, t^{n+1})}(\boldsymbol{x}, t),$$

where $\psi_K^n = 1/|K| \int_K \psi(\boldsymbol{x}, t^n)$ and χ_P is the characteristic function of the set P. To any discrete family, $(f_K^n)_{K \in \mathcal{M}}^{n \in \mathbb{N}, n \leq N}$, the following fuction of $\mathrm{S}_\mathcal{M}(\Omega \times [0,T))$ is naturally associated:

$$f_\mathcal{M}(\boldsymbol{x}, t) = \sum_{n \in \mathbb{N}} \sum_{K \in \mathcal{M}} f_K^n \, \chi_{K \times [t^n, t^{n+1})}(\boldsymbol{x}, t).$$

From here on, a function or a discrete family indexed by $\mathcal{M}$ will refer to the corresponding function of $\mathrm{S}_\mathcal{M}(\Omega \times [0,T))$. For any $g_\mathcal{M}$, the discrete $\mathrm{L}^1([0,T); \mathrm{BV}(\Omega))$ and $\mathrm{L}^1(\Omega; \mathrm{BV}([0,T)))$ norms read:

$$\|g_\mathcal{M}\|_{\mathrm{BV}x} = \sum_{n \in \mathbb{N}} \delta t \sum_{\sigma = K|L} |\sigma| |g_K^n - g_L^n|, \qquad \|g_\mathcal{M}\|_{\mathrm{BV}t} = \sum_{K \in \mathcal{M}} |K| \sum_{n \in \mathbb{N}} |g_K^{n+1} - g_K^n|.$$

The space of piecewisely constant functions in $D_\sigma \times [t^n, t^{n+1})$, for any $n \in \mathbb{N}, n \leq N$ and $\sigma \in \mathcal{E}$, is denoted by $\mathrm{S}_\mathcal{D}(\Omega \times [0,T))$. It is defined in analogy to $\mathrm{S}_\mathcal{M}(\Omega \times [0,T))$, but the interpolates here are defined by the mean value of the function over the primal edges, instead of the mean value over the primal the dual cell. Thus, for any regular function ψ, its interpolate in $\mathrm{S}_\mathcal{D}(\Omega \times [0,T))$ is defined by

$$\psi_\mathcal{D} = \sum_{n \in \mathbb{N}} \sum_{\sigma \in \mathcal{E}_{\mathrm{int}}} \psi_\sigma^n \, \chi_{D_\sigma \times [t^n, t^{n+1})}(\boldsymbol{x}, t),$$

where $\psi_\sigma^n = 1/|\sigma| \int_\sigma \psi(\boldsymbol{x}, t^n)$. To any discrete family $(f_\sigma^n)_{\sigma \in \mathcal{E}}^{n \in [\![0, N-1]\!]}$, the following function of $\mathrm{S}_\mathcal{D}(\Omega \times [0,T))$ is naturally associated:

$$f_\mathcal{D} = \sum_{n \in \mathbb{N}} \sum_{\sigma \in \mathcal{E}} f_\sigma^n \, \chi_{D_\sigma \times [t^n, t^{n+1})}(\boldsymbol{x}, t).$$

From here on, a function or discrete family indexed by $\mathcal{D}$, will refer to the corresponding function of $\mathrm{S}_\mathcal{D}(\Omega \times [0,T))$. For any $g_\mathcal{D} \in \mathrm{S}_\mathcal{D}(\Omega \times [0,T))$, its discrete $\mathrm{L}^1([0,T); \mathrm{BV}_0(\Omega))$ and $\mathrm{L}^1(\Omega; \mathrm{BV}([0,T)))$ norms read, respectively:

$$\|g_\mathcal{D}\|_{\mathrm{BV}x} = \sum_{n \in \mathbb{N}} \delta t \sum_{\epsilon = D_\sigma | D_{\sigma'}} h_K |g_{\sigma'}^n - g_\sigma^n|, \qquad \|g_\mathcal{D}\|_{\mathrm{BV}t} = \sum_{\sigma \in \mathcal{E}} |D_\sigma| \sum_{n \in \mathbb{N}} |g_\sigma^{n+1} - g_{\sigma'}^n|.$$

Let $\mathcal{L}$ be a differential operator. The notations $(\mathcal{L} f_i)_j$, $(i,j) \in \{\mathcal{M}, \mathcal{D}\}^2$, refer to the piecewise constant functions associated to the family obtained by applying the discrete operator to the family $(f_K^n)_{K \in \mathcal{M}}^{n \in \mathbb{N}, n \leq N}$ if $i = \mathcal{M}$, and $(f_\sigma^n)_{\sigma \in \mathcal{E}}^{n \in \mathbb{N}, n \leq N}$ if $i = \mathcal{D}$. In the case where $i = j$, the index j will be dropped.

A result similar to the one to be announced in Theorem 2.6.1, has already been stated and proven in [22] for non-reactive case, where it is shown that the limit of a sequence of discrete solutions, satisfies the equation of state and the non-reactive (2.13). What changes here, is that the total energy equation contains reactive terms. Before proceeding to the proof of the consistency theorem, let us state and prove two preliminary results.

LEMMA 2.6.9.
For any $n \in \mathbb{N}, n \leq N$, the following inequality holds:

$$\|\mathrm{div}(\rho \boldsymbol{u})^n_{\mathcal{M}}\|_{\mathrm{L}^1(\Omega)} \leq \|\rho^n_{\mathcal{M}}\|_\infty \|\boldsymbol{u}^n_{\mathcal{D}}\|_{\mathrm{BV}x} + \|\rho^n_{\mathcal{M}}\|_{\mathrm{BV}x} \|\boldsymbol{u}^n_D\|_\infty.$$

Proof. The index n being the same for all variables, it will be dropped. By definition,

$$\|\mathrm{div}(\rho \boldsymbol{u})_{\mathcal{M}}\|_{\mathrm{L}^1(\Omega)} = \sum_{K \in \mathcal{M}} \Big| \sum_{\sigma \in \mathcal{E}(K)} |\sigma| \rho_\sigma u_{K,\sigma} \Big|.$$

Let us rewrite for any $K \in \mathcal{M}$,

$$\sum_{\sigma \in \mathcal{E}(K)} |\sigma| \rho_\sigma u_{K,\sigma} = \rho_K \sum_{\sigma \in \mathcal{E}(K)} |\sigma| u_{K,\sigma} + \sum_{\sigma \in \mathcal{E}(K)} |\sigma| (\rho_\sigma - \rho_K) u_{K,\sigma} = T_1(K) + T_2(K),$$

and since for any $\sigma = K|L,\ \rho_\sigma \in [\![\rho_K, \rho_L]\!]$,

$$\sum_{K \in \mathcal{M}} |T_1(K)| \leq \sum_{K \in \mathcal{M}} \sum_{\sigma \in \mathcal{E}(K)} |\sigma| \, |\rho_K - \rho_L| \, |u_{K,\sigma}| \leq \|\boldsymbol{u}\|_\infty \|\rho\|_{\mathrm{BV}x}.$$

Given that for $1 \leq i \leq d$ and $K \in \mathcal{M}$, $\sum_{\sigma \in \mathcal{E}(K)} |\sigma| n_{\sigma,i} = 0$, where $n_{\sigma,i}$ stands for the i-th component of $\boldsymbol{n}_{K,\sigma}$, we obtain that

$$\begin{aligned} T_2(K) = \rho_K \sum_{\sigma \in \mathcal{E}(K)} |\sigma| \boldsymbol{u}_\sigma \cdot \boldsymbol{n}_{K,\sigma} &= \rho_K \sum_{i=1}^{d} \sum_{\sigma \in \mathcal{E}(K)} |\sigma| u_{\sigma,i} n_{\sigma,i} \\ &= \rho_K \sum_{i=1}^{d} \sum_{\sigma \in \mathcal{E}(K)} |\sigma| \big(u_{\sigma,i} - \frac{1}{M} \sum_{\sigma' \in \mathcal{E}(K)} u_{\sigma',i}\big) n_{\sigma,i}, \end{aligned}$$

where $M = \mathrm{card}\{\sigma \in \mathcal{E}(K)\}$, thus,

$$\sum_{K \in \mathcal{M}} |T_2(K)| = \sum_{K \in \mathcal{M}} \rho_K \sum_{i=1}^{d} \sum_{\sigma' \in \mathcal{E}(K)} \sum_{\sigma \in \mathcal{E}(K)} \frac{|\sigma|}{M} |u_{\sigma,i} - u_{\sigma',i}| \leq \|\rho\|_\infty \|\boldsymbol{u}\|_{\mathrm{BV}x},$$

and finally,

$$\|\mathrm{div}(\rho \boldsymbol{u})_{\mathcal{M}}\|_{\mathrm{L}^1(\Omega)} = \sum_{K \in \mathcal{M}} |T_1(K) + T_2(K)| \leq \|\rho_{\mathcal{M}}\|_\infty \|\boldsymbol{u}_{\mathcal{D}}\|_{\mathrm{BV}x} + \|\rho_{\mathcal{M}}\|_{\mathrm{BV}x} \|\boldsymbol{u}_D\|_\infty.$$

□

LEMMA 2.6.10.
Let $(\rho^0_K)_{K \in \mathcal{M}}$ be the solution of (2.14d) for $n = 0$ and $\rho^0_{\mathcal{M}}(\boldsymbol{x})$ the associated piecewisely constant function. Then, $\rho^0_{\mathcal{M}}(\boldsymbol{x})$ converges to $\rho_0(\boldsymbol{x})$ in $\mathrm{L}^p(\Omega)$, $1 \leq p < \infty$, when $m \to \infty$.

Proof. Firstly, using (2.14d) and Lemma 2.6.9, we obtain

$$\int_\Omega |\rho^0_{\mathcal{M}} - \rho_0| \mathrm{d}\boldsymbol{x} \leq \delta t \big(\|\rho^0_{\mathcal{M}}\|_\infty \|\boldsymbol{u}^0_{\mathcal{D}}\|_{\mathrm{BV}x} + \|\rho^0_{\mathcal{M}}\|_{\mathrm{BV}x} \|\boldsymbol{u}^0_{\mathcal{D}}\|_\infty \big),$$

thus $\rho^0_{\mathcal{M}}$ converges to ρ_0 when $m \to \infty$, and secondly, $\rho^0_{\mathcal{M}}$ is bounded in $\mathrm{L}^\infty(\Omega)$, thus $\rho^0_{\mathcal{M}}$ converges to ρ_0 in $\mathrm{L}^p(\Omega),\ 1 \leq p < \infty$:

$$\begin{aligned} &\int_\Omega |\rho^0_{\mathcal{M}} - \rho_0|^p \mathrm{d}\boldsymbol{x} \leq \|\rho^0_{\mathcal{M}} - \rho_0\|^{p-1}_\infty \|\rho^0_{\mathcal{M}} - \rho_0\|_{\mathrm{L}^1(\Omega)}, \text{ thus} \\ &\|\rho^0_{\mathcal{M}} - \rho_0\|_{\mathrm{L}^p(\Omega)} \leq \|\rho^0_{\mathcal{M}} - \rho_0\|^{p-1/p}_\infty \|\rho^0_{\mathcal{M}} - \rho_0\|^{1/p}_{\mathrm{L}^1(\Omega)} \overset{m\to\infty}{\longrightarrow} 0. \end{aligned}$$

□

Theorem 2.6.1 (Consistency)
Let $\Omega \subset \mathbb{R}^d$ be an open bounded domain and suppose initial conditions satisfying:

$$(\rho^0, p^0, h^0_s, \boldsymbol{u}^0) \in (\mathrm{L}^\infty(\Omega) \times \mathrm{BV}(\Omega) \times \mathrm{L}^\infty(\Omega) \times \mathrm{L}^\infty(\Omega)^d).$$

Let $(\mathcal{M}^{(m)}, \delta t^{(m)})_{m\in\mathbb{N}}$ be a sequence of discretizations in space and time, such that both the size of the mesh, $h^{(m)}$, and the time step, $\delta t^{(m)}$, tend to zero when $m \to \infty$. Let $(\rho_{\mathcal{M}}, p_{\mathcal{M}}, (h_s)_{\mathcal{M}}, \boldsymbol{u}_{\mathcal{D}}, \tilde{\boldsymbol{u}}_{\mathcal{D}})_{(m)}$ be the corresponding sequence of solutions. Suppose that this sequence verifies the following assertions:

(*i*) The sequence is uniformly bounded in $\mathrm{L}^\infty(\Omega \times [0,T))^5$, *i.e.* there exists $C \in \mathbb{R}$ such that, for $m \in \mathbb{N}$ and $0 \leq n \leq N$,

$$\max\left\{\rho^n_K, p^n_K, (h_s)^n_K\right\} \leq C,\ \forall K \in \mathcal{M}^{(m)} \quad \text{and} \quad \max\left\{|\boldsymbol{u}^n_\sigma|, |\tilde{\boldsymbol{u}}^n_\sigma|\right\} \leq C,\ \forall \sigma \in \mathcal{E}^{(m)}.$$

(*ii*) The sequence satisfies the following BV-stability assumption,

$$\lim_{m\to\infty} (h+\delta t)\big[\|\rho_{\mathcal{M}}\|_{\mathrm{BV}x} + \|p_{\mathcal{M}}\|_{\mathrm{BV}x} + \|(h_s)_{\mathcal{M}}\|_{\mathrm{BV}x} + \|\boldsymbol{u}_{\mathcal{D}}\|_{\mathrm{BV}x} + \|\boldsymbol{u}_{\mathcal{D}}\|_{\mathrm{BV}t} + \|\tilde{\boldsymbol{u}}_{\mathcal{D}}\|_{\mathrm{BV}x} + \|\tilde{\boldsymbol{u}}_{\mathcal{D}}\|_{\mathrm{BV}t}\big] = 0.$$

(*iii*) The sequence converges in $\mathrm{L}^p(\Omega\times[0,T))^{3+d}$, for $1 \leq p < \infty$, to $(\bar{\rho}, \bar{p}, \bar{h}_s, \bar{\boldsymbol{u}}, \bar{\tilde{\boldsymbol{u}}}) \in \mathrm{L}^p(\Omega\times[0,T))^{3+2d}$.

Then, $\bar{\tilde{u}} = \bar{u}$ and the limit $(\bar{\rho}, \bar{p}, \bar{h}_s, \bar{\boldsymbol{u}})$ satisfies (2.13).

Proof. The proof that follows is for the Ranacher Turek and Crouzeix Raviart discretisations, since for the MAC discretisation the arguments are essentially the same.

The line proposed in [[22],[73]], to show that the "weak form" of the total energy equation is respected by the scheme, follows three steps:

(*i*) multiply the discrete internal energy balance equation (which in the Euler case coincides with the discrete internal energy equation (2.18)) by $\delta t \phi^{n+1}_K$ and sum over $n \in \mathbb{N}, n \leq N$ and $K \in \mathcal{M}$,

(*ii*) multiply the discrete kinetic energy balance equation (2.20) by $\delta t \phi^{n+1}_\sigma$ and sum over $n \in \mathbb{N}, n \leq N$, and $\sigma \in \mathcal{E}$,

(*iii*) show that the sum of the equations obtained in (*i*) and (*ii*) converges to the "weak form" of the total energy equation, when m tends to infinity.

The only difference here, is the chemical fraction balance equations and that the discrete sensible energy equation contains reaction terms. All these equations are multiplied by $\delta t \phi^{n+1}_K$ and summed over $n \in \mathbb{N}, n \leq N$ and $K \in \mathcal{M}$.

The chemical fraction balance equations become, for $i \in \mathcal{I}$:

$$(Y_i)_1^{(m)} + (Y_i)_2^{(m)} = (Y_i)_3^{(m)}$$

where

$$(Y_i)_1^{(m)} = \sum_{n\in\mathbb{N}} \delta t \sum_{K\in\mathcal{M}} \frac{|K|}{\delta t} \big[\rho_K^n (y_i)_K^{n+1} - \rho_K^{n-1}(y_i)_K^n\big]\phi_K^{n+1},$$
$$(Y_i)_2^{(m)} = \sum_{n\in\mathbb{N}} \delta t \sum_{K\in\mathcal{M}} \sum_{\sigma\in\mathcal{E}(K)} F_{K,\sigma}^n (y_i)_\sigma^{n+1} \phi_K^{n+1}, \qquad (Y_i)_3^{(m)} = \zeta_i \nu_i W_i \sum_{n\in\mathbb{N}} \delta t \sum_{K\in\mathcal{M}} \dot{\omega}_K^{n+1} \phi_K^{n+1},$$

with ζ_i denoting the sign of the source term for the i-th chemical species, thus $-\zeta_F = -\zeta_O = \zeta_P = 1$ and $\zeta_N = 0$. Recasting the summation on the first term yields:

$$\begin{aligned}
(Y_i)_1^{(m)} &= \sum_{n\in\mathbb{N}}^{N} \sum_{K\in\mathcal{M}} |K| \rho_K^n (y_i)_K^{n+1} - \rho_K^{n-1}(y_i)_K^n\big]\phi_K^{n+1} \\
&= \sum_{n=1}^{N} \sum_{K\in\mathcal{M}} |K| \rho_K^{n-1}(y_i)_K^n \phi_K^n - \sum_{n\in\mathbb{N}} \sum_{K\in\mathcal{M}} |K| \rho_K^{n-1}(y_i)_K^n \phi_K^{n+1} \\
&= \sum_{n=0}^{N} \delta t \sum_{K\in\mathcal{M}} |K| \rho_K^{n-1}(y_i)_K^n \frac{\phi_K^n - \phi_K^{n+1}}{\delta t} - \sum_{K\in\mathcal{M}} |K| \rho_K^{-1}(y_i)_K^0 \phi_K^0 \\
&= -\int_0^T \int_\Omega \rho_\mathcal{M}\,(y_i)_\mathcal{M}\, \partial_t \phi_\mathcal{M} - \int_\Omega \rho_\mathcal{M}^0\,(y_i^0)_\mathcal{M}\, \phi_\mathcal{M}^0,
\end{aligned}$$

thus,

$$(Y_i)_1^{(m)} \overset{m\to\infty}{\longrightarrow} -\int_0^T \int_\Omega \bar{\rho}(\boldsymbol{x},t)\, \bar{y_i}(\boldsymbol{x},t)\, \partial_t \phi(\boldsymbol{x},t)\, \mathrm{d}\boldsymbol{x}\mathrm{d}t - \int_\Omega \rho_0(\boldsymbol{x})\, y_{i,0}(\boldsymbol{x})\, \phi(\boldsymbol{x},0)\, \mathrm{d}\boldsymbol{x}.$$

The second term reads:

$$\begin{aligned}
(Y_i)_2^{(m)} &= \sum_{n\in\mathbb{N}} \delta t \sum_{K\in\mathcal{M}} \sum_{\sigma\in\mathcal{E}(K)} F_{K,\sigma}^n (y_i)_\sigma^{n+1} \phi_K^{n+1} = \sum_{\sigma=K|L} \rho_\sigma^n (y_i)_\sigma^{n+1} \boldsymbol{u}_\sigma^n \cdot (\phi_L^{n+1} - \phi_K^{n+1}) \boldsymbol{n}_{K,\sigma} \\
&= -\sum_{n\in\mathbb{N}} \delta t \sum_{\sigma=K|L} \big[|D_{K,\sigma}| \rho_K^n (y_i)_K^{n+1} + |D_{L,\sigma}| \rho_L^n (y_i)_L^{n+1}\big] \boldsymbol{u}_\sigma^n \cdot \frac{|\sigma|}{|D_\sigma|} (\phi_L^{n+1} - \phi_K^{n+1}) \boldsymbol{n}_{K,\sigma} \\
&\quad + \sum_{n\in\mathbb{N}} \delta t \sum_{\sigma=K|L} \big[|D_{K,\sigma}| \rho_K^n (y_i)_K^{n+1} + |D_{L,\sigma}| \rho_L^n (y_i)_L^{n+1} - \rho_\sigma^n (y_i)_\sigma^n\big] \boldsymbol{u}_\sigma^n \cdot \frac{|\sigma|}{|D_\sigma|} (\phi_L^{n+1} - \phi_K^{n+1}) \boldsymbol{n}_{K,\sigma} \\
&= -\int_0^T \int_\Omega \rho_\mathcal{M}\,(y_i)_\mathcal{M}\, \boldsymbol{u}_\mathcal{D} \cdot (\boldsymbol{\nabla}\phi_\mathcal{M})_\mathcal{D} + (R_i)_{2,2}^{(m)}.
\end{aligned}$$

Using the identity $ab - cd = \frac{1}{2}(a-c)(b+d) + (a+c)(b-d)$ for any $(a,b,c,d) \in \mathbb{R}^4$, and the fact that $\rho_\sigma^n \in [\![\rho_K^n, \rho_L^n]\!]$, $(y_i)_\sigma^n \in [\![(y_i)_K^n, (y_i)_L^n]\!]$ for any $\sigma = K|L$ and $n \in \mathbb{N}, n \le N$, for any $i \in \mathcal{I}$,

$$\begin{aligned}
\big|(R_i)_{2,2}^{(m)}\big| &= \frac{1}{2}\Big| \sum_{n\in\mathbb{N}} \delta t \sum_{\sigma=K|L} \Big(|D_{K,\sigma}| \big[(\rho_K^n - \rho_\sigma^n)((y_i)_K^{n+1} + (y_i)_\sigma^{n+1}) + (\rho_K^n + \rho_\sigma^n)((y_i)_K^{n+1} - (y_i)_\sigma^{n+1})\big] \\
&\qquad + |D_{L,\sigma}| \big[(\rho_L^n - \rho_\sigma^n)((y_i)_L^{n+1} + (y_i)_\sigma^{n+1}) + (\rho_L^n + \rho_\sigma^n)((y_i)_L^{n+1} - (y_i)_\sigma^{n+1})\big] \Big) \boldsymbol{u}_\sigma^n \cdot (\boldsymbol{\nabla}\phi_\mathcal{M})_\sigma^{n+1} \Big| \\
&\le \frac{1}{2} \sum_{n\in\mathbb{N}} \delta t \sum_{\sigma=K|L} \Big(|D_{K,\sigma}| \big[2\|\rho_\mathcal{M}\|_\infty |(y_i)_K^{n+1} - (y_i)_L^{n+1}| + 2\|(y_i)_\mathcal{M}\|_\infty |\rho_K^n - \rho_L^n|\big] \Big) \|\boldsymbol{u}\|_\infty C_{\boldsymbol{\nabla}\phi} \\
&= C_{\boldsymbol{\nabla}\phi} \|\boldsymbol{u}\|_\infty \sum_{n\in\mathbb{N}} \delta t \sum_{\sigma=K|L} |D_\sigma| \big[\|\rho_\mathcal{M}\|_\infty |(y_i)_K^{n+1} - (y_i)_L^{n+1}| + \|(y_i)_\mathcal{M}\|_\infty |\rho_K^n - \rho_L^n|\big] \\
&\le h\, C_{\boldsymbol{\nabla}\phi} \|\boldsymbol{u}\|_\infty \big[\|\rho_\mathcal{M}\|_\infty \|(y_i)_\mathcal{M}\|_{\mathrm{BV}x} + \|(y_i)_\mathcal{M}\|_\infty \|\rho_\mathcal{M}\|_{\mathrm{BV}x}\big] \overset{m\to\infty}{\longrightarrow} 0,
\end{aligned}$$

where $\|\cdot\|_\infty$ denotes the usual norm of the space $\mathrm{L}^\infty(\Omega\times[0,T))$ and $C_{\boldsymbol{\nabla}\phi}\geq\|\boldsymbol{\nabla}\phi\|_\infty$. Thus,

$$(Y_i)_2^{(m)} \overset{m\to\infty}{\longrightarrow} -\int_0^T\int_\Omega \bar{\rho}(\boldsymbol{x},t)\,\bar{y_i}(\boldsymbol{x},t)\,\bar{\boldsymbol{u}}(\boldsymbol{x},t)\cdot\boldsymbol{\nabla}\phi(\boldsymbol{x},t)\,\mathrm{d}\boldsymbol{x}\mathrm{d}t.$$

Finally, in what concerns the third term, since by hypothesis $\dot{\omega}$ is only a function of y_F and y_O, the boundedness of the mass fractions implies, by continuity, the boundedness of $\dot{\omega}$, thus the dominated convergence theorem allows the following passage to the limit:

$$\sum_{n\in\mathbb{N}}\delta t\sum_{K\in\mathcal{M}}|K|\dot{\omega}_K^{n+1}=\int_{\delta t}^T\int_\Omega \dot{\omega}_{\mathcal{M}}(\boldsymbol{x},t)\,\phi_{\mathcal{M}}(\boldsymbol{x},t)\,\mathrm{d}\boldsymbol{x}\mathrm{d}t\overset{m\to\infty}{\longrightarrow}\int_0^T\int_\Omega\dot{\omega}(\boldsymbol{x},t)\,\phi(\boldsymbol{x},t)\,\mathrm{d}\boldsymbol{x}\mathrm{d}t,$$

and

$$(Y_i)_3^{(m)}\overset{m\to\infty}{\longrightarrow}\zeta_i\nu_i W_i\int_0^T\int_\Omega\dot{\omega}(\boldsymbol{x},t)\,\phi(\boldsymbol{x},t)\,\mathrm{d}\boldsymbol{x}\mathrm{d}t,$$

which concludes the proof that the discrete chemical species balance equations converge to the weak formulation of the continuous problem.

Let us now turn to the sensible energy equation, which reads:

$$E_1^{(m)}+E_2^{(m)}+E_3^{(m)}=S^{(m)},$$

where

$$\begin{aligned}
E_1^{(m)}&=\sum_{n\in\mathbb{N}}\delta t\sum_{K\in\mathcal{M}}\frac{|K|}{\delta t}\Big[\big[\rho_K^{n+1}(e_s)_K^{n+1}-\rho_K^n(e_s)_K^n\big]+\sum_{i\in\mathcal{I}}\Delta h_{f,i}^0\big[\rho_K^n(y_i)_K^{n+1}-\rho_K^{n-1}(y_i)_K^n\big]\Big]\phi_K^{n+1}\\
&=E_{1,1}^{(m)}+E_{1,2}^{(m)},\\
E_2^{(m)}&=\sum_{n\in\mathbb{N}}\delta t\sum_{K\in\mathcal{M}}\sum_{\sigma\in\mathcal{E}(K)}\Big[F_{K,\sigma}^{n+1}(e_s)_\sigma^{n+1}+\sum_{i\in\mathcal{I}}\Delta h_{f,i}^0F_{K,\sigma}^n(y_i)_\sigma^{n+1}\Big]\phi_K^{n+1}=E_{2,1}^{(m)}+E_{2,2}^{(m)},\\
E_3^{(m)}&=\sum_{n\in\mathbb{N}}\delta t\sum_{K\in\mathcal{M}}|K|p_K^{n+1}\mathrm{div}(\boldsymbol{u})_K^{n+1}\phi_K^{n+1},\qquad\text{and } S^{(m)}=\sum_{n\in\mathbb{N}}\delta t\sum_{K\in\mathcal{M}}S_K^n\phi_K^{n+1}.
\end{aligned}$$

All non-reactive terms having been treated, we focus in showing that the reactive terms $E_{1,2}^{(m)}$ and $E_{2,2}^{(m)}$ converge to the correct limit, so that following the steps, (*ii*) and (*iii*), lead to the "weak form" of the total energy equation. In fact, the reactive terms have already been treated above in the consistency of the chemical fraction balance equations, since they may be rewritten as

$$E_{1,2}^{(m)}=\sum_{i\in\mathcal{I}}\Delta h_{f,i}^0(Y_i)_1^{(m)},\text{ and}\qquad E_{2,2}^{(m)}=\sum_{i\in\mathcal{I}}\Delta h_{f,i}^0(Y_i)_2^{(m)},$$

thus, it is immediate that they both converge to the expected limit:

$$\begin{aligned}
E_{1,2}^{(m)}&\overset{m\to\infty}{\longrightarrow}-\sum_{i\in\mathcal{I}}\Delta h_{f,i}^0\Big[\int_0^T\int_\Omega\bar{\rho}(\boldsymbol{x},t)\,\bar{y_i}(\boldsymbol{x},t)\,\partial_t\phi(\boldsymbol{x},t)\,\mathrm{d}\boldsymbol{x}\mathrm{d}t+\int_\Omega\rho_0(\boldsymbol{x})\,y_{i,0}(\boldsymbol{x})\,\phi(\boldsymbol{x},0)\,\mathrm{d}\boldsymbol{x}\Big],\\
E_{2,2}^{(m)}&\overset{m\to\infty}{\longrightarrow}-\sum_{i\in\mathcal{I}}\Delta h_{f,i}^0\int_0^T\int_\Omega\bar{\rho}(\boldsymbol{x},t)\,\bar{y_i}(\boldsymbol{x},t)\,\bar{\boldsymbol{u}}(\boldsymbol{x},t)\cdot\boldsymbol{\nabla}\phi(\boldsymbol{x},t)\,\mathrm{d}\boldsymbol{x}\mathrm{d}t.
\end{aligned}$$

□

2.7 Numerical tests

At the continuous level, the boundedness of the chemical mass fractions formally implies that, when $\varepsilon \to 0$, the relaxed model converges to the asymptotic one. Indeed, integrating any of the reactive species mass balance equations with respect to time and space, we observe that $||\dot{\omega}||_{\mathrm{L}^1(\Omega\times(0,T))}$ tends to zero as ε, and thus two separate zones appear: a zone characterized by $G < 0.5$ and where the reaction is complete, and a zone corresponding to $G \geq 0.5$, where no reaction has occured.

A closed form of the solution of the Riemann problem for the asymptotic model is available [2]. In order to perform numerical tests, a Riemann problem with initial conditions such that the analytic solution has the profile presented in Figure 2.1 is chosen. Moreover, the selected configuration imposes zero amplitude for the contact discontinuity and the left non linear wave, thus the solution consists of three different constant states: $\mathbf{W}_R^*, \mathbf{W}^{**}$ and $\mathbf{W}_R$. The right state corresponds to a stoechiometric mixture of hydrogen and air (so the molar fractions of Hydrogen, Oxygen and Nitrogen are 2/7, 1/7 and 4/7 respectively) at rest, at the pressure $p = 9.9\,10^4$ Pa and the temperature $T = 283°$ K. The velocity is supposed to be zero in the left state, which is sufficient to determine the solution, supposing that the initial discontinuity lies at $x = 0$; physically, this situation corresponds to the left part of a (symetrical) constant velocity plane deflagration starting at $x = 0$.. The flame velocity is $u_f = 63$ m/s and the formation enthalpies are zero except for the product (*i.e.* steam), with $\Delta h^0_{f,O} = -13.255\,10^6$ J (Kg K)$^{-1}$. The quantity ρ_u is the analytical density in the intermediate state (so the total velocity of the flame brush is equal to the sum of u_f and the material velocity after the reactive shock, see [2]). The computation is initialized by the analytical solution at $t = 0.002$ and the final time is $t = 0.005$. The computational domain is the interval $(0, 4.5)$.

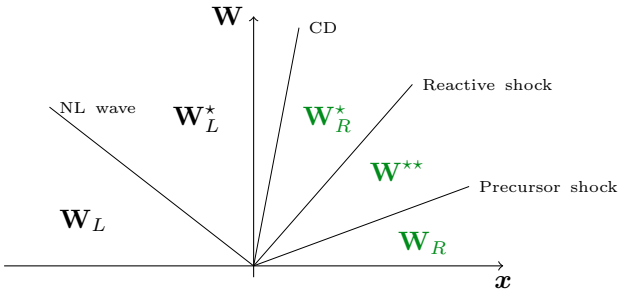

Figure 2.1: The analytic solution of the numerical test configuration.

The numerical tests performed aim at checking the convergence of the scheme to such a solution, which in fact may result from two different properties: the convergence of the relaxed model to the asymptotic model when ε tends to zero, and the convergence of the scheme towards a numerical solution when the time and space steps tend to zero. To this purpose, we choose ε proportional to the space step and make it tend to zero, with a constant CFL number. We test the scheme behaviour with three different discretizations of the convection operator in the chemical mass species balances: the standard upwind scheme, a MUSCL-like discretizatin which is an extension to variable density flows of the scheme proposed in [67] and is described in Appendix 2.A, and a first-order anti-diffusive scheme proposed in [17] and given in Apendix 2.B for the sake of completeness.

Results obtained at $t = 0.005$ with the upwind scheme, the MUSCL-like scheme and the anti-diffusive scheme, for more and more refined meshes, are shown on Figures 2.2 and 2.3, Figures 2.4 and 2.5 and Figures 2.6 and 2.7 respectively, together with the analytical solution. The expected convergence is indeed observed but, with the upwind discretization, the rate of convergence is poor.

This seems to be due to the interaction between the numerical diffusion of the upwind scheme, which artificially introduces unburnt reactive masses to the burnt zone, and the stiffness of the reaction term. As expected in such a case, the results are significantly improved by the use of a less diffusive scheme for the chemical species balance equations. Indeed, passing from the upwind to the MUSCL-like and, last, the anti-diffusive discretization improves the accuracy of the scheme, as may be observed in Figures 2.8 and 2.9, where the results obtained by the three discretizations for a regular mesh composed of 500 cells are plotted together with the continuous solution. This observation is conforted by the measures, in L^1-norm, of the difference between the discrete and continuous solutions gathered in the following table. Black values correspond to the errors obtained with the upwind discretization, blue ones to the MUSCL discretization and the orange ones to the anti-diffusive scheme; we denote by $h_0 = 4.5/250$ the measure of the control volume of the least refined mesh. For every meshes and variables, the anti-diffusive scheme is the most accurate and the upwind one the least accurate. The calculated orders of convergence are respectively close to 0.5 and 1 for the upwind scheme, on one part, and the MUSCL-like and anti-diffusive schemes, on the other part.

h	$\|\|p - p_{ex}\|\|_{L^1} \times 10^{-4}$			$\|\|\boldsymbol{u} - \boldsymbol{u}_{ex}\|\|_{L^1} \times 10^{-2}$			$\|\|\rho - \rho_{ex}\|\|_{L^1} \times 10$		
h_0	16.5	7.26	4.59	2.17	1.56	1.07	7.69	3.71	2.74
$h_0/2$	12.5	3.88	2.43	1.64	0.787	0.579	6.16	2.23	1.65
$h_0/4$	9.66	2.05	1.38	1.23	0.471	0.371	4.73	1.26	0.913
$h_0/8$	7.58	1.17	0.708	0.958	0.263	0.175	3.63	0.691	0.476
$h_0/20$	5.78	0.673	0.375	0.728	0.160	0.103	2.77	0.382	0.267
$h_0/40$	4.31	0.414	0.194	0.543	0.0786	0.0458	2.03	0.201	0.134

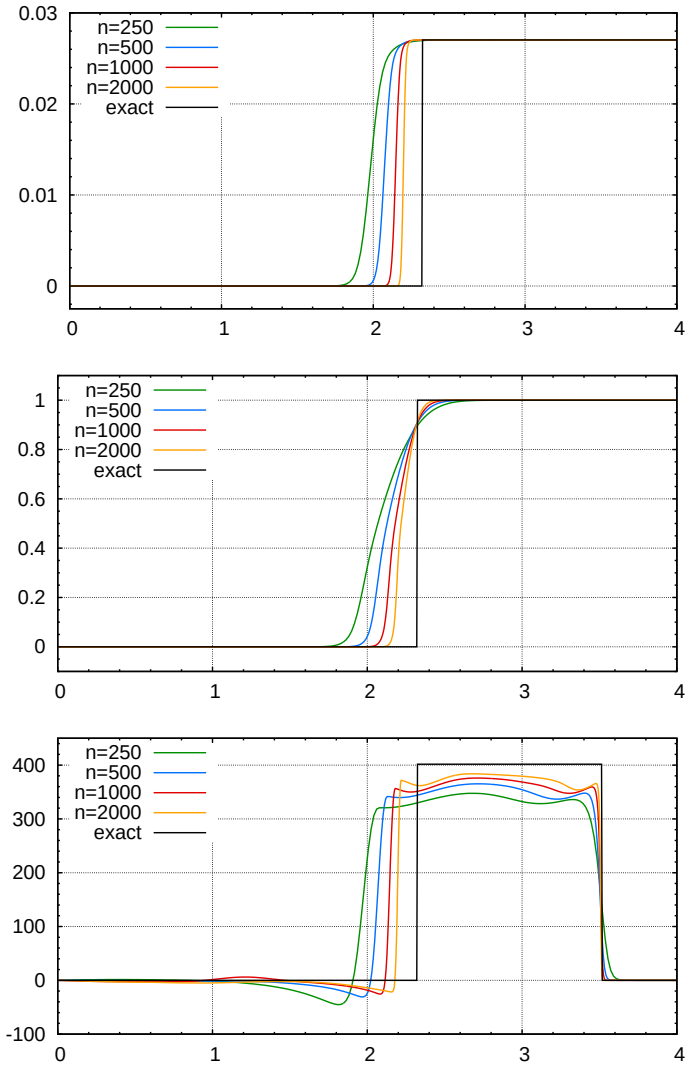

Figure 2.2: Upwind scheme – From top to bottom, fuel mass fraction, G and velocity at $t = 0.005$, as a function of the space variable. Results obtained with more and more refined meshes (the label $n = num$ on the figures means that the mesh is a uniform grid with num cells) and exact solution.

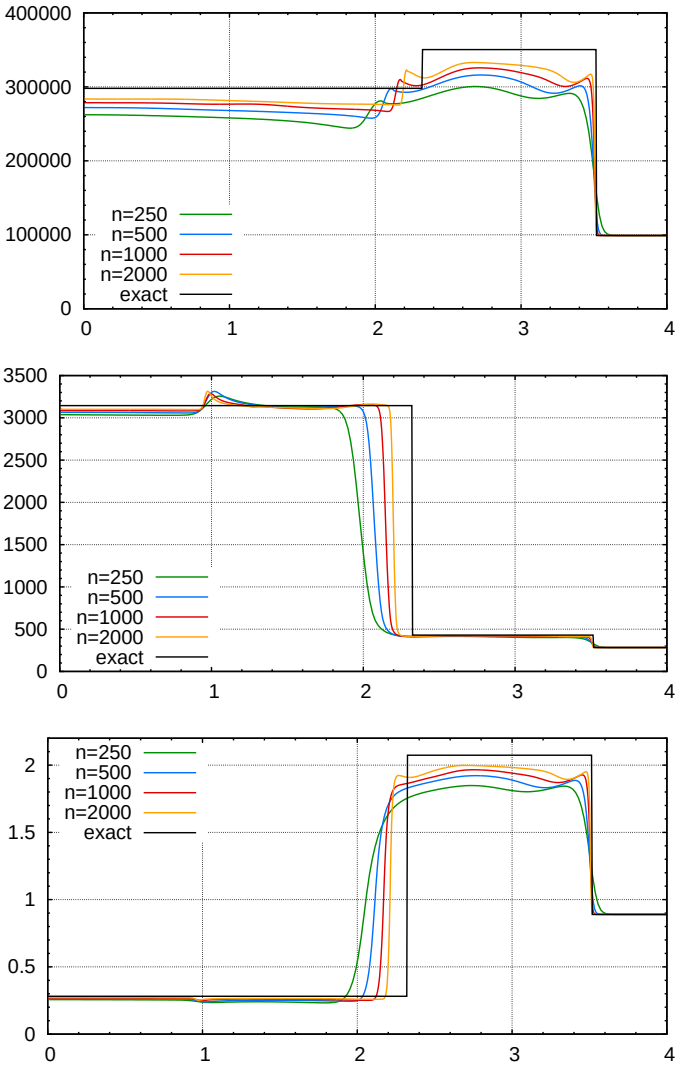

Figure 2.3: Upwind scheme – From top to bottom, pressure, temperature and density at $t = 0.005$, as a function of the space variable. Results obtained with more and more refined meshes (the label $n = num$ on the figures means that the mesh is a uniform grid with num cells) and exact solution.

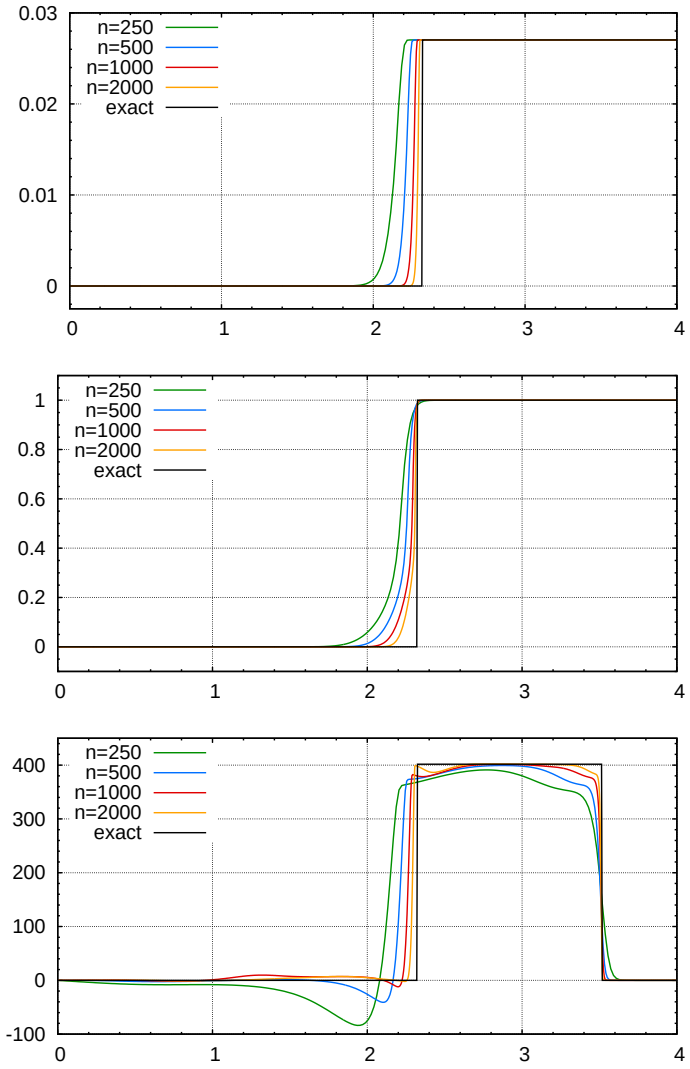

Figure 2.4: MUSCL scheme – From top to bottom, fuel mass fraction, G and velocity at $t = 0.005$, as a function of the space variable. Results obtained with more and more refined meshes (the label $n = num$ on the figures means that the mesh is a uniform grid with num cells) and exact solution.

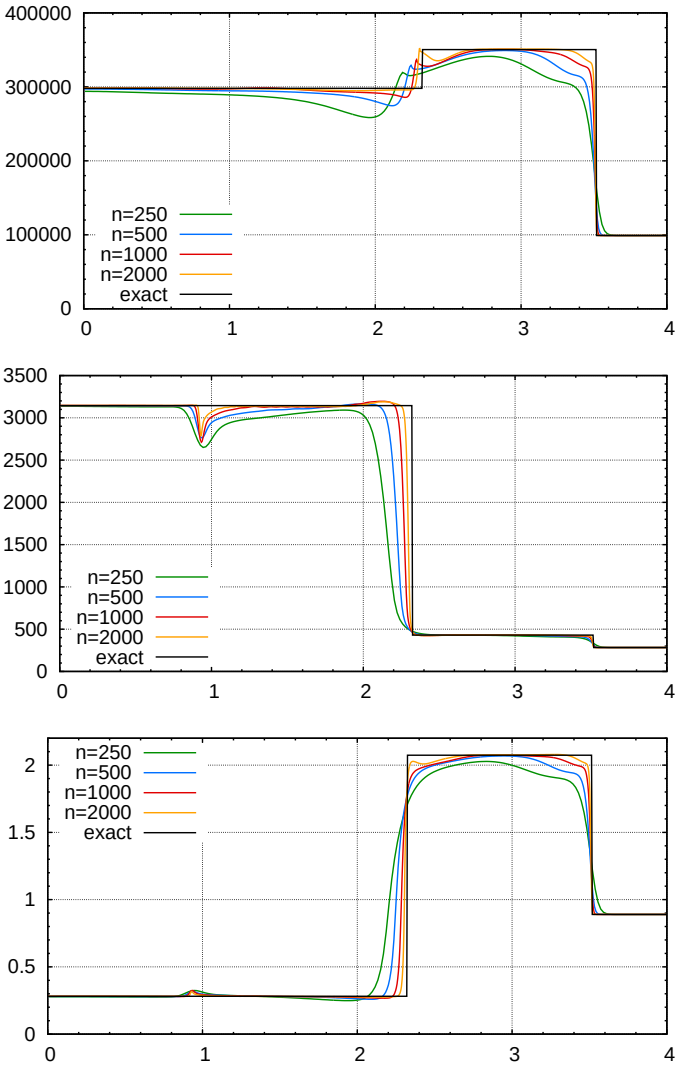

Figure 2.5: MUSCL scheme – From top to bottom, pressure, temperature and density at $t = 0.005$, as a function of the space variable. Results obtained with more and more refined meshes (the label $n = num$ on the figures means that the mesh is a uniform grid with num cells) and exact solution.

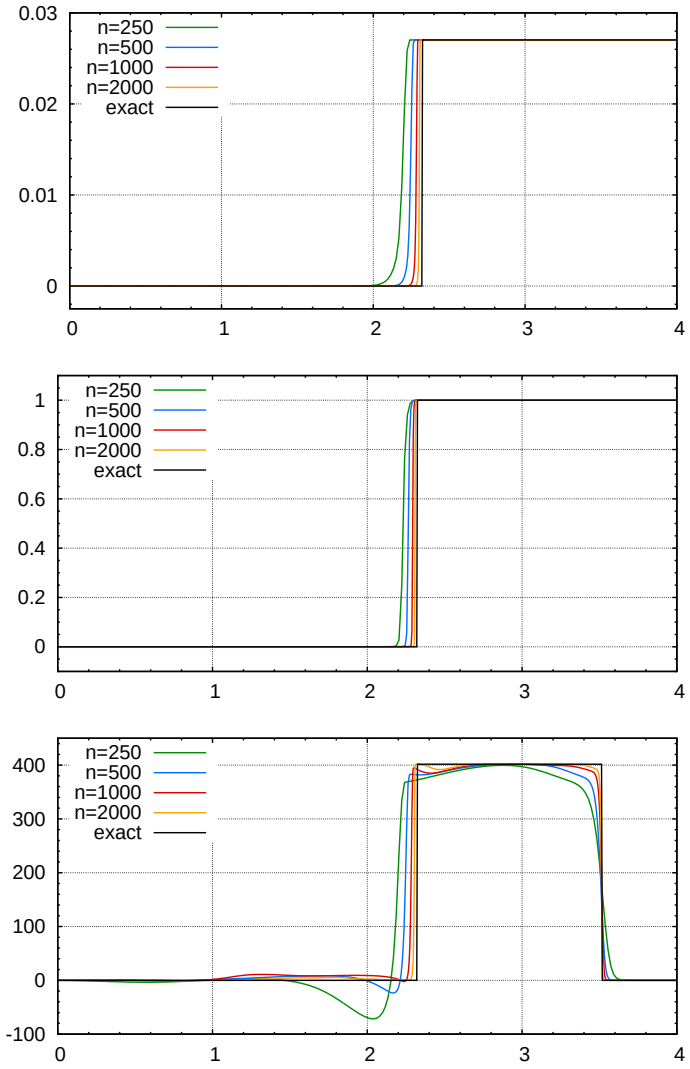

Figure 2.6: Anti-diffusive scheme – From top to bottom, fuel mass fraction, G and velocity at $t = 0.005$, as a function of the space variable. Results obtained with more and more refined meshes (the label $n = num$ on the figures means that the mesh is a uniform grid with num cells) and exact solution.

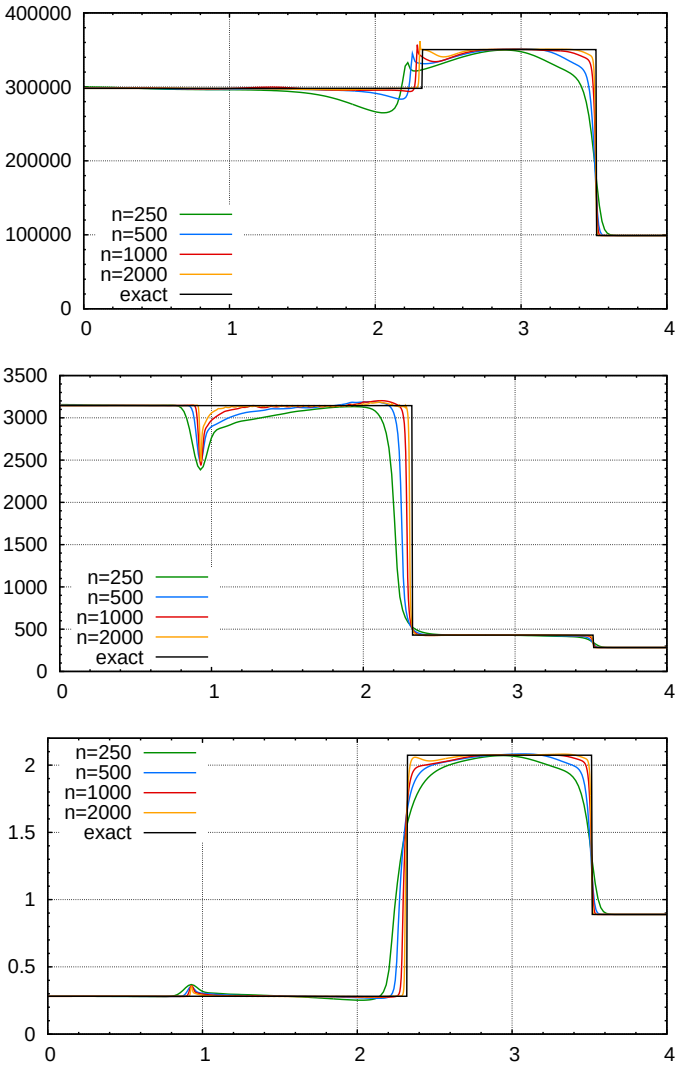

Figure 2.7: Anti-diffusive scheme – From top to bottom, pressure, temperature and density at $t = 0.005$, as a function of the space variable. Results obtained with more and more refined meshes (the label $n = num$ on the figures means that the mesh is a regular mesh composed of num cells) and exact solution.

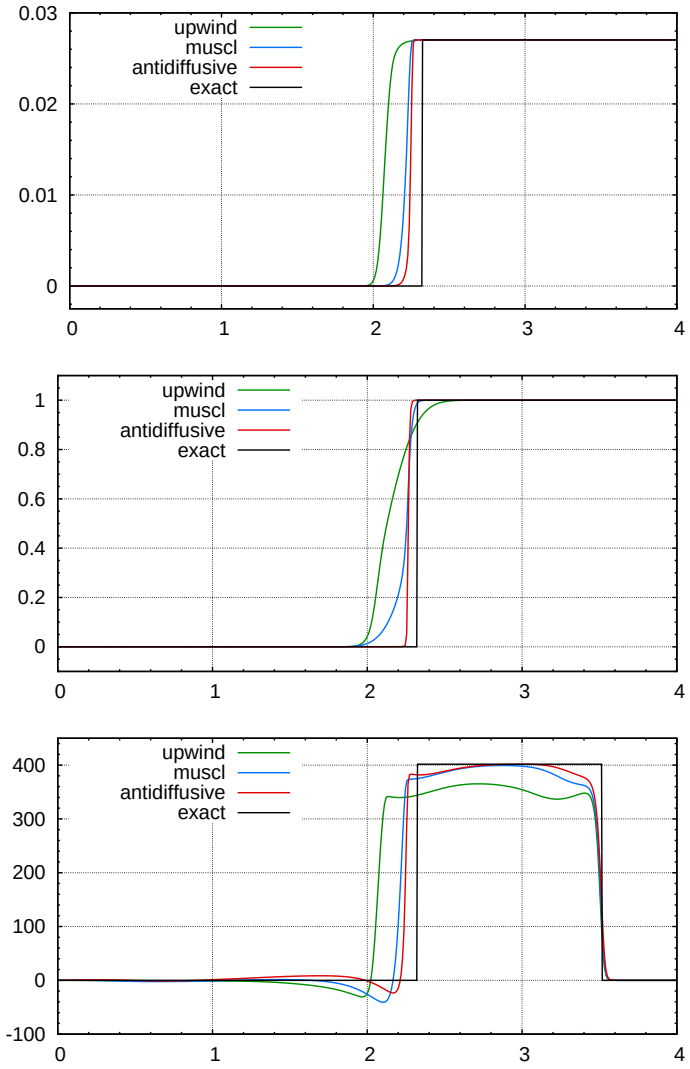

Figure 2.8: Comparison of the solutions obtained with the upwind, MUSCL and anti-diffusive scheme – From top to bottom, fuel mass fraction, G and velocity at $t = 0.005$, as a function of the space variable. Results obtained with a regular mesh composed of $n = 500$ cells.

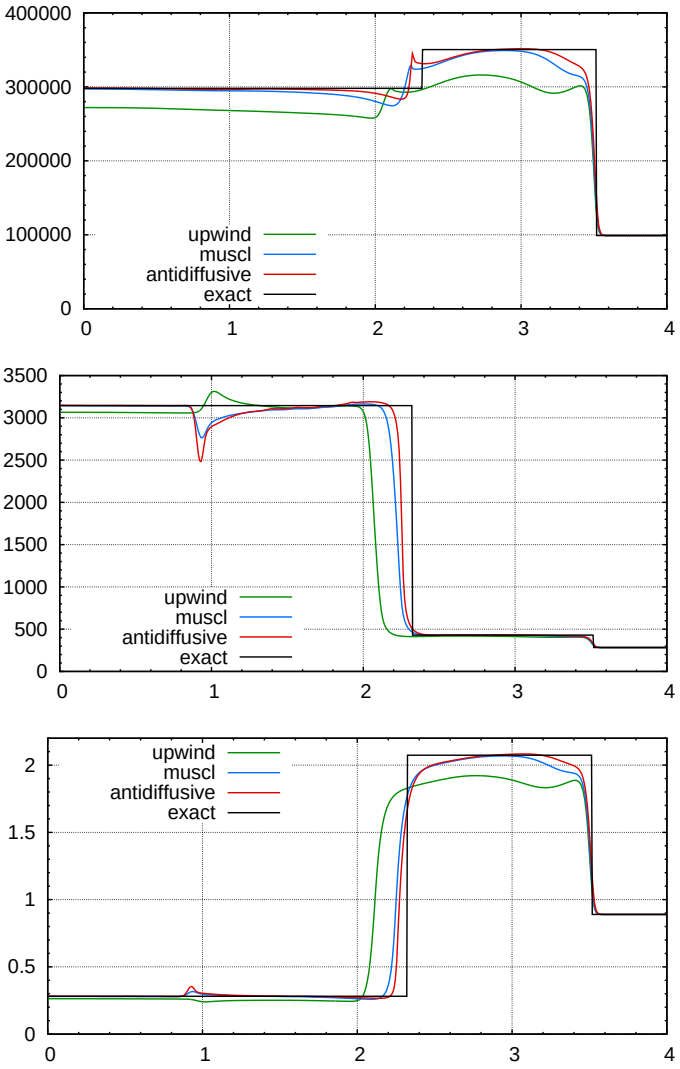

Figure 2.9: Comparison of the solutions obtained with the upwind, MUSCL and anti-diffusive scheme – From top to bottom, pressure, temperature and density at $t = 0.005$, as a function of the space variable. Results obtained with a regular mesh composed of $n = 500$ cells.

Appendix

2.A The MUSCL scheme

The MUSCL discretisation of the convection operators of the chemical species balance and G-equation is inspired by the discretisation proposed in [67]. Let us use the following system of equations,

$$\partial_t \rho + \mathrm{div}(\rho \boldsymbol{u}) = 0$$
$$\partial_t (\rho \boldsymbol{u}) + \mathrm{div}(\rho \boldsymbol{u} y) = 0,$$

in order to explain here the MUSCL discretization of the convection operator in the transport equation of y.

The discretization of the above system reads:

$$\forall K \in \mathcal{M}, \qquad \frac{\rho_K^{n+1} - \rho_K^n}{\delta t} + \frac{1}{|K|} \sum_{\sigma \in \mathcal{E}(K)} F_{K,\sigma}^{n+1} = 0,$$
$$\frac{\rho_K^{n+1} y_K^{n+1} - \rho_K^n y_K^n}{\delta t} + \frac{1}{|K|} \sum_{\sigma \in \mathcal{E}(K)} F_{K,\sigma}^{n+1} y_\sigma^n = 0.$$

For any $\sigma \in \mathcal{E}$, the procedure consists in three steps:

- Calculate a tentative value for y_σ as a linear interpolate of nearby values.
- Calculate an interval for y_σ which guarantees the stability of the scheme.
- Project the tentative value y_σ to the stability interval.

For the tentative value of y_σ, let us choose some real coefficients $(\alpha_K^\sigma)_{K \in \mathcal{M}}$ such that

$$\boldsymbol{x}_\sigma = \sum_{K \in \mathcal{M}} \alpha_K^\sigma \boldsymbol{x}_K, \qquad \sum_{K \in \mathcal{M}} \alpha_K^\sigma = 1.$$

The coefficients used in this interpolation are chosen in such a way that as little as possible of the closest cells to σ take part. For example, for $\sigma = K|L$ and if $\boldsymbol{x}_K$, $\boldsymbol{x}_\sigma$, $\boldsymbol{x}_L$ are aligned, only two non-zero coefficients exist in the family $(\alpha_K^\sigma)_{K \in \mathcal{M}}$, namely the α_K^σ and α_K^σ. Then, these coefficients are used to calculate the tentative value of y_σ by

$$y_\sigma = \sum_{K \in \mathcal{M}} \alpha_K^\sigma y_K.$$

The construction of the stability interval lies on the following hypothesis:

$$\forall K \in \mathcal{M},\ \forall \sigma \in \mathcal{E}(K) \cap \mathcal{E}_{\mathrm{int}},\ \exists \beta_K^\sigma \in [0,1] \text{ and } M_K^\sigma \in \mathcal{M} \text{ such that}$$

$$y_\sigma - y_K = \begin{cases} \beta_K^\sigma (y_K - y_{M_K^\sigma}), \text{ if } F_{K,\sigma} \geq 0, \\ \beta_K^\sigma (y_{M_K^\sigma} - y_K), \text{ otherwise.} \end{cases} \tag{2.21}$$

Under this hypothesis and a CFL condition, the scheme preserves the initial of y.

Definition. Note that in this work the presence of Neumann homogeneous boundary conditions limits our study to the internal faces, but what follows may be naturally generalized for non-homegneous Dirichlet or/and Neumann boundary conditions.

Definition. The so-called CFL number reads for any $n \in \mathbb{N}, n \leq N$:

$$\mathrm{CFL}^n = \max_{K \in \mathcal{M}} \Big\{ \frac{\delta t}{|K|} \sum_{\sigma \in \mathcal{E}(K)} \big|u_{K,\sigma}^{n+1}\big| \Big\}.$$

Lemma 2.A.1.
Let us suppose that $\mathrm{CFL}^{n+1} \leq 1$. For $K \in \mathcal{M}$, let us note by $\mathcal{V}(K)$ the set of cells $M_K^\sigma,\ \sigma \in \mathcal{E}(K)$ such that (2.21) holds. Then $\forall K \in \mathcal{M}$, the value of y_K^{n+1} is a convex combination of $\{y_K^n, (y_M^n)_{M \in \mathcal{V}(K)}\}$.

Proof. Reordering the discretised form of the mass balance equation, gives:

$$\rho_K^n = \rho_K^{n+1} + \frac{\delta t}{|K|} \sum_{\sigma \in \mathcal{E}(K)} F_{K,\sigma}^{n+1}.$$

Replacing this expression of ρ_K^n in the discrete balance equation of y and using the relations provided by (2.21), yields:

$$\begin{aligned}
\rho_K^{n+1} y_K^{n+1} &= \rho_K^n y_K^n - \frac{\delta t}{|K|} \sum_{\sigma \in \mathcal{E}(K)} F_{K,\sigma}^{n+1} y_\sigma^n \\
&= \rho_K^{n+1} y_K^n - \frac{\delta t}{|K|} \sum_{\sigma \in \mathcal{E}(K)} F_{K,\sigma}^{n+1} (y_\sigma^n - y_K^n) \\
&= \rho_K^{n+1} y_K^n - \frac{\delta t}{|K|} \sum_{\sigma \in \mathcal{E}(K)} \big(F_{K,\sigma}^{n+1}\big)^+ (y_\sigma^n - y_K^n) + \frac{\delta t}{|K|} \sum_{\sigma \in \mathcal{E}(K)} \big(F_{K,\sigma}^{n+1}\big)^- (y_\sigma^n - y_K^n) \\
&= \rho_K^{n+1} y_K^n - \frac{\delta t}{|K|} \sum_{\sigma \in \mathcal{E}(K)} \big(F_{K,\sigma}^{n+1}\big)^+ \beta_K^\sigma (y_K^n - y_{M_K^\sigma}^n) + \frac{\delta t}{|K|} \sum_{\sigma \in \mathcal{E}(K)} \big(F_{K,\sigma}^{n+1}\big)^- (y_{M_K^\sigma}^n - y_K^n),
\end{aligned}$$

and since the discretization of the mass balance equation is such that $\forall K \in \mathcal{M}$ and $n \in \mathbb{N}, n \leq N$, $\rho^{n+1} > 0$,

$$y_K^{n+1} = y_K^n \Big(1 - \frac{\delta t}{|K|} \sum_{\sigma \in \mathcal{E}(K)} \beta_K^\sigma |u_{K,\sigma}^{n+1}|\Big) + \frac{\delta t}{|K|} \sum_{\sigma \in \mathcal{E}(K)} y_{M_K^\sigma}^n \beta_K^\sigma |u_{K,\sigma}^{n+1}|,$$

which concludes the proof under the hypothesis that $\mathrm{CFL} \leq 1$. □

In order to construct the stability interval, we will use a stronger version of (2.21), which allows us to be more precise in the choice of the control volumes $M_K^\sigma,\ \forall K \in \mathcal{M}$ and $\forall \sigma \in \mathcal{E}(K)$. Let $\sigma \in \mathcal{E}$, let us denote by V^- and V^+ the upstream and downstream cell separated by σ, and by $\mathcal{V}_\sigma(V^-)$ and $\mathcal{V}_\sigma(V^+)$ two sets of neighbouring cells of V^- and V^+ respectively, and let us suppose:

(H1) – there exists $M \in \mathcal{V}_\sigma(V^+)$ such that $u_\sigma^n \in |[u_M^n, u_M^n + \frac{\zeta^+}{2}(u_{V^+}^n - u_M^n)]|$,

(H2) – there exists $M \in \mathcal{V}_\sigma(V^-)$ such that $u_\sigma^n \in |[u_{V^-}^n, u_{V^-}^n + \frac{\zeta^-}{2}(u_{V^-}^n - u_M^n)]|$,

where for $a,\ b \in \mathbb{R}$, we denote by $|[a,b]|$ the interval $\{\alpha a + (1-\alpha)b,\ \alpha \in [0,1]\}$, and ζ^+ and ζ^- are two numerical parameters lying in the interval $[0,2]$.

Definition (1D case). Let us take the example of an interface σ separating K_i and K_{i+1} in a 1D case (see Figure 2.A.1 for the notations), with a uniform meshing and a positive advection velocity, so that $V^- = K_i$ and $V^+ = K_{i+1}$. In 1D, a natural choice is $\mathcal{V}_\sigma(K_i) = \{K_{i-1}\}$ and $\mathcal{V}_\sigma(K_{i+1}) = \{K_i\}$. On Figure 2.A.1, we sketch: on the left, the admissible interval given by (H1) with $\zeta^+ = 1$ (green) and $\zeta^+ = 2$ (orange); on the right, the admissible interval given by (H2) with $\zeta^- = 1$ (green) and $\zeta^- = 2$ (orange). The parameters ζ^- and ζ^+ may be seen as limiting the admissible slope between $(\boldsymbol{x}_i, y_i^n)$ and $(\boldsymbol{x}_\sigma, y_\sigma^n)$ (with $\boldsymbol{x}_i$ the abscissa of the mass centre of K_i and $\boldsymbol{x}_\sigma$ the abscissa of σ), with respect to a left and right slope, respectively. For $\zeta^- = \zeta^+ = 1$, one recognises the usual minmod limiter (*e.g.* [29, Chapter III]). Note that, since, on the example depicted on Figure 2.A.1, the discrete function y^n has an extremum in K_i, the combination of the conditions (H1) and (H2) imposes that, as usual, the only admissible value for y_σ^n is the upwind one.

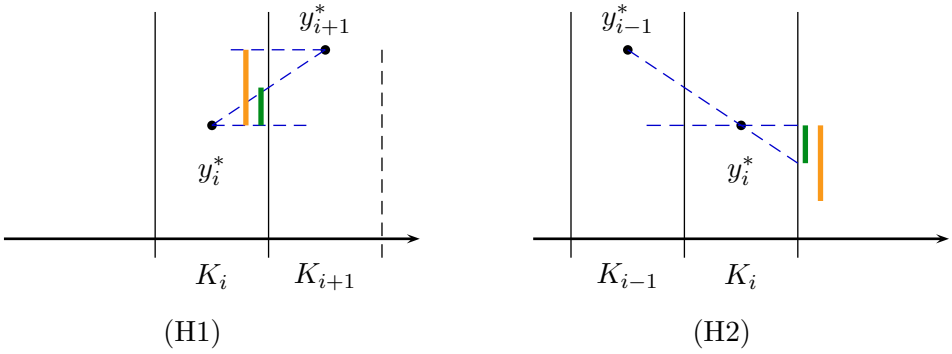

Figure 2.A.1: Conditions (H1) and (H2) in 1D.

(H1)-(H2) and (2.21) are linked in the following way: let $K \in \mathcal{M}$ and $\sigma \in \mathcal{E}(K)$. If $F^n_{K,\sigma} \leq 0$, *i.e.* K is the downstream cell for σ, denoted above by V^+, since $\zeta^+ \in [0, 2]$, condition (H1) yields that there exists $M \in \mathcal{M}$ such that $u^n_\sigma \in |[u^n_K, u^n_M]|$, which is (2.21). Otherwise, *i.e.* if $F^n_{K,\sigma} \geq 0$ and K is the upstream cell for σ, denoted above by V^-, condition (H2) yields that there exists $M \in \mathcal{M}$ such that $y^n_\sigma \in |[y^n_K, 2y^n_K - y^n_M]|$, so $y^n_\sigma - y^n_K \in |[0, y^n_K - y^n_M]|$, which is once again (2.21).

Definition. For $\sigma \in \mathcal{E}$, if $V^- \in \mathcal{V}_\sigma(V^+)$, the upstream choice $y^n_\sigma = y^n_{V^-}$ always satisfies the conditions (H1)-(H2), and is the only one to satisfy them if we choose $\zeta^- = \zeta^+ = 0$.

Finally, we need to precise the choice of the sets $\mathcal{V}_\sigma(V^-)$ and $\mathcal{V}_\sigma(V^+)$. Here, we just set $\mathcal{V}_\sigma(V^+) = \{V^-\}$; such a choice guarantees that at least the upstream choice is in the intersection of the intervals defined by (H1) and (H2), as explained in Remark 2.A. $\mathcal{V}_\sigma(V^-)$ may be defined in two different ways (*cf.* Figure 2.A.2):

- as the "upstream cells" to V^-, *i.e.* $\mathcal{V}_\sigma(V^-) = \{L \in \mathcal{M},\ L$ shares a face σ with V^- and $F_{V^-,\sigma} < 0\}$,
- when this makes (*i.e.* with a mesh obtained by Q_1 mappings from the $(0,1)^d$ reference element), the opposite cells to σ in V^- are chosen. Note that for a structured mesh, this choice allows to recover the usual minmod limiter.

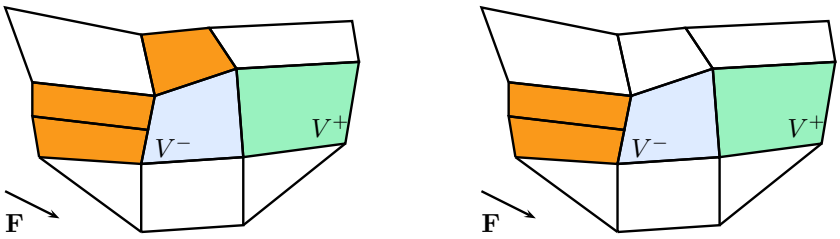

(a) (b)

Figure 2.A.2: Notations for the definition of the limitation process. In orange, control volumes of the set $\mathcal{V}_\sigma(V^-)$ for $\sigma = V^-|V^+$, with a constant advection field $\mathbf{F}$: upwind cells (a) or opposite cells (b).

2.B An anti-diffusive scheme

The scheme of Després-Lagoutière [17] for the constant velocity advection problem presents some interesting proporties in one-dimensional (or structured multi-dimensional) space, among which is the fact that it notably limits the numerical diffusion. In this work, in order to treat convection operators of the chemical variables, which read in a simplified case

$$\partial_t(\rho y) + \mathrm{div}(\rho y \boldsymbol{u}) = 0,$$

we used the following generalization, which allows us to work in untructured meshes:

$$\forall K \in \mathcal{M}, \qquad y_K^{n+1} = \frac{\rho_K^{n-1}}{\rho_K^n} y_K^n + \frac{\delta t}{|K|} \frac{1}{\rho_K^n} \sum_{\sigma \in \mathcal{E}(K)} F_{K,\sigma}^n y_\sigma^n,$$

where for $\sigma = K|L$ and given that $F_{K,\sigma}^n \geq 0$, at first we estimate $y_\sigma^n = y_L^n$ and second, to ensure stability, we project to the interval $[y_K^n, y_K^n + \frac{1}{\alpha}\frac{1-\nu}{\nu}(y_K - y_O)]$, where $\nu = \delta t/|K|$, α is a numerical parameter that depends on the space dimension and $O \in \mathcal{M}$ is the control volume which stands at the opposite side of K with respect to L.

Chapter 3

A model and a numerical scheme to compute laminar flames in dust suspensions

Abstract

We address in this paper a system of balance equations which models the low Mach number one-dimensional reactive flow generated by the combustion of a dust suspension. This model features rather general diffusion terms, with, in particular, mass diffusion coefficients which depend on the local composition and differ in function of the considered chemical species. For the resolution of this system, we develop a fractional step finite volume algorithm which preserves by construction the stability properties of the continuous problem, namely the positivity of the chemical species mass fractions, the fact that their sum is equal to one, and the non-decrease of the temperature, provided that the chemical reaction is exothermic.

3.1 Introduction

We address in this paper a model for the combustion of dust suspensions. This model is dedicated to the simulation of laminar flames, for which a one-dimensional representation, supposing a low Mach number flow, is sufficient. Particular care has to be paid to the formulation of the diffusion fluxes, since they determine the structure of the flame; in particular, the mass diffusion coefficients depend on the local composition of the mixture, and differ from one chemical species to another. Consequently, (standard) simplifications performed to derive the model will yield balance equations for the mass of the chemical species which preserve the positivity of the mass fractions and the fact that their sum is equal to 1, but do not satisfy a maximum principle (*i.e.* non-physical local accumulation of a species can not be excluded). On the opposite, the energy balance equation does satisfy a maximum principle so, provided that the chemical reaction is exothermic, the minimal temperature cannot decrease. The aim of this chapter is to develop a fractional step finite volume scheme for the resolution for a model that uses a rather general simplification for the mass diffusion coefficients, to show that it has at least one solution and that any possible solution satisfies the above-mentionned physical bounds.

The exposition is structured as follows. The physical model is introduced in the next section, then the scheme is given in Section 3.3. Its properties are analysed in Section 3.4.

3.2 The physical model

We first give the balance equations, then the closure laws for the mass diffusion terms.

3.2.1 The system of balance equations

The flow is supposed to be governed by the balance equations modelling a variable density flow in the asymptotic limit of low Mach number flows [61], namely the mass balance of the chemical species and of the mixture, the enthalpy balance, and the momentum balance equations. For a one-dimensional flow in such a quasi-incompressible situation, the role played by the mass and momentum balance equations is quite different than in the multi-dimensional case: indeed, since, in one space dimension, both the divergence and the gradient may be considered as transport operators, the velocity may be seen as the solution of the mass balance equation, and the momentum balance yields the dynamic pressure. Since this latter unknown does not appear in the other equations, its computation is of poor interest, and the momentum balance equation may be disregarded; this is what we do in the following. Except for this aspect, equations in this section are written in the usual multi-dimensional form.

The computational domain is denoted by Ω, and its boundary $\partial\Omega$ is supposed to be split in an inflow part $\partial\Omega_I$ (where the flow enters the domain, *i.e.* $\boldsymbol{u}\cdot\boldsymbol{n}_{\partial\Omega} < 0$, with $\boldsymbol{u}$ the flow velocity and $\boldsymbol{n}_{\partial\Omega}$ the normal vector to $\partial\Omega$ outward Ω) and an outflow one $\partial\Omega_O$ (where the flow leaves the domain, *i.e.* $\boldsymbol{u}\cdot\boldsymbol{n}_{\partial\Omega} \geq 0$) of positive $(d-1)$-measure, with $\partial\Omega = \partial\Omega_I \cup \partial\Omega_O$. The problem is supposed to be posed over the time interval $[0, T]$.

Mass balance equations – The mass balance reads:

$$\partial_t(\rho) + \mathrm{div}(\rho\boldsymbol{u}) = 0, \tag{3.1}$$

where ρ stands for the fluid density. In the present quasi-incompressible model, this relation may be seen as a constraint on the velocity (and even, in the present one-dimensional case, allows to compute the velocity), while the density may be expressed from the other unknowns of the problem (temperature and chemical species mass fractions) by the equation of state (see below). It must be complemented by a initial condition for the velocity u_0 and by the data of the velocity u_I on the inflow part of the domain boundary $\partial\Omega_I$, while the initial and inflow density, denoted by ρ_0 and ρ_I will be deduced from the initial and inflow temperature and composition of the flow. Thanks to the formulation of the equation of state and natural bounds for the unknowns (see below), ρ_0, ρ_I and ρ are non negative.

Only four chemical species are supposed to be present in the flow, namely the dust, or fuel (denoted by F), the oxydant (O), the product (P) of the reaction, and a neutral gas (N). We denote by $\mathcal{I}$ the set $\mathcal{I} = \{F, O, N, P\}$ and the set of mass fractions of the chemical species in the flow reads $\{y_i,\ i \in \mathcal{I}\}$ (*i.e.* $\{y_F,\ y_O,\ y_N,\ y_P\}$). A one-step irreversible total chemical reaction is considered, which is written:

$$\nu_F F + \nu_O O + N \to \nu_P P + N,$$

where ν_F, ν_O and ν_P are the molar stoichiometric coefficients of the reaction. The system of the mass balance equations for the chemical species reads:

$$\partial_t(\rho y_i) + \mathrm{div}(\rho y_i \boldsymbol{u}) + \mathrm{div}(\boldsymbol{j}_i) = \dot{\omega}_i, \qquad \text{for } i \in \mathcal{I}, \tag{3.2}$$

where y_i, $\boldsymbol{j}_i$ and $\dot{\omega}_i$ stand respectively for the mass fraction, the mass diffusion flux and the reaction rate of the species i. System (3.2) must be complemented by initial and boundary conditions for

$(y_i)_{i\in\mathcal{I}}$. At the inflow boundary, the total flux (*i.e.* the sum of the convection and of the diffusion fluxes) is prescribed and, at the outflow boundary, the diffusion flux is supposed to vanish:

$$\text{on } \partial\Omega_I, \quad (\rho y_i \boldsymbol{u} + \boldsymbol{j}_i)\cdot \boldsymbol{n}_{\partial\Omega} = (y_i)_I\, \boldsymbol{u}\cdot\boldsymbol{n}_{\partial\Omega}, \tag{3.3a}$$

$$\text{on } \partial\Omega_O, \quad \boldsymbol{j}_i\cdot\boldsymbol{n}_{\partial\Omega} = 0. \tag{3.3b}$$

The prescribed values of the mass fractions $(y_i)_{i\in\mathcal{I}}$ at the initial time and the quantities $((y_i)_I)_{i\in\mathcal{I}}$ given on the inflow boundary lie in the interval $[0,1]$. The reaction rate of each chemical species may be written as:

$$\dot\omega_F = -\nu_F W_F\,\dot\omega, \quad \dot\omega_O = -\nu_O W_O\,\dot\omega, \quad \dot\omega_P = \nu_P W_P\,\dot\omega \quad \text{and } \dot\omega_N = 0,$$

where W_F, W_O and W_P stand for the molar masses of the fuel, oxydant and product respectively, and $\dot\omega$ is a non-negative reaction rate, which is supposed to vanish when either $y_F = 0$ or $y_O = 0$. Under these assumptions (positivity of the initial and boundary values, form of the reaction rate), with the specific form of the diffusion fluxes $\boldsymbol{j}_i$, $i\in\mathcal{I}$, considered here (see Section 3.2.2), Equation (3.2) only has non-negative solutions.

Since $\nu_F W_F + \nu_O W_O = \nu_P W_P$, we have:

$$\dot\omega_F + \dot\omega_O + \dot\omega_P = 0. \tag{3.4}$$

In addition, the sum of the mass diffusion fluxes of the chemical species is supposed to vanish everywhere in $\Omega\times(0,T)$ (see once again Section 3.2.2):

$$\sum_{i\in\mathcal{I}} \boldsymbol{j}_i = 0. \tag{3.5}$$

Let the variable Σ stand for $\Sigma = \sum_{i\in\mathcal{I}} y_i$. Summing the chemical species mass balance equations (3.2) and using relations (3.4) and (3.5) yields:

$$\partial_t(\Sigma\rho) + \operatorname{div}(\Sigma\rho\boldsymbol{u}) + \operatorname{div}(\sum_{i\in\mathcal{I}} \boldsymbol{j}_i) = \dot\omega_F + \dot\omega_O + \dot\omega_P,$$

and thus, by (3.4) and (3.5),

$$\partial_t(\Sigma\rho) + \operatorname{div}(\Sigma\rho\boldsymbol{u}) = 0. \tag{3.6}$$

We now suppose that the quantity Σ is precribed to 1 at the initial time and at the boundaries (*i.e.* that $\sum_{i\in\mathcal{I}}(y_i)_0(\boldsymbol{x}) = 1$ a.e. in Ω and that $\sum_{i\in\mathcal{I}}(y_i)_I(\boldsymbol{x},t) = 1$ a.e. in $\partial\Omega_I\times(0,T)$). Then, thanks to the mass balance equation (3.1), $\Sigma = 1$ is solution. Provided that the problem (3.6) is well posed (*i.e.* admits only one solution), relation (3.6) thus implies that $\Sigma(\boldsymbol{x},t) = 1$ for any $\boldsymbol{x}\in\Omega$ and $t\in[0,T]$. Note that, together with the fact that $y_i \geq 0$, for $i\in\mathcal{I}$, this implies that $y_i \leq 1$.

Energy balance – In the low Mach number approximation (*i.e.* neglecting the work of the pressure forces because of the quasi-incompressibility of the flow) and disregarding the viscous dissipation, the total enthalpy balance reads:

$$\partial_t(\rho h) + \operatorname{div}(\rho h\boldsymbol{u}) + \operatorname{div}(\boldsymbol{q}) = 0, \tag{3.7}$$

where h is the so-called sensible+chemical enthalpy. This quantity is defined as the sum of the enthalpies of the chemical species:

$$h = \sum_{i\in\mathcal{I}} y_i\, h_i, \quad \text{with } h_i = c_{\mathrm{p},i}\,\theta + \Delta h^0_{f,i}, \text{ for } i\in\mathcal{I}, \tag{3.8}$$

where θ stands for the temperature, $c_{\mathrm{p},i}$ for the specific heat of the species i (supposed to be constant) and $\Delta h^0_{f,i}$ for the formation enthalpy at 0°K. The enthalpy flux $\boldsymbol{q}$ is:

$$\boldsymbol{q} = -\lambda \boldsymbol{\nabla}\theta + \sum_{i\in\mathcal{I}} h_i \, \boldsymbol{j}_i \tag{3.9}$$

with λ thermal conductivity. Substituting the expression (3.8) of h in (3.7) yields:

$$\sum_{i\in\mathcal{I}} c_{\mathrm{p},i} \, \Big[\partial_t(\rho y_i \theta) + \mathrm{div}(\rho y_i \theta \boldsymbol{u}) + \mathrm{div}(\theta \boldsymbol{j}_i)\Big] + \sum_{i\in\mathcal{I}} \Delta h^0_{f,i} \Big[\partial_t(\rho y_i) + \mathrm{div}(\rho y_i \boldsymbol{u}) + \mathrm{div}(\boldsymbol{j}_i)\Big] - \mathrm{div}(\lambda \boldsymbol{\nabla}\theta) = 0.$$

Using the species conservation equations (3.2) leads to:

$$\sum_{i\in\mathcal{I}} c_{\mathrm{p},i} \, \Big[\partial_t(\rho y_i \theta) + \mathrm{div}(\rho y_i \theta \boldsymbol{u}) + \mathrm{div}(\theta \boldsymbol{j}_i)\Big] + \sum_{i\in\mathcal{I}} \Delta h^0_{f,i} \, \dot{\omega}_i - \mathrm{div}(\lambda \boldsymbol{\nabla}\theta) = 0.$$

Let $\dot{\omega}_\theta$ be the heat production rate due to the chemical reaction, defined by:

$$\dot{\omega}_\theta = -\sum_{i\in\mathcal{I}} \Delta h^0_{f,i} \, \dot{\omega}_i. \tag{3.10}$$

With this definition, we get the following form of the enthalpy balance:

$$\sum_{i\in\mathcal{I}} c_{\mathrm{p},i} \, \Big[\partial_t(\rho y_i \theta) + \mathrm{div}(\rho y_i \theta \boldsymbol{u}) + \mathrm{div}(\theta \boldsymbol{j}_i)\Big] - \mathrm{div}(\lambda \boldsymbol{\nabla}\theta) = \dot{\omega}_\theta. \tag{3.11}$$

This equation must be complemented by a positive initial condition for the temperature and boundary conditions. Once again, we assume a total flux condition at the inlet boundary, and that the diffusion flux vanishes at the outlet boundary:

$$\text{on } \partial\Omega_I, \quad \sum_{i\in\mathcal{I}} c_{\mathrm{p},i} \theta (\rho y_i \boldsymbol{u} + \boldsymbol{j}_i) \cdot \boldsymbol{n}_{\partial\Omega} = \sum_{i\in\mathcal{I}} c_{\mathrm{p},i} \theta_I \rho_I \, (y_i)_I \boldsymbol{u} \cdot \boldsymbol{n}_{\partial\Omega}, \tag{3.12a}$$

$$\text{on } \partial\Omega_O, \quad -\lambda \boldsymbol{\nabla}\theta \cdot \boldsymbol{n}_{\partial\Omega} = 0 \quad (\text{and } \boldsymbol{j}_i \cdot \boldsymbol{n}_{\partial\Omega} = 0 \text{ by (3.3b)}), \tag{3.12b}$$

where θ_I stands for a positive function defined on $\partial\Omega_I \times (0,T)$. Thanks to the species mass balance equations (3.2), we can obtain the so-called non-conservative form of the enthalpy balance (3.11), which reads:

$$\Big[\sum_{i\in\mathcal{I}} c_{\mathrm{p},i} y_i\Big] \rho \partial_t \theta + \Big[\sum_{i\in\mathcal{I}} c_{\mathrm{p},i} (\rho y_i \boldsymbol{u} + \boldsymbol{j}_i)\Big] \cdot \boldsymbol{\nabla}\theta - \mathrm{div}(\lambda \boldsymbol{\nabla}\theta) + \beta \, \dot{\omega} \, \theta = \dot{\omega}_\theta, \tag{3.13}$$

where the coefficient $\bar{c}_p$ reads:

$$\beta = -\nu_F W_F (c_p)_F - \nu_O W_O (c_p)_O + \nu_P W_P (c_p)_P = \nu_F W_F \big[(c_p)_P - (c_p)_F\big] + \nu_O W_O \big[(c_p)_P - (c_p)_O\big].$$

Let $\underline{\theta} > 0$ be defined as the minimum value of θ_0 on Ω and of θ_I on $\partial\Omega_I \times (0,T)$. The first three terms at the left-hand side of the relation (3.13) may be seen as a transport-diffusion operator applied to θ; since this operator satisfies a maximum principle, supposing that the chemical reaction is exothermic (*i.e.* $\dot{\omega}_\theta \geq 0$) and that $\beta \leq 0$, we obtain that $\theta(\boldsymbol{x},t) \geq \underline{\theta}$ for a.e. $(\boldsymbol{x},t) \in \Omega \times (0,T)$. Still for an exothermic reaction, if $\beta > 0$, only the non-negativity of θ is warranted.

Equation of state – Finally, we must give an equation of state to close the system. Let us denote by ρ_i the density of the component i, let $\mathcal{I}_s$ be the set of indices corresponding to solid species and $\mathcal{I}_g$ the set of the indices corresponding to gaseous species (so $\mathcal{I}_s \cup \mathcal{I}_g = \{i \in \mathcal{I}\}$). We suppose that the

gas phase is a mixture of perfect gases. Assuming that the density of the solid phase is constant, the usual mixture law reads:

$$\rho = \varrho\big(\theta, (y_i)_{i\in\mathcal{I}}\big) = \frac{1}{\dfrac{R\theta}{P_{th}}\displaystyle\sum_{i\in\mathcal{I}_g}\frac{y_i}{W_i} + \sum_{i\in\mathcal{I}_s}\frac{y_i}{\rho_i}}, \tag{3.14}$$

where $R = 8.31451\,\mathrm{JK}^{-1}\mathrm{mol}^{-1}$ stands for the perfect gases constant and P_{th} is the so-called thermodynamic pressure. Since we assumed that the measure of $\partial\Omega_O$ is positive (*i.e.* the computational domain is not closed), this latter quantity is constant in time and space, and given by the initial state. The initial and boundary values of the density are naturally supposed to satisfy the equation of state applied to the initial and boundary values of the temperature and the mass fractions:

$$\rho_0 = \varrho\big(\theta_0, ((y_i)_0)_{i\in\mathcal{I}}\big), \quad \rho_I = \varrho\big(\theta_I, ((y_i)_I)_{i\in\mathcal{I}}\big).$$

3.2.2 Expression of the chemical species diffusion fluxes

Since the size of the particles is large compared to the molecular Brownian motion ranges, we suppose that the diffusion of dust vanishes, so the diffusion phenomena only occur in the gas phase. We define the gas mass fraction as $y_g = \sum_{i\in\mathcal{I}_g} y_i$ and, for $i \in \mathcal{I}_g$, the mass fraction of the species i in the gas phase as $\tilde{y}_i = y_i/y_g$. A general expression of the diffusion fluxes reads:

$$\text{for } i \in \mathcal{I}_s,\ \boldsymbol{j}_i = 0\ ; \quad \text{for } i \in \mathcal{I}_g, \quad \boldsymbol{j}_i = -\rho \sum_{j\in\mathcal{I}_g} D_{i,j}\boldsymbol{\nabla}\tilde{y}_j,$$

where the coefficients $(D_{i,j})_{i,j\in\mathcal{I}_g}$ depend on the local mixture concentration (*i.e.* on the mass fractions $(\tilde{y}_i)_{i\in\mathcal{I}_g}$ themselves). However, using a full tensor D and computing its coefficients is cost-consuming, and, moreover, the complete data necessary to their accurate computation is usually not available. This tensor is thus generally approximated. For instance, a "quasi-diagonal" approximation to this purpose for pure gaseous mixtures reads:

$$\text{for } i \in \mathcal{I}_g, \quad \boldsymbol{j}_i = \boldsymbol{j}_i^e + \tilde{y}_i\boldsymbol{J}, \quad \boldsymbol{j}_i^e = -\rho D_i \frac{W_i}{W}\boldsymbol{\nabla}\tilde{x}_i,$$

where $\tilde{x}_i$ stands for the molar mass fraction of the component i, so

$$\tilde{x}_i = \tilde{y}_i\,\frac{W}{W_i}, \quad \text{with } \frac{1}{W} = \sum_{i\in\mathcal{I}_g}\frac{\tilde{y}_i}{W_i}. \tag{3.15}$$

The quantity W is the so-called gaseous mixture molar mass. Complemented by a suitable expression of the coefficient D_i (see Equation (3.16) below), this formula is known as the Hirschfelder and Curtiss approximation (see [28, 45] and [68, pp. 14-15]). The term $\tilde{y}_i\,\boldsymbol{J}$ is a correction term added to ensure that $\sum_{j\in\mathcal{I}_g}\boldsymbol{j}_j = 0$, and so a suitable expression for $\boldsymbol{J}$ reads $\boldsymbol{J} = -\sum_{j\in\mathcal{I}_g}\boldsymbol{j}_j^e$ (note that, by definition, $\sum_{i\in\mathcal{I}_g}\tilde{y}_i = 1$). Under the Hirschfelder and Curtiss approximation, the diffusion coefficients read:

$$\text{for } i \in \mathcal{I}_g,\ D_i = \frac{1-\tilde{y}_i}{\displaystyle\sum_{j\in\mathcal{I}_g,\ j\neq i}\frac{\tilde{x}_j}{D_{ji}}}, \tag{3.16}$$

where D_{ji} is the binary diffusion coefficient of the species j into species i. Exploiting the expression (3.15) of the molar fractions as a function of the mass fractions, we obtain the following expression for the diffusion fluxes:

$$\text{for } i \in \mathcal{I}_g,\ \boldsymbol{j}_i^e = -\rho D_i\frac{1}{y_g}\boldsymbol{\nabla}y_i - \rho D_i y_i\big[\boldsymbol{\nabla}(\frac{1}{y_g}) + \frac{1}{y_g}\boldsymbol{\nabla}(\log(W))\big]. \tag{3.17}$$

In this model, the operator $y_i \mapsto \mathcal{D}(y_i) = \mathrm{div}\big(\boldsymbol{j}(y_i)\big)$ can thus be split in two parts:

$$\mathcal{D}(y_i) = \mathcal{D}_1(y_i) + \mathcal{D}_2(y_i), \quad \mathcal{D}_1(y_i) = -\mathrm{div}(\rho D_i \frac{1}{y_g} \boldsymbol{\nabla} y_i), \quad \mathcal{D}_2(y_i) = -\mathrm{div}(y_i \boldsymbol{q}_d),$$

with:

$$\boldsymbol{q}_d = \rho D_i \big[\boldsymbol{\nabla}(\frac{1}{y_g}) + \frac{1}{y_g}\boldsymbol{\nabla}(\log(W))\big] - \frac{1}{y_g}\boldsymbol{J}. \tag{3.18}$$

The operator $\mathcal{D}_1$ satisfies a maximum principle, while $\mathcal{D}_2$ is only positivity-preserving, since the divergence of the vector $\boldsymbol{q}_d$ is not zero in the general case. For instance, this means that, because of the approximation made for the diffusion tensor, the dust mass fraction may locally exceed the maximum of its initial and boundary values, which is of course unphysical (within the framework of the present model, where a possible drift of the particles with respect to the bulk flow velocity is not taken into account). Hopefully, the occurrence of this phenomenon may be limited in time and space.

3.2.3 Bounds for the unknowns

Let us now collect the different bounds for the unknowns that we mentioned in the previous sections:

mass fractions: $0 \leq y_i \leq 1,\ \sum_{i\in\mathcal{I}} y_i = 1$
if $\boldsymbol{q}_d = 0$ (or $\mathrm{div}(\boldsymbol{q}_d) = 0$), $y_F \leq \overline{y}_F,\ y_O \leq \overline{y}_O,\ y_P \geq \underline{y}_P, \underline{y}_N \leq y_N \leq \overline{y}_N$.

temperature: if $\dot{\omega}_\theta \geq 0,\ \theta \geq 0$,
if $\dot{\omega}_\theta \geq 0$ and $\beta \leq 0,\ \theta \geq \underline{\theta}$.

3.3 The numerical scheme

For the resolution of the model equations, we define the variable z as follows:

$$z = \frac{y_F + s(1 - y_O)}{1 + s}, \qquad s = \frac{\nu_F W_F}{\nu_O W_O}$$

Note that, combining the fuel and the oxydant mass balance equations, the variable z satisfies a homogeneous equation; for this reason, we replace the oxydant mass balance equation by the balance equation for z (since, given the values of z and y_F, we may deduce y_O).

Let us consider a partition $0 = t_0 < t_1 < \ldots < t_N = T$ of the time interval $(0, T)$, which we suppose uniform. Let $\delta t = t_{n+1} - t_n$ for $n = 0, 1, \ldots, N-1$ be the constant time step. We suppose that the interval Ω is split in a family of control volumes (sub-intervals of Ω) which realizes a partition of Ω; we denote these control volumes by $(K)_{K\in\mathcal{M}}$, where $\mathcal{M}$ is the set of all the control volumes of the mesh. The scalar unknowns, *i.e.* the density, the mass fractions and the temperature, are associated to the control volumes, and the corresponding unknowns read ρ_K^n, $(y_i)_K^n$, θ_K^n for $K \in \mathcal{M}$ and $0 \leq n \leq N$. The velocity is discretized at faces of the mesh, which we denote by $(\sigma)_{\sigma\in\mathcal{E}}$, where $\mathcal{E}$ stands for the set of all faces of the mesh, so the corresponding unknowns are u_σ^n for $\sigma \in \mathcal{E}$ and $0 \leq n \leq N$. The sets of the internal faces, the external faces (*i.e.* the two faces located on the boundary of Ω) and the faces of K are denoted by $\mathcal{E}_{\mathrm{int}}$, $\mathcal{E}_{\mathrm{ext}}$ and $\mathcal{E}(K)$ respectively, and the face separating two neighbour cells K and L is denoted by $K|L$. For $K \in \mathcal{M}$, x_K stands for the mass center of K and, for $\sigma = K|L \in \mathcal{E}_{\mathrm{int}}$, we define d_σ by $d_\sigma = |x_K - x_L|$. For short, we use indifferently ρ^n (resp. $(y_i)^n$, θ^n, u^n) and $(\rho_K^n)_{K\in\mathcal{M}}$ (resp. $((y_i)_K^n)_{K\in\mathcal{M}}$, $(\theta_K^n)_{K\in\mathcal{M}}$, $(u_\sigma^n)_{\sigma\in\mathcal{E}}$).

Using the initial conditions, we define the following variables on the time level t_0:

$$\forall K \in \mathcal{M}, \qquad \rho_K^{-1} = \frac{1}{|K|}\int_K \rho_0(\boldsymbol{x})\,\mathrm{d}\boldsymbol{x}, \quad \theta_K^0 = \frac{1}{|K|}\int_K \theta_0(\boldsymbol{x})\,\mathrm{d}\boldsymbol{x}, \quad (y_i)_K^0 = \frac{1}{|K|}\int_K y_{i,0}(\boldsymbol{x})\,\mathrm{d}\boldsymbol{x} \text{ for } i \in \mathcal{I},$$
$$\forall \sigma \in \mathcal{E}, \qquad u_\sigma^0 = u_0(\sigma).$$

Then, we implement a fractional step algorithm, which consists in four steps, in order to calculate recursively the unknowns ρ^n, ρ^{n+1}, $(y_i)_{i\in\mathcal{I}}^{n+1}$, θ^{n+1} and u^{n+1} for $0 \le n < N$:

Reactive step:

$\forall K \in \mathcal{M}$:

Reduced variable computation – Solve for z^{n+1}:

$$\frac{1}{\delta t}(\rho_K^n z_K^{n+1} - \rho_K^{n-1} z_K^n) + \mathrm{div}(\rho^n z^k \boldsymbol{u}^n)_K = 0. \tag{3.19a}$$

Neutral gas mass fraction computation – Solve for y_N^{n+1}:

$$\frac{1}{\delta t}\big[\rho_K^n (y_N)_K^{n+1} - \rho_K^{n-1}(y_N)_K^n\big] + \mathrm{div}(\rho^n y_N^k \boldsymbol{u}^n)_K = 0. \tag{3.19b}$$

Fuel mass fraction computation – Solve for y_F^{n+1}:

$$\frac{1}{\delta t}\big[\rho_K^n (y_F)_K^{n+1} - \rho_K^{n-1}(y_F)_K^n\big] + \mathrm{div}(\rho^n y_F^{n+1} \boldsymbol{u}^n)_K = (\dot\omega_F)_K^{n+1}. \tag{3.19c}$$

Oxydant mass fraction computation – $(y_O)_K^{n+1} = 1 + \frac{1}{s}(y_F)_K^{n+1} - z_K^{n+1}(1+\frac{1}{s})$. (3.19d)

Product mass fraction computation – $(y_P)_K^{n+1} = 1 - (y_F)_K^{n+1} - (y_O)_K^{n+1} - (y_N)_K^{n+1}$. (3.19e)

Hydrodynamics step:

Energy balance – Solve for θ^{n+1}:

$$\forall K \in \mathcal{M}, \qquad \sum_{i\in\mathcal{I}} c_{\mathrm{p},i}\Big[\frac{1}{\delta t}\big[\rho_K^n (y_i)_K^{n+1}\theta_K^{n+1} - \rho_K^{n-1}(y_i)_K^n\theta_K^n\big] + \mathrm{div}\big[\rho^n y_i^{n+1}\theta^{n+1}\boldsymbol{u}^n\big]_K + \mathrm{div}\big[\theta^{n+1}\boldsymbol{j}_i^n\big]_K\Big] - \mathrm{div}(\lambda\boldsymbol{\nabla}\theta^{n+1})_K = (\dot\omega_\theta)_K^{n+1}. \tag{3.20a}$$

Equation of state – $\rho_K^{n+1} = \varrho\big(\theta_K^{n+1}, ((y_i)_K^{n+1})_{i\in\mathcal{I}}\big), \quad$ for $K \in \mathcal{M}$. (3.20b)

Mass balance – Solve for $\boldsymbol{u}^{n+1}$:

$$\forall K \in \mathcal{M}, \qquad \frac{1}{\delta t}\big[\rho_K^{n+1} - \rho_K^n\big] + \mathrm{div}\big[\rho^{n+1}\boldsymbol{u}^{n+1}\big]_K = 0. \tag{3.20c}$$

Let us define the function $f : (y_F, y_O) \mapsto \min(y_F/(\nu_F W_F),\ y_O/(\nu_O W_O))$. From a practical point of view, it is interesting to note that $f(y_F, y_O)$ may be deduced from the value of z; indeed,

$$z = \frac{y_F + (1-y_O)s}{1+s} \ \Leftrightarrow\ \frac{y_F}{\nu_F W_F} - \frac{y_O}{\nu_O W_O} = z\Big(\frac{1}{\nu_F W_F} + \frac{1}{\nu_O W_O}\Big) - \frac{1}{\nu_O W_O}.$$

So, once the equation (3.19a) is solved for z^{n+1}, $f(y_F^{n+1}, y_O^{n+1})$ is known. But the function f vanishes as soon as y_F or y_O vanishes; we thus have at hand the possibility to write a reactive term satisfying this latter property (and so preserving the positivity of the mass fractions) while appearing in the

algorithm as a linear quantity (thus avoiding to implement an iterative technique, like a Newton algorithm, to cope with a nonlinear algebraic problem). So, either f appears in the expression of $\dot{\omega}$ and the expression that follows is exact, either we use it to linearize $\dot{\omega}$ in the time scale:

$$\dot{\omega}^{n+1} = \dot{\omega}(y_F^n, y_O^n)\ \frac{f(y_F^{n+1}, y_O^{n+1})}{f(y_F^n, y_O^n)}.$$

This last technique is used in the applications presented hereafter.

Supposing the rest of the mass fractions given, the product mass fraction equation is equivalent to the simple algebraic relation (3.19e), since, on the discrete level, the sum of all mass fractions is equal to 1 (*cf.* Section 3.4, Theorem 3.4.1).

Equations (3.19b)-(3.20c) are resolved successively. We now give the expression of the fluxes appearing in these relations.

Convection fluxes – The guideline for the definition of the convection fluxes is that we want the numerical scheme to respect "by construction" the physical bounds satisfied by the variables in the continuous case. To this purpose, we first remark that an operator which satisfies a maximum principle must vanish when applied to constant functions. Indeed, denoting by $\mathcal{L}$ such an operator, an initially constant solution ξ to the equation $\partial_t \xi + \mathcal{L}(\xi) = 0$ must remain constant, since the upper and lower bounds of the solution have to be preserved (provided, of course, that boundary conditions are consistent with this constant solution); this yields $\partial_t \xi = 0$ and so $\mathcal{L}(\xi) = 0$. In fact, when $\mathcal{L}$ is a discrete convection operator, using an upwind approximation of the unknown at the faces, this condition of preservation is not only mandatory but also sufficient [54]. In the system under consideration, two such convection operators have to be approximated, namely the convection operator for the species mass balance equations and for the energy balance, and the fact that these operators vanish when applied to constant functions is closely related to the fact that these equations may be recast under the so-called non-conservative form thanks to the mixture mass balance and to the species mass balance, respectively. So, let the convection fluxes in this latter relation read:

$$\mathrm{div}\big[\rho \boldsymbol{u}\big]_K = \frac{1}{|K|} \sum_{\sigma \in \mathcal{E}(K)} F_{K,\sigma}.$$

We then define the convection fluxes in the species mass balance equations as:

$$\mathrm{div}\big[\rho y_i \boldsymbol{u}\big]_K = \frac{1}{|K|} \sum_{\sigma \in \mathcal{E}(K)} F_{K,\sigma} (y_i)_\sigma^{\mathrm{up}},$$

where $(y_i)_\sigma^{\mathrm{up}}$ stands for the upwind approximation of y_i on the face σ with respect to $F_{K,\sigma}$. Similarly, let the convection and diffusion fluxes in this equation be written as:

$$\mathrm{div}\big[\rho y_i \boldsymbol{u}\big]_K + \mathrm{div}\big[\boldsymbol{j}_i\big]_K = \frac{1}{|K|} \sum_{\sigma \in \mathcal{E}(K)} G_{K,\sigma},$$

where, for short, we skip the index i for the flux $G_{K,\sigma}$. Then, in the energy mass balance,

$$\mathrm{div}\big[\rho y_i \theta \boldsymbol{u}\big]_K + \mathrm{div}\big[\theta \boldsymbol{j}_i\big]_K = \sum_{\sigma \in \mathcal{E}(K)} G_{K,\sigma}\ \theta_\sigma^{\mathrm{up}},$$

where $\theta_\sigma^{\mathrm{up}}$ stands for the upwind approximation of θ on the face σ with respect to $G_{K,\sigma}$. This upwind discretization for y_i and θ for an internal face $\sigma = K|L$ is defined as follows:

$$(y_i)_\sigma^{\mathrm{up}} = (y_i)_K \text{ if } F_{K,\sigma} \geq 0, \quad (y_i)_\sigma^{\mathrm{up}} = (y_i)_L \text{ otherwise,}$$

$$\theta_\sigma^{\mathrm{up}} = \theta_K \text{ if } G_{K,\sigma} \geq 0, \qquad \theta_\sigma^{\mathrm{up}} = \theta_L \text{ otherwise.}$$

For an external face adjacent to K, lying on the outlet part of the boundary, we have $(y_i)_\sigma^{\rm up} = (y_i)_K$, which is consistent with the above definition since $F_{K,\sigma}$ is supposed to be non-negative, and $\theta_\sigma^{\rm up} = \theta_K$, which, once again, is consistent with the upwind definition on the internal faces since the mass species diffusion flux is supposed to vanish, and so $G_{K,\sigma} = F_{K,\sigma}\ (y_i)_\sigma^{\rm up}$ has the same sign as $F_{K,\sigma}$, *i.e.* it is also non-negative (provided that we are able to prove that the chemical species mass fractions remain non negative, which is indeed done in Section 3.4 below). For an external face adjacent to K lying on the inlet part of the boundary, both $(y_i)_\sigma$ and θ_σ are computed as an approximation of the mass fractions and the temperature prescribed on the boundary, and, by similar arguments, both $F_{K,\sigma}$ and $G_{K,\sigma}$ are non-positive.

The mass flux through the face σ reads:

$$F_{K,\sigma} = \rho_\sigma u_{K,\sigma}$$

where $u_{K,\sigma}$ stands for the value of the velocity oriented outward K, *i.e.* $u_{K,\sigma} = u_\sigma$ if K is situated "on the left part" of σ and $u_{K,\sigma} = -u_\sigma$ otherwise, and ρ_σ stands for any reasonable approximation of ρ on σ; here, we choose a centered approximation: $\rho_\sigma = \frac{1}{2}(\rho_K + \rho_L)$ for $\sigma = K|L$, $\rho_\sigma = \rho_K$ for an outlet external face adjacent to K and ρ_σ is computed from the equation of state as a function of the data for the species mass fractions and the temperature for an inlet external face.

Diffusion fluxes – The mass diffusion fluxes vanish for the solid species. For the gaseous chemical species, we have:

$$\mathrm{div}\big[\boldsymbol{\jmath}_i^n\big]_K = \frac{1}{|K|}\sum_{\sigma=K|L}(J_i)_{K,\sigma}^n.$$

Note that the sum is restricted to the internal faces of K since, by assumption, the diffusion fluxes vanish at the boundaries (more precisely speaking, they are supposed to vanish at the outlet boundary and the total flux is written as a convection flux at the inlet boundary, so already taken into account in the definition of $G_{K,\sigma}$ above). For a scalar variable ξ and an internal face $\sigma = K|L$, let us define $-(\partial_x f(\xi))_{K,\sigma}$ and $\{f(\xi)\}_\sigma$ as:

$$-\big(\partial_x f(\xi)\big)_{K,\sigma} = \frac{1}{d_\sigma}\big(f(\xi_K) - f(\xi_L)\big) \quad \text{and} \quad \{f(\xi)\}_\sigma = \frac{1}{2}\big(f(\xi_K) + f(\xi_L)\big).$$

For $i \in \mathcal{I}_g$, we then define $(J_i^d)_{K,\sigma}$ as:

$$(J_i^d)_{K,\sigma} = -\big\{\rho D_i \frac{1}{y_g}\big\}_\sigma (\partial_x y_i)_{K,\sigma}. \tag{3.21}$$

Note that, in this definition, the quantity $\{\rho\, D_i\, /y_g\}_\sigma$ may be replaced by any reasonable approximation of $\rho\, D_i\, /y_g$ on the face (so, for instance, by the harmonic mean of the cell aproximations of this expression, which may possibly give more accurate results when it varies quickly from cell to cell). Let us then introduce the following quantities:

$$(q_i)_{K,\sigma} = -\big\{\rho D_i\big\}_\sigma \big(\partial_x(\frac{1}{y_g})\big)_{K,\sigma} - \big\{\rho D_i \frac{1}{y_g}\big\}_\sigma \big(\partial_x(\log(W))\big)_{K,\sigma}, \qquad (J_i^c)_{K,\sigma} = (q_i)_{K,\sigma}(y_i)_\sigma^{{\rm up}/q_i},$$

where $(y_i)_\sigma^{{\rm up}/q_i}$ stands for the upwind approximation of y_i at the face σ with respect to $(q_i)_{K,\sigma}$. Finally, let us denote by $q_{K,\sigma}$ the following quantity:

$$q_{K,\sigma} = \sum_{i\in\mathcal{I}_g}(J_i^d)_{K,\sigma} + (J_i^c)_{K,\sigma}.$$

With this notation, the diffusion flux $(J_i)_{K,\sigma}$ reads:

$$(J_i)_{K,\sigma} = (J_i^d)_{K,\sigma} + (J_i^c)_{K,\sigma} + \frac{(y_i)_\sigma^{\mathrm{up}/q}}{(y_g)_\sigma^{\mathrm{up}/q}}\, q_{K,\sigma},$$

where $(y_i)_\sigma^{\mathrm{up}/q}$ and $(y_g)_\sigma^{\mathrm{up}/q}$ stand for an upwind approximation at the face σ with respect to $q_{K,\sigma}$ of y_i and y_g respectively. Note that this latter upwinding is performed with respect to the same quantity for all the species, and thus $\sum_{i\in\mathcal{I}_g}(y_i)_\sigma^{\mathrm{up}/q} = (y_g)_\sigma^{\mathrm{up}/q}$.

The discrete heat diffusion term in the enthalpy energy balance reads:

$$-\mathrm{div}[\lambda\boldsymbol{\nabla}\theta^{n+1}]_K = \sum_{\sigma=K|L} H_{K,\sigma}, \text{ with } H_{K,\sigma} = \lambda_\sigma \left(\partial_x\theta\right)_{K,\sigma},$$

where λ_σ stands for an approximation of the diffusion coefficient λ on σ; for instance, if λ depends on the temperature, a possible choice is $\lambda_\sigma = \{\lambda(\theta)\}_\sigma$.

3.4 Properties of the scheme

In this section we prove that the set of solutions of the scheme is not empty and that, at the discrete level, the mass fractions, the temperature and the density preserve the same physical bounds as at the continuous level.

Let us now introduce some notations. For any real valued function f we denote by f^+ (respectively f^-) its positive part (respectively its negative part), *i.e.* $f^+ = \max(f, 0)$ (respectively $f^- = -\min(f, 0)$). M-matrices play a fundamental role in this section.

Definition. $A \in \mathcal{M}_n(\mathbb{R})$ is an M-matrix if and only if it verifies:

- (a) All diagonal entries are positive, $A_{ii} > 0$.
- (b) All off-diagonal entries are non-positive, $A_{ij} \leq 0$ for $i \neq j$.
- (c) It is strictly diagonally dominant, $A_{ii} > -\sum_{j\neq i} A_{ij}$.

Lemma 3.4.1 (M-matrix properties).
Let A be an M-matrix, the following results hold:

- (i) A is invertible.
- (ii) If $x \in \mathbb{R}^n$ is such that $(Ax)_i \geq 0$, for all i, then $x_i \geq 0$ for all i.
- (iii) Let $x, b \in \mathbb{R}^n$ be such that $(Ax)_i = (\sum_j A_{ij})b_i$. Then, for all i, $\min_j b_j \leq x_i \leq \max_j b_j$.

Proof. (i) Let us suppose that $\ker(A) \neq \{\varnothing\}$: there exists $x \in \mathbb{R}^n$, $x \neq 0$, such that $Ax = 0$. We choose i such that $x_i = \min_j(x_j)$. By hypothesis,

$$|x_i| = \frac{1}{A_{ii}}\Big|\sum_{j\neq i} A_{ij}x_j\Big| \leq \frac{\sum_{j\neq i}|A_{ij}|}{A_{ii}} \max_{j\neq i}|x_j| < \max_{j\neq i}|x_j|,$$

which is a contradiction, thus $\ker(A) = \varnothing$ and A is invertible.

(ii) There exists i such that $x_i = \min_j x_j$ and let us suppose $x_i < 0$. The equation verified by x reads:

$$A_{ii}x_i = \sum_{j\neq i}|A_{ij}|x_j = \sum_{\substack{j\neq i,\\ x_j\geq 0}}|A_{ij}|x_j + \sum_{\substack{j\neq i,\\ x_j<0}}|A_{ij}|x_j \geq \sum_{\substack{j\neq i,\\ x_j<0}}|A_{ij}|x_j,$$

and since both sides are negative

$$|x_i| \leq \frac{\sum_{\substack{j\neq i,\\ x_j<0}} |A_{ij}|}{A_{ii}} |x_j| < \max_{\substack{j\neq i,\\ x_j<0}} |x_j|,$$

which is a contradiction, thus for all $i,\ x_i \geq 0$.

(iii) Let $\underline{b} = \min_i b_i$. Substracting the quantity $\sum_j A_{ij}\underline{b}$ from the i-th line of the system $Ax = b$, yields:

$$\sum_j A_{ij}(x_j - \underline{b}) = \sum_j A_{ij}(b_i - \underline{b}).$$

The terms $b_i - \underline{b}$ are all non-negative and since by hypothesis A is diagonally dominant, the right-hand side is non-negative. If this holds for an arbitrary line i, it holds for all lines of the system, thus, by *(ii)*, $x_i \geq \underline{b}$ for all i. To prove that $x_i \geq \overline{b}$ for all i, where $\overline{b} = \max_i b_i$, substract $\sum_j A_{ij}\overline{b}$ from the i-th line of $Ax = b$ and follow the same steps. □

Replacing equations (3.19a) and (3.19e) by their equivalents, the system of equations (3.19b)-(3.19e) may be written in the following form:

$$\forall i \in \mathcal{I},\ \forall K \in \mathcal{M}, \quad \mathcal{A}_K^{n+1} \cdot (y_i)^{n+1} = \frac{|K|}{\delta t}\rho_K^{n-1}(y_i)_K^n - (\mathcal{D}_i)_K^{n+1} \cdot (y_i)^n + (\dot{\omega}_i)_K^{n+1}. \tag{3.22}$$

$\mathcal{A}_K^{n+1}$ denotes the K-th line of the discretized convection operator $\mathcal{A}^{n+1}$, and $\mathcal{A}_K^{n+1} \cdot (y_i)^{n+1}$ is the inner product between these two vectors. In the same way, $(\mathcal{D}_i)_K^{n+1}$ denotes the K-th line of the discretized diffusion operator $(D_i)^{n+1}$, and $(\mathcal{D}_i)_K^{n+1} \cdot (y_i)^n$ is the inner product between thsese two vectors.

Lemma 3.4.2 (Properties of the discrete operator $\mathcal{A}^{n+1}$).
If for $0 \leq n < N$ and for any $K \in \mathcal{M},\ \rho_K^n > 0$, then $\mathcal{A}^{n+1}$ is an invertible operator. Now consider the system of equations:

$$\mathcal{A}^{n+1} \cdot y^{n+1} = b^n, \qquad \text{with } b_K^n = \frac{|K|}{\delta t}\rho_K^{n-1} y_K^n \text{ for } K \in \mathcal{M},$$

and let us suppose that (3.20c) holds. Then, for all $K \in \mathcal{M}$, $\min_{K\in\mathcal{M}}(y_i)_K^n \leq (y_i)_K^{n+1} \leq \max_{K\in\mathcal{M}}(y_i)_K^n$ (*i.e.* $\mathcal{A}^{n+1}$ is "bound-preserving").

Proof. For $0 \leq n \leq N$ and any $K \in \mathcal{M}$, the only non-zero terms of the K-th line of $\mathcal{A}^{n+1}$, read:

$$\begin{aligned} &\frac{|K|}{\delta t}\rho_K^n + (F_{K,\sigma}^n)^+, && \text{on the diagonal,} \\ &-(F_{L,\sigma}^n)^+, && \text{on any column } L \text{ such that } \sigma = K|L. \end{aligned}$$

It is straightforward that the diagonal entries are positive and the off-diagonal non-positive. Thanks to the mass balance equation, the sum of the entries of $\mathcal{A}_K^{n+1}$ is equal to $|K|/\delta t\, \rho_K^{n-1} > 0$, thus $\mathcal{A}^{n+1}$ is an M-matrix and a unique solution exists for the chemical mass fraction balance equations. Furthermore, the entries of $\mathcal{A}_K^{n+1}$ sum up to the coefficient of $(y_i)_K^n$ on the right-hand side and Lemma 3.4.1-*(iii)* concludes the proof. □

For $0 \leq n \leq N$, let us define the so-called *CFL*-number by

$$CFL^n = \max(CFL_{\mathcal{D}}^n, CFL_{\dot{\omega}}^n),$$

where

$$CFL_{\mathcal{D}}^n = \max_{i\in\mathcal{I}} \max_{K\in\mathcal{M}} \frac{\delta t}{|K|\,\rho_K^{n-1}(y_i)_K^n} \sum_{\sigma=K|L} \{\rho^n D_i \frac{1}{y_g^n}\}_\sigma \frac{1}{d_\sigma} + \big((q_i)_{K,\sigma}^n\big)^+ + (q_{K,\sigma}^n)^+$$

and

$$CFL_{\dot\omega}^n = \max_{K\in\mathcal{M}} \frac{\delta t \sum_i c_{\mathrm{p},i}(\dot\omega_i)_K^{n+1}}{\rho_K^{n-1}\sum_i c_{\mathrm{p},i}(y_i)_K^n}.$$

Let us also introduce the following quantity,

$$\forall i\in\mathcal{I},\ \forall K\in\mathcal{M},\quad \frac{|K|}{\delta t}\rho_K^{n-1}(y_i)_K^{n+\frac12} = \frac{|K|}{\delta t}\rho_K^{n-1}(y_i)_K^n - (\mathcal{D}_i)_K^{n+1}\cdot(y_i)^n,$$

and the neighbourhood of a cell K, denoted $\mathcal{V}(K)$, which is the set of cells sharing an edge with K.

Lemma 3.4.3.
For $0\le n\le N$, the following statements hold:

(*i*) If $(q_d)^n = 0$, then for all $i\in\mathcal{I}$ and $K\in\mathcal{M}$, $\min\limits_{K\in\mathcal{V}(K)}(y_i)_K^n \le (y_i)_K^{n+\frac12} \le \max\limits_{K\in\mathcal{V}(K)} y_K^n$.

(*ii*) If $(q_d)^n \neq 0$, then, under the condition $CFL_{\mathcal{D}}^n \le 1$, for all $i\in\mathcal{I}$, $(y_i)^{n+\frac12}\ge 0$.

Proof. Ignoring the contribution of the reaction term, the right-hand side of the mass fraction balance equations (3.22), reads:

$$\forall i\in\mathcal{I},\ \forall K\in\mathcal{M},\quad \frac{|K|}{\delta t}\rho_K^{n-1}(y_i)_K^{n+\frac12} = \frac{|K|}{\delta t}\rho_K^{n-1}(y_i)_K^n + \sum_{\sigma=K|L}\{\rho D_i\frac{1}{y_g}\}_{K,\sigma}^n(\partial_x y_i)_{K,\sigma}^n + (q_d)_{K,\sigma}^n(y_i)_s^n,$$

where

$$\forall K\in\mathcal{M},\ \forall\sigma\in\mathcal{E}(K),\quad (q_d)_{K,\sigma}(y_i)_s = (q_i)_{K,\sigma}(y_i)_\sigma^{\mathrm{up}/q_i} + \frac{(y_i)_\sigma^{\mathrm{up}/q}}{(y_g)_\sigma^{\mathrm{up}/q}} q_{K,\sigma}.$$

(*i*) The right-hand side may be written in the following way:

$$\forall i\in\mathcal{I},\ \forall K\in\mathcal{M},\quad \frac{|K|}{\delta t}\rho_K^{n-1}(y_i)_K^{n+\frac12} = \sum_{L\in\mathcal{V}(K)}\alpha_L^n(y_i)_L^n,$$

where $\sum_{L\in\mathcal{V}(K)}\alpha_L^n = \rho_K^{n-1}|K|/\delta t$, thus the result is straightforward in virtue of Lemma 3.4.2.

(*ii*) If $CFL\le 1$, the positivity of the right-hand side is guaranteed. □

Lemma 3.4.4 (Boundedness of the chemical mass fractions).
For $0\le n\le N$, suppose that for all $i\in\mathcal{I}$ and $K\in\mathcal{M}$, $(y_i)_K^n\ge 0$, $CFL_{\mathcal{D}}^n\le 1$ and that the discrete mass balance (3.20c) is verified.

(*i*) For all $i\in\mathcal{I}$ and $K\in\mathcal{M}$, $(y_i)_K^{n+1}\ge 0$.

(*ii*) Now let us suppose that $q_d^n = 0$ (in the sense that $(q_d)_{K,\sigma}^n = 0,\ K\in\mathcal{M},\ \sigma\in\mathcal{E}(K)$). Then $\overline{y}_F^{n+1}\le\overline{y}_F^n$, $\overline{y}_O^{n+1}\le\overline{y}_O^n$, $\underline{y}_P^{n+1}\le\underline{y}_P^n$ and $\underline{y}_N^n\le\underline{y}_N^{n+1}\le\overline{y}_N^{n+1}\le\overline{y}_N^n$.

Proof. The mass fraction balance equations equivalently read:

$$\begin{aligned}\forall i \in \mathcal{I},\ \forall K \in \mathcal{M}, \quad & \big(\frac{|K|}{\delta t}\rho_K^n + (F_{K,\sigma}^n)^+\big)(y_i)_K^{n+1} - \sum_{\sigma=K|L}(F_{K,\sigma}^n)^-(y_i)_L^{n+1} \\ & = \frac{|K|}{\delta t}\rho_K^{n-1}(y_i)_K^n + \sum_{\sigma=K|L}\big\{\rho D_i \frac{1}{y_g}\big\}_{K,\sigma}^n (\partial_x y_i)_{K,\sigma}^n + (q_d)_{K,\sigma}(y_i)_s^n + (\tilde{\omega}_i)_K^{n+1},\end{aligned} \tag{3.23}$$

where

$$\forall K \in \mathcal{M},\ \forall \sigma \in \mathcal{E}(K), \quad (q_d)_{K,\sigma}(y_i)_s = (q_i)_{K,\sigma}(y_i)_\sigma^{\mathrm{up}/q_i} + \frac{(y_i)_\sigma^{\mathrm{up}/q}}{(y_g)_\sigma^{\mathrm{up}/q}} q_{K,\sigma},$$

and where for $i \in \mathcal{I}$, $\widetilde{\omega}_i^{n+1}$ denotes the continuation of the i-th reaction rate for negative values of y_F^n and y_O^n, defined by:

$$\forall i \in \mathcal{I}, \quad \widetilde{\omega}_i^{n+1} = \left| \begin{array}{ll} 0, & \text{if } \min\{y_F, y_O\}^{n+1} \leq 0, \\ \dot{\omega}_i^{n+1}, & \text{otherwise.} \end{array} \right.$$

(i) For $i \in \{N, P\}$, given the non-negative sign of the reactive term and the condition $CFL_{\mathcal{D}} \leq 1$, the right-hand side is positive and the result is a direct application of Lemma 3.4.1-(ii). When the reaction term may take negative values, *i.e.* for $i \in \{F, O\}$, let us rewrite:

$$\text{for } i = F \text{ or } O, \quad \widetilde{\omega}_i^{n+1} = \left| \begin{array}{ll} 0, & \text{if } \min\Big\{\frac{y_F}{\nu_F W_F}, \frac{y_O}{\nu_F W_F}\Big\}^{n+1} \leq 0, \\ y_i^{n+1}\dfrac{\dot{\omega}_i^{n+1}}{y_i^{n+1}}, & \text{otherwise.} \end{array} \right.$$

Passing this non-positive term on the left-hand side, the left-hand side operator becomes:

$$\forall K \in \mathcal{M}, \quad \widetilde{\mathcal{A}}_K^{n+1} = \mathcal{A}_K^{n+1} + \frac{(\dot{\omega}_i)_K^{n+1}}{(y_i)_K^{n+1}} I_K,$$

where I_K denotes the K-th line of the identity matrix. By definition of $\widetilde{\omega}_i$, the terms added on the diagonal of $\widetilde{\mathcal{A}}^{n+1}$ are non-negative, thus $\widetilde{\mathcal{A}}^{n+1}$ is an M-matrix and since the right hand side is non-negative, any solution will be non-negative.

(ii) For all $i \in \mathcal{I}$ and $K \in \mathcal{M}$, let us denote by $(b_i)_K^n$ the value of the right-hand side of (3.23) at the time level t_n, which may be written as:

$$(b_i)_K^n = \sum_{L \in \mathcal{V}(K)} \alpha_L^n (y_i)_L^n + (\widetilde{\omega}_i)_K^{n+1},$$

where $\sum_{L\in\mathcal{V}(K)} \alpha_L^n = |K|/\delta t \rho_K^{n-1}$, which is exactly the sum of the entries of $\mathcal{A}_K^{n+1}$. Taking also into consideration the sign of the reactive term and Lemma 3.4.2, the results are immediate. □

Lemma 3.4.5.
For $0 \leq n \leq N$, let us suppose that for all $K \in \mathcal{M}$, $\sum_{i\in\mathcal{I}}(y_i)_K^n = 1$ and that (3.20c) holds. Then any solution to the discrete chemical fraction balance equations satisfies for all $K \in \mathcal{M}$, $\sum_{i\in\mathcal{I}}(y_i)_K^{n+1} = 1$.

Proof. Summing over $i \in \mathcal{I}$ the discrete chemical fraction balance equations, yields:

$$\forall K \in \mathcal{M}, \quad \mathcal{A}_K^{n+1} \cdot \Big(\sum_{i\in\mathcal{I}}(y_i)^{n+1}\Big) = \frac{|K|}{\delta t}\rho_K^{n-1}\sum_{i\in\mathcal{I}}(y_i)_K^{n+1} + \mathrm{div}\Big(\sum_{i\in\mathcal{I}}(\boldsymbol{j}_i)_K^{n+1}\Big) + \sum_{i\in\mathcal{I}}(\dot{\omega}_i)_K^{n+1}.$$

Let us recall that by construction, $\forall K \in \mathcal{M}$, $\sum_{i\in\mathcal{I}}(\dot{\omega}_i)_K^{n+1} = 0$ and for all $\sigma \in \mathcal{E}(K)$, $\sum_{i\in\mathcal{I}}(\boldsymbol{j}_i)_{K,\sigma}^n = 0$. Thus, what remains on the right-hand side is the sum of the entries of the vector b^n, where for all $K \in \mathcal{M}$, $b_K^n = \sum_j (A_K^{n+1})_j$. Applying the result of Lemma 3.4.2, concludes the proof. □

Now we may state and prove our main result. Some of its statements have already been treated, but are also present here for the sake of clarity.

Theorem 3.4.1 (Existence and boundedness of solutions)
For $0 \leq n \leq N$, let us suppose that for all $i \in \mathcal{I}$ and $K \in \mathcal{M}$, $(y_i)_K^n \geq 0$, $\sum_{i\in\mathcal{I}}(y_i)_K^n = 1$ and $CFL^n \leq 1$. Then, there exists at least one solution to (3.19)-(3.20), satisfying the following assertions:

(i) for any $i \in \mathcal{I}$, $(y_i)^{n+1} \in [0,1]$; If, in addition, $q_d^n = 0$, then $\overline{y}_F^{n+1} \leq \overline{y}_F$, $\overline{y}_O^{n+1} \leq \overline{y}_O$, $\underline{y}_P^{n+1} \leq \underline{y}_P$ and $\underline{y}_N \leq \underline{y}_N^{n+1} \leq \overline{y}_N^{n+1} \leq \overline{y}_N$.

(ii) $\theta^{n+1} \geq 0$;

(iii) if $\beta \leq 0$, then $\underline{\theta}^{n+1} \geq \underline{\theta}$ and $0 \leq \rho^{n+1} \leq \max\Big\{\dfrac{P_{th}}{R\underline{\theta}}W_i,\ \text{for } i \in \mathcal{I}_g\ ;\ \rho_i,\ \text{for } i \in \mathcal{I}_s\Big\}$.

Proof. In the first place, let us suppose the existence of a solution and prove that the announced bounds hold. We proceed by induction, supposing that the announced bounds hold at t_n, $0 \leq n \leq N$.

Assertion *(i)* – Under the assumption of existence of a solution, the positivity of $(y_i)_K^{n+1}$ for all $i \in \mathcal{I}$ and $K \in \mathcal{M}$ is guaranteed by Lemma 3.4.4. Thus, the sdought bounds are guaranteed by Lemma 3.4.5.

Assertion *(ii)* – Let us rewrite the linear system (3.20a) in the following form,

$$\sum_{i\in\mathcal{I}} c_{\mathrm{p},i}\mathcal{M}_K^{n+1}\theta^{n+1} = \sum_{i\in\mathcal{I}} c_{\mathrm{p},i}\rho_K^{n-1}(y_i)_K^n\theta_K^n + (\dot{\omega}_\theta)_K^{n+1}.$$

For $0 \leq n \leq N$ and any $K \in \mathcal{M}$, the only non-zero terms of the K-th line of $\mathcal{M}^{n+1}$, read:

$$\begin{aligned}
&\frac{|K|}{\delta t}\rho_K^n(y_i)_K^{n+1} + (G_{K,\sigma}^{n+1})^+ + \frac{\lambda_\sigma}{d_\sigma}, && \text{on the diagonal,}\\
&-(G_{K,\sigma}^{n+1})^- - \frac{\lambda_\sigma}{d_\sigma}, && \text{on any column } L \text{ such that } \sigma = K|L.
\end{aligned}$$

The matrix $\mathcal{M}^{n+1}$ has the same properties as the matrix $\mathcal{A}^{n+1}$, since under the condition $CFL_{\dot{\omega}}^n \leq 1$, the sum over a line of the matrix is non-negative. Note also that for an exothermic chemical reaction, such as the combustion, $\forall K \in \mathcal{M}$, $(\dot{\omega}_\theta)_K^{n+1}$ must be by definition non-negative. Thus, the sign of the right-hand side is positive and since $\mathcal{M}^{n+1}$ is an M-matrix, the temperature at t_{n+1} cannot be negative.

Assertion *(iii)* – By the discrete equation of state, for all $K \in \mathcal{M}$, ρ_K^{n+1} is non-negative since neither of the elements of $\{(y_i)_K^{n+1}\}_{i\in\mathcal{I}}$ and θ_K^{n+1} is negative. The upper bound for ρ^{n+1} is obtained from the same relation with a simple computation.

Let us now turn to the question of existence of a solution. For the density and temperature, it is directly given by the invertibility of the associated linear operators. For the chemical mass fractions, let us rewrite the corresponding systems in the following form,

$$\forall i \in \mathcal{I},\ \forall K \in \mathcal{M},\quad \frac{|K|}{\delta t}(\rho_K^n(y_i)_K^{n+1} - \rho_K^{n-1}(y_i)_K^n) + \mathrm{div}\big[\rho^n y_i^{n+1}\boldsymbol{u}^n\big]_K + \mathrm{div}\big[\boldsymbol{\jmath}_i^n\big] = \alpha(\widetilde{\omega}_i)_K^{n+1}, \quad (3.24)$$

where α is a real number lying in the interval $[0,1]$. For $\alpha = 0$ system (3.24) admits a unique solution, $(y_N^{n+1}, y_F^{n+1}, y_O^{n+1}, y_P^{n+1})$, thanks to the invertibility of the corresponding linear operators and let us suppose the existence of a solution for $\alpha \in (0,1]$. For any value of $\alpha \in [0,1]$, any solution is bounded in

$[0,1]$: firstly, for any value of α the solution is bounded below by 0 in virtue of Lemma 3.4.4. Secondly, it is easy to check that for any $\alpha \in (0,1]$ the solution is bounded above by 1, by summing over $i \in \mathcal{I}$ equations (3.24) and exploiting the facts that for all $K \in \mathcal{M}$ the sum over $i \in \mathcal{I}$ of the reaction rates vanishes, such a the sum over $i \in \mathcal{I}$ of the mass diffusion fluxes on the edges, and that the mass balance must hold. We conclude to the existence of a solution $(y_N^{n+1}, y_F^{n+1}, y_O^{n+1}, y_P^{n+1}) \in [0,1]^4$ for $\alpha = 1$ (*i.e.* for the discrete mass fraction balance equations) thanks to a topological degree argument stated in the Appendix 3.A. □

3.5 Numerical results

Computations presented in this section are performed with MATLAB for the primitive formulation and by the open-source CALIF^{3}S software developped at IRSN [6] for the flame-velocity model.

Data is chosen in order to check the scheme properties (*i.e.* to avoid unrealistic simplifications, as, for instance, a same specific heat diffusion coefficient for all the chemical species), and to be in the range of practical applications. The mixture is initially at rest, homogeneous and with an uniform temperature:

$$(y_F)_0 = (y_O)_0 = 0.4, \quad (y_N)_0 = 0.2, \quad (y_P)_0 = 0, \quad \theta_0 = 300°K.$$

The reaction rate is given by the following Arrhenius law:

$$\dot{\omega}_K = 10^4 \, y_F \, y_O \, e^{-900/\theta}. \tag{3.25}$$

The molar masses of the chemical species are considered to be equal to 20 g/mol for all the species, so the combustion reaction reads $F + O + N \longrightarrow 2P + N$, and the initial atmosphere composition is stoichiometric. The binary mass diffusion coefficients are

$$D_{NO} = 0.25 * 10^{-5}, \quad D_{NP} = 0.5 * 10^{-5}, \quad \text{and } D_{OP} = 10^{-5}.$$

The temperature diffusion coefficient is $\lambda = 0.005$, the specific heat coefficients (J/(Kg K)) are $c_{\mathrm{p},N} = 3.\,10^3$, $c_{\mathrm{p},F} = 1.\,10^3$, $c_{\mathrm{p},O} = 2.\,10^3$ and $c_{\mathrm{p},P} = 4.\,10^3$ and the formation enthalpies (J/Kg) are $\Delta h^0_{f,N} = 3.\,10^6$, $\Delta h^0_{f,F} = 1.\,10^6$, $\Delta h^0_{f,O} = -2.\,10^6$ and $\Delta h^0_{f,P} = -4.\,10^6$ (so the reaction is exothermic). The fuel density is equal to 100 Kg/m^3, and the density of the gaseous atmosphere is given by the ideal gases law.

Flame profiles obtained with the Hirschfelder and Curtiss diffusion coefficients – We first perform computations with mass diffusion coefficients calculated by the Hirschfelder and Curtis approximation. To initiate the transient, the reaction ignition is forced at the left part of the domain; then, the flame brush propagates to the right, while the solution progressively tends to a progressive wave (*i.e.* the translation at a constant speed of a constant profile). This establishment is quite long (for present computations, the final time is $t = 2\,$s), and to capture this phenomena with a reasonable number of cells, we use a mobile frame attached to the flame front (or, equivalently, we impose a constant inlet flow rate of fresh gases at the right-hand section of the domain). However, the velocity of the flame front is influenced by the mesh, so the frame velocity (or the inlet flowrate) depends on the number of cells; to compare the established profiles, we thus have performed an abscissa translation up to obtain solutions as close as possible.

Obtained results with various meshes are plotted on Figures 3.1 and 3.2. First, we observe that numerical convergence (at least for an engineering point of view) is obtained for the coarsest mesh except for the velocity, which, unfortunately, is an important quantity, since the plane flame laminar velocity is a parameter often used to characterize the mixture, for instance to compute the turbulent

flame velocity in the so-called TFC (for Turbulent Flame velocity Closure) deflagration mdels [85, 59]. For the velocity in the fresh gases, we obtain 3.343 cm/s, 3.017 cm/s 2.931 cm/s and 2.862 cm/s for $n = 500$, $n = 1000$, $n = 2000$ and $n = 4000$ cells respectively, which suggests a first order convergence of this parameter, since the difference between two successive meshes roughly varies as the space step (of the coarsest or finest one, equivalently). Second, as expected, the expression of the mass diffusion operator produces, with the chosen binary diffusion coefficients, rather large (up to around 25% locally) unphysical variations of the inert gases mass fractions, which should remain constant in space and time. The temperature is larger in the burnt zone than in the fresh one (the reaction is exothermic); however, we observe a small temperature decrease on the upstream side (*i.e.* near the fresh zone) of the flame brush, which is not unconsistant with the theoretical study, since the β parameter of Equation (3.13) is positive.

Since the profile in the interface does not vary in space and time up to a translation velocity u_p (the velocity of the flame brush), we may write the usual jump conditions for the mixture mass balance equation (3.1), to obtain:

$$(\rho_u - \rho_b)\ u_p = \rho_u u_u - \rho_b u_b,$$

where ρ_b and u_b (resp. ρ_u and u_u) stand for the constant density and velocity in the burnt (resp. unburnt) zone. Thanks to symetry conditions (due to the fact that the combustion takes place in an atmosphere initially at rest), $u_b = 0$ and we deduce from the previous relation that the flame velocity is given by:

$$u_f = u_p - u_u = \frac{\rho_b}{\rho_u - \rho_b}\ u_u.$$

The obtained flame velocity is equal to $u_f = 0.75$ cm/s.

Comparison between the two formulas for the diffusion coefficients – We now assess the influence of an approximation often done in practice, namely considering mass diffusion coefficients which do not vary as a function of the mixture composition. To this purpose, we set these coefficients to the average of their value calculated thanks to the Hirschfelder and Curtiss formula in the unburnt and the burnt phase, under the hypothesis of a complete reaction. Obtained profiles are plotted on Figures 3.3 and 3.4. They show a reasonably weak impact of the approximation. The flame velocity for the constant mass diffusion coefficients is equal to 0.84 cm/s (to be compared with $u_f = 0.75$ cm/s for the Hirschfelder and Curtiss approximation).

Dependence on the magnitude of the reactive source and the thermal diffusion coefficient – We now assess the influence of mass difusion, setting the mass diffusion coefficients to zero, an then of the chemical reaction rate and the thermal diffusion coefficient. The established profiles obtained with 1000 cells (when turning off the mass diffusion, the space convergence is obtained faster) are shown on Figures 3.5 and 3.6. We first observe that the inert gases mass fraction (not shown here) is now constant, which is consistent with the theoretical expectations (when the mass diffusion coefficients are the same for all the chemical species, the scheme satisfies a discrete maximum principle). We then collect the flame velocity and the flame brush thickness for various thermal diffusion coefficients and reaction rates in the tables below. The flame brush thickness is evaluated as:

$$\delta_f = x_{0.39} - x_{0.02}$$

where, from the left to the right, $x_{0.39}$ (respectively $x_{0.02}$) stands for the first (respectively last) location where the fuel mass fraction is greater that 0.39 (respectively, lower than 0.02).

	$\lambda/2$	λ	$2\,\lambda$
flame velocity (cm s^{-1})	2.02	2.82	3.95
flame brush thickness (mm)	0.76	1.04	1.44

	$\dot{\omega}/2$	$\dot{\omega}$	$2\,\dot{\omega}$
flame velocity (cm s^{-1})	1.97	2.82	4.04
flame brush thickness (mm)	0.77	1.04	1.45

The flame velocity is much greater when the mass diffusion vanishes: compared to the diffusive cases presented in the previous sections, u_f is multiplied by a factor greater than 3. In addition, this velocity is larger and larger when the thermal diffusion or the chemical reaction rate increase, with a dependence which seems to be close to linear with respect to the square root of both these parameters. The flame brush thickness seems to be roughly proportional to u_f.

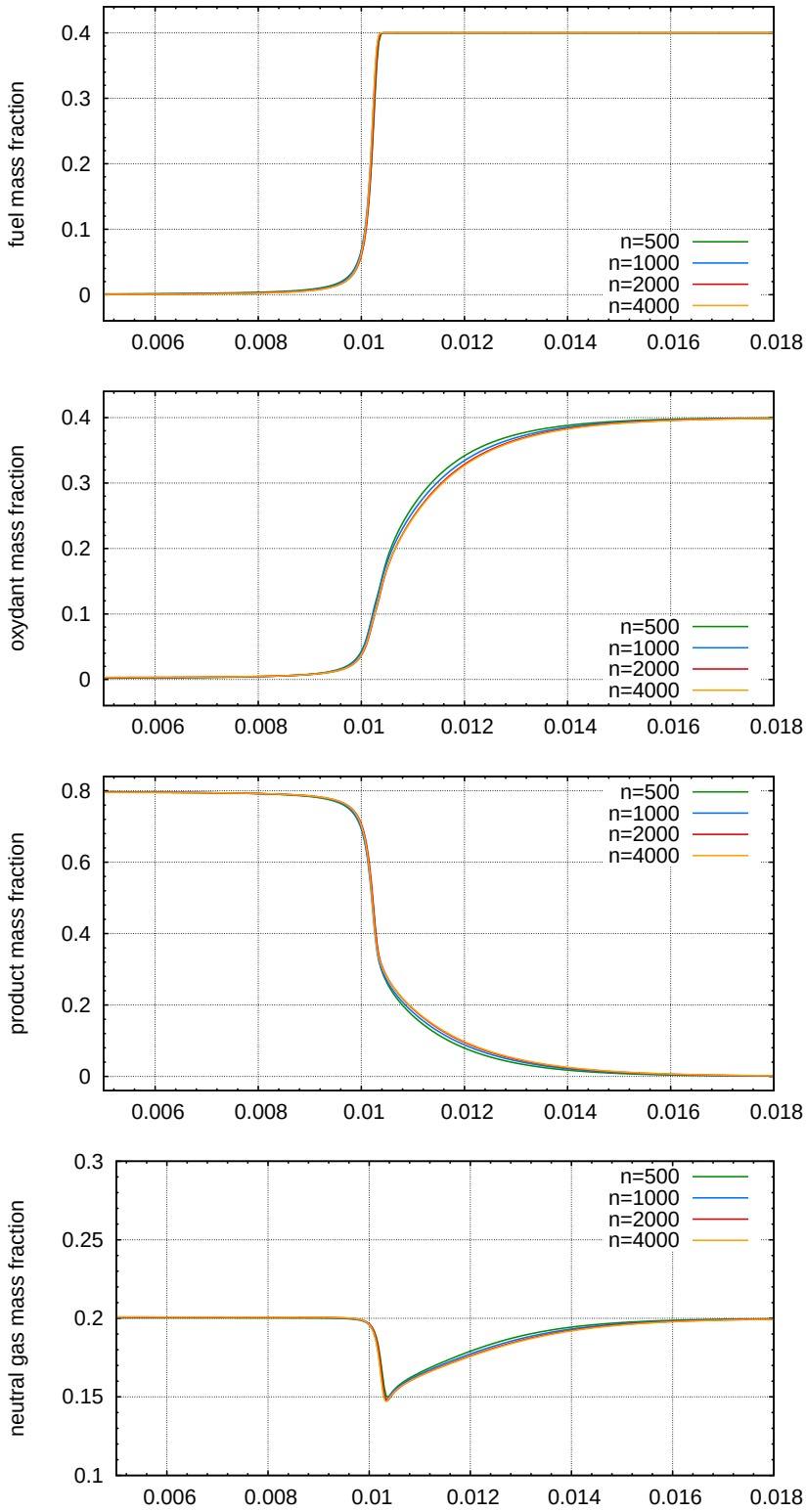

Figure 3.1: Results obtained with the Hirschfelder and Curtiss formula for the diffusion coefficients – From the top to the bottom, fuel, oxydant, product and neutral gas mass fractions obtained with 500 (green), 1000 (blue), 2000 (red) and 4000 (orange) cells.

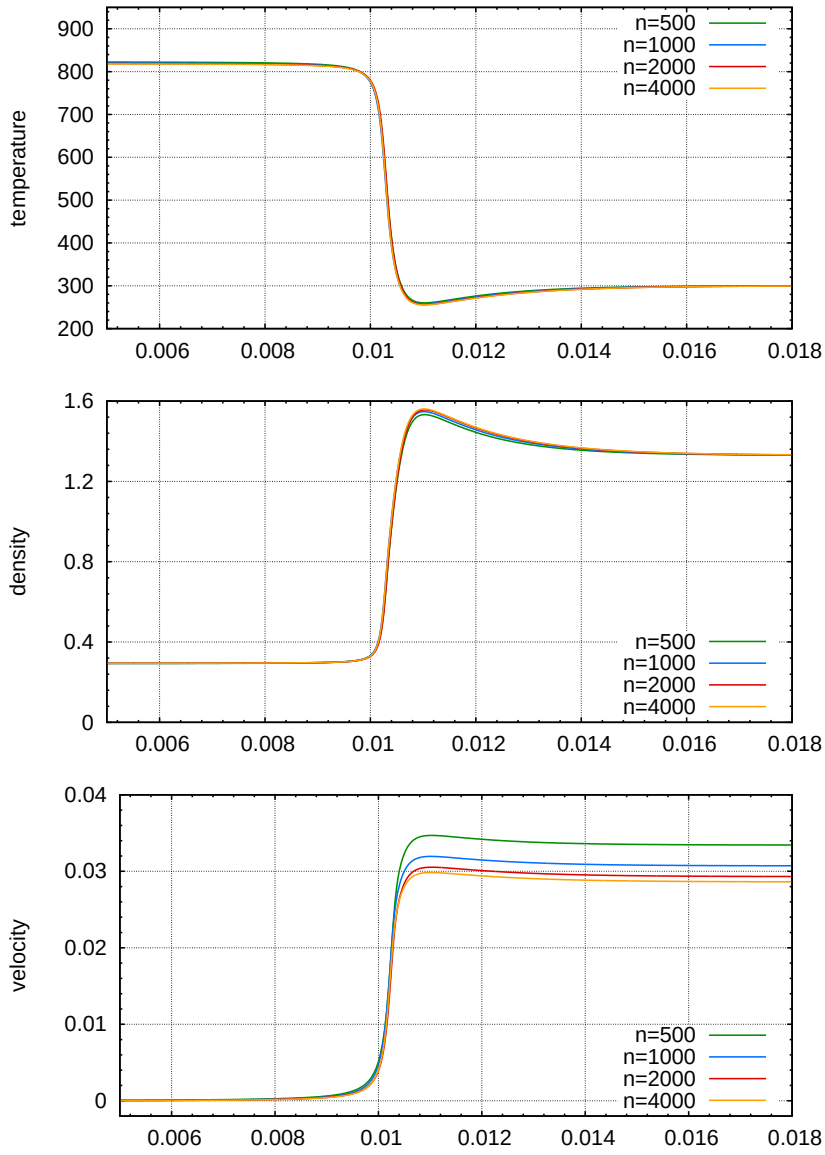

Figure 3.2: Results obtained with the Hirschfelder and Curtiss formula for the diffusion coefficients – From the top to the bottom, temperature, density and velocity obtained with 500 (green), 1000 (blue), 2000 (red) and 4000 (orange) cells.

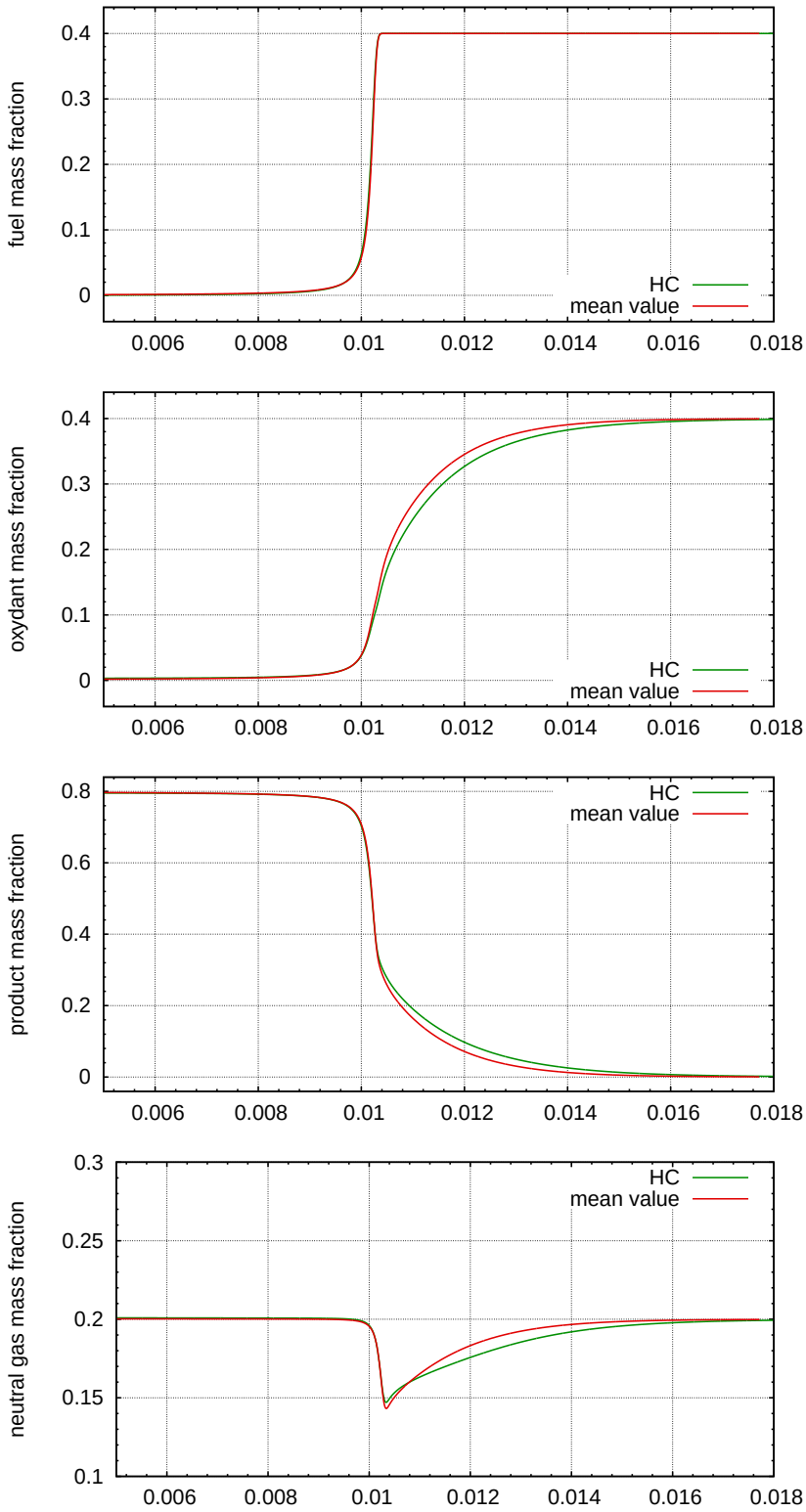

Figure 3.3: Results obtained with the Hirschfelder and Curtiss formula (green) and with a mean value (red) for the diffusion coefficients – From the top to the bottom, fuel, oxydant, product and neutral gas mass fractions.

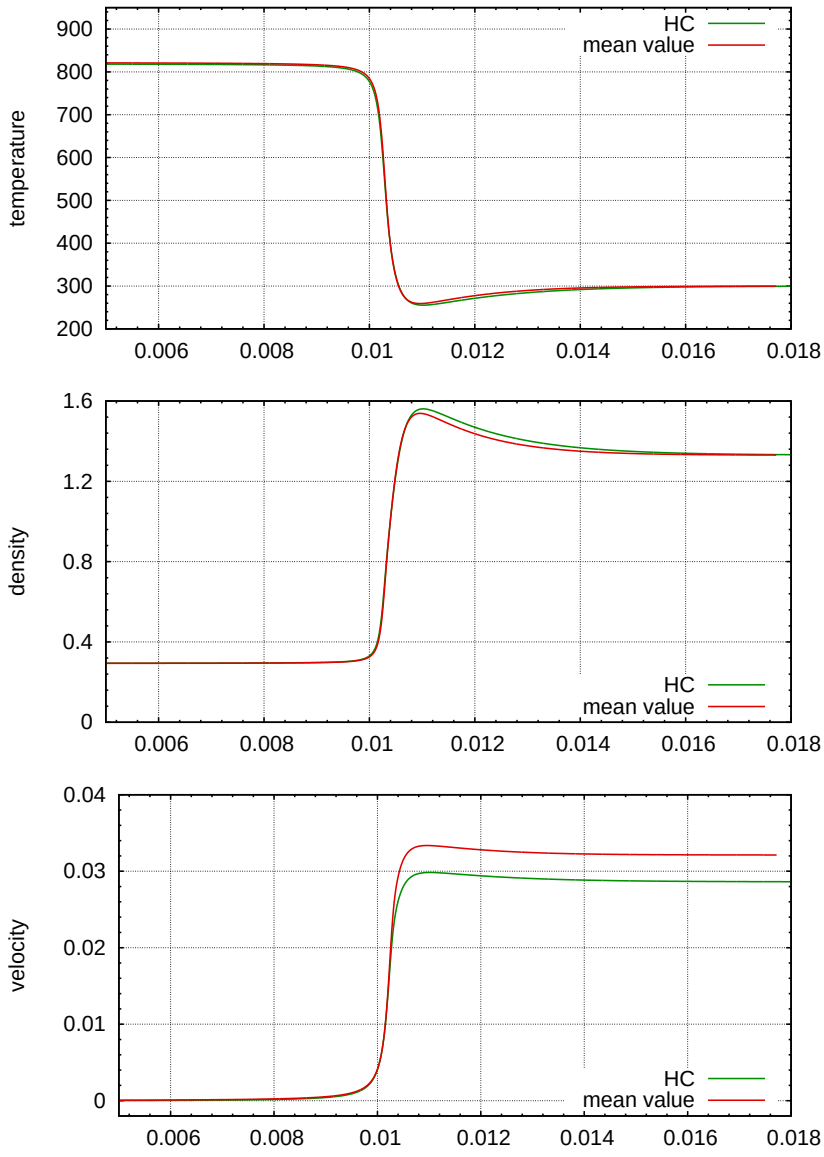

Figure 3.4: Results obtained with the Hirschfelder and Curtiss formula (green) and with a mean value (red) for the diffusion coefficients – From the top to the bottom, temperature, density and velocity.

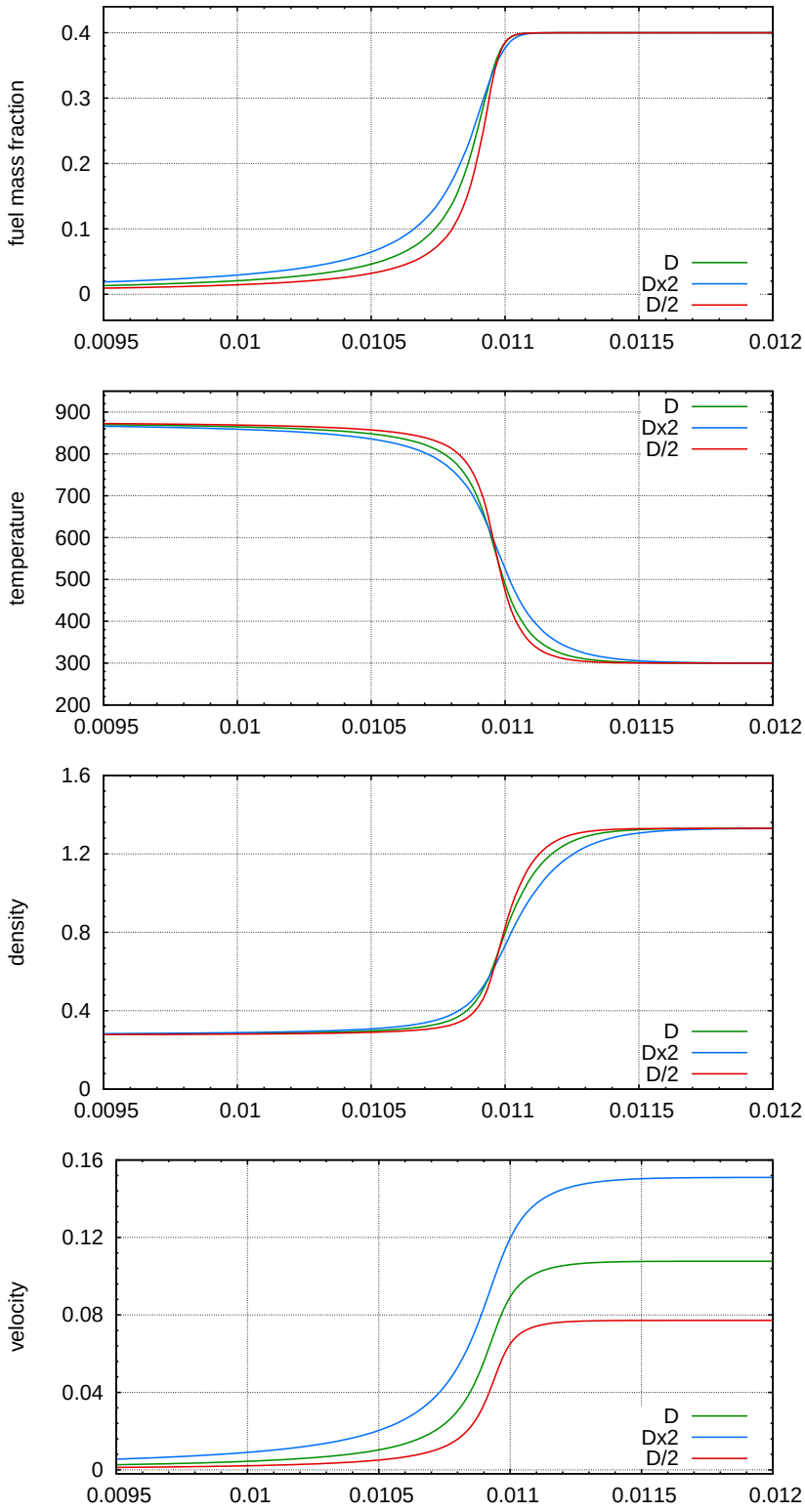

Figure 3.5: From the top to the bottom, fuel mass fraction, temperature, density and velocity travelling profiles obtained with a constant thermal diffusion coefficient $\lambda = 0.005$, $2\,\lambda$ (blue) and $\lambda/2$ (red).

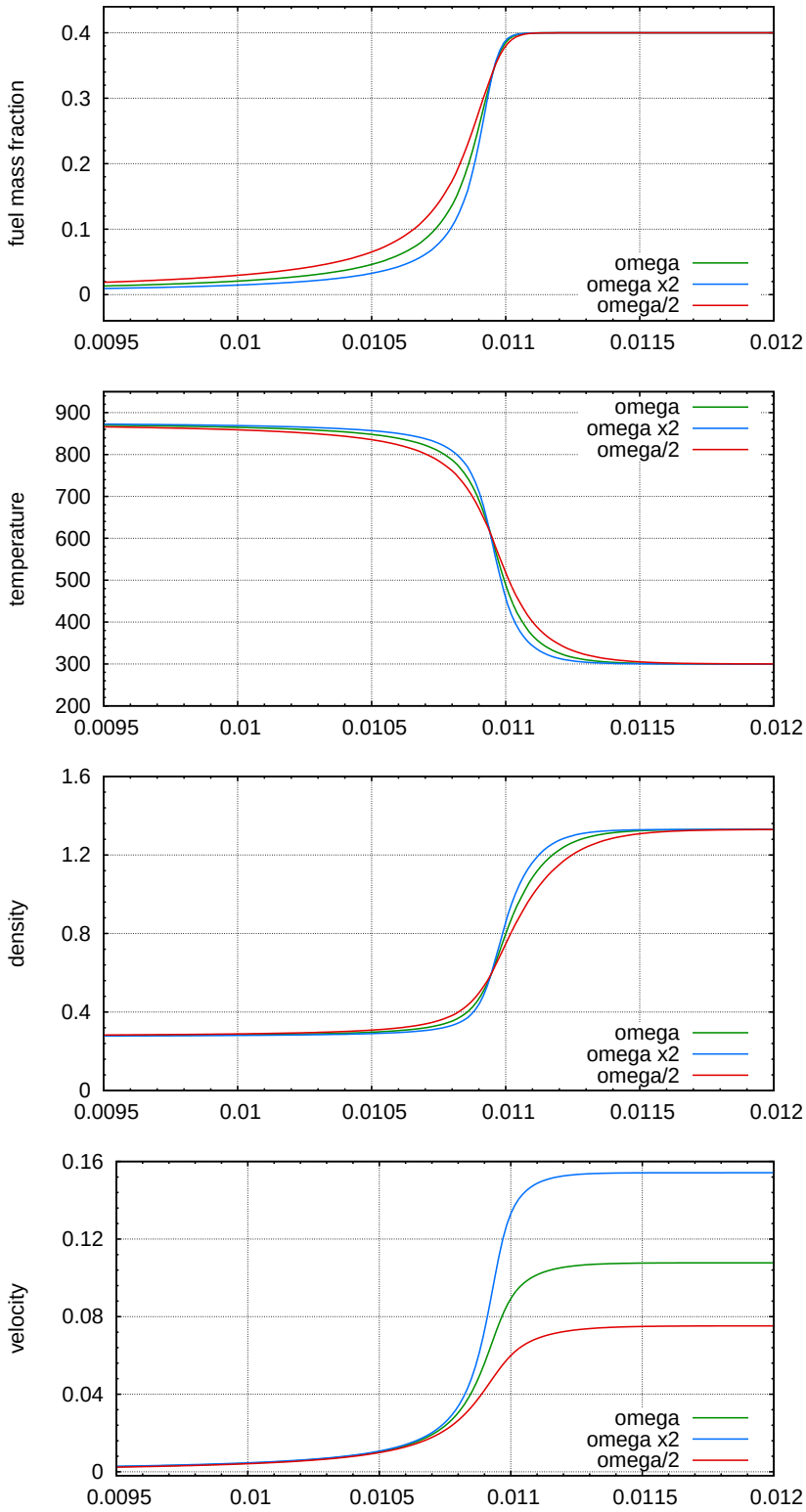

Figure 3.6: From the top to the bottom, fuel mass fraction, temperature, density and velocity travelling profiles obtained with $\dot{\omega}$ given by Equation (3.25) (green), $2\,\dot{\omega}$ (blue) and $\dot{\omega}/2$ (red).

3.6 Comparison with an alternative approach

We compare in this section two descriptions of the combustion phenomenon:

- The first one is the model considered up to now in this chapter. It is obtained by collecting the mass balance for the chemical species, the energy balance and the momentum balance for the mixture; the reaction term $\dot{\omega}$ is expressed by a closure law depending of the temperature, derived on the basis of physical arguments. This model will be refered to in the following of this section as the *primitive formulation*.
- The second one is the model considered in the previous chapter. It relies on the assumption that the solution consists in a travelling reaction thin interface (the so-called flame front) separating a zone where the combustion is complete (the "burnt zone") from a zone where no combustion yet occured (the "fresh zone"). This representation offers the possibility to reduce the problem to an explicit tracking of the front location, through the solution of a transport equation for a color function G ($G \in [0,1]$, $G < 0.5$ in the burnt zone, $G \geq 0.5$ in the fresh atmosphere); the reaction term is governed by the value of G: $\dot{\omega} = 0$ if $G \geq 0.5$ and $\dot{\omega}$ is proportional to $1/\tau$ otherwise, where τ is a time-scale closely correlated to the flame front thickness (see Equation (3.27) below for its actual expression). In the rest of this section, we will call this model as the *flame velocity formulation*.

The first option is standard for the computation of laminar flames. Variants of the flame velocity formulation are often chosen to compute turbulent deflagrations in industrial applications [66, 59], for at least two reasons: first, it reduces the modelling of a complex physical phenomenon to the construction of a suitable closure law for a quantity accessible through experiments, namely the turbulent flame velocity (note, however, that the accurate prediction of this parameter turns to be in practice a rather intricate task, not much easier than the estimation of an effective burning rate in turbulent flows); second, specially in tri-dimensional situations, the mesh requirement for an accurate solution of the flame velocity formulation is dramatically less stringent than for the primitive one.

The recall the transport equation governing the evolution of the level-set function G:

$$\partial_t(\rho G) + \mathrm{div}(\rho G \boldsymbol{u}) + \rho_u u_f |\boldsymbol{\nabla} G| = 0, \tag{3.26}$$

associated to the initial conditions $G = 0$ at the location where the flame starts and $G = 1$ elsewhere. The quantity ρ_u is a constant density, which, from a physical point of view, stands for a characteristic value for the unburnt gases density, and u_f is the flame brush velocity. The reactive term $\dot{\omega}$ is given by:

$$\dot{\omega} = \frac{u_f}{\delta}\ \eta(y_F, y_O)\ (G - 0.5)^-, \quad \eta(y_F, y_O) = f(y_F, y_O) = \min(\frac{y_F}{\nu_F W_F}, \frac{y_O}{\nu_O W_O}), \tag{3.27}$$

where δ is a quantity homogeneus to a length scale, which governs the thickness of the reaction zone. Besides the addition of Equation (3.26) and the modification of the expression of $\dot{\omega}$, the other equations of the primitive formulation are left unchanged.

The numerical algorithm differs from the scheme (3.19)-(3.20) for the primitive formulation by the insertion, as a first step, of a dicrete analog of (3.26), with a discretization of G on the primal mesh (so the associated discrete unknowns are $(G_K)_{K\in\mathcal{M}}$), which we recall:

Solve for G^{n+1}:

$$\forall K \in \mathcal{M}, \qquad \frac{1}{\delta t}\left[\rho_K^n G_K^{n+1} - \rho_K^{n-1} G_K^n\right] + \mathrm{div}\Big[\rho^n G^{n+1} \boldsymbol{u}^n\Big]_K + \rho_u u_f |\boldsymbol{\nabla} G|_K^{n+1} = 0.$$

The discretization of the time derivative and convection terms is the same as for fuel mass fractions. for the latst term, at the continuous level, we observe that:

$$|\boldsymbol{\nabla} G| = \frac{\boldsymbol{\nabla} G}{|\boldsymbol{\nabla} G|} \cdot \boldsymbol{\nabla} G$$

and the last term in (3.28) is approximated by writing:

$$|\boldsymbol{\nabla} G|_K^{n+1} = (\mathbf{W}^n \cdot \boldsymbol{\nabla} G^{n+1})_K,$$

where $\mathbf{W}$ is an approximation of the advection field $\boldsymbol{\nabla} G/|\boldsymbol{\nabla} G|$ and we use the standard upwind finite volume formulation of the transport operator (*i.e.* the formulation obtained by writing $\mathbf{W} \cdot \boldsymbol{\nabla} G = \mathrm{div}(G\,\mathbf{W}) - G\,\mathrm{div}\mathbf{W}$ and using a usual finite volume discretization of the convection operator). In the solution of this system of equations, the convection operators are discretized by an explicit MUSCL-like technique, as described in [67].

We compare the profiles obtained with the flame velocity formulation with those obtained in the previous section in the non-diffusive case. To this purpose, the obtained value for the flame velocity is injected in the flame velocity model, and we choose the length δ_f to fit as closely as possible the travelling profiles of the unknowns. Results for the fuel mass fraction and the temperature are given on Figure 3.1. We observe that, as expected, the thickness of the combustion zone is scaled by δ_f and that a reasonable agreement is obtained with $\delta_f = 0.2\,\mathrm{mm}$.

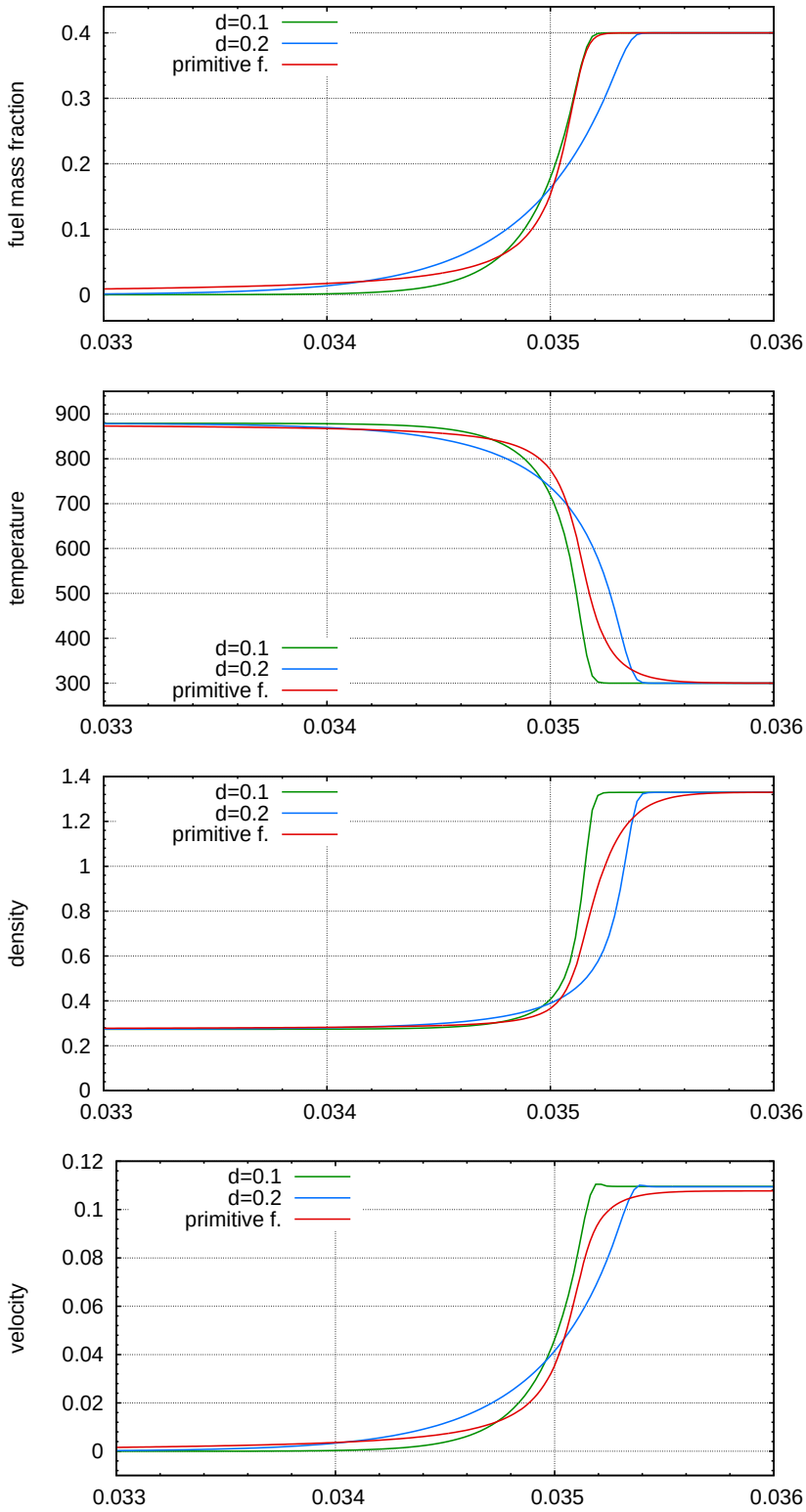

Figure 3.1: From the top to the bottom, fuel mass fraction, temperature, density and velocity travelling profiles obtained with the primitive formulation of the equations (red) and with the flame velocity model, with $\delta = 0.1\,\mathrm{mm}$ (green) and $\delta = 0.1\,\mathrm{mm}$ (blue).

Appendix

3.A A result from the topological degree theory

Theorem 3.A.1 (Application of the topological degree, finite dimensional case)
Let V be a finite dimensional vector space on $\mathbb{R}$, $\|.\|$ a norm on V, let f be a continuous function from V to V and let $R > 0$. Let us assume that there exists a continuous function $F : V \times [0,1] \to V$ satisfying:

(i) $F(.,1) = f$,

(ii) $\forall \alpha \in [0,1]$, if $v \in V$ is such that $F(v,\alpha) = 0$ then $v \in B_R = \{v \in V \ ; \|v\| < R\}$,

(iii) the topological degree of $F(.,0)$ with respect to 0 and B_R is equal to $d_0 \neq 0$.

Then the topological degree of $F(.,1)$ with respect to 0 and to B_R is also equal to $d_0 \neq 0$; consequently, there exists at least a solution $v \in B_R$ such that $f(v) = 0$.

3.B On the Hirschfelder and Curtiss approximation

Hirschfelder and Curtiss model and Fick's law for a binary mixture – In the case of a binary gaseous mixture, the difusion flux for the first species reads (see Section 3.2.2):

$$\boldsymbol{j}_1^e = -\rho D_1 \frac{W_1}{W} \boldsymbol{\nabla} x_1, \quad \text{with } D_1 = \frac{1 - y_1}{\dfrac{x_2}{D}},$$

where D stands for the diffuxion coefficient for the species 1 in species 2. Using the fact that $1 - y_1 = y_2$ and that $y_2/x_2 = W_2/W$, we thus get:

$$\boldsymbol{j}_1^e = -\rho D \frac{W_1 W_2}{W^2} \boldsymbol{\nabla} x_1. \tag{3.29}$$

We have

$$x_1 = \frac{W}{W_1}\, y_1,$$

thus

$$\boldsymbol{\nabla} x_1 = \frac{W}{W_1}\, \boldsymbol{\nabla} y_1 + \frac{1}{W_1} y_1 \boldsymbol{\nabla} W. \tag{3.30}$$

The mixture molar mass W is given by:

$$W = \frac{1}{\dfrac{y_1}{W_1} + \dfrac{y_2}{W_2}},$$

with $y_2 = 1 - y_1$, thus:

$$\boldsymbol{\nabla} W = W^2 \left(\frac{1}{W_2} - \frac{1}{W_1}\right) \boldsymbol{\nabla} y_1.$$

Inserting in (3.30) yields:

$$\begin{aligned}\boldsymbol{\nabla} x_1 &= \frac{W^2}{W_1}\left(\frac{1}{W}+(\frac{1}{W_2}-\frac{1}{W_1})y_1\right)\boldsymbol{\nabla} y_1 = \frac{W^2}{W_1}\left(\frac{y_1}{W_1}+\frac{y_2}{W_2}+\frac{y-1}{W_2}-\frac{y-1}{W_1}\right)\boldsymbol{\nabla} y_1 \\ &= \frac{W^2}{W_1}\,\frac{y_1+y_2}{W_2}\,\boldsymbol{\nabla} y_1 = \frac{W^2}{W_1 W_2}\,\boldsymbol{\nabla} y_1.\end{aligned}$$

Inserting this expression in (3.29) yields:

$$\boldsymbol{j}_1^e = -\rho D \boldsymbol{\nabla} y_1.$$

In addition, since $y_1 + y_2 = 1$, we get that $\boldsymbol{j}_1^e + \boldsymbol{j}_2^e = 0$, so the corrective term $\boldsymbol{J}$ is equal to zero, and $\boldsymbol{j}_1 = \boldsymbol{j}_1^e$ is given by the previous expression, which is exactly Fick's law.

Another expression for the diffusion flux – For a species i in a gaseous mixture, the diffusion flux given by the Hirschfelder and Curtiss model may be reformulated as:

$$\boldsymbol{j}_i^e = -\rho\,\frac{y_i\,(1-y_i)}{x_i\,(1-x_i)}\;\bar{D}_i\;\boldsymbol{\nabla} x_i \quad \text{with } \bar{D}_i = \frac{1-x_i}{\displaystyle\sum_{j\neq i}\frac{x_j}{D_{ji}}}.$$

The diffusion coefficient $\bar{D}_i$ is the harmonic mean value of the binary diffusion coefficients of the species i in the species $j \neq i$.

Appendix A

A Large Eddy Simulation model and scheme

A.1 Navier-Stokes equations

The three dimensional Navier-Stokes system of equations under the enthalpy formulation, reads:

$$\begin{aligned} &\partial_t \rho + \mathrm{div}(\rho \boldsymbol{u}) = 0, \\ &\partial_t (\rho \boldsymbol{u}) + \mathrm{div}(\rho \boldsymbol{u} \otimes \boldsymbol{u}) + \boldsymbol{\nabla} p = \mathrm{div}\boldsymbol{\sigma}, \\ &\partial_t (\rho h) + \mathrm{div}(\rho h \boldsymbol{u}) = \partial_t p + \boldsymbol{u} \cdot \boldsymbol{\nabla} p + \mathrm{div}(\kappa \boldsymbol{\nabla} T) + \Phi, \\ &p = \rho R T, \end{aligned} \tag{A.1}$$

where $\partial_t f$ and $\partial_i f$, $i = 1, 2, 3$, denote the partial derivatives of the function f with respect to the time (t) and spatial ($\boldsymbol{x} = (x_1, x_2, x_3)$) coordinates. The unknowns are the density ρ, the velocity $\boldsymbol{u} = (u_1, u_2, u_3)$, the pressure p and the enthalpy h.

Under the Stoke's hypothesis, the shear-stress tensor for a Newtonian fluid is given by:

$$\sigma_{ij} = 2\mu(T)\big(S_{ij} - \frac{1}{3}\delta_{ij} \sum_{k=1}^{3} \mathrm{Tr}(S)\big),$$

where

$$S_{ij} = \frac{1}{2}(\partial_j u_i + \partial_i u_j).$$

In this work the dynamic viscosity $\mu(T)$ will be considered constant and will simply be denoted by μ. The viscous dissipation is given by

$$\Phi = \sum_{i=1}^{3} \sum_{j=1}^{3} \sigma_{ij} \partial_j u_i.$$

The gas constant is $R = c_p - c_v$, where c_p and c_v are the specific heat constants at constant pressure and constant volume respectively. For air, $R = 287.03\ \mathrm{m^2\,s^2\,K}$. The temperature T is linked to the enthalpy h through the relation

$$h = c_p T,$$

The thermal conductivity may be expressed by $\kappa = \mu c_p / \mathrm{Pr}$, where the Prandtl number Pr is the ratio of the kinematic viscosity $\nu = \mu/\rho$ and the thermal diffusivity $\kappa/(\rho c_p)$ and is assumed to be constant equal to 0.72 for air.

A.2 Filtering operator

Scales are separated using a scale high-pass filter which is also a low-pass filter in frequency. Filtering is represented mathematically in the physical space as a convolution product. The resolved part $\overline{\phi}(\boldsymbol{x},t)$ of a space-time variable $\phi(\boldsymbol{x},t)$ is defined by

$$\overline{\phi}(\boldsymbol{x},t)=\frac{1}{\Delta^3}\frac{1}{\tau_c}\int_{\mathbb{R}^3}\int_{-\infty}^{+\infty}G\Big(\frac{\boldsymbol{x}-\boldsymbol{\xi}}{\Delta},\frac{t-\tau}{\tau_c}\Big)\phi(\boldsymbol{\xi},\tau)\,\mathrm{d}\tau\,\mathrm{d}\boldsymbol{\xi},$$

where the convolution kernel G is characteristic of the filter used and is associated with the cut-off scale in space Δ and time τ_c.

To manipulate the Navier-Stokes equations after the filtering, the three properties given below are required. The first one is satisfied by the convolution form of the filtering, while the latter ones depend on the filtering function G.

- Linearity,
$$\overline{\phi+\psi}=\overline{\phi}+\overline{\psi}.$$
- Consistency,
$$\overline{\phi}=\phi\iff\int_{\mathbb{R}^3}\int_{-\infty}^{+\infty}G(\boldsymbol{\xi},\tau)\mathrm{d}\tau\,\mathrm{d}^3\xi=1,\qquad\text{if }\phi\text{ is constant.}$$
- Commutation with differentiation,
$$\overline{\partial_s\phi}=\partial_s\overline{\phi},\quad s=\boldsymbol{x},t.$$

Moreover, we assume that the space-time convolution kernel is obtained by tensorial extension of the one-dimensional kernel, *i.e.*

$$G(\boldsymbol{\xi},\tau)=G_t(\tau)\prod_{i=1}^{3}G_i(\xi_i).$$

Since up to now there is no example of LES of compressible flow based on temporal filtering, we restrict our discussion to spatial filtering. Mathematically, this additional restriction is expressed by

$$G_t(\tau)=\delta_0(\tau).$$

Nevertheless, one has to keep in mind that the spatial filtering implies a temporal filtering since the dynamics of the Navier-Stokes equations make it possible to associate a characteristic time scale with a length scale.

Most authors dealing with LES of compressible flows have used a change of variable in which filtered variables are weighted by the density. Mathematically, this change of variables is written as

$$\overline{\rho\phi}=\overline{\rho}\frac{\overline{\rho\phi}}{\overline{\rho}}=\overline{\rho}\widetilde{\phi}.\tag{A.2}$$

The $\widetilde{(\cdot)}$ operator is linear but does not commute with the derivation operators.

A.3 Filtering

Applying the filtering operator defined in (A.2) to the system (A.1), yields

$$\begin{aligned}
&\partial_t\bar{\rho} + \mathrm{div}(\bar{\rho}\widetilde{\boldsymbol{u}}) = 0\\
&\partial_t(\bar{\rho}\widetilde{\boldsymbol{u}}) + \mathrm{div}(\bar{\rho}\widetilde{\boldsymbol{u}}\otimes\widetilde{\boldsymbol{u}}) + \boldsymbol{\nabla}\bar{p} - \mathrm{div}\widetilde{\boldsymbol{\sigma}} = -\mathrm{div}\boldsymbol{\tau} + \mathrm{div}(\bar{\boldsymbol{\sigma}} - \widehat{\boldsymbol{\sigma}}),\\
&\partial_t(\bar{\rho}\widetilde{h}) + \mathrm{div}(\bar{\rho}\widetilde{h}\widetilde{\boldsymbol{u}}) - \partial_t\bar{p} - \widetilde{\boldsymbol{u}}\cdot\boldsymbol{\nabla}\bar{p} + \mathrm{div}\widehat{\boldsymbol{q}} - \widehat{\Phi}\\
&\qquad = -\Big[\mathrm{div}\big(\bar{\rho}c_p(\widetilde{T\boldsymbol{u}} - \widetilde{T}\widetilde{\boldsymbol{u}})\big) - (\overline{\boldsymbol{u}\cdot\boldsymbol{\nabla}p} - \widetilde{\boldsymbol{u}}\cdot\boldsymbol{\nabla}\bar{p}) - (\bar{\Phi} - \widehat{\Phi}) + \mathrm{div}(\bar{\boldsymbol{q}} - \widehat{\boldsymbol{q}})\Big],\\
&\bar{p} = \bar{\rho}R\widetilde{T}.
\end{aligned} \tag{A.3}$$

The subgrid scale (SGS) stress tensor reads

$$\tau_{ij} = \bar{\rho}(\widetilde{u_iu_j} - \widetilde{u}_i\widetilde{u}_j).$$

The filtered enthalpy $\widetilde{h}$ is equal to $c_p\widetilde{T}$ and the filtered computable viscous dissipation $\widehat{\Phi}$ is defined as

$$\widetilde{\Phi} = \sum_{i=1}^{3}\sum_{j=1}^{3}\widehat{\sigma}_{ij}\partial_j\widetilde{u}_i,$$

where

$$\widehat{\sigma}_{ij} = 2\mu(\widetilde{T})\big(\widetilde{S}_{ij} - \frac{1}{3}\delta_{ij}\sum_{k=1}^{3}\mathrm{Tr}(\widetilde{S})\big),$$

which depends on the computable rate-of-strain tensor

$$\widetilde{S}_{ij} = \frac{1}{2}\big(\partial_j\widetilde{u}_i + \partial_i\widetilde{u}_j\big).$$

The computable heat flux is

$$\widehat{\boldsymbol{q}} = -\kappa(\widetilde{T})\boldsymbol{\nabla}\widetilde{T}.$$

Using the following decomposition of the filtered pressure-gradient velocity correlation

$$\begin{aligned}
\overline{\boldsymbol{u}\cdot\boldsymbol{\nabla}p} &= \overline{\mathrm{div}(p\boldsymbol{u})} - \overline{p\mathrm{div}\boldsymbol{u}}\\
&= \mathrm{div}(\overline{\rho RT\boldsymbol{u}}) - \overline{p\mathrm{div}\boldsymbol{u}}\\
&= \mathrm{div}(\bar{\rho}R\widetilde{T}\widetilde{\boldsymbol{u}}) + \mathrm{div}\big(\bar{\rho}R(\widetilde{T\boldsymbol{u}} - \widetilde{T}\widetilde{\boldsymbol{u}})\big) - \overline{p\mathrm{div}\boldsymbol{u}}\\
&= \bar{p}\mathrm{div}\widetilde{\boldsymbol{u}} + \widetilde{\boldsymbol{u}}\cdot\boldsymbol{\nabla}\bar{p} + \mathrm{div}\big(\bar{\rho}R(\widetilde{T\boldsymbol{u}} - \widetilde{T}\widetilde{\boldsymbol{u}})\big) - \overline{p\mathrm{div}\boldsymbol{u}}
\end{aligned}$$

in (A.3), leads to the following form of the enthalpy balance equation:

$$\partial_t\bar{\rho}\widetilde{h} + \mathrm{div}(\bar{\rho}\widetilde{h}\widetilde{\boldsymbol{u}}) - \partial_t\bar{p} - \widetilde{\boldsymbol{u}}\cdot\boldsymbol{\nabla}\bar{p} + \mathrm{div}\widehat{\boldsymbol{q}} - \widehat{\Phi} = -\big[\mathrm{div}(c_v\boldsymbol{Q}) + \Pi_{dil} - \varepsilon_v + \mathrm{div}(\bar{\boldsymbol{q}} - \widehat{\boldsymbol{q}})\big].$$

In this last equation, the SGS temperature flux $\boldsymbol{Q}$ is defined by

$$\boldsymbol{Q} = \bar{\rho}(\widetilde{\boldsymbol{u}T} - \widetilde{\boldsymbol{u}}\widetilde{T}),$$

the SGS pressure dilatation Π_{dil} reads

$$\Pi_{dil} = \overline{p\mathrm{div}\boldsymbol{u}} - \bar{p}\mathrm{div}\widetilde{\boldsymbol{u}}$$

and the SGS viscous dissipation ε_v follows the expression

$$\varepsilon_v = \bar{\Phi} - \widehat{\Phi}.$$

A.4 Modelling choices

Following a Boussinesq type hypothesis, the deviatoric part of the stress tensor reads

$$\tau_{ij}^d = \tau_{ij} - \frac{1}{3}\delta_{ij}\sum_{k=1}^{3}\mathrm{Tr}(\tau) = -2\bar{\rho}\nu_{sgs}(\widetilde{S}_{ij} - \frac{1}{3}\delta_{ij}\sum_{k=1}^{3}\widetilde{S}_{kk}).$$

The simplest expression for scalar subgrid kinematic viscosity ν_{sgs} is given by the Smagorinsky model:

$$\nu_{sgs} = c_s^2\Delta^2|\widetilde{S}|,$$

where

$$|\widetilde{S}| = \big(2\sum_{i=1}^{3}\sum_{j=1}^{3}\widetilde{S}_{ij}\widetilde{S}_{ij}\big)^{1/2}, \qquad c_s = \frac{1}{\pi}\big(\frac{3K_0}{2}\big)^{-3/4} \sim 0.18,$$

with K_0 the Kolmogorov constant, equal to 1.4. The modeling proposed by Yoshizawa for the isotropic part of the SGS stress tensor reads

$$\mathrm{Tr}(\boldsymbol{\tau}) = \frac{2}{3}c_I\bar{\rho}\Delta^2|\widetilde{S}|^2,$$

where the value of the constant c_I maximizing the correlation of the modeled stress with the exact stress is 0.0066 according to Erleacher et al.

The SGS thermal conductivity κ_{sgs} is linked to the SGS dynamic visosity through the relation

$$\kappa_{sgs} = \frac{\mu_{sgs}c_p}{\mathrm{Pr}_{sgs}},$$

where Pr_{sgs} is the SGS Prandtl number, chosen in the interval $[0.3, 0.9]$. The EDQNM theory gives a value of 0.6 for this quantity. The temperature flux $\boldsymbol{Q}$ reads

$$\boldsymbol{Q} = -\frac{\bar{\rho}\nu_{sgs}}{\mathrm{Pr}_{sgs}}\boldsymbol{\nabla}\widetilde{T}.$$

The SGS viscous dissipation is modelled by

$$\varepsilon_v = \frac{c_\varepsilon\bar{\rho}k^{\frac{3}{2}}}{\Delta},$$

where $k = \frac{1}{2}\mathrm{Tr}(\tau)$ and c_ε is a constant (to be defined). Finally, in the enthalpy balance equation, the SGS pressure-dilatation Π_{dil}, the term $(\widetilde{\boldsymbol{u}}\cdot\boldsymbol{\nabla}\bar{p} - \overline{\boldsymbol{u}\cdot\boldsymbol{\nabla}p})$ and $\mathrm{div}(\bar{\boldsymbol{q}} - \widehat{\boldsymbol{q}})$ are neglected, such as the term $\mathrm{div}(\widehat{\boldsymbol{\sigma}} - \bar{\boldsymbol{\sigma}})$ in the momentum balance equation.

A.5 The filtered equations

According to the above discussion, the final filtered model equations read

$$\begin{aligned}
&\partial_t\bar{\rho} + \mathrm{div}(\bar{\rho}\widetilde{\boldsymbol{u}}) = 0\\
&\partial_t(\bar{\rho}\widetilde{\boldsymbol{u}}) + \mathrm{div}(\bar{\rho}\widetilde{\boldsymbol{u}}\otimes\widetilde{\boldsymbol{u}}) + \boldsymbol{\nabla}\bar{p} - \mathrm{div}\widehat{\boldsymbol{\sigma}} = -\mathrm{div}\boldsymbol{\tau}^d + \frac{2}{3}\boldsymbol{\nabla}k,\\
&\partial_t\bar{\rho}\widetilde{h} + \mathrm{div}(\bar{\rho}\widetilde{h}\widetilde{\boldsymbol{u}}) - \partial_t\bar{p} - \widetilde{\boldsymbol{u}}\cdot\boldsymbol{\nabla}\bar{p} + \mathrm{div}\widehat{\boldsymbol{q}} - \widehat{\Phi} = -\mathrm{div}(c_v\boldsymbol{Q}),\\
&\bar{p} = \frac{\gamma-1}{\gamma}\bar{\rho}\widetilde{h},
\end{aligned} \tag{A.4}$$

where $\gamma = c_p/c_v$ is the adiabatic index.

Replacing the enthalpy in the enthalpy balance equation by the expression $\widetilde{h} = \widetilde{e} + \bar{p}/\bar{\rho}$, yields the internal energy balance equation:

$$\partial_t(\bar{\rho}\widetilde{e}) + \mathrm{div}(\bar{\rho}\widetilde{e}\widetilde{\boldsymbol{u}}) + \mathrm{div}(\bar{p}\widetilde{\boldsymbol{u}}) - \widetilde{\boldsymbol{u}} \cdot \boldsymbol{\nabla}\bar{p} + \mathrm{div}(\widehat{\boldsymbol{q}}) - \widehat{\Phi} = -\mathrm{div}(c_v Q). \tag{A.5}$$

The kinetic energy balance equation is obtaining by the inner product of the filtered momentum balance equation with the filtered velocity:

$$\frac{1}{2}\partial_t(\bar{\rho}|\widetilde{\boldsymbol{u}}|^2) + \frac{1}{2}\mathrm{div}(\bar{\rho}|\widetilde{\boldsymbol{u}}|^2\widetilde{\boldsymbol{u}}) + \widetilde{\boldsymbol{u}} \cdot \boldsymbol{\nabla}\bar{p} - \widetilde{\boldsymbol{u}} \cdot \mathrm{div}(\widehat{\boldsymbol{\sigma}}) = -\widetilde{\boldsymbol{u}} \cdot \mathrm{div}(\boldsymbol{\tau}^d) + \frac{2}{3}\widetilde{\boldsymbol{u}} \cdot \boldsymbol{\nabla}k, \tag{A.6}$$

where $k = \frac{1}{2}\mathrm{Tr}(\boldsymbol{\tau})$ is the subgrid energy. Summing equations (A.5) and (A.6) gives rise to the total energy balance equation:

$$\partial_t(\bar{\rho}\widetilde{E}) + \mathrm{div}(\bar{\rho}\widetilde{E}\widetilde{\boldsymbol{u}}) + \mathrm{div}(\bar{p}\widetilde{\boldsymbol{u}}) - \mathrm{div}(\widehat{\boldsymbol{\sigma}}\widetilde{\boldsymbol{u}}) + \mathrm{div}(\widehat{\boldsymbol{q}}) = \widetilde{\boldsymbol{u}} \cdot \mathrm{div}(\boldsymbol{\tau}^d) + \frac{2}{3}\widetilde{\boldsymbol{u}} \cdot \boldsymbol{\nabla}k - \mathrm{div}(c_v Q), \tag{A.7}$$

where the total energy is defined by $E = e + \frac{1}{2}|\widetilde{\boldsymbol{u}}|^2$.

A.6 The pressure correction scheme

Let us consider a partition $0 = t_0 < t_1 < \ldots < t_N = T$ of the time interval $(0, T)$, which we suppose uniform. Let $\delta t = t_{n+1} - t_n$ for $n = 0, 1, \ldots, N-1$ be the constant time step. In order to reduce the notations, in what follows we will drop the notations corresponding to the operators of the filtering process, for example ρ_K is the approximation of the mean value of $\bar{\rho}$ over the control volume $K \in \mathcal{M}$ and so on. The pressure correction scheme considered here consists in the two following steps:

Pressure gradient scaling step:

$$\forall \sigma \in \mathcal{E}_{\mathrm{int}}, \quad (\boldsymbol{\nabla}P)_\sigma^{n+1} = \Big(\frac{\rho_{D_\sigma}^n}{\rho_{D_\sigma}^{n-1}}\Big)^{1/2} (\boldsymbol{\nabla}p^n)_\sigma. \tag{A.8a}$$

Prediction step – Solve for $\boldsymbol{v}^{n+1}$:

$$\begin{aligned} \text{For } 1 \le i \le d,\ \forall \sigma \in \mathcal{E}_{\mathcal{S}}^{(i)}, \qquad & \frac{1}{\delta t}\left(\rho_{D_\sigma}^n v_{\sigma,i}^{n+1} - \rho_{D_\sigma}^{n-1} u_{\sigma,i}^n\right) + \mathrm{div}(\rho^n v_i^{n+1}\boldsymbol{u}^n)_\sigma \\ & -\mathrm{div}\big(\boldsymbol{\tau}^d(\boldsymbol{v}^{n+1})\big)_{\sigma,i} + \frac{2}{3}\big(\boldsymbol{\nabla}k(\boldsymbol{v}^{n+1})\big)_{\sigma,i} + (\boldsymbol{\nabla}P)_{\sigma,i}^{n+1} = 0. \end{aligned} \tag{A.8b}$$

Correction step – Solve for p^{n+1}, h^{n+1}, ρ^{n+1} and $\boldsymbol{u}^{n+1}$:

$$\text{For } 1 \le i \le d,\ \forall \sigma \in \mathcal{E}_{\mathcal{S}}^{(i)}, \qquad \frac{1}{\delta t}\ \rho_{D_\sigma}^n\ (u_{\sigma,i}^{n+1} - v_{\sigma,i}^{n+1}) + (\boldsymbol{\nabla} p^{n+1})_{\sigma,i} - (\boldsymbol{\nabla} P)_{\sigma,i}^{n+1} = 0, \tag{A.8c}$$

$$\forall K \in \mathcal{M}, \quad \frac{1}{\delta t}(\rho_K^{n+1} - \rho_K^n) + \operatorname{div}(\rho^{n+1}\boldsymbol{u}^{n+1})_K = 0, \tag{A.8d}$$

$$\begin{aligned}\forall K \in \mathcal{M}, \quad \frac{1}{\delta t}(\rho_K^{n+1} h_K^{n+1} - \rho_K^n e_K^n) + \operatorname{div}(\rho^{n+1} h^{n+1}\boldsymbol{u}^{n+1})_K - \frac{1}{\delta t}(p_K^{n+1} - p_K^n) \\ -(\boldsymbol{u}^{n+1} \cdot \boldsymbol{\nabla} p^{n+1})_K + \operatorname{div}(c_v \boldsymbol{q}^{n+1})_K = \left(\boldsymbol{\tau}(\boldsymbol{v}^{n+1}) : \boldsymbol{\nabla}\boldsymbol{v}^{n+1}\right)_K + S_K^{n+1},\end{aligned} \tag{A.8e}$$

$$\forall K \in \mathcal{M}, \quad p_K^{n+1} = \frac{\gamma - 1}{\gamma} \rho_K^{n+1} h_K^{n+1}. \tag{A.8f}$$

Bibliography

[1] G. Ansanay-Alex, F. Babik, J.-C. Latché, and D. Vola. An L^2-stable approximation of the Navier-Stokes convection operator for low-order non-conforming finite elements. *International Journal for Numerical Methods in Fluids*, 66:555–580, 2011.

[2] A. Beccantini and E. Studer. The reactive Riemann problem for thermally perfect gases at all combustion regimes. *International Journal for Numerical Methods in Fluids*, 64:269–313, 2010.

[3] C. Berthon, F. Coquel, and P. G. LeFloch. Why many theories of shock waves are necessary. Kinetic relations for nonconservative systems. *Proceedings of the Royal Society of Edinburgh*, 142:1–37, 2012.

[4] H. Bijl and P. Wesseling. A unified method for computing incompressible and compressible flows in boundary-fitted coordinates. *Journal of Computational Physics*, 141:153–173, 1998.

[5] F. Boyer, F. Dardalhon, C. Lapuerta, and J.-C. Latché. Stability of a Crank-Nicolson pressure correction scheme based on staggered discretizations. *International Journal for Numerical Methods in Fluids*, 74:34–58, 2014.

[6] CALIF^{3}S. A software components library for the computation of reactive turbulent flows. `https://gforge.irsn.fr/gf/project/isis`.

[7] V. Casulli and D. Greenspan. Pressure method for the numerical solution of transient, compressible fluid flows. *International Journal for Numerical Methods in Fluids*, 4:1001–1012, 1984.

[8] C. Chalons, M. Girardin, and S. Kokh. Large time step and asymptotic preserving numerical schemes for the gas dynamics equations with source terms. *SIAM Journal on Scientific Computing*, 35:A2874–A2902, 2013.

[9] C. Chalons, M. Girardin, and S. Kokh. An all regime Lagrange-projection like scheme for the gas dynamics equations on unstructured meshes. *Communications in Computational Physics*, 20:188–233, 2016.

[10] P. G. Ciarlet. Handbook of numerical analysis volume II : Finite elements methods – Basic error estimates for elliptic problems. In P. Ciarlet and J.L. Lions, editors, *Handbook of Numerical Analysis, Volume II*, pages 17–351. North Holland, 1991.

[11] S. Clain, S. Diot, and R. Loubère. A high-order finite volume method for systems of conservation laws – Multi-dimensional Optimal Order Detection (MOOD). *Journal of Computational Physics*, 230:4028–4050, 2011.

[12] B. Cockburn and C.-W. Shu. The Runge-Kutta Discontinuous Galerkin method for conservation laws V – multidimensional systems. *Journal of Computational Physics*, 141:199–224, 1998.

[13] P. Colella and K. Pao. A projection method for low speed flows. *Journal of Computational Physics*, 149:245–269, 1999.

[14] M. Crouzeix and P.A. Raviart. Conforming and nonconforming finite element methods for solving the stationary Stokes equations. *RAIRO Série Rouge*, 7:33–75, 1973.

[15] F. Dardalhon, J.-C. Latché, and S. Minjeaud. Analysis of a projection method for low-order non-conforming finite elements. *IMA Journal of Numerical Analysis*, 33:295–317, 2013.

[16] S. Dellacherie. Analysis of Godunov type schemes applied to the compressible Euler system at low Mach number. *Journal of Computational Physics*, 229:978–1016, 2010.

[17] B. Després and F. Lagoutière. Contact discontinuity capturing schemes for linear advection and compressible gas dynamics. *Journal of Scientific Computing*, 16:479–524, 2001.

[18] P. Drábek and J. Milota. Methods of nonlinear analysis. Birkhäuser Advanced Texts. 2007.

[19] R. Eymard, T. Gallouët, and R. Herbin. Finite volume methods. In P. Ciarlet and J.L. Lions, editors, *Handbook of Numerical Analysis, Volume VII*, pages 713–1020. North Holland, 2000.

[20] T. Gallouët, L. Gastaldo, R. Herbin, and J.-C. Latché. An unconditionally stable pressure correction scheme for compressible barotropic Navier-Stokes equations. *Mathematical Modelling and Numerical Analysis*, 42:303–331, 2008.

[21] T. Gallouët, R. Herbin, J.-C. Latché, and N. Therme. Entropy estimates for a class of schemes for the Euler equations. *In preparation*, 2017.

[22] T. Gallouët, R. Herbin, N. Therme, and J.-C. Latché. Consistency of some staggered schemes for the euler equations. *in preparation*, 2017.

[23] L. Gastaldo, D. Grapsas, R. Herbin, and J.-C. Latché. A staggered pressure correction numerical scheme to compute a travelling reactive interface between two compressible media. *in preparation*, 2016.

[24] L. Gastaldo, R. Herbin, W. Kheriji, C. Lapuerta, and J.-C. Latché. Staggered discretizations, pressure correction schemes and all speed barotropic flows. In *Finite Volumes for Complex Applications VI - Problems & Perspectives - Prague, Czech Republic*, volume 2, pages 39–56. Springer, 2011.

[25] L. Gastaldo, R. Herbin, and J.-C. Latché. A discretisation of the phase mass balance in fractional step algorithms for the drift-flux model. *IMA J.Numer. Anal.*, 2011.

[26] L. Gastaldo, R. Herbin, and J.-C. Latché. A discretization of the phase mass balance in fractional step algorithms for the drift-flux model. *IMA Journal of Numerical Analysis*, 31:116–146, 2011.

[27] L. Gastaldo, R. Herbin, J.-C. Latché, and N. Therme. A MUSCL-type segregated staggered scheme with explicit steps for the euler equations. *under revision*, 2017.

[28] V. Giovangigli. *Multicomponent flow modeling*. Birkhäuser, 1999.

[29] E. Godlewski and P.-A. Raviart. *Numerical Approximation od Hyperbolic Systems of Conservation Laws*. Springer, 1991.

[30] D. Grapsas, R. Herbin, W. Kheriji, and J.-C. Latché. An unconditionally stable finite element-finite volume pressure correction scheme for the compressible Navier-Stokes equations. *SMAI Journal of Computational Mathematics*, 2016.

[31] D. Grapsas, R. Herbin, and J.-C. Latché. A model and a numerical scheme to compute laminar flames in dust suspensions. *in preparation*, 2017.

[32] J.-L. Guermond and L. Quartapelle. A projection FEM for variable density incompressible flows. *Journal of Computational Physics*, 165:167–188, 2000.

[33] J.L. Guermond, R. Pasquetti, and B. Popov. Entropy viscosity method for nonlinear conservation laws. *Journal of Computational Physics*, 230:4248–4267, 2011.

[34] H. Guillard. Recent developments in the computation of compressible low Mach flows. *Flow, Turbulence and Combustion*, 76:363–369, 2006.

[35] H. Guillard and A. Murrone. On the behaviour of upwind schemes in the low Mach number limit: II. Godunov type schemes. *Computers & Fluids*, 33:655–675, 2004.

[36] H. Guillard and C. Viozat. On the behaviour of upwind schemes in the low Mach number limit. *Computers & Fluids*, 28:63–86, 1999.

[37] F.H. Harlow and A.A. Amsden. Numerical calculation of almost incompressible flow. *Journal of Computational Physics*, 3:80–93, 1968.

[38] F.H. Harlow and A.A. Amsden. A numerical fluid dynamics calculation method for all flow speeds. *Journal of Computational Physics*, 8:197–213, 1971.

[39] F.H. Harlow and J.E. Welsh. Numerical calculation of time-dependent viscous incompressible flow of fluid with free surface. *Physics of Fluids*, 8:2182–2189, 1965.

[40] R. Herbin, W. Kheriji, and J.-C. Latché. On some implicit and semi-implicit staggered schemes for the shallow water and euler equations. *Mathematical Modelling and Numerical Analysis*, 48:1807–1857, 2014.

[41] R. Herbin and J.-C. Latché. Kinetic energy control in the MAC discretisation of the compressible Navier-Stokes equations. *International Journal of Finite Volumes*, 7, 2010.

[42] R. Herbin, J.-C. Latché, and T.T. Nguyen. On some consistent explicit staggered schemes for the shallow water and Euler equations. *submitted*, 2014.

[43] R. Herbin, J.-C. Latché, and K. Saleh. Low mach number limit of some staggered schemes for compressible barotropic flows. *In preparation*, 2017.

[44] R. Herbin, J.-C. Latché, and C. Zaza. A cell-centered pressure-correction scheme for the compressible euler equations. *in revision*, 2017.

[45] R. Hilbert, F. Tap, H. El-Rabii, and D. Thévenin. Impact of detailed chemistry and transport models on turbulent combustion simulations. *Progress in Energy and Combustion Science*, 30:61–117, 2004.

[46] R.I. Issa. Solution of the implicitly discretised fluid flow equations by operator splitting. *Journal of Computational Physics*, 62:40–65, 1985.

[47] R.I. Issa, A.D. Gosman, and A.P. Watkins. The computation of compressible and incompressible recirculating flows by a non-iterative implicit scheme. *Journal of Computational Physics*, 62:66–82, 1986.

[48] K.C. Karki and S.V. Patankar. Pressure based calculation procedure for viscous flows at all speeds in arbitrary configurations. *AIAA Journal*, 27:1167–1174, 1989.

[49] W. Kheriji, R. Herbin, and J.-C. Latché. Pressure correction staggered schemes for barotropic monophasic and two-phase flows. *Computers & Fluids*, 88:524–542, 2013.

[50] S. Kudriakov, F. Dabbene, E. Studer, A. Beccantini, J.P. Magnaud, H. Paillère, A. Bentaib, A. Bleyer, J. Malet, E. Porcheron, and C. Caroli. The TONUS CFD code for hydrogen risk analysis: physical models, numerical schemes and validation matrix. *Nuclear Engineering and Design*, 238:551–565, 2008.

[51] A. Kurganov and E. Tadmor. Solution of two-dimensional Riemann problems for gas dynamics without Riemann problem solvers. *Numerical Methods for Partial Differential Equations*, 18:584–608, 2002.

[52] D. Kuzmin, R. Löhner, and S. Turek. *Flux-Corrected transport*. Springer, 2005.

[53] N. Kwatra, J. Su, J.T. Grétarsson, and R. Fedkiw. A method for avoiding the acoustic time step restriction in compressible flow. *Journal of Computational Physics*, 228:4146–4161, 2009.

[54] B. Larrouturou. How to preserve the mass fractions positivity when computing compressible multi-component flows. *Journal of Computational Physics*, 95:59–84, 1991.

[55] J.-C. Latché, B. Piar, and K. Saleh. A discrete kinetic energy preserving convection operator for variable density flows on locally refined staggered meshes. *In preparation*, 2017.

[56] P. Lax and X.-D. Liu. Solution of two-dimensional riemann problems of gas dynamics by positive schemes. *SIAM Journal on Scientific Computing*, 19:319–340, 1998.

[57] M.-S. Liou. A sequel to AUSM, part II: AUSM+-up. *Journal of Computational Physics*, 214:137–170, 2006.

[58] M.-S. Liou and C.J. Steffen. A new flux splitting scheme. *Journal of Computational Physics*, 107:23–39, 1993.

[59] A.N. Lipatnikov and J. Chomiak. Turbulent flame speed and thickness: phenomenology, evaluation, and application in multi-dimensional simulations. *Progress in Energy and Combustion Science*, 28:1–74, 2002.

[60] C. Liu and N.J. Walkington. Convergence of numerical approximations of the incompressible Navier-Stokes equations with variable density and viscosity. *SIAM Journal on Numerical Analysis*, 45:1287–1304, 2007.

[61] A. Majda and J. Sethian. The derivation and numerical solution of the equations for zero Mach number solution. *Combustion Science and Techniques*, 42:185–205, 1985.

[62] J.J. McGuirk and G.J. Page. Shock capturing using a pressure-correction method. *AIAA Journal*, 28:1751–1757, 1990.

[63] S. Minjeaud. An unconditionally stable uncoupled scheme for a triphasic Cahn-Hilliard/Navier-Stokes model. *Numerical Methods for Partial Differential Equations*, 29:584–618, 2013.

[64] K. Nerinckx, J. Vierendeels, and E. Dick. Mach-uniformity through the coupled pressure and temperature correction algorithm. *Journal of Computational Physics*, 206:597–623, 2005.

[65] K. Nerinckx, J. Vierendeels, and E. Dick. A Mach-uniform algorithm: coupled versus segregated approach. *Journal of Computational Physics*, 224:314–331, 2007.

[66] N. Peters. *Turbulent Combustion*. Cambridge Monographs of Mechanics. Cambridge University Press, 2000.

[67] L. Piar, F. Babik, R. Herbin, and J.-C. Latché. A formally second order cell centered scheme for convection-diffusion equations on general grids. *International Journal for Numerical Methods in Fluids*, 71:873–890, 2013.

[68] T. Poinsot and D. Veynante. *Theoretical and Numerical Combustion*. Editions R.T Edwards Inc., 2005.

[69] R. Rannacher and S. Turek. Simple nonconforming quadrilateral Stokes element. *Numerical Methods for Partial Differential Equations*, 8:97–111, 1992.

[70] M. Schäfer and S. Turek. *Benchmark Computations of Laminar Flow Around a Cylinder*, volume 52 of *Notes on Numerical Fluid Mechanics*. 1996.

[71] C.W. Schulz-Rinne, J.P. Collins, and H.M. Glaz. Numerical solution of the Riemann problem for two-dimensional gas dynamics. *SIAM Journal on Scientific Computing*, 14:1394–1414, 1993.

[72] J.L. Steger and R.F. Warming. Flux vector splitting of the inviscid gaz dynamics equations with applications to finite difference methods. *Journal of Computational Physics*, 40:263–293, 1981.

[73] N. Therme. *Schémas numériques pour la simulation de l'explosion*. PhD thesis, Université d'Aix-Marseille, 2015.

[74] E.F. Toro and M.E. Vázquez-Cendón. Flux splitting schemes for the Euler equations. *Computers & Fluids*, 70:1–12, 2012.

[75] D.R. Van der Heul, C. Vuik, and P. Wesseling. Stability analysis of segregated solution methods for compressible flow. *Applied Numerical Mathematics*, 38:257–274, 2001.

[76] D.R. Van der Heul, C. Vuik, and P. Wesseling. A conservative pressure-correction method for flow at all speeds. *Computers & Fluids*, 32:1113–1132, 2003.

[77] J.P. Van Dormaal, G.D. Raithby, and B.H. McDonald. The segregated approach to predicting viscous compressible fluid flows. *Transactions of the ASME*, 109:268–277, 1987.

[78] D. Vidović, A. Segal, and P. Wesseling. A superlinearly convergent Mach-uniform finite volume method for the Euler equations on staggered unstructured grids. *Journal of Computational Physics*, 217:277–294, 2006.

[79] C. Wall, C.D. Pierce, and P. Moin. A semi-implicit method for resolution of acoustic waves in low Mach number flows. *Journal of Computational Physics*, 181:545–563, 2002.

[80] I. Wenneker, A. Segal, and P. Wesseling. A Mach-uniform unstructured staggered grid method. *International Journal for Numerical Methods in Fluids*, 40:1209–1235, 2002.

[81] P. Woodward and P. Colella. The numerical simulation of two-dimensional fluid flow with strong shocks. *Journal of Computational Physics*, 54:115–173, 1984.

[82] Z. Xu, Y. Liu, H. Du, G. Lin, and C.-W. Shu. Point-wise hierarchical reconstruction for discontinuous Galerkin and finite volume methods for solving conservation laws. *Journal of Computational Physics*, 230:6843–6865, 2011.

[83] S.Y. Yoon and T. Yabe. The unified simulation for incompressible and compressible flow by the predictor-corrector scheme based on the CIP method. *Computer Physics Communications*, 119:149–158, 1999.

[84] G.-C. Zha and E. Bilgen. Numerical solution of Euler equations by a new flux vector splitting scheme. *International Journal for Numerical Methods in Fluids*, 17:115–144, 1993.

[85] V.L. Zimont. Gas premixed combustion at high turbulence. turbulent flame closure combustion model. *Experimental Thermal and Fluid Science*, 21:179–186, 2000.